A Current-Only Faulted Section Identification Scheme for Power System Protection

Pannita Rajakrom

A thesis submitted for the degree of Doctor of Philosophy to the
Department of Electronic and Electrical Engineering
University of Strathclyde
Glasgow, United Kingdom

June 9, 2025

This thesis is the result of the author's original research. It has been composed by the author and has not previously submitted for examination which has led to the award of a degree.

The copyright of this thesis belongs to the author under the terms of the United Kingdom Copyright Acts as qualified by University of Strathclyde Regulation 3.50. Due acknowledgement must always be made of the use of any material contained in, or derived from, this thesis.

Signed:

Date:

Abstract

This thesis presents a faulted section identification scheme designed for modern distribution networks, which is applicable to power system protection and/or to the emergent "fault location, isolation, and service restoration" (FLISR) set of functions (often also termed "distribution automation" or "distribution system automation"). The scheme relies solely on current measurements and employs a binary coded data exchange mechanism between measurement and processing locations that is used to compare the current angle and magnitude changes from pre- to during-fault conditions. The system can be implemented in distributed or centralised architectures.

The scheme addresses many of the challenges arising from the increasing integration of distributed energy resources (DERs), which are described in detail in the thesis, and include reduced and variable system strength and short-circuit capacity (or fault level), bi-directional power flows and protection-specific issues such as blinding and sympathetic tripping.

The reliability, selectivity, and accuracy of the scheme have been validated through extensive non-real-time simulation in MATLAB/Simulink, as well as hardware-in-the-loop (HIL) testing using a real-time digital simulator (RTDS). Simulations cover a range of scenarios including variation in fault location, fault resistance, short-circuit level, and load conditions. The HIL results, which include actual processing hardware and communications links, confirmed the scheme's ability to meet the timing and performance requirements of contemporary distribution protection and monitoring systems. In the concluding section, a range of areas for future work is suggested.

Acknowledgements

I would like to express my deepest gratitude to my supervisor, Professor Campbell Booth, for his invaluable guidance, encouragement, and unwavering support throughout the course of this research. His expertise, insightful advice, and generous provision of opportunities, both academic and financial, have been fundamental to the completion of this thesis. I am truly grateful for his mentorship, which has been a constant source of inspiration.

I would like to offer my sincere thanks to my second supervisor, Dr Qiteng Hong, for his constructive feedback, the sharing of knowledge, and provision of essential materials which greatly contributed to the progress of this work.

My thanks are extended to Mr Richard Munro and Mr Jiaxuan Han for their technical assistance, particularly in the laboratory and during the real-time simulation testing. Their support was instrumental in the practical aspects of this research.

I am also grateful to my colleagues in the Advanced Electrical Systems group at the University of Strathclyde for their friendship and collaboration throughout my studies, in particular Shuxiu Cao, Kevin Kawal, Dr Di Liu, Lu Shen, and Qi Dong for their generous assistance.

Finally, I owe my heartfelt thanks to my parents, Asawin and Ngamta Rajakrom, my sister, Puthita, and all my relatives and friends for their unconditional support and encouragement throughout the years. This thesis is dedicated to them.

Contents

List of Figures

List of Tables

Glossary of Abbreviations

5G	Fifth-Generation (mobile communications)
AMI	Advanced Metering Infrastructure
BESS	Battery Energy Storage System
CAT-M1	Category M1
CAT-M2	Category M2
CB	Circuit Breaker
CCW	Counterclockwise
CDMA	Code Division Multiple Access
CEGB	Central Electricity Generating Board
CI	Customer Impact
CML	Customer Minutes Lost
CSI	Current Source Inverter
CT	Current Transformer
CW	Clockwise
DD	Directional Detector
DER	Distribution Energy Resource
DFT	Discrete Fourier Transform
DG	Distributed Generation
DMS	Distribution Management System
DNP	Directional Normal Power
DOCR	Directional Overcurrent Relay
DSL	Digital Subscriber Line
DSP	Digital Signal Processing
eMTC	enhanced Machine-Type Communication
ETAP	Electrical Transient Analyser Programme
EU	European Union

FFT	Fast Fourier Transform
FLISR	Fault Location, Isolation, and Service Restoration
GOOSE	Generic Object Oriented Substation Event
GTNET-SKT	Gigabit Transceiver Network Socket
HIF	High Impedance Fault
HIL	Hardware-in-the-Loop
IDMT	Inverse Definite Minimum Time
IED	Intelligent Electronic Device
IIDG	Inverter-Interfaced Distributed Generation
ISDN	Integrated Service Digital Network
Kbps	Kilobits per second
LTE-M	Long-Term Evolution for Machine
MTA	Maximum Torque Angle
NB-IoT	Narrow-Band Internet-of-Thing
NIST	National Institute of Standards and Technology
OCR	Overcurrent Relay
OPGW	Optical Ground Wires
PLC	Power Line Communication
PMS	Plug Multiplier Setting
PQ	Real and Reactive Power
p.u.	per unit
PV	Photovoltaic
RES	Renewable Energy Resource
RoCoF	Rate of Change of Frequency
RTDS	Real-Time Digital Simulator
RTU	Remote Terminal Unit
SAU	Substation Automation Unit
SCADA	Supervisory Control and Data Acquisition
SEP	Smart Energy Profile
TDMA	Time Division Multiple Access
TMS	Time Multiplier Setting

UHF	Ultra High Frequency
UK	United Kingdom
URLLC	Ultra-Reliable Low-Latency Communication
US	United States
VHF	Very High Frequency
VSAT	Very Small Aperture Terminal
VSI	Voltage Source Inverter
VT	Voltage Transformer
WSN	Wireless Sensor Network

Chapter 1

Introduction

1.1 Objectives and motivations of research

1.1.1 Context: decarbonisation of global energy systems

Climate change, emission of greenhouse and other harmful gases and the global push for decarbonisation of energy has led to the need for government intervention and policy change on a global scale, with the goal of managing and decreasing pollution and emissions. In June 2019, the United Kingdom (UK) amended the Climate Change Act, which established a legally-binding commitment to achieve net zero greenhouse gas emissions by the year 2050. This commitment is commonly referred to as the UK's net zero target, which was reaffirmed during the discussion at COP27 [1.1]. This necessity, combined with the growing demand for energy, has driven many changes and innovations in the electricity supply industry. One of these changes includes the widespread incorporation of small-scale renewable energy sources (RES) integrated directly into power grids, particularly at the distribution level. The transition to cleaner, low-carbon energy sources is further supported by technological advancements in areas such as hydroelectric, wind, solar, and nuclear power. This global shift can be illustrated by the renewable and non-renewable energy generation and consumption in the United Kingdom.

The UK has positioned itself as a global leader in the transition from fossil fuels to RES. The UK government has outlined targets for expanding both offshore wind, including floating installations, and solar PV capacity, aiming for 50 GW and 70 GW of installed capacity respectively, by 2030 and 2035 [1.2]. Over the past two decades, the UK has witnessed a remarkable increase in the contribution of renewables to its national energy mix, as shown in Figure 1.1. In 2000, RESs only accounted for 2.8% of total energy generation [1.3]. This figure was projected to reach an estimated 50.8% by 2024 [1.4]. This marked the first time that more than half of the UK's electricity supply has originated from renewable sources. It can be attributed to several key factors, including supportive government policies, advancements in renewable energy technologies, and a growing public commitment to environmental sustainability.

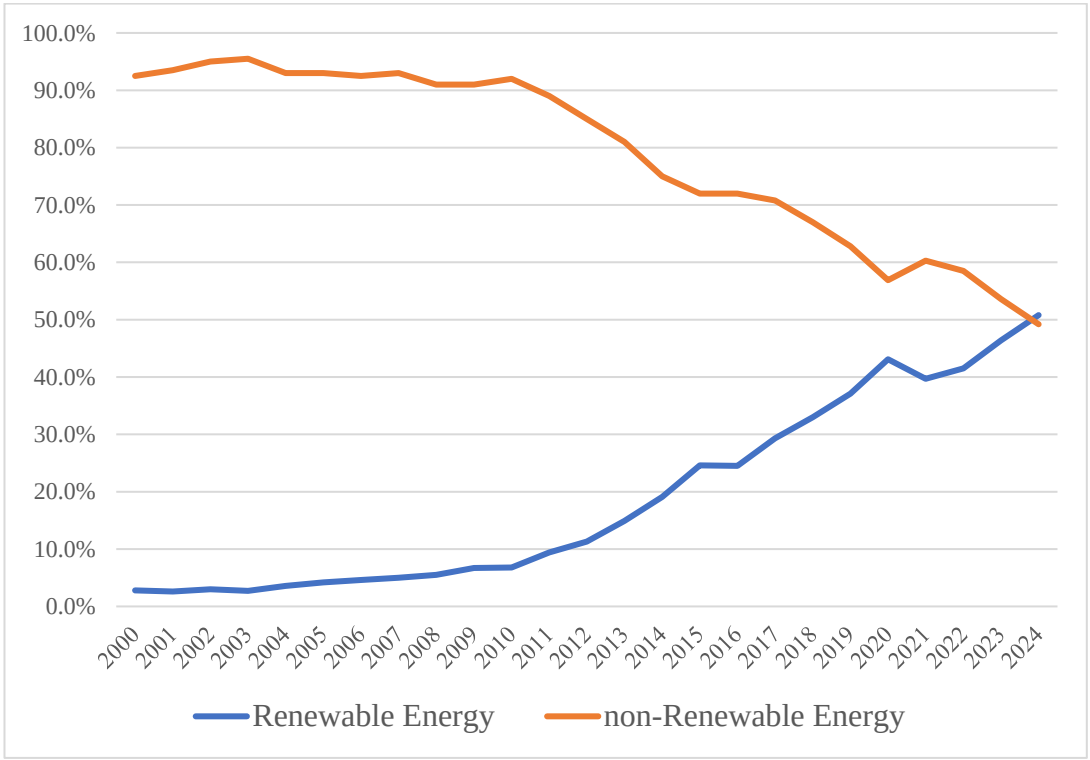

Figure 1.1: Electricity generated by fuel type in the UK during year 2000 – 2024 [1.3] – [1.27]

Wind energy, encompassing both onshore and offshore installations, currently is the UK's leading source of renewable energy. It contributed an estimated 60.61% of the total renewable energy generation in 2023. Solar photovoltaic (PV) systems are playing an increasingly significant role, accounting for approximately 10.24% in 2023. Biomass and hydropower further diversify the UK's renewable energy portfolio [1.27].

Despite the significant progress made in transitioning towards renewables, non-renewable energy sources still hold a substantial share of the UK's energy mix. In 2000, non-renewable energy accounted for roughly 92.5% of total generation [1.3]. However, by 2024, this figure was projected to decrease to less than 50% [1.4], highlighting a noteworthy shift toward cleaner energy sources. This shift aligns with government policies aimed at reducing carbon emissions from fossil fuels and gas used in electricity generation to 5% by 2030 [1.28], ultimately targeting net-zero carbon emissions by 2050 [1.1] – [1.2], [1.28].

The global trend towards renewable energy adoption is not limited to the UK; many other countries are experiencing similar shifts. This can be illustrated through the data presented in Figure 1.2, which depicts renewable and non-renewable energy generation from 2000 to 2023 in the United States (US), European Union (EU), China and Thailand (the author's home country). The data clearly indicates a significant increase in RES consumption worldwide, reflecting the effectiveness of government policies and public support for clean energy initiatives. This growth is indicative of a broader commitment to sustainability and environmental stewardship.

Although the reduction in the use of fossil fuels for electricity generation is not uniform for the various countries illustrated, it does show that there is an ongoing and persistent global effort to reduce carbon footprints and transition towards a low-carbon economy. This shift is particularly evident in the gradual phase-out of coal and the increasing reliance on natural gas as a transition fuel [1.29], as shown in Figure 1.3.

Figure 1.2: Share of electricity production from renewables for a range of different countries [1.30]

Figure 1.3: Share of electricity production from fossil fuels for a range of different countries [1.29]

The comparative analysis of renewable and non-renewable energy consumption highlights the complexities and challenges inherent in the transition towards renewables and low/zero-carbon energy systems. Although the growth of RES is commendable, it is essential to recognise the need for a balanced approach to energy policy [1.31]. The energy landscape is characterised by a dynamic interplay between the push for RES and the realities of existing infrastructure and market conditions.

1.1.2 Decarbonisation: implications for electrical power systems

The widespread adoption of RES presents both positive and negative implications for modern power systems. In addition to transmission-connected renewables, a great deal of future energy will be generated and connected at the distribution voltage levels, leading to a growing presence of distributed energy resources (DER) – especially those in the form of distributed generation (DG) derived from RES – within distribution networks. By generating power closer to the point of consumption, DER reduces transmission losses and can alleviate congestion on the "upstream" grid [1.32]. In terms of resilience and enhancing reliability, if the transmission or centralised generation is lost or reduced, DER can provide backup power to critical infrastructure, contributing to a more robust energy infrastructure, although the ability to operate power systems in "island" mode is often limited due to DER capabilities and/or policies that do not allow islanded operation due to operational and safety reasons [1.33].

Despite offering considerable environmental and economic advantages, the integration of DERs also introduces a range of technical considerations that must be addressed. Traditional electricity systems were structured around large, centralised energy generation, with unidirectional power flows transmitting electricity over long distances to end users. However, the increasingly penetration of DERs has significantly altered the structure and

behaviour of modern power networks. Existing grid infrastructure – particularly at the distribution level (medium and low voltage) – was not originally designed to accommodate the decentralised and bidirectional nature of power flows introduced by RES [1.3]. As more DERs are integrated, substantial upgrades to infrastructure and operational paradigms are required. This transition also introduces regulatory and market complexities, as existing policies and frameworks may not adequately support the technical and economic requirements of decentralised energy integration. Moreover, the coordination among diverse stakeholders – including utilities, regulators, aggregators, and consumers – becomes increasingly complex. Enhancing grid flexibility and resilience, both technically and institutionally, is therefore critical to the success of this energy transition.

1.1.3 Specific challenges for power system protection

Among the various technical systems affected by this transition, power system protection remains particularly vulnerable. Malfunction of protection systems can lead to severe consequences, including equipment damage, personnel hazards, and wide-area outages. Conventional protection schemes, which were developed for centralised generation and largely passive networks, are often based on static settings and operate under the assumption of predictable fault current behaviour. However, the integration of DERs introduces variability in fault characteristics and network topology, making traditional protection methods increasingly unreliable (either in the form of unnecessary operation or non-operation – both of which are extremely undesirable), leading to unnecessary outages and economic losses, as well as potential physical damage to system assets and customers. The specific limitation of conventional protection in DER-rich environments are discussed further in Chapter 3 of this thesis.

Moreover, modern power networks increasingly rely on advanced monitoring systems and digital technologies to support more efficient, intelligent, and resilient grid operations [1.34]. The growing availability of digital tools, such as intelligent electronic devices (IEDs) and IoT-based sensors, provides new opportunities to enhance protection systems [1.35]. In the distribution context, these technologies underpin applications such as the Distribution Management System (DMS) for real-time monitoring and control, as well as automation function like Fault Location, Isolation, and Service Restoration (FLISR). These systems enable real-time measurement, fast data exchange, and decentralised decision-making – capabilities that are crucial for operating networks with DER-rich [1.36].

1.1.4 Responding to the challenge – motivation and objectives for the research reported in this thesis

Rather than presenting a challenge, the widespread adoption of digital infrastructure acts as an enabler for more selective, responsive, and scalable protection schemes. Leveraging these technologies allows the transition from conventional protection to intelligent, communication-assisted methods that are better suited to the evolving characteristics of distribution networks. This shift has motivated many researchers to develop novel protection schemes, as discussed further in literature review in Chapter 3. These solutions typically incorporate advanced technologies and strategies to improve reliability and performance. However, several of these approaches are overly complex or resource-intensive, making them less suitable for practical implementation in distribution-level systems where simplicity and cost-effectiveness are critical [1.37]. Furthermore, few studies have thoroughly evaluated the actual benefits or effectiveness of the approaches in term of realistic deployment. There is also a lack of in-depth analysis regarding the supporting systems required for these schemes – such as the underlying communication networks, monitoring

infrastructure, or applications that facilitate protection coordination and system-wide integration.

Based on the above discussion, the objectives of this thesis are defined as follows:

- To address the challenges posed by the changing network behaviour resulting from high penetration of DERs, particularly those connected at the distribution level, which may compromise the performance of conventional protection methods.
- To develop a protection scheme specifically designed for modern grid-connected distribution networks with multiple infeed sources, which are becoming increasingly common due to the widespread integration of RE technologies.
- To conduct a comprehensive review and comparative analysis of communication technologies suitable for use within the protection scheme, with particularly focus on key technical aspects such as requirements of bandwidth, latency, and architecture.
- To ensure that the proposed protection scheme achieves a balance between technical effectiveness and cost-efficiency, and operational simplicity, making it not only robust but also practical and easy to implement in modern digital network environments.

1.2 Research contributions

This research has delivered a principal contribution to knowledge, which is to present and demonstrate a novel faulted section identification algorithm using solely current measurements, that can be applied to both protection and monitoring applications. It can be used over a wide area, could be deployed as either a centralised or distributed scheme in terms of the decision-making hardware, and is ideally suited for application to networks including significant penetrations of DERs. The main features of the system, which address many of the issues and shortcomings associated with related research, include the

fact that it can cope with widely variable short-circuit levels (that may be apparent in modern and future systems due to different energy sources/converter types and responses being connected to the system in an intermittent fashion), plus the facts that voltage measurements are not required, and that communications, while necessary, is not required continuously, only being required when the operation of the system is initiated. It can also operate with a very low-bandwidth communications system, and is insensitive to variations in latency, meaning that relatively inexpensive communications technologies would be suitable for an actual installation.

Another aspect of novelty and contribution lies in the fact that this approach utilises readily-available measurement data to perform analysis of the differences between pre- and during-fault currents from different measurement locations. Specifically, the scheme analyses current angle and magnitude changes, eliminating the need for complex and high-fidelity measurements, time synchronisation or costly communications equipment (simple transfer of logical codes is all that is required, as shown later). The robustness and adaptability of the proposed technique are comprehensively validated through a range of simulations encompassing a diverse range of fault and system configuration scenarios.

The research demonstrates the adaptability of the proposed method by showcasing its applicability for both protection and monitoring purposes. The system offers flexibility in implementation, allowing for either distributed (node-to-node) or centralised (node-to-centre) configurations. This enables authorities to select the most appropriate option according to their specific optimisation requirements.

There are several secondary contributions associated with this research:

- Detailed review, critique and comparison of various novel and proposed solutions for protection and/or monitoring of future electrical power systems, including analysis of pros and cons, and illustration of how the system proposed and demonstrated in this thesis addresses many of the identified issues and shortcomings associated with others' works.

- A review of associated communications technologies that can be used as part of the proposed scheme, focusing on several key aspects including bandwidth requirements for data exchange between measuring points, latency and the nature of the architecture – for example distributed processors, or a centralised master processor, with descriptions of the associated measurement locations and communications architectural requirements. This comparison of various communication options to determine their effectiveness for protection and faulted section identification also represents a useful contribution to knowledge.
- Evaluation of system performance and practical implementation through both non-real-time simulation using MATTLAB/Simulink software, and real-time simulation using Hardware-in-the-Loop (HIL) with a Real-Time Digital Simulator (RTDS) system, ensuring accurate and realistic testing conditions. This also completes initial work towards an actual hardware implementation of the system for faulted section identification and protection in the future.
- An analysis of the benefits and cost-effectiveness of the proposed protection scheme in the context of modern distribution networks, demonstrating its suitability for practical deployment and alignment with the operational needs of future digital power systems.
- Recognition and descriptions of future challenges and proposals for various areas of future work, which should assist other researchers in establishing areas for research.

1.3 Thesis structure

The structure of the remainder of this thesis is as follows.

Chapter 2 explores the historical development of electrical distribution networks. It outlines the transition from conventional systems to the integration of DERs and other low-carbon technologies. The chapter also

details protection schemes employed in traditional distribution systems, and outlines network behaviours (in terms of behaviour during both normal and fault conditions) compared to the past. This analysis serves as a foundation for the following chapters exploring the challenges these changes pose to traditional protection schemes. This chapter also includes the potential application of the scheme to monitoring and automation functions, e.g., FLISR application in future distribution network operations. Finally, it explores the communication technologies supported in distribution networks and the proposed faulted section identification scheme.

Chapter 3 outlines the challenges to conventional protection schemes arising from the evolving power network, as introduced in the previous chapter. It also forms the fundamental literature review component of the thesis, containing reviews of several potential solutions reported by other researchers, critically examining the proposals, their benefits, practical application and potential issues or gaps in their work. By identifying the contributions and limitations of other reported and relevant work, this chapter also justifies the choice and design of methods used in the proposed faulted section identification algorithm for protection and/or monitoring/FLISR applications.

Chapter 4 describes fully the principles of the proposed faulted section identification scheme, and shows how it utilises current-only angle/direction and magnitude measurements, comparing the transitions of the measurements from pre- to during-fault conditions, with relatively simple and cheap communications to transfer logical codes describing these transitions between measurement locations. The detail of the data transmission process between neighbouring measurement point is also described in this chapter.

Chapter 5 demonstrates and validates the developed scheme through case studies, simulation results, and performance verification. The chapter utilises a modelled system created in MATLAB/Simulink to demonstrate the reliability of the faulted section identification algorithm by simulating various fault and non-fault scenarios, and a wide variety of conditions.

Chapter 6 elaborates upon the scheme's performance as described in Chapter 5, but uses an implementation of the system in a Real-Time Digital Simulator (RTDS) with Hardware-in-the-Loop (HIL) testing, incorporating actual hardware and communications technology available at the University of Strathclyde. This approach effectively evaluates the practical efficiency and robustness of the protection protocol under realistic operating conditions and further demonstrates the scheme's operation in a more realistic experimental arrangement.

Finally, Chapter 7 completes the thesis by presenting the key conclusion drawn from this research, along with the economic implications and cost-benefit aspects of the proposed scheme. The final chapter also explores and discusses potential avenues for future work.

1.4 Publications

In the course of completing this PhD, the following publications have been produced:

1.4.1 Journal articles

A journal paper entitled "A Protection Scheme for DER-Rich Distribution Networks Using Current-Based Fault Section Identification" is currently in preparation and is expected to be submitted to the *International Journal of Electrical Power & Energy Systems* by August 2025.

1.4.2 Conference papers

1. **P. Rajakrom**, C. Booth and Q. Hong, "Analysis and Simulation of Current-Only Directional Protection Incorporating Simple Communications," *2022 57th International Universities Power Engineering Conference (UPEC)*, Istanbul, Turkey, 2022, pp. 1-6

2. **P. Rajakrom**, C. Booth, Q. Hong and A. Rajakrom, "Fault Location, Isolation, and Service Restoration Using Current-Only Directional Approach with Simple Low-Cost Communication," *2023 IEEE PES 15th Asia-Pacific and Energy Engineering Conference (APPEEC)*, Chiang Mai, Thailand, 2023, pp. 1-6
3. **P. Rajakrom**, C. D. Booth and Q. Hong, "Current-Only Directional Protection of Distribution Network Using Low-Cost Communication," *17th International Conference on Developments in Power System Protection (DPSP 2024)*, Manchester, UK, 2024, pp. 1-7

Chapter references

[1.1] Department of Energy Security and Net Zero, "Net Zero Government Initiative: UK roadmap to net zero government emissions". December 2023. Available: https://www.gov.uk/government/publications/net-zero-government-emissions-uk-roadmap

[1.2] R. Davies, "Solar and wind "will miss 2030 clean energy target without £48bn funding"," *The Guardian*, July 22, 2024. Available: https://www.theguardian.com/environment/article/2024/jul/22/solar-wind-uk-clean-energy-cornwall-insight

[1.3] National Statistics, Department of Trade and Industry (DTI), "UK Energy in Brief 2001," July 2001. Available: https://webarchive.nationalarchives.gov.uk/ukgwa/20030731215915mp_/http://www.dti.gov.uk:80/EPA/eib/ukeb072001.pdf

[1.4] 'Energy Trends March 2025'. Department for Energy Security & Net Zero, March 27, 2025. [Online]. Available: https://assets.publishing.service.gov.uk/media/67e4f5d855239fa04d412067/Energy_Trends_March_2025.pdf

[1.5] National Statistics, Department of Trade and Industry (DTI), "UK Energy in Brief 2002," December 2002. Available: https://webarchive.nationalarchives.gov.uk/ukgwa/20030731205557mp_/http://www.dti.gov.uk:80/energy/inform/energy_in_brief/ene_in_brief.pdf

[1.6] National Statistics, Department of Trade and Industry (DTI), "UK Energy in Brief 2003," July 2003. Available: https://webarchive.nationalarchives.gov.uk/ukgwa/20031221111216mp

_/http://www.dti.gov.uk/energy/inform/energy_in_brief/energyinbrief2003.pdf

[1.7] National Statistics, Department of Trade and Industry (DTI), "UK Energy in Brief 2004," July 2004. Available: https://webarchive.nationalarchives.gov.uk/ukgwa/20050303044710mp_/http://www3.dti.gov.uk/energy/inform/energy_in_brief/energyinbrief2004.pdf

[1.8] National Statistics, Department of Trade and Industry (DTI), "UK Energy in Brief 2005," July 2005. Available: https://webarchive.nationalarchives.gov.uk/ukgwa/20060715170216mp_/http://www.dti.gov.uk/files/file10738.pdf

[1.9] National Statistics, Department of Trade and Industry (DTI), "UK Energy in Brief 2006," July 2006. Available: https://webarchive.nationalarchives.gov.uk/ukgwa/20070507013054mp_/http://www.dti.gov.uk/files/file32387.pdf

[1.10] National Statistics, Department of Business, Enterprise, and Regulatory Reform (BERR), "UK Energy in Brief 2007," July 2007. Available: https://webarchive.nationalarchives.gov.uk/ukgwa/20080611001706mp_/http://www.berr.gov.uk/files/file39881.pdf

[1.11] National Statistics, Department of Business, Enterprise, and Regulatory Reform (BERR), "UK Energy in Brief 2008," July 2008. Available: https://webarchive.nationalarchives.gov.uk/ukgwa/20090203210041mp_/http://www.berr.gov.uk/files/file46983.pdf

[1.12] National Statistics, Department of Energy and Climate Change (DECC), "UK Energy in Brief 2009," July 2009. Available: https://webarchive.nationalarchives.gov.uk/ukgwa/20100104173135mp_/http://www.decc.gov.uk/media/viewfile.ashx?filepath=statistics/publications/ukenergyinbrief/1_20090728165537_e_@@_energyinbrief2009.pdf&filetype=4

[1.13] National Statistics, Department of Energy and Climate Change (DECC), "UK Energy in Brief 2010," July 2010. Available: https://webarchive.nationalarchives.gov.uk/ukgwa/20111205171829mp_/https://www.decc.gov.uk/assets/decc/Statistics/publications/brief/190-uk-energy-in-brief-2010.pdf

[1.14] National Statistics, Department of Energy and Climate Change (DECC), "UK Energy in Brief 2011," July 2011. Available: https://webarchive.nationalarchives.gov.uk/ukgwa/20111205171848mp_/https://www.decc.gov.uk/assets/decc/11/stats/publications/energy-in-brief/2286-uk-energy-in-brief-2011.pdf

[1.15] National Statistics, Department of Energy and Climate Change (DECC), "UK Energy in Brief 2012," July 2012. Available: https://www.gov.uk/government/statistics/uk-energy-in-brief-2012

[1.16] National Statistics, Department of Energy and Climate Change (DECC), "UK energy in Brief 2013," July 2013. Available: https://www.gov.uk/government/statistics/uk-energy-in-brief-2013

[1.17] National Statistics, Department of Energy and Climate Change (DECC), "UK Energy in Brief 2014," July 2014. Available: https://www.gov.uk/government/statistics/uk-energy-in-brief-2014

[1.18] National Statistics, Department of Energy and Climate Change (DECC), "UK Energy in Brief 2015," July 2015. Available: https://www.gov.uk/government/statistics/uk-energy-in-brief-2015

[1.19] National Statistics, Department Business, Energy and Industrial Strategy (BEIS), UK Energy in Brief 2016, July 2016. Available at: https://www.gov.uk/government/statistics/uk-energy-in-brief-2016

[1.20] National Statistics, Department Business, Energy and Industrial Strategy (BEIS), UK Energy in Brief 2017, July 2017. Available at: https://www.gov.uk/government/statistics/uk-energy-in-brief-2017

[1.21] National Statistics, Department Business, Energy and Industrial Strategy (BEIS), UK Energy in Brief 2018, July 2018. Available at: https://www.gov.uk/government/statistics/uk-energy-in-brief-2018

[1.22] National Statistics, Department Business, Energy and Industrial Strategy (BEIS), UK Energy in Brief 2019, July 2019. Available at: https://www.gov.uk/government/statistics/uk-energy-in-brief-2019

[1.23] National Statistics, Department Business, Energy and Industrial Strategy (BEIS), UK Energy in Brief 2020, July 2020. Available at: https://www.gov.uk/government/statistics/uk-energy-in-brief-2020

[1.24] National Statistics, Department Business, Energy and Industrial Strategy (BEIS), UK Energy in Brief 2021, July 2021. Available at: https://www.gov.uk/government/statistics/uk-energy-in-brief-2021

[1.25] National Statistics, Department Business, Energy and Industrial Strategy (BEIS), UK Energy in Brief 2022, August 2022. Available at: https://www.gov.uk/government/ statistics/uk-energy-in-brief-2022

[1.26] National Statistics, Department Business, Energy and Industrial Strategy (BEIS), UK Energy in Brief 2023, September 2023. Available at: https://www.gov.uk/government/ statistics/uk-energy-in-brief-2023

[1.27] National Statistics, Department Business, Energy and Industrial Strategy (BEIS), UK Energy in Brief 2024, September 2024. Available at: https://www.gov.uk/government/ statistics/uk-energy-in-brief-2024

[1.28] HM Government Department of Business, Energy & Industrial Strategy, "British Energy Security Strategy," April 2022. Available: https://assets.publishing.service.gov.uk/media/626112c0e90e07168e3fdba3/british-energy-security-strategy-web-accessible.pdf

[1.29] H. Ritchie and P. Rosado, 'Fossil fuels', *Our World in Data*, October 2017, [Online]. Available: https://ourworldindata.org/fossil-fuels

[1.30] H. Ritchie, M. Roser, and P. Rosado, "Renewable Energy," *Our World in Data*, December 2020. Available: https://ourworldindata.org/renewable-energy

[1.31] The International Renewable Energy Agency (IRENA), "Renewable Capacity Statistics," March 2020. Available: https://www.irena.org/-/media/Files/IRENA/Agency/%20Publication/2020/Mar/IRENA_RE_Capacity_Statistics_2020.pdf

[1.32] O. US EPA, 'Distributed Generation of Electricity and its Environmental Impacts'. [Online]. Available: https://www.epa.gov/energy/distributed-generation-electricity-and-its-environmental-impacts

[1.33] I. Waseem, M. Pipattanasomporn, and S. Rahman, "Reliability benefits of distributed generation as a backup source," in *2009 IEEE Power & Energy Society General Meeting*, Calgary, AB, Canada, July 2009, pp. 1–8.

[1.34] 'Power system digitalisation is crucial for clean energy transitions and security in developing markets, but investment is lagging', *International Energy Agency (IEA)*, June 06, 2023. [Online]. Available: https://www.iea.org/news/power-system-digitalisation-is-crucial-for-clean-energy-transitions-and-security-in-developing-markets-but-investment-is-lagging

[1.35] C. Pritchard and F. Steinhauser, 'The Digital Transformation of Protection, Automation, and Control System', PAC World. September 2024. [Online]. Available: https://www.pacw.org/the-digital-transformation-of-protection-automation-and-control-system

[1.36] D. A. Kisinga, P. Makolo, and P. Trodden, "A Neural Network-based Online Estimation of Stochastic Inertia in a Power System," in *2022 IEEE PES/IAS PowerAfrica*, Kigali, Rwanda, August 2022, pp. 1–5.

[1.37] L. Ding, F. Li, Z. Zhang, and J. Hu, 'Multi-terminal Optical Fiber Tuning Method for Distribution Network Relay Protection Based on Reinforcement Learning Algorithm', presented at the 2023 Asia-Pacific Conference on Image Processing, Electronics and Computers (IPEC), IEEE Computer Society, April 2023, pp. 182–186.

Chapter 2

Evolution of Electrical Power Distribution Systems

2.1 Chapter overview

This chapter presents an overview of the evolution of electrical power distribution networks, with a particular emphasis on the transition from conventional systems to modern and future systems incorporating DERs, which can include both generation and storage of electricity. Various forms of DG are described, along with their potential impacts on the behaviours of traditional distribution networks. Furthermore, with the advancement of various technologies, several notable applications relevant to modern distribution systems are also described.

The chapter also contains an explanation of the fundamental principles underlying conventional protection schemes, highlighting characteristics that may be challenged by the increasing complexity and evolution of electricity distribution networks. As the scheme developed in this research employs communications, this chapter also contains a review of communication systems and technologies that are used within electrical power systems, with reference to those technology options that may be most appropriate for the scheme if it were to be further developed into a practical application.

2.2 Overview of electrical power networks

In 1881, the world's first public electricity supply for street lighting commenced operation in Britain, marking the beginning of the country's electrification journey. A significant milestone followed in 1935, with the creation of the original 132 kV national grid – the first integrated transmission network of its kind globally [2.1]. This pioneering infrastructure was managed by the Central Electricity Generating Board (CEGB), which oversaw the centralised planning and operation of the network until the electricity sector underwent major privatisation reforms in the 1990s. There reforms led to the unbundling of generation, transmission, and distribution activities, fundamentally transforming the structure of the UK electricity market [2.2].

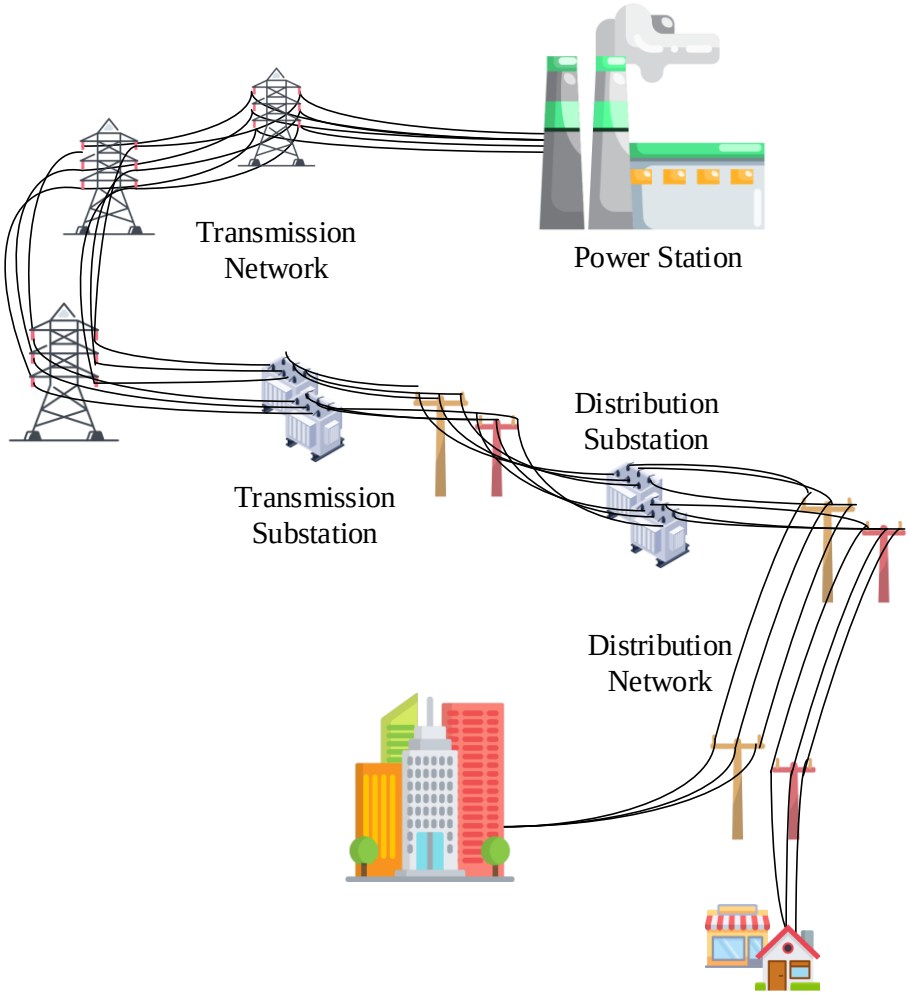

Figure 2.1: Traditional electricity network adapted from [2.3]

The structure of the traditional electricity network in the UK is illustrated in Figure 2.1 and Figure 2.2. Historically, the UK electrical system was characterised by centralised generation and a top-down, hierarchical transmission and distribution network. Electricity production was dominated by large-scale thermal power stations, primarily fuelled by coal and, to a lesser extent, oil and gas. These facilities were typically situated near fuel sources and water bodies to ensure logistical efficiency and effective cooling. At its peak, coal-fired power plants accounted for nearly 80% of total electricity generation, while the remaining 20% was derived from a mix of other sources, including oil, natural gas, nuclear, hydro, wind, and solar energy [2.4].

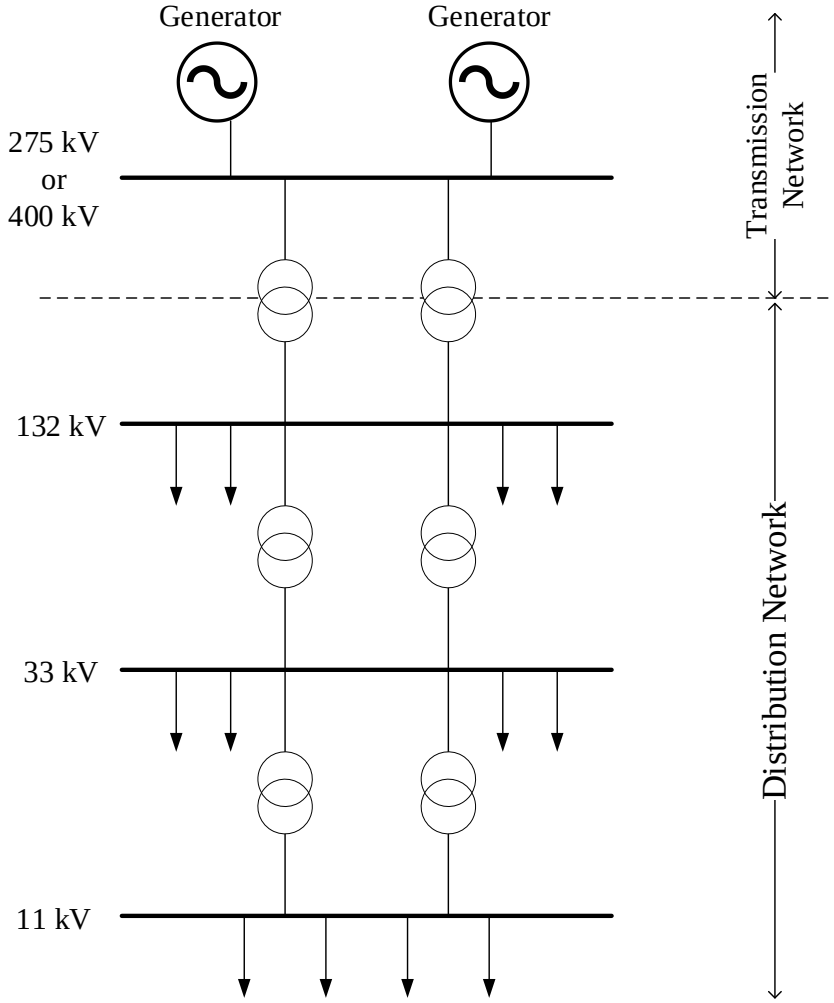

Figure 2.2: Traditional UK electricity transmission and distribution network layout

Due to the often-remote locations (typically near coal fields and often in coastal areas or near rivers for cooling) these power stations, electricity had to be transmitted over long distances to reach end-users. This necessitated the development of a high-voltage transmission system, initially operating at 132 kV and later upgraded to 275 kV and 400 kV to accommodate growing demand and to ensure that thermal ratings and losses (driven largely by current levels) were optimised. The transmission grid was designed to transport bulk power efficiently to regional substations, where the voltage would be stepped down for distribution. At the distribution level, power flow was conventionally unidirectional – from the transmission network to the consumers – and the system was designed as a passive infrastructure, with limited flexibility or local/distributed generation integration.

2.3 Decarbonisation and increased penetration of renewable energy and DERs

By the early 2000s, the UK began integrating RES into its energy system. However, their uptake was not yet widespread due to the continued dominance of a centralised generation and associated network structure. A significant turning point occurred in 2008, when the UK became the first country in the world to enact a legally-binding carbon reduction framework through the Climate Change Act [2.5]. The Act initially aimed to reduce greenhouse gas emissions by 80% by 2050 (a target that was later revised in 2019 to a more ambitious goal of achieving net zero carbon emissions by the 2050 [2.6]).

According to recent statistics, in 2024, renewable generation in the UK produced 144.7 TWh of electricity, accounting for 50.8% of the total electricity generation. This marks the first time that more than half of the nation's electricity supply has originated from renewable sources [2.7]. The percentage share and generation capacity of each type of RES in 2024 are illustrated in

Figure 2.3. Furthermore, the UK reached a significant milestone in the same year with the decommissioning of its last remaining coal-fired power station [2.8].

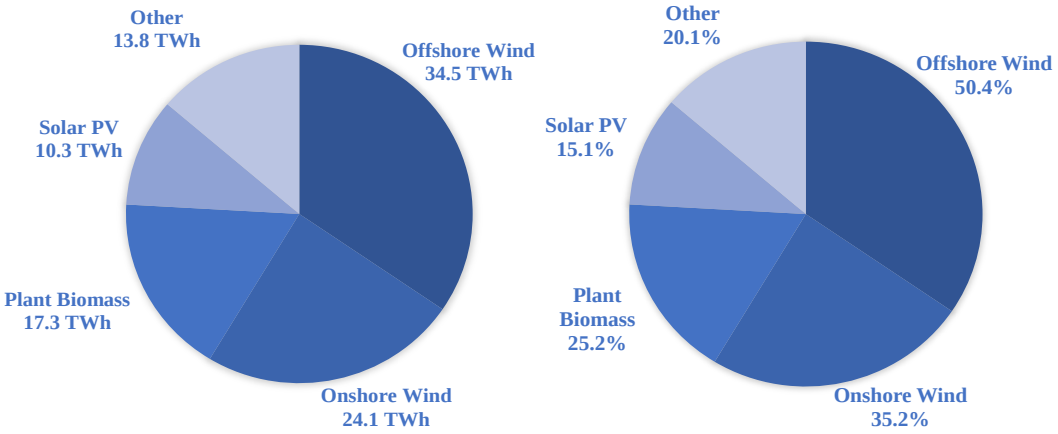

(a) (b)

Figure 2.3: Renewable generation in the UK in 2024 (a) by TWh (b) by percentage [2.7]

As the author is Thai, some reflections on the situation in Thailand are included. Although the outcomes are not yet as evident as those observed in the UK, government policies – particularly following Thailand's participation in the COP26 summit [2.9] – Thailand has demonstrated a growing commitment to clean energy. The Thai government has outlined a national energy policy aimed at increasing the proportion of clean energy. The target has been set at 51% by the year 2037, up from the current level of 25.6% [2.10].

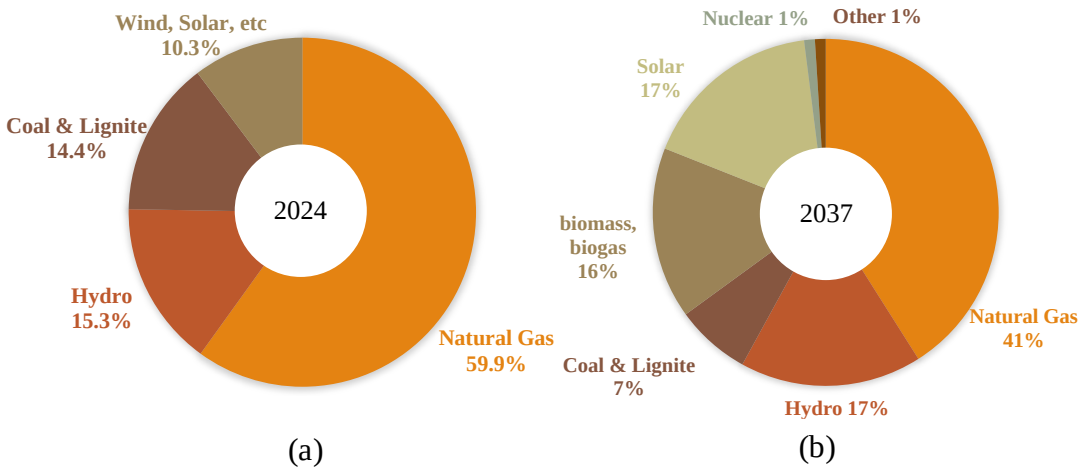

Figure 2.4: Electricity generation in Thailand (a) in 2024 (b) expected in 2037 [2.10]

The enactment of this legislation has significantly elevated the role of RES, positioning them as essential components within the UK's (as well as Thailand's) decarbonisation strategy. As a result, the deployment of DERs – particularly in the form of DG – has expanded steadily in the years that have followed. This growing integration of DERs, especially at the distribution level, has fundamentally reshaped the electricity network, shifting it from traditionally passive infrastructure to a more dynamic and active system, as depicted in Figure 2.5.

DERs encompasses a wide spectrum of decentralised technologies, including DG and energy storage systems, all typically situated relatively close to the point of consumption. Among these, DG, often renewable in nature, has exerted the most significant influence on conventional power system, primarily due to its decentralised and often intermittent nature. Therefore, this thesis focuses specifically on the concept of DG, given its prominent role and substantial impact on the transformation of traditional power systems.

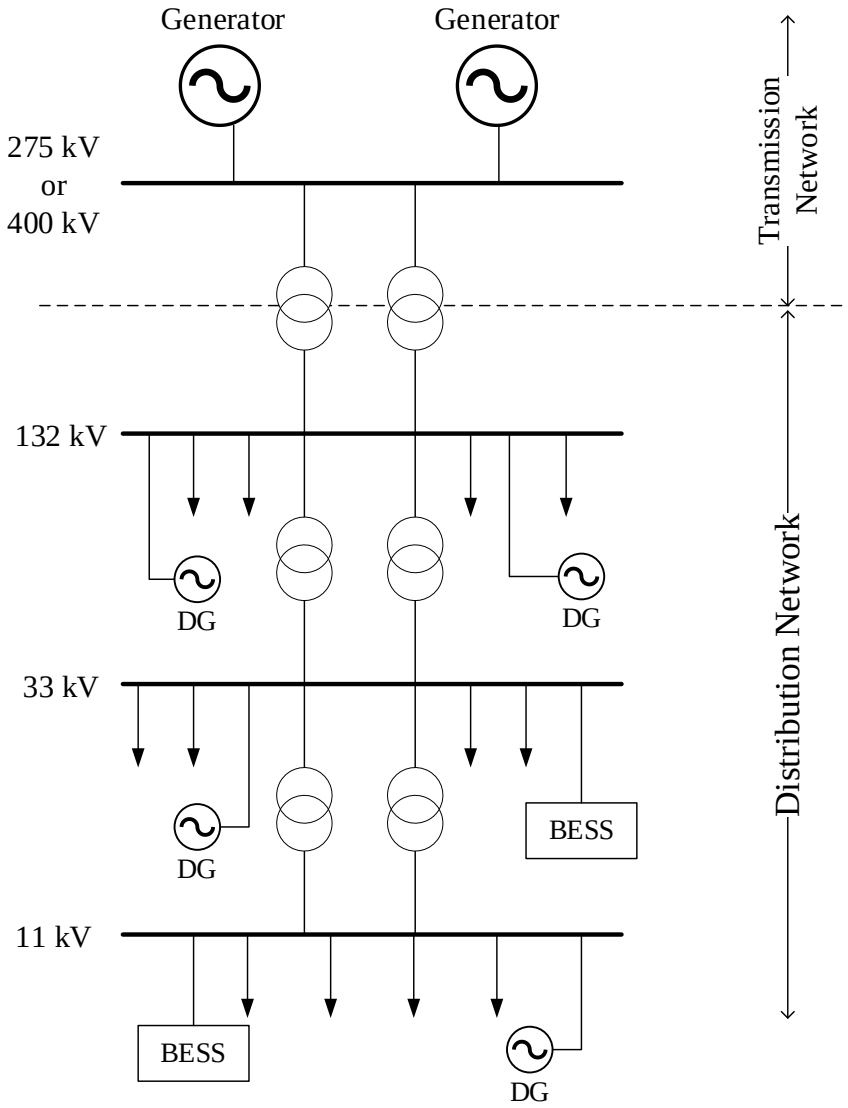

Figure 2.5: UK's electricity network with DER integration

2.3.1 Distributed generation (DG)

DG refers to the generation of electrical energy from relatively small-scale power sources located close to the point of consumption or integrated within distribution network, thus eliminating or significantly reducing the reliance on long-distance transmission [2.11]. In generally, DG can comprise both renewable and non-renewable energy sources, although renewables are clearly the most popular and will grow in future.

One common classification distinguishes between synchronised and non-synchronised DG systems [2.12].

- **Synchronised DG**: typically includes synchronous generators such as diesel generator or small-scale hydroelectric turbines driving synchronous machines. Some non-synchronous sources that are interfaced via inverter-based systems capable of grid-forming or grid-supporting functionalities (sometimes termed as virtual synchronous machines as they can provide inertial and frequency-control/droop functions) could arguably belong lie in this category.
- **Non-synchronised DG**: typically includes non-synchronous generation technologies such as wind or solar, that are connected via inverter interfaces that are grid-following in nature and therefore do not behave as "virtual" synchronous machines.

DG is generally divided into micro, small, and medium scales based upon their output capacities [2.12]. Micro DG refers to systems with a capacity of less than 5 kW, while small DG includes units ranging from 5 kW to 5 MW. Finally, medium DG generally encompasses system with capacities of between 5 MW and 50 MW.

2.3.2 Impact of DGs on power systems

The increasing penetration of DG has significantly altered the characteristic of modern power system in the following ways:

- **Reduction in system inertia:** the widespread integration of DG – especially inverter-based resources such as solar PV and wind energy systems – can result in a substantial reduction in system inertia, as this is coupled with the decommissioning and reduction of directly-connected large synchronous generators. Traditional synchronous generators inherently provide rotational inertia. However, DG units, particularly those interfaced via power electronic inverters, contribute negligible or no inertia [2.13]. This can increase the frequency volatility of systems

and increase the risk of significant (and faster) frequency excursions following loss of infeed/load events (which are often initiated by faults and protection actions).

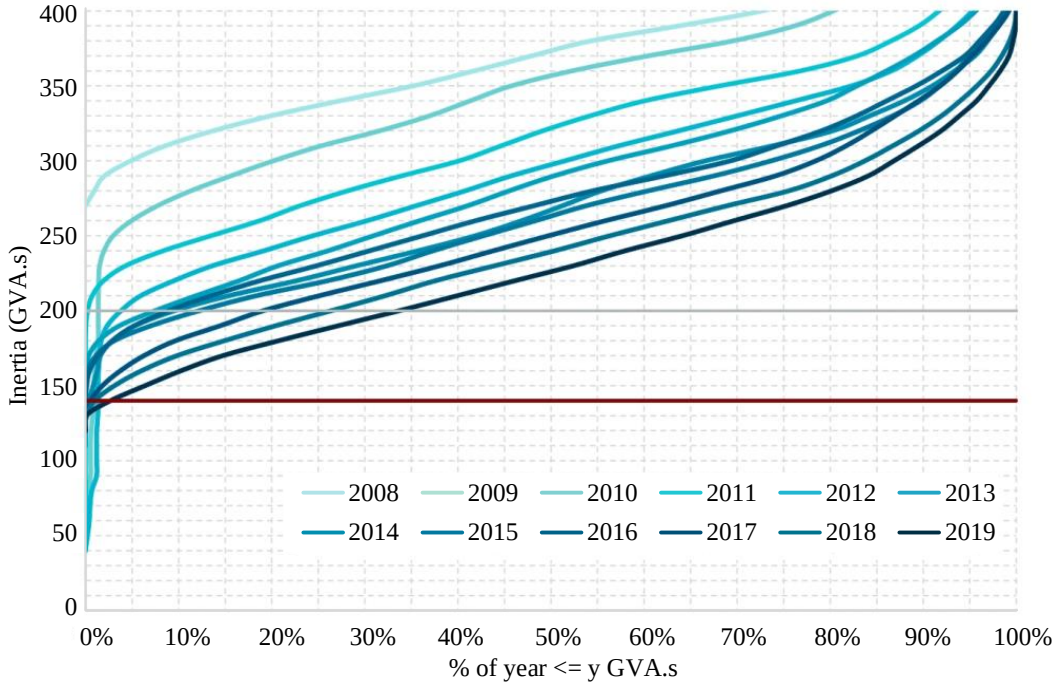

Figure 2.6: Declining inertia levels in Great Britain from 2008 – 2019 adapted from [2.13]

- **Transition of power flow dynamics:** the traditional model of power systems was characterised by unidirectional power flow – from centralised generation through transmission and distribution networks to end-users. However, with the increasing deployment of DG units, especially at the distribution level, this framework has shifted. Power may now flow in both directions, a phenomenon referred to as bidirectional power flow, depending on real-time generation and demand across the network [2.14]. This also changes fault behaviour, as described in the next point.
- **Change in short-circuit levels:** inverter-based generators inherently limit the amount of short-circuit current they can contribute, typically to protect the power electronics components within the inverter from

damage. As a result, the short-circuit level, particularly in transmission systems, may decrease considerably, and this can be more pronounced in some parts of the country [2.15], as depicted in Figure 2.7. However, in distribution systems, the short-circuit level may either increase or decrease, and will certainly vary in some way due to the rising number of DG installations [2.16] – [2.17].

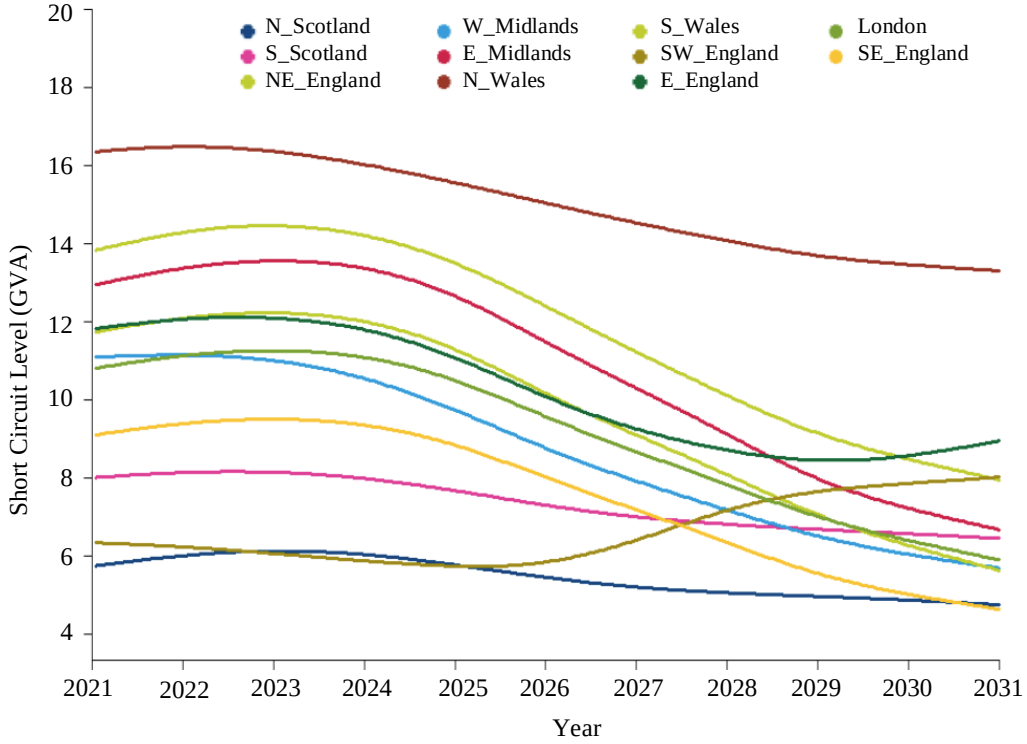

Figure 2.7: Mean short circuit level in different areas in the UK over a range of years, showing a general decline [2.15]

2.3.3 Benefits and challenges associated with DERs

DERs, and DG specifically, provide numerous benefits to distribution networks, providing technical, economic, and environmental benefits (when compared with conventional centralised, often fossil-fuelled power generation). There are, however, a number of challenges associated with incorporating DERS and DG into networks. These are discussed in the following subsections.

2.3.3.1 Benefits of incorporating DG within power distribution networks

The key benefits can be details as follows:

- **Reduction in energy losses:** by generating electricity close to the point of consumption, DG minimises the distance electricity travels through transmission and distribution networks, thus considerably decreasing the energy losses typically experienced in centralised generation systems with power being transmitted over long distances [2.11].
- **Potentially enhanced network reliability:** localised generation enables the distribution system to maintain operation or recover quickly form disturbance or outages, thus ensuring uninterrupted electricity supply during peak demand periods or emergency scenarios – although this depends on having the appropriate control and protection technology, as well as rules and regulations that permit this to happen [2.18].
- **Acceleration of uptake and increased proportion of renewable energy produced:** DG facilitates greater integration of RES directly into local distribution systems. This decentralised approach not only reduces dependency on fossil fuels but also contributes to lowering greenhouse gas emissions, aligning with global environment and sustainability goals [2.17].
- **Increased system flexibility and scalability and cost-effective energy solutions:** the modular nature of DG allows for incremental expansion, enhancing the flexibility and scalability of networks. This adaptability enables utilities to respond rapidly and economically to changing electricity demands and evolving market conditions, without substantial disruption or financial burden [2.18] – [2.19].

Although DG offers numerous advantages, it is also accompanied by a range of technical challenges. These challenges can be broadly categorised into three core areas as outlined in the following subsections.

2.3.3.2 Challenges – control and system stability

Power stability in distribution systems with high DG penetration has become an increasing concern due to the dynamic and variable nature of generation sources. In particular, low inertia and intermittent generation profiles have made voltage and frequency less stable and more sensitive to system disturbances. The resulting instability can manifest in both short-term and sustained operating issues.

When sudden load changes or generation fluctuation occur, the system experiences rapid frequency excursions that are more difficult to control compared to traditional networks. One of the key indicators of this instability is the Rate of Change of Frequency (RoCoF). In systems with low inertia, RoCoF becomes significantly higher, meaning that frequency can deviate beyond acceptable limits within fractions of a second [2.20]. If RoCoF exceeds the threshold configured in DG or inverter control and protection systems (which are defined by standards in the UK [2.21]), it may trigger automatic disconnection to protect the equipment, further compounding the instability as the mismatch between supply and demand will be increased, as well as reducing a source of voltage support from the network [2.16]. Such events increase the likelihood of loss of synchronisation, unintentional islanding, and degraded frequency regulation. These issues can cause cascading effects in weak grids [2.13], leading to supply interruptions, potential system-wide blackouts, and generally reduced system stability [2.22].

Intermittency in generation also introduces substantial voltage control challenges. Rapid drops in power output can lead to voltage flicker, while the opposite condition – overgeneration during periods of low demand – can cause voltage rise. This will also affect systems frequency.

2.3.3.3 Challenges – protection

In traditional radial system configurations, protection devices are designed based on the assumption of unidirectional power flow and predictable fault current levels. However, with the inclusion of DG, both of these assumptions become invalid. Firstly, short-circuit level becomes increasingly variable [2.14]. Secondly, bidirectional power flow can disrupt traditional coordination among protective devices, which are typically arranged based on the assumption of downstream fault current flow [2.13]. These results are increased risk of protection problems. Furthermore, the fast dynamic introduced by weak infeed can lead to frequent relay operations in response to minor transient or fluctuations. This increases the stress on protective equipment, accelerating its wear and potentially reducing long-term system stability [2.16].

Detailed discussion on protection-related challenges, including fault detection limitations, coordination issues, and possible solution strategies, are presented in Chapter 3.

2.3.3.4 Challenges – system design and operation

The shift from passive to active distribution networks, driven by the proliferation of DG, also necessitates a fundamental rethinking of system design and operation. Distribution network with high amount of DGs complicates planning, voltage control, thermal loading, and contingency management [2.23]. For example, voltage rise, especially at locations close to DG sources, is now common. The conventional placement of voltage regulators or capacitor banks may no longer be sufficient or even appropriate [2.24]. Additionally, hosting capacity – the maximum amount of DG that a feeder can accommodate without violating voltage, thermal, or protection constraints – becomes a key design constraint. This often necessitates the use of detailed time-series simulations, probabilistic modelling, and advanced planning tools, which may not be available to all utilities, particularly in developing regions. Furthermore, it can require expensive upgraded implementations such as network automation,

advanced metering, and local energy storage [2.25]. Some of automation applications are described later in this chapter. In many cases, the economic burden of these enhancements is significant, and without proper policy or incentive structures, utilities may be reluctant to approve further DG interconnection. Thus, technical challenges at the design level have direct regulatory, financial, and operational implications that cannot be overlooked.

2.4 Overview of automation and related applications for systems incorporating DERs

With the rapid advancement of technology, utility providers are increasingly seeking automated systems to reduce operational expenditures and mitigate potential risked to personnel. Traditional distribution networks, which has historically depended on manual operation and reactive maintenance, are now undergoing a transformative shift driven by digital innovation. The integration of smart sensors, advanced metering infrastructure sophisticated communication platforms, and intelligent control systems in paving the way towards more efficient, reliable, and resilient future distribution networks. Designing and operating microgrids effectively requires balancing multiple considerations – technical feasibility, economic viability, and environment impact – all of which often present conflicting objective [2.26]. Automation not only accelerates fault detection and restoration processes, but also supports the integration of DERs, thereby enhancing grid flexibility and resilience. These capabilities are becoming increasingly essential in addressing rising energy demands, enabling the adoption of renewable energy, and ensuring the long-term sustainability of power system.

This section explores examples of automation applications that play a key role in enhancing the performance and intelligence of future distribution networks.

2.4.1 Distribution management systems (DMS)

DMS is typically a platform designed to enable real-time supervision, analysis, and control of modern distribution networks, particularly as these systems increasingly accommodate DERs [2.27]. The DMS operates by collecting and analysing data from diverse sources, including Supervisory Control and Data Acquisition (SCADA) systems, Advanced Metering Infrastructure (AMI), remote terminal units (RTUs), and various smart sensors deployment across the network [2.28]. This continuous stream of data, integrated from a variety of sources, enables DMS controllers to monitor voltage levels, power flows, and system status in real time, associated which high-speed communication networks, allowing for fast and accurate decision-making, thereby providing the situational awareness required for intelligent and automated control actions.

The fundamental objective of the DMS controller is to support intelligent grid operations through a suite of functions, such as load flow analysis, automatic voltage regulation (e.g. Volt/VAR optimisation), load forecasting, fault location and isolation, and feeder reconfiguration [2.29]. These functions are essential not only for maintaining the operational balance of the grid but also for maximising system reliability and minimising losses [2.28].

2.4.2 Fault location, isolation, and service restoration (FLISR)

FLISR is an emerging term, and could be viewed as a component of a DMS system. It is very relevant to this these as the scheme developed could be part of an FLISR scheme. It is an increasingly prevalent application in modern distribution networks, gaining significant traction in numerous countries, including the UK and Thailand [2.30] – [2.31]. This application is particularly well-suited to distribution systems incorporating DERs, as it facilitates the automatic restoration of power following disturbance within the network.

FLISR addresses both temporary and permanent faults through a structured sequence: identifying the fault location and isolating the affected networks segments, then restoring power service to unaffected areas [2.32]. This sequential process aims to maximise the number of customers restored in the shortest possible time, thereby minimising the scale of outage and improve key reliability indices such as Customer Interruptions (CI) and Customer Minutes Lost (CML) associated with such faults [2.33] – [2.34].

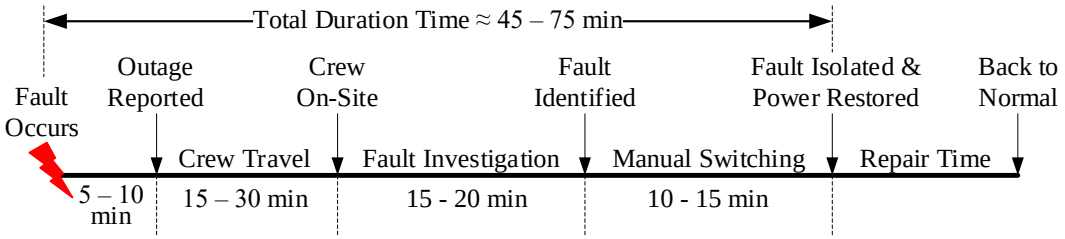

Time for occurrence of fault for current distribution network without FLISR

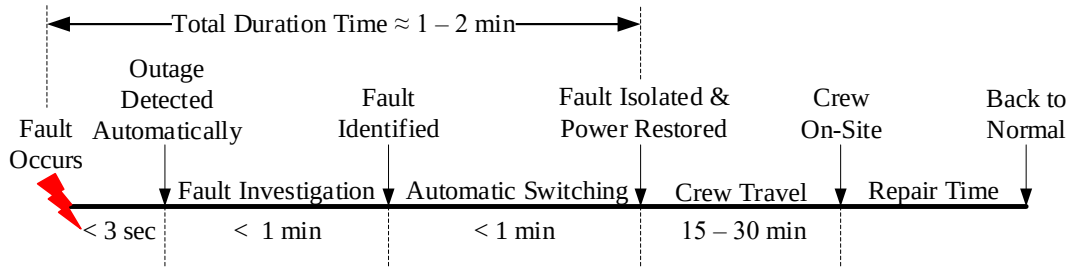

Time for occurrence of fault for current distribution network with FLISR

Figure 2.8: Example of outage time reduction using FLISR application adapted from [2.33]

FLISR can be implemented through various architectures, depending on the existing system implementation and available sensing infrastructure. A number of architecture options are is outlined in the following subsections.

2.4.2.1 Centralised FLISR

In this configuration, FLISR functionalities are managed through DMS or SCADA, with measurements and commands being exchanged between a central and many distributed measurement locations and control devices (e.g. remotely-controllable switchgear). The DMS coordinates fault detection,

isolation, and restoration actions based on real-time data collected from the network. This allows for system-wide operation and optimisation of responses to events, but relies heavily on reliable communication infrastructure and data integration across multiple substation and devices, which often comes with a significant cost [2.29], [2.33].

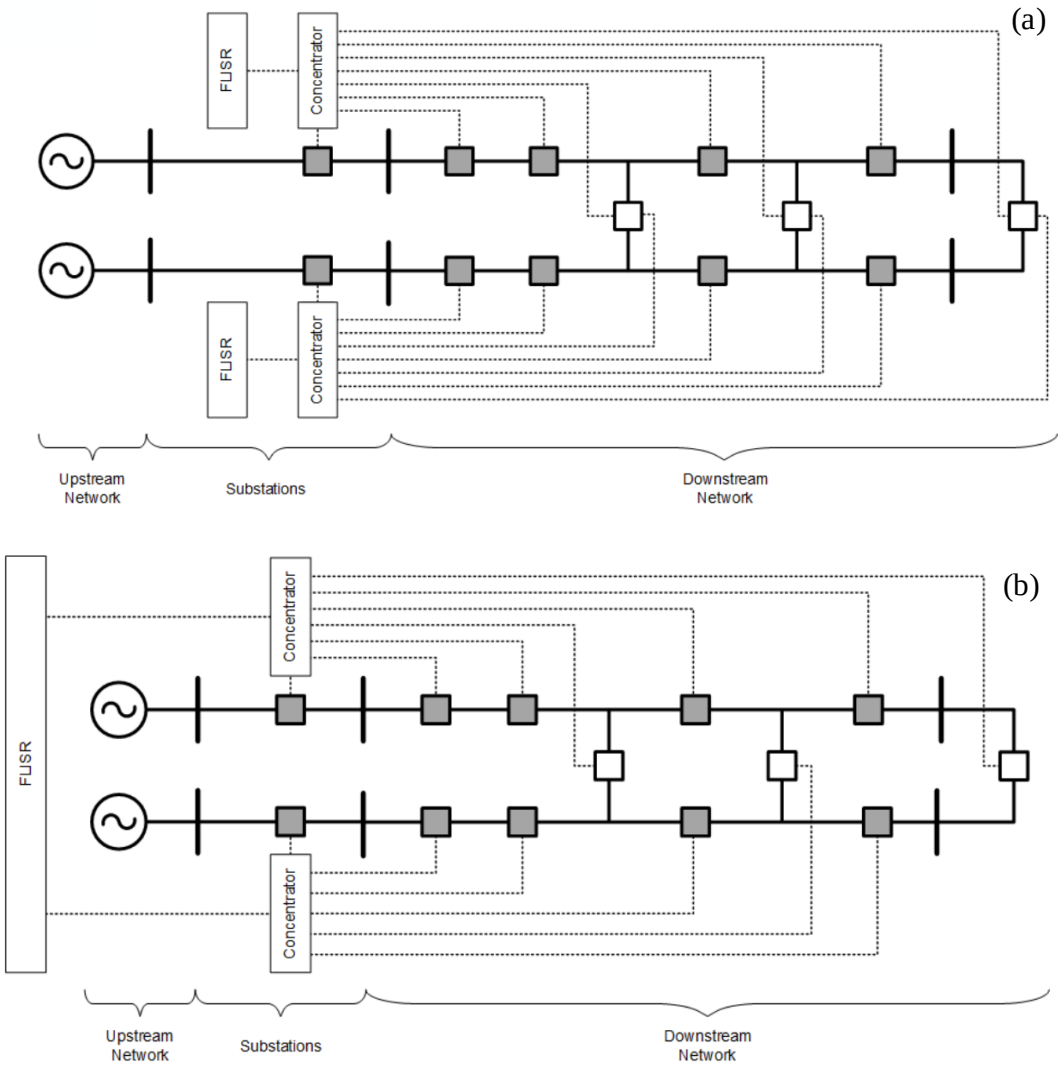

Figure 2.9: FLISR architecture: (a) Distributed and (b) Centralised [2.32]

2.4.2.2 Distributed FLISR

Autonomous field devices – such as IEDs, reclosers, and sectionalising switches – carry out FLISR actions independently. These devices use local measurements and predefined logic associated with peer-to-peer

communication to identify and isolate faults and reconfigure the network without central or regional oversight. However, this requires controllers at each switch location, instead of solely sensors [2.32] – [2.33].

In practice, FLISR play a critical role in the realisation of self-healing grid strategies, wherein the network autonomously reconfigures itself in response to faults without the need for manual intervention. This capability not only accelerates service restoration but also reduces the operational burden on human operators, thus prompting more streamlined and efficient management of large-scale distribution networks.

2.5 Protection schemes

Electrical faults and disturbances predominantly arise from short-circuit events, which in turn result from a wide range of issues. These include insulation ageing, adverse weather conditions such as wind, rain, snow, and ice, as well as external objects like trees or animals. Additionally, equipment malfunctions that lead to overvoltage, along with human error, contribute to the occurrence of faults. However, these causes are inherently unpredictable and thus cannot be prevented with certainly.

Faults can generally be categorised into two types: balanced faults, which are typically three-phase (3-PH) faults, and unbalanced faults. Unbalanced faults include single-phase-to-earth (P-E) faults, phase-to-phase (P-P) faults, and double-phase-to-earth (P-P-E) faults. The likelihood of each fault type occurring varies. According to [2.35], the most common fault is P-E, accounting for approximately 85% of all occurrence, followed by P-P (8%), P-P-E (5%), and, 3-PH, with only 2% of all faults being of this type.

These electrical faults and disturbances can result in significant thermal stress, fires, explosions, and mechanical damage, posing severe risks to power equipment, assets, and human safety. Moreover, they can often severely impact power system stability and efficiency, often resulting in power outages. Such events may lead to broader cascading consequences. Faults and sometimes the

incorrect operation of power system protection has often been a root or major contributory cause to the majority of major blackouts experienced [2.36].

The extent of damage can be mitigated if disturbances are detected promptly and effectively. Protection systems are implemented to reduce the impact of faults, especially given their unpredictable nature. The principal function of such systems is to isolate the affected equipment or faulty feeder section as swiftly as possible, minimising disruption to the remainder of the system. The accuracy and efficiency of a protection system rely on the coordination of the following core components [2.37].

- **Measurement devices:** these include voltage transformers (VT) and current transformers (CT), which measure voltage and current levels, respectively, reducing them to analogue values that can then typically be input directly to devices such as protection relays or merging units.
- **Relay:** acting as the "brain" of the protection system, the relay processes the data received from the measurement devices in order to detect the presence of faults or disturbances and make decisions on whether to take any action – they may also communicate with other measurement devices or relays in order to make the decisions.
- **Circuit breaker (CB):** CBs are switches that are capable of interrupting fault currents (as well as carrying out routine switching for reclosing or reconfiguration. Circuit breakers are responsible for physically isolating the faulted equipment from the network and reconnecting it once the fault has been cleared. In protection systems, it operates upon receiving commands from relay(s), which could be local or remote.

In power system protection, schemes are generally classified into unit or non-unit protection, depending on the principle of operation and effectively whether their zones of protection are clearly and unambiguously defined (unit) or not (non-unit). Typically, both systems are used throughout the system. While unit

is attractive, it has no inherent backup, so non-unit schemes are required almost everywhere.

Unit protection schemes are designed to protect a specific and clearly defined section of the power system, such as generator, transformer, or a line (or even section of line). They operate based on the principle of comparing the current (and sometime voltage) at the boundaries of the protected zone. If a discrepancy is detected (typically when the vector sum of the compared currents from a phase do not add to zero, or close to zero), the protection scheme will trigger. These system relay on measurements devices at both ends of the equipment or line, or from multiple measurements in multi-terminal circuits or for busbar protection applications. Unit protection schemes are highly selective and fast-acting, minimising the risk of affecting adjacent system components.

Non-unit protection schemes, on the other hand, do not confine their operation to a clearly defined zone (no boundaries). Instead, they typically protect larger areas of the system and determine the presence of faults based on measurements taken at a single location. These schemes may operate for faults occurring outside the immediate zone or as "backup" of the protected equipment, and hence, discrimination with other protection schemes is crucial. Time grading and coordination with downstream protection devices are typically employed to ensure selectively and avoid unnecessary disconnections, whereby the relay operates fastest for faults that are closer to the relay's location (directional capability can also be embedded), and progressively slower for faults further away (to operate in backup zone as other protection systems should clear the fault before the backup time delay expires).

Note that in the diagrams included in this section, only relays are shown. Circuit breakers would normally be located very close to the relays shown, along with measurement transformers, but for simplicity and to aid clarity, they are omitted.

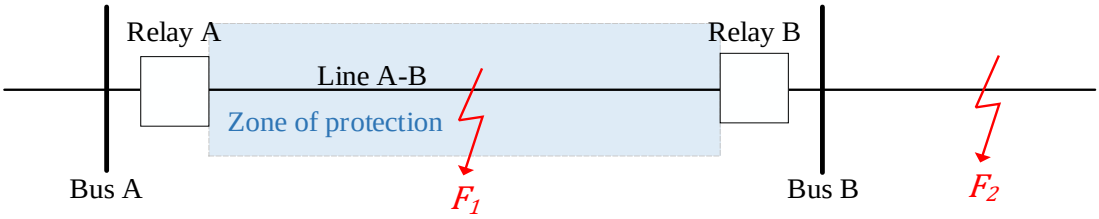

Figure 2.10: Unit protection system showing zone of protection

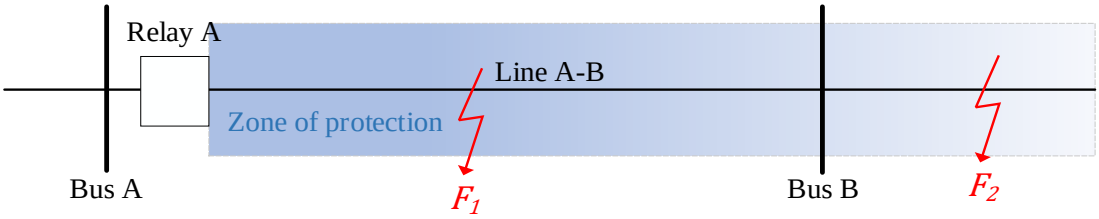

Figure 2.11: Non-unit protection system – zone of protection not accurately defined

A variety of protection schemes widely used in power systems generally are outlined in the following section. The majority of distribution systems are protected using relatively simple overcurrent protection, but in some cases distance and differential are used for network protection, so a brief overview of these types of protection is also included.

2.5.1 Differential protection

Differential protection is one of the most precise and widely applied unit protection schemes, operates based on the continuous comparison of measurements (which are monitored by CTs installed at the boundaries of the protected equipment) – typically current – at both ends of the protected zone (in a line protection application described here and in the figure). This method can be implemented as a single-relay scheme, as shown in Figure 2.12, when applied to the protection of single items of plant (e.g. busbar, transformer, generator) or short lines. However, for the protection of longer lines, a differential scheme employing dual relays may also be used. In such configurations, a communication like is established between the relays at both

ends to ensure coordinated and synchronised operation, as depicted in Figure 2.13.

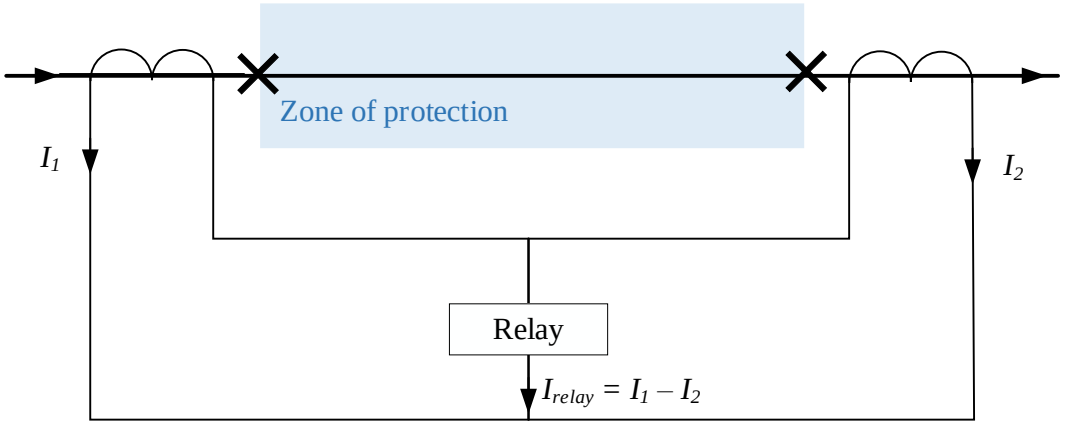

Figure 2.12: Single-relay current differential protection scheme

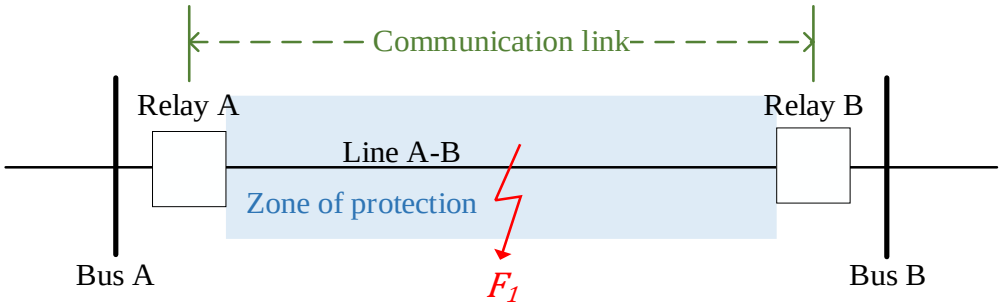

Figure 2.13: Dual relay current differential protection scheme

The operation of both schemes is shown in Figure 2.12 and Figure 2.13. They are identical conceptually, in that they compare currents measured from two or more locations to establish whether there is a difference between the currents, that may be indicative of a fault condition. Single relay schemes are typically applied to local equipment such as busbars and transformers, with the interconnections from the CTs made directly to the relay, while dual relay schemes would be used, with communications, between locations for the protection of interconnecting lines.

Under normal operating conditions, the magnitude and phase of I_1 and I_2 are equal, thus I_{relay} is zero. In external fault conditions, I_1 and I_2 will be much larger than normal, but still equal in magnitude and phase. However, if an

internal fault occurs within the protected zone, a difference (or "differential) arises between I_1 and I_2, which lead to I_{relay} is not equal to zero. That means the fault is detected by the relay, which then initiates a trip signal to the CBs, isolating the faulted section. In practical applications, a restraint or bias is often included in the relay algorithm to avoid false tripping during CT saturation or through-fault conditions.

The main advantages of differential protection include its high sensitivity, fast operating time, and selectivity, as it only responds to faults within the defined protection zone. However, it requires accurate matching and proper coordination of CTs and may involve more complex wiring and configuration. It also does not inherently provide backup, and is therefore typically deployed with a non-unit scheme also protecting the same items of equipment.

2.5.2 Overcurrent protection

An overcurrent protection scheme, which is a non-unit protection scheme, is typically based on measurement of current magnitudes only. It operates by detecting current levels that exceed a predefined threshold (or "pickup"), which typically indicates the presence of a fault such as a short-circuit or an undesirable overload condition.

Overcurrent relays may operate with varying time delays depending on the magnitude of fault current. If the fault occurs at a progressively greater distance from the relay location, the relay will normally respond progressively more slowly. This delayed response allows time for other relays that are located closer to the fault to operate first and isolate the faulted section more rapidly. However, if the primary relay nearest to the fault fails to operate and the fault persists, the more distant overcurrent relay can still respond and trip the circuit. In the way, it acts as a "backup" to the primary relay. For example, as illustrated in Figure 2.14, if a fault F_1 occurs near relay A, relay A will operate quickly and relay B should not operate (as long as there is no fault current infeed from beyond relay B). Conversely, if a fault F_2 occurs closer to relay B,

relay B will detect and clear the fault first. Should relay B fail to operate and the fault remain on the system, relay A will still be capable of detecting the fault and initiating tripping (with a time delay that is set to be slower than the operate time of relay B, for a fault at B). In this scenario, relay A effectively serves as a backup to relay B, thereby enhancing system reliability through redundancy.

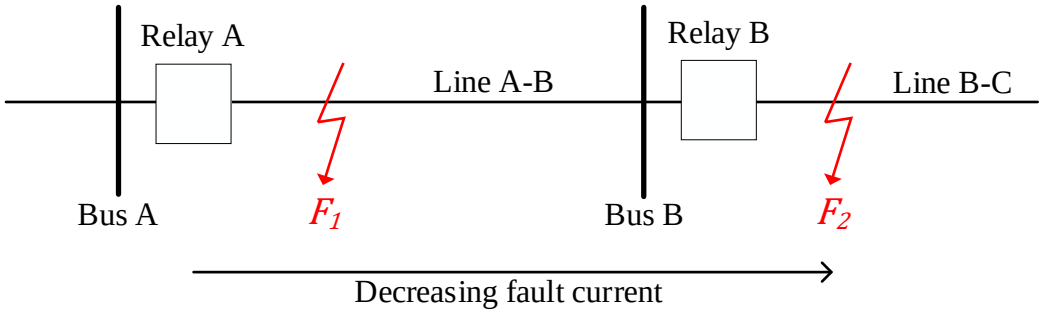

Figure 2.14: Overcurrent protection

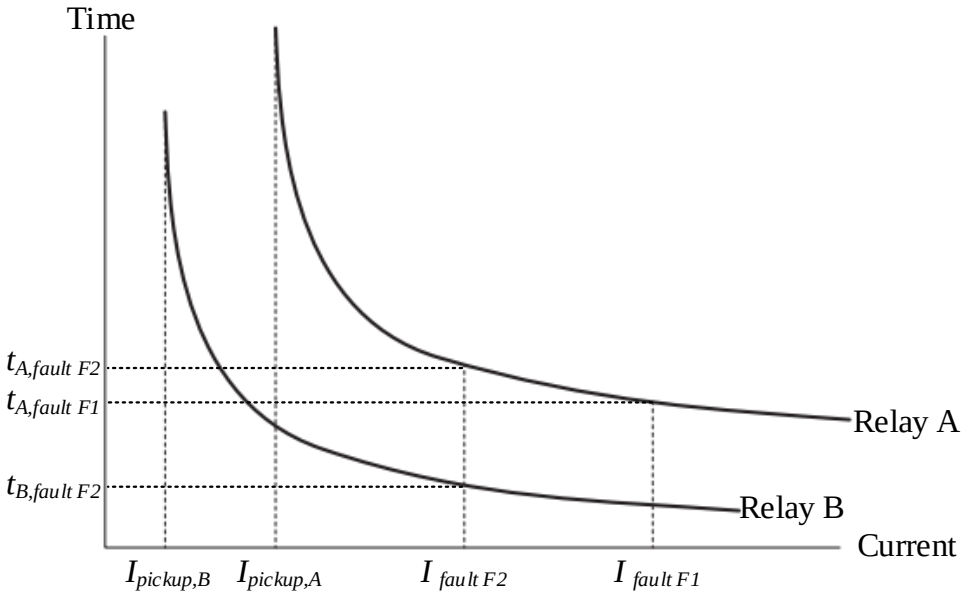

Figure 2.15: Time-current characteristic curve

Overcurrent protection can be implemented using various time-current characteristic, including instantaneous, definite-time, and inverse time curves, depending on the application and coordination requirement. The IEC 60255 standard [2.38] provides guidelines for calculating trip curve equation of the

inverse definite minimum time (IDMT) characteristic of overcurrent relays. These calculation methods are summarised in Table 2.1. An example of a standard inverse-time characteristic curve, approximated from relay operation as displayed in Figure 2.14, is illustrated in Figure 2.15, where each relay (A and B) has the same curve shapes (which are defined by the equations in Table 2.1., but are configured, via their settings, to lie in different locations on the current vs time plane as shown.

Table 2.1: Definition of IDMT relay characteristic [2.39]

Relay Characteristic	**Equation**
Standard Inverse	$t = TMS \times \frac{0.14}{I_r^{0.01} - 1}$
Very Inverse	$t = TMS \times \frac{13.5}{I_r - 1}$
Extremely Inverse	$t = TMS \times \frac{80}{I_r^2 - 1}$
Long time standby earth fault	$t = TMS \times \frac{120}{I_r - 1}$

In the table above, t is the time of operation of the relay for a given input current, I_r is the current input to the relay, which can be modified by a setting knows as the PMS – plug multiplier setting – which reduces or increases the CT current used by the relay via the setting value (e.g. 50-200%). This effectively defines where the curve will lie on the x-axis (current). TMS is the time multiplier setting, and changes the operating time of the relay by a factor, and this effectively defines the location of the characteristic curve with respect to the y axis on the figure. One of the key advantages of overcurrent protection is its simplicity and cost-effectiveness. It does not require communication between relays or extensive equipment, making it ideal for radial network configurations. However, it is less selective and often slower than other schemes, particularly in meshed or interconnected systems where fault discrimination is more complex. Despite its limitations, overcurrent protection remains a vital component of distribution system design, serving as both primary and backup

protection, due to its simplicity and relatively low cost. However, it is being increasingly challenged by changes to power systems as outlined in section 3.2.1 in the thesis.

2.5.3 Distance protection

Distance protection, also known as impedance protection, is a non-unit protection scheme, typically applied to medium and high voltage transmission networks. Unlike overcurrent protection, which relies solely on current magnitude measurements, distance protection determines the location of a fault by measuring the impedance (calculated from the measured voltages and currents) between the relay location and the point of the fault. Since impedance is proportional to the length of the line, the relay can estimate the distance to the fault from the measurement location (although other factors such as CT/VT errors and fault resistance may affect accuracy). Although distance protection is generally classified as a non-unit protection scheme, it is sometimes implemented with a communication link between relays to enhance its performance. In some cases, the scheme can effectively function as a unit protection system, allowing for faster and more selective fault clearance.

This method compares the ratio of measured voltage to current during a fault condition to calculate the apparent impedance – the ratio is complex, and the voltage and current phasors are used to calculate the magnitude and angle of the complex impedance being measured. If this impedance falls within a predefined protection zone which is set with using known line(s) impedance data, the relay operates and issues a trip command to the CB. As an illustrative case, consider a scenario where the relay detects an impedance equivalent to 90% of the total line impedance. Under the assumption of negligible fault resistance, this implies that the fault has occurred approximately 90% along the line length, measured form the relay position.

Distance relay are typically configured in multiple zones of protection (normally 3 zones, although sometimes there can be more), each covering

progressively longer sections of the line with increasing time delays to provide both primary and backup protection.

- **Zone 1:** this zone is typically configured to operate instantaneously for faults occurring within approximately 80% of the protection line's length (i.e., less than 80% of the line impedance). The remaining 20% margin is reserved to accommodate potential measurement inaccuracies arising from both current and voltage transformers, which are used in the calculation of impedance.
- **Zone 2:** this zone generally covers 125 – 150% of the line length (or line impedance), extending beyond the protected section to offer backup protection for the adjacent line segment. It operates with a delayed response, typically in the range of 500 ms, to allow time for Zone 1 of the downstream protection to clear the fault first.
- **Zone 3:** designed to provide additional backup protection for faults locate further down the network, Zone 3 covers approximately 200 – 250% of the line length. It is associated with a longer time delay, usually around 1 s, to ensure proper coordination with Zones 1 and 2 under fault conditions.

Figure 2.16 and Figure 2.17 show the operating zones of distance protection. Figure 2.16 presents the zone coverage along the transmission line together with their respective time delays, while Figure 2.17 depicts the zone boundaries represented in the complex impedance plane.

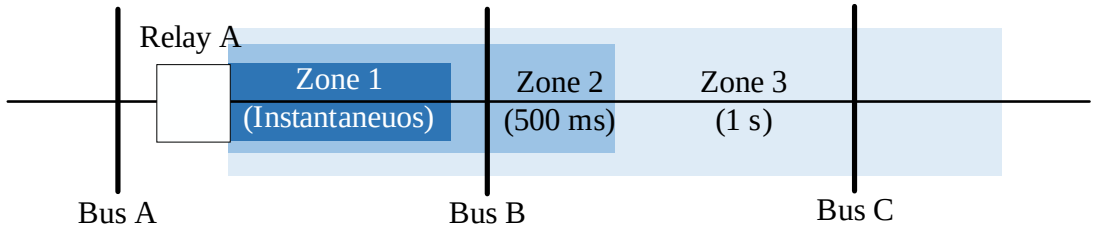

Figure 2.16: Operating zone of distance protection

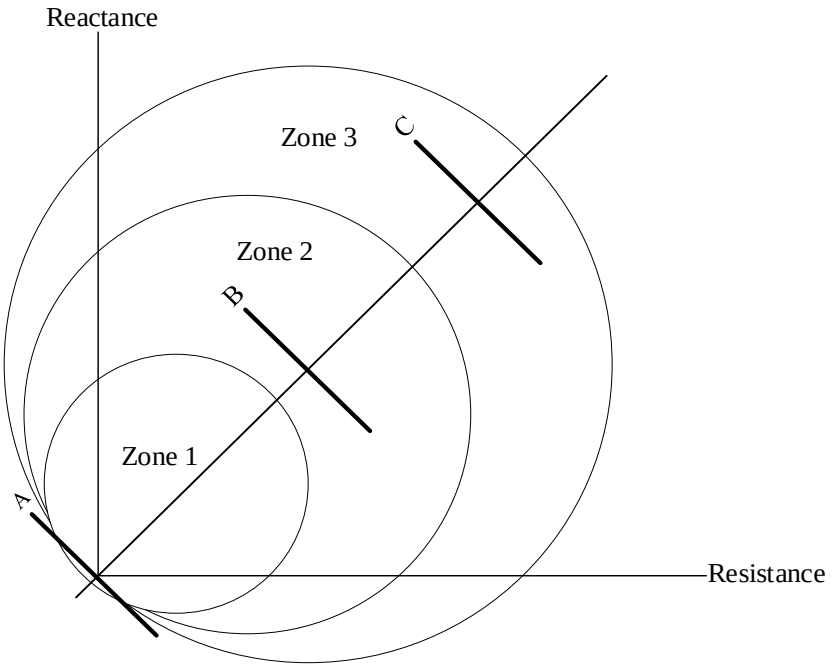

Figure 2.17: Zone boundaries of distance protection in the complex impedance plane

One of the main advantages of distance protection is its ability to provide fast and selective fault clearance over wide areas. Another major benefit is that, unlike overcurrent protection, it is not affected by variations in system fault levels, as the measured impedance to faults will not change (the values of voltage and current may change, but their ration – impedance – will normally remain constant). However, for complex or heavily loaded systems, such as those with multiple infeed points or series compensation, relay performance can be affected by power swings, load encroachment, very weak infeeds (from local or remote line-end sources) and fault resistance. The often non-sinusoidal waveforms output from converters during faults may also challenge measurement and subsequent relay operation (for all protection schemes).

2.6 Communications for power systems

Communication systems are integral to the efficient operation of both transmission and distribution networks, particularly in modern grids. As the

demand for reliable and optimised energy delivery increases, the importance of robust and adaptive communication infrastructures becomes increasingly evident. These systems facilitate real-time data exchange between key network components, including power generation plants, substations, distribution infrastructure, and end-users. Effective communication enables precise power flow management, enhances fault detection and response mechanisms, and supports advanced automation and control strategies. Furthermore, it plays a crucial role in ensuring grid stability, resilience, and cybersecurity by enabling rapid coordination between protection devices and control systems. As distribution networks evolve, sophisticated communication technologies will remain essential in achieving enhanced operational efficiency and a more sustainable energy future.

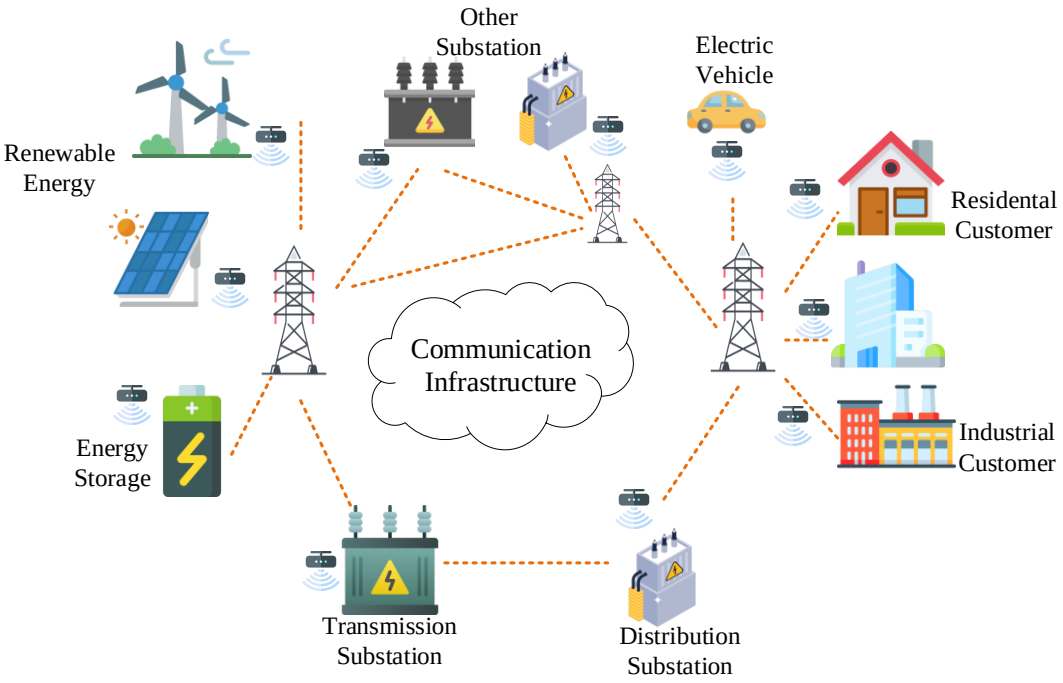

Figure 2.18: Overview of communication infrastructure in "smart grid" adapted from [2.40]

2.6.1 Communication for distribution networks

In the context of distribution networks specifically, various applications requiring some form of communications exist [2.41] These include:

- **Managing customers' loads:** enhancing demand-side management by optimising energy distribution and consumption based on real-time and predictive demand patterns.
- **Monitoring system performance:** ensuring operational stability by detecting inefficiencies, identifying faults, and mitigating risks before they impact grid functionality.
- **Reading customers' meters:** enabling frequent and automated meter readings, potentially several times per hour, to improve billing accuracy and support real-time consumption tracking.
- **Detecting stolen energy:** identifying anomalies in power usage patterns that may indicate instances of electricity theft, helping utilities mitigate revenue losses and enhance system integrity.
- **Controlling voltage levels:** regulating voltage across the power system to maintain stability, improve power quality, and ensure compliance with operational standards.
- **Reconfiguring the system post-fault:** adjusting system configurations following a disturbance or failure to restore power safely, efficiently, and with minimal disruption.
- **Detecting outages:** continuously monitoring system parameters to identify service interruptions, enabling rapid response and restoration efforts.
- **Balancing loads:** ensuring optimal system operation by distribution loads efficiently, preventing overloading, and enhancing grid resilience.
- **Collecting load data:** gathering and analysing data to support strategic system planning, demand forecasting, and infrastructure expansion.

Each of these applications requires a reliable and robust communication infrastructure to function effectively [2.42]. As distribution networks evolve towards smart grids, the integration of advanced communication technologies

becomes increasingly critical to ensuring grid intelligence, resilience, and sustainability.

2.6.2 Communication for protection

Communication systems are often integral to the functionally of modern transmission protection systems (differential and distance), but are not often deployed as key components of distribution protection systems, although many modern and emerging applications (including the faulted section identification scheme presented in this thesis) are employing various forms of communications – from simple and cheap to complex and expensive. This is necessary to address the changing nature and complexity of distribution systems and to cater for the increasing penetration of DERs and DG.

Some researchers and companies have shown how communications can enhance reliability and efficiency of fault detection and response mechanisms, enabling faster and more precise fault clearing to help reduce fault clearing time and increase selectivity and stability, thereby limiting the impact of short-circuit currents and mitigating potential equipment damage [2.43].

Communication systems can be used to enhance selective tripping, allowing for the isolation of only the affected section rather than triggering widespread disconnections, which in turn minimises the outage area and enhances system reliability [2.44].

Communications can also be used for transmitting alarm signals and logging events [2.45], which are important for monitoring system performance and conducting thorough post-event analyses. They also support the implementation of adaptive protection strategies, permitting dynamic adjustments to protective settings in response to evolving system conditions and thereby optimising overall protection system performance, which in turn can enhance power system reliability, resilience and safety.

2.7 Analysis of communications requirements for the faulted section identification scheme

In this thesis, the focus is solely on communication used for signal transmission and information exchange between two relays in a distributed application of the scheme, although in a centralised implementation there could be communications between multiple measurement points (which are often termed "relays" in this thesis, although in monitoring applications they may be more akin to simple processing devices or IEDs with no tripping responsibility). Specifically, a point-to-point communication approach is employed, similar to pilot-wire protection, where data is transmitted in packet format [2.46]. Each packet consists of seven digital binary code bits, making the proposed fault identification algorithm highly bandwidth-efficient. Consequently, this approach requires low bandwidth, thereby expanding the rang of potential communication applications, particularly within low-bandwidth communication networks.

Nonetheless, since this communication system is an integral part of a protection scheme, which must be a near real-time process, low latency remains a critical requirement [2.44] . However, it is important to note that the latency requirements in distribution network protection are generally less stringent compared to those found in transmission networks. Typically, fault clearing in distribution networks must be executed within a range from 12 to 20 cycles [2.47], which is equivalent to 240 to 400 ms in a 50 Hz power system, such as those in the UK and Thailand.

Furthermore, in terms of area coverage, medium-range communication is sufficient, as the average length of a distribution line typically ranges from very short to 30 km. Moreover, mobility is not a requirement, as the sensors and relays are permanently installed within substations or as fixed pole-mounted equipment [2.48] – [2.49].

2.7.1 Review of candidate communication technologies

The effectiveness of any protection scheme in a distribution network is significantly influenced by the choice of communication technology. An appropriate communication system ensures reliable data exchange, low latency, and secure signal transmission, all of which are essential for maintaining system stability and fault response efficiency. Given the diverse range of available communication technologies available, selecting the most suitable approach requires careful evaluation of performance parameters, infrastructure constraints, and network requirements.

Communication technologies for protection schemes can be broadly classified into wired and wireless communication methods, each offering distinct advantages and limitations.

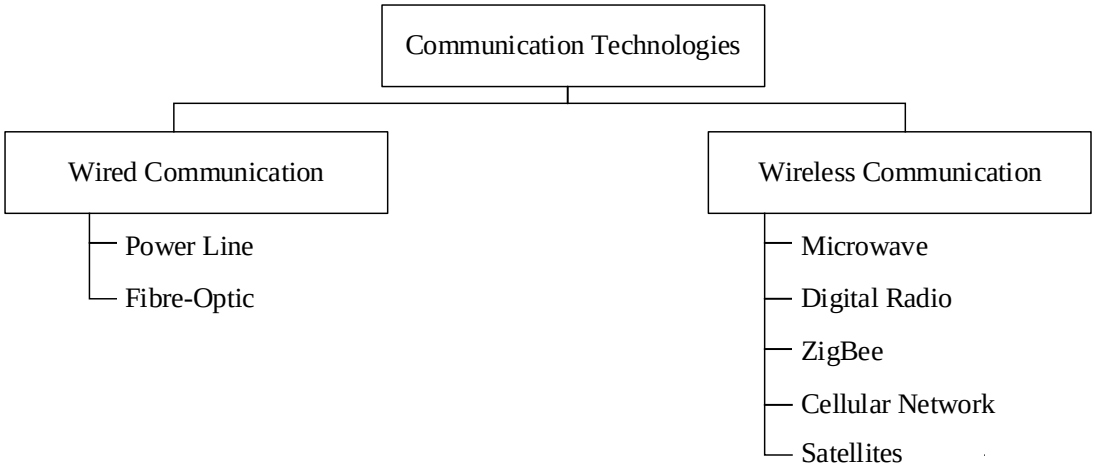

Figure 2.19: Hierarchy of communication technologies

The following sections explores wired and wireless communication candidates that are relevant to the proposed protection scheme, analysing their suitability, challenges, and potential implementation considerations in the context of distribution network protection.

2.7.1.1 Wired communication

Wired communication remains a fundamental choice for protection systems due to its high reliability, low latency, and resistance to external interference. In critical applications, where precision and security and paramount, wired networks provide dedicated and stable communication channels, ensuring fast and accurate data transmission between protection devices. Specific implementations and practical examples of wired communication are discussed in the context.

2.7.1.1.1. Power line communication

Power Line Communication (PLC) is a technology that enables the transmission of data over metallic conductors, which are primarily used for electric power distribution. Over the past few decades, utility companies worldwide have increasingly adopted PLC for applications such as remote metering and load control [2.50]. The extensive installed base of metallic infrastructure and the relative ease of interfacing make PLC an attractive option for integrating digital communication into power transmission systems. Additionally, enhancements have been made to metallic media to better accommodate digital communication requirements [2.45], [2.51].

PLC is anticipated to be particularly well-suitable for distribution grids as traditional substations within medium-voltage distribution networks typically lack integrated communication capabilities [2.52]. This technology is considered one of the most cost-effective communication solutions, as existing power lines can be leveraged for data transmission without the need for extensive additional infrastructure [2.52]. Furthermore, the data transmission speeds of PLC have been significantly improved, making them sufficient for pilot wire protection applications [2.43], [2.45].

However, security concerns remain a significant challenge due to the inherent vulnerabilities of power lines in broadband PLC access systems and their exposure to field deployment risks [2.53]. In practice, PLC-based protection schemes have demonstrated a failure rate of approximately 17.5 %, primarily

caused by pilot wires becoming shorted, open, or reversed [2.43]. Although installation costs for PLC are relatively low, the expenses associated with safeguarding personnel and equipment against damaging power surges can be moderately high due to protective equipment requirements and maintenance considerations [2.43]. Additionally, PLC faces challenges related to buffering, retransmission, error correction, and unpredictable transmission speeds in noisy conditions, which can negatively impact the reliability and performance of protection [2.45]. PLC may also be affected by changes in impedances and the presence of power transformers in the path (and of course if a disconnector or breaker is opened, the signal will not pass) – hence they are normally used for point-point applications in protection.

Given these limitations, PLC is often integrated with other communication technologies, such as cellular networks, to develop hybrid solutions for smart grid communication. A fully PLC-based network is considered impractical, as the technology is highly susceptible to external disturbances, limiting its effectiveness for comprehensive connectivity solutions [2.54].

Nevertheless, advancements in Integrated Services Digital Network (ISDN) and Digital Subscriber Line (DSL) technologies have led to higher data transmission speed and reduced latency, making PLC more promising for protection applications.

2.7.1.1.2. Fibre-optic communication

Fibre optic technology involves the transmission of data as light pulses through strands of glass or plastic fibres. Due to its high bandwidth capacity, low signal attenuation, and resistance to electromagnetic and radio interference, fibre optics have been widely adopted across various industrial applications over the past 30 years [2.45], [2.55] – [2.56].

In the telecommunications infrastructure of electrical networks, fibre optics are often integrated into optical ground wires (OPGW), or are deployed in underground environments [2.45]. This integration allows for effective utilisation of available bandwidth, enabling the consolidation of multiple

communication needs within the electric utility sector, including SCADA systems [2.45]. Owing to its high reliability and resilience, fibre optics is commonly chosen as a backbone communication solution, minimising common-mode failures and ensuring a stable and secure network [2.57].

Fibre optic technology offers exceptional performance characteristics, including high data transmission rates, minimal end-to-end delay (typically below 1 ms unless the distance is extremely high), and extremely low bit error rates [2.45]. These attributes make fibre optics highly suitable for protection systems, particularly in current differential relay, as their design mitigates the impacts of induced noise, ground potential rise, and other interference sources, making them an ideal choice for point-to-point protection schemes [2.43].

However, the primary drawback of fibre optic communication is its high cost, both in terms of installation and maintenance. Deploying fibre optic cables requires significant time and resources, making them unsuitable for immediate deployment in urgent scenarios [2.54]. Additionally, installing fibre optic infrastructure in geographically challenging regions, such as rocky or mountainous terrains, presents considerable difficulties, which is similar to other wired communication technologies. Despite these limitations, some researchers argue that the superior performance characteristics of fibre optics make it a worthwhile investment, even in light of its high initial costs. It can often be used for other purposes (e.g. leasing some fibre cores to other users such as commercial telecommunications companies) [2.58] – [2.59] .

2.7.1.2 Wireless communication

Wireless communication has emerged as a viable alternative to traditional wired communication in protection systems, offering flexibility, scalability, and cost-effectiveness. Unlike wired solutions, which require physical infrastructure and extensive cabling, wireless communication enables rapid deployment and remote connectivity, making it particularly beneficial in challenging environments where wired installation is impractical or cost-prohibitive [2.43].

Various wireless communication technologies are examined to assess their suitability for the proposed protection scheme, along with their key performance characteristics, implementation challenges, and practical considerations.

2.7.1.2.1 Microwave

Microwave communication had traditionally been employed for analogue signal transmission, including its use in protection systems. For instance, electric utilities have long-relied on microwave radio links to facilitate essential communications for pilot protection schemes, particularly when transferring control commands in point-to-point relay protection schemes between Intelligent Electronic Devices (IEDs) for power lines protection [2.60]. This widespread application is attributed to the small wavelengths of microwave signals, which enable the deployment of compact directional antennas to maintain secure and efficient data transmission [2.58].

In recent years, the adoption of digital microwave communication has been steadily increasing. Terrestrial digital microwave signals operate within the radio frequency spectrum, typically ranging from 890 MHz to 20 GHz [2.45]. This technology is implemented within licensed private networks [2.60], incorporating sophisticated digital encryption techniques, thereby providing robust reliability while maintaining lower equipment costs [2.45]. As a result of these advantages, digital microwave communication sometimes serves as a backup solution for fibre-optic wired communication systems [2.61]. Moreover, microwave communication offers exceptionally low transmission time delays. In particularly, digital microwave technologies exhibit a worst-case time delay of approximately 600 µs [2.62].

In spite of its benefits, microwave communication is highly sensitive to external interference. Due to its susceptibility to electromagnetic interference, line-of-sight transmission is required to ensure uninterrupted data exchange [2.63]. Additionally, weather-related disruptions pose a significant challenge, as severe atmospheric conditions can degrade signal quality leading to data loss

or transmission errors [2.64] – [2.65], which can be problematic in mission-critical protection applications.

2.7.1.2.2 Digital radio

Digital radio technology is increasingly being adopted within the electric utility industry, supporting a wide range of general and emerging specialised applications. Various types of radio communications systems – including very high frequency (VHF), ultra high frequency (UHF), and trunked radio networks – are primarily used for portable, mobile operation [2.45].

In general, digital radio is utilised in a mesh communication topology, often referred to as a "wireless mesh network." This approach offers several advantages, including cost-effectiveness, dynamic self-organisation, self-healing capabilities, self-configuration, and high scalability. These features enhance network performance, optimise load distribution, and extend coverage range, making wireless mesh technology a viable communication solution [2.40], [2.65]

Both VHF (30 – 172 MHz) and UHF (450 – 5112 MHz) radio systems, particularly narrow-band UHF, enable direct communication, offering performance comparable to that of microwave communication systems. However, they may provide greater reliability due to their lower system complexity. Despite these advantages, VHF and UHF systems are not typically deployed for general protection purposes due to potential unavailability and propagation constraints. As a result, their applications have been largely confined to direct transfer trip schemes for low-speed, less critical protection applications [2.45].

Furthermore, radio channels may be disrupted by antenna-pointing errors and advised weather conditions. Although mechanical damage to the infrastructure is unlikely to interfere with radio signals, these environmental factors can significantly impact communication reliability [2.45].

Trunked radio systems operating in the 800 MHz band were originally developed for shared voice communication. However, these systems are unsuitable for protection channels due to variable user congestion and

insufficient security measures, making them impractical for mission-critical power system protection application [2.45].

2.7.1.2.3 ZigBee

ZigBee is a wireless communication technology based on the IEEE 802.15.4 standard, specially developed for radio-frequency applications that demand low data transmission rates, prolonged battery life (of the communicating devices), secure networking, and low-cost application [2.58], [2.67] – [2.68]. It is considered one of the most widely-adopted communication technologies within customer home networks. Moreover, ZigBee and its Smart Energy Profile (SEP) have been established as key communication standards for use in customer premise network domains within the smart grid infrastructure, as defined by the United States National Institute of Standards and Technology (NIST) [2.69] – [2.70].

ZigBee is particularly well-suited for smart metering applications [2.25], as it provides a standardised platform for the exchange of data between smart meters and household appliances. The SEP supports several advanced functionalities, including demand response, real-time pricing, advanced metering infrastructure, text messaging, and load control mechanisms [2.70]. Given its technical characteristics, ZigBee operates at a data rate of approximately 250 kilobits per second (Kbps), making it predominantly used for establishing home automation networks and wireless sensor networks (WSNs) [2.54], [2.70].

Despite its advantages in low-power, secure, and cost-effective application, ZigBee has significant limitations when applied to protection systems. One of its primary drawbacks is its high latency, which can reach up to 5000 ms [2.47]. This delay is excessive for protection systems, which require real-time, low-latency communication to support critical applications. Another disadvantage of ZigBee is that it operates in unlicensed frequency bands, making it highly susceptible to noise and interference issues, particularly in dense communication environments [2.54]. Additionally, ZigBee offers limited

coverage area – typically less than 1 km – which further restricts its applicability in wide-area protection schemes [2.71].

2.7.1.2.4 Cellular network

Cellular mobile radio, operating within the 700 – 900 MHz frequency band, is classified as a Machine-Type Communication (MTC) technology aimed at enabling direct data transfers between MTC devices. One of the primary advantages of cellular communication is its pre-existing network infrastructure, which removes the need for deploying separate antenna towers. This significantly accelerates the installation process, facilitating seamless connectivity for IEDs in power systems [2.60]. Due to its high data rates, widespread adoption, and improve data reliability, cellular communication is considered one of the fastest-growing technologies globally [2.54].

A diverse range of MTC access technologies is available, spanning from 2G, 3G, NB-IoT, LET-M, 4G, to 5G. Below is an overview of key MTC technologies:

A. Narrow-band Internet-of-Thing (NB-IoT)

NB-IoT is characterised by extensive coverage, enabling communications with devices in remote areas. By utilizing a narrow bandwidth, it ensures efficient spectrum usage, making it particularly advantageous for massive device connectivity applications, such as smart city infrastructure. Furthermore, it is an energy-efficient technology, resulting in lower power consumption [2.72]. However, its latency ranges between 1.6 to 10 seconds, rendering it unsuitable for real-time mission-critical application [2.73].

B. Long-Term Evolution for Machine (LTE-M)

Particularly enhanced Machine-Type Communication (eMTC) includes LTE Category M1 (CAT-M1), and Category M2 (CAT-M2), both of which also offer wide coverage [2.72]. However, compared to NB-IoT, LTE-M offers a wider bandwidth, supporting higher data rates for applications such as video surveillance [2.72]. additionally, LTE-M has a latency of approximately 10 – 15

ms, making it more appropriate for time-sensitive tasks, including protection relaying, despite its higher power consumption relative to NB-IoT [2.73].

C. Fifth-Generation (5G) Cellular network

Ongoing research is exploring the practical deployment of 5G, which promise ultra-fast data rates of up to 100 Gbps with end-to-end latency as low as 5 ms and a reliability of 99.999 percent, making them a viable candidate for high-speed and low-latency applications in the power industry, positioning it as a highly promising option for time-critical application. [2.46], [2.54].

Despite its numerous advantages, cellular communication has inherent limitations. One of the primary concerns is network sharing, as multiple users access the same cellular infrastructure simultaneously. When a user requests access to a communication path from a central controller, which then assigns an available channel for data transfer. However, this channel assignment may remain static or switch dynamically during transmission, introducing security vulnerabilities. Consequently, mission-critical applications that require uninterrupted, real-time communication may not be fully supported, making cellular communication unsuitable for high-priority protection system [2.45], [2.54].

However, as the introduction of personal digital service, digital cellular technology has led to the development of devices specifically designed for data transport. As Time Division Multiple Access (TDMA) and Code Division Multiple Access (CDMA) technologies continue to evolve, their ability to meet real-time communication requirements for protection applications is improving, enabling limited use in selected relay protection schemes [2.45]. Future advancements in CDMA technology are of particularly interest due to its secure spread spectrum techniques, which hold potential for digital power line carrier applications. Additionally, there is increasing research into private cellular technologies, such as Ultra-Reliable Low-Latency Communication (URLLC) within private 5G networks. For instance, universities – including the University of Strathclyde – have begun experimenting with private cellular SIM

cards within laboratory settings, further advancing the development of dedicated cellular communication of power system applications [2.74].

2.7.1.2.5 Satellite communications

Satellite networks provide almost universal coverage, making them a potential solution for various utility applications. With advancement in Very Small Aperture Terminal (VSAT) technology – such as smaller dish sizes, reduced costs, and lower-orbiting satellites – this method has become a viable option for applications including supervisory and adaptive control. However, a significant drawback of VSAT technology is its inherent signal delay, as signals must travel several hundred kilometres to and from satellites [2.54]. This substantial latency makes VSAT largely unsuitable for real-time monitoring and control application, particularly in protection systems, where low-latency communication is essential for ensuring rapid fault detection and maintaining system stability [2.45].

2.7.2 Most suitable communication technologies for faulted section identification scheme

Following the presentation of communication technologies in the previous section, their suitability can be assessed in relation to the defined criteria, which include:

- Low bandwidth requirements
- Low latency, keeping the fault clearing time within 400 ms – ideally less (for a 50 Hz system)
- Resistance to noise interference
- Coverage area of approximately 30 km

Wired (or optical) communication technologies typically present no significant issues concerning bandwidth, latency, or noise immunity, as data transmission occurs within a controlled and isolated medium. Nevertheless, for systems requiring extensive coverage areas, such solutions may impractical due

to the installation complexity and associated costs of physical infrastructure over long distances.

Considering coverage limitations, wireless communication technologies present a more appropriate alternative. A comparative analysis of their suitability is provided in Table 2.2.

Table 2.2: Comparison of wireless communication options

Technology	**Bandwidth**	**Latency**	**Noise Tolerance**	**Coverage**	**Cost**
Microwave	✓	✓	⚠ (need line-of -sight)	✓	Medium - high
Digital radio	✓	✓	⚠	✓	Low - medium
ZigBee	✓	✓	✓	✗ (< 1 km)	Very low
Cellular	✓	✓	✓	✓	High
Satellite	✓	✗	✗	✓	Very high

In the context of faulted section identification schemes, microwave, digital radio, and cellular networks may all be considered viable communication technologies. However, when cost-effectiveness is taken into account, digital radio emerges as the most reasonable choice among the three.

One aspect that requires careful consideration is the system's tolerance to noise, which can be influence by actors such as antenna quality and weather conditions. For the application discussed in this thesis – binary-code signal transmission – noise is expected to have a minimal impact. This is due to the extremely low data complexity, which provides a higher margin for signal interpretation.

For example, a binary '0' may be transmitted using a 0 V signal, while a '1' may correspond to a 5 V signal. In this case, even if noise causes minor voltage fluctuations, the receiver can still reliably distinguish between the two logical states, thus maintaining communication integrity.

2.8 Chapter summary

This chapter has described the evolution of electrical power systems, beginning with a detailed overview of conventional networks structures. It outlined the roles of transmission and distribution networks in delivering electricity from centralised generation sources to consumers, thereby establishing a foundation for understanding the subsequent transformation of these systems.

The growing integration of DERs into existing distribution networks was also presented. This shift, motivated by global sustainability objectives and the drive towards net-zero emission, has introduced many changes and complexities into the system. While the chapter summarised the key benefits of DG adoption, it has also been acknowledged that there are several characteristics presenting challenges to network protection (and operation). These protection-related issues are be discussed in greater detail in the next chapter. A number of other innovations enhancing real-time monitoring, decentralised control, and dynamic optimisation, were also described, which are beneficial in DER-rich environments.

The chapter also provided a review of traditional protection schemes and their inadequacies when applied to modern distribution systems.

This chapter has also provided a detailed overview of communications system technologies and their application in power systems generally. Commentary on candidate technologies for protection in general, and more specifically for the faulted section identification scheme reported in this thesis, has also been included.

Chapter references

[2.1] 'The history of energy in the UK', national grid. [Online]. Available: https://www.nationalgrid.com/stories/energy-explained/history-of-energy

[2.2] 'Selected landmarks in The History of Electricity Generation | Distribution | Utilisation', The Institution of Engineering and Technology (IET).

[2.3] K. Blacklaws, 'What next for the electricity grid?', Isonomia. [Online]. Available: https://www.isonomia.co.uk/what-next-for-the-electricity-grid/

[2.4] T. McGarry, 'UK Electricity capacity and generation by fuel between 1920 and 2020'. Department for Energy Security & Net Zero, June 29, 2023.

[2.5] 'Climate change', GOV.UK. [Online]. Available: https://www.gov.uk/guidance/climate-change

[2.6] 'Climate Change Act 2008 as Amended – Policies', IEA. [Online]. Available: https://www.iea.org/policies/1449-climate-change-act-2008-as-amended

[2.7] 'Energy Trends March 2025'. Departmetn for Energy Security & Net Zero, March 27, 2025. [Online]. Available: https://assets.publishing.service.gov.uk/media/67e4f5d855239fa04d412067/Energy_Trends_March_2025.pdf

[2.8] 'Britain's last coal-fired electricity plant is closing. It ends 142 years of coal power in the UK', AP News. [Online]. Available: https://apnews.com/article/uk-last-coal-power-station-closing-9e6b792f27513e3b02904da1eaedfbf3

[2.9] G. Network, 'COP26 and Thailand's Role in Addressing Climate Change', Green Network. [Online]. Available: https://www.greennetworkthailand.com/cop26-%e0%b8%9b%e0%b8%a3%e0%b8%b0%e0%b9%80%e0%b8%97%e0%b8%a8%e0%b9%84%e0%b8%97%e0%b8%a2/

[2.10] N. S, 'The 2025 National Energy Policy: Government Commitment to Promoting Clean Energy', Energy News Center. [Online]. Available: https://www.energynewscenter.com/เปิดนโยบายพลังงานปี-2568-รั/

[2.11] O. US EPA, 'Distributed Generation of Electricity and its Environmental Impacts'. [Online]. Available: https://www.epa.gov/energy/distributed-generation-electricity-and-its-environmental-impacts

[2.12] T. Ackermann, G. Andersson, and L. Söder, 'Distributed generation: a definition', *Electr. Power Syst. Res.*, vol. 57, no. 3, pp. 195–204, April 2001.

[2.13] I. Dytham, 'System Inertia Monitoring National Grid ESO', 2019. [Online]. Available: https://www.naspi.org/sites/default/files/2021-06/20210630_naspi_webinar_system_inertia.pdf

[2.14] A. Dagar, P. Gupta, and V. Niranjan, 'Microgrid protection: A comprehensive review', *Renew. Sustain. Energy Rev.*, vol. 149, p. 111401, October 2021.

[2.15] National Grid ESO, 'National Trends and Insights: A System Operability Framework Document'. nationalgridESO, March 2021. [Online]. Available: https://www.neso.energy/document/190151/download

[2.16] C. Su, Z. Liu, Z. Chen, and Y. Hu, 'Short circuit analysis of distribution system with integration of DG', in *2014 International Conference on Power System Technology*, October 2014, pp. 2921–2926.

[2.17] S. Gordon, C. McGarry, and K. Bell, 'The growth of distributed generation and associated challenges: A Great Britain case study', *IET Renew. Power Gener.*, vol. 16, no. 9, pp. 1827–1840, July 2022.

[2.18] T. B. Nadeem, M. Siddiqui, M. Khalid, and M. Asif, 'Distributed energy systems: A review of classification, technologies, applications, and policies', *Energy Strategy Rev.*, vol. 48, p. 101096, July 2023.

[2.19] G. Pepermans, J. Driesen, D. Haeseldonckx, R. Belmans, and W. D'haeseleer, 'Distributed generation: definition, benefits and issues', *Energy Policy*, vol. 33, no. 6, pp. 787–798, April 2005.

[2.20] C. Broderick, 'Rate of Change of Frequency (RoCoF) withstand capability'. European Network of Tranmission System Operators for Electricity (ENTSO-E), January 31, 2018.

[2.21] *Engineering Recommendation G99*, March 04, 2024. [Online]. Available: https://dcode.org.uk/assets/uploads/files/ENA_EREC_G99_Issue_1_Amendment_10_(2024).pdf

[2.22] S. Saha, M. I. Saleem, and T. K. Roy, 'Impact of high penetration of renewable energy sources on grid frequency behaviour', *Int. J. Electr. Power Energy Syst.*, vol. 145, p. 108701, February 2023.

[2.23] B. Amjad, M. A. A. Al-Ja'afreh, and G. Mokryani, 'Active Distribution Networks Planning Considering Multi-DG Configurations and Contingency Analysis', *Energies*, vol. 14, no. 14, Art. no. 14, January 2021.

[2.24] K. Turitsyn, P. Sulc, S. Backhaus, and M. Chertkov, 'Local Control of Reactive Power by Distributed Photovoltaic Generators', in *2010 First*

IEEE International Conference on Smart Grid Communications, October 2010, pp. 79–84.

[2.25] H. Farhangi, 'The path of the smart grid', *IEEE Power Energy Mag.*, vol. 8, no. 1, pp. 18–28, January 2010.

[2.26] F. A. Kassab, B. Celik, F. Locment, M. Sechilariu, S. Liaquat, and T. M. Hansen, 'Optimal sizing and energy management of a microgrid: A joint MILP approach for minimization of energy cost and carbon emission', *Renew. Energy*, vol. 224, p. 120186, April 2024.

[2.27] G. de Donato, J. A. Aguado, C. Gonzales-Moran, and J. Garcia, 'Power System Smart Power Engineering', in *Encyclopedia of Electrical and Electronic Power Engineering*, Elsevier, 2023. [Online]. Available: http://www.sciencedirect.com:5070/referencework/9780128232118/encyclopedia-of-electrical-and-electronic-power-engineering

[2.28] W. R. Cassel, 'Distribution management systems: functions and payback', *IEEE Trans. Power Syst.*, vol. 8, no. 3, pp. 796–801, August 1993.

[2.29] R. A. Jabr and I. Džafić, 'Distribution Management Systems for Smart Grid: Architecture, Work Flows, and Interoperability', *J. Mod. Power Syst. Clean Energy*, vol. 10, no. 2, pp. 300–308, March 2022.

[2.30] P. Westwater, 'UK Power Networks Expands Wide Area Restoration Abilities', GE VERNOVA. [Online]. Available: https://www.gevernova.com/software/blog/forward-thinking-uk-power-networks-expands-digital-wide-area-restoration-abilities

[2.31] 'MEA enhances the potential of the electrical systemm with FLISR and FFM technology, reducing all problem statistics', Metropolitan Electricity Autority. [Online]. Available: https://www.mea.or.th/public-relations/corporate-news-activities/announcement/mea-power-quality-flisr-ffm

[2.32] J. Smith *et al.*, 'Case Study: A Subtransmission-Level Fault Location, Isolation, and Service Restoration (FLISR) Scheme', presented at the 78th Annual conference for Protective Relay Engineering at Texas A&M, College Station, TX, USA, April 2025.

[2.33] P. Parikh, I. Voloh, and M. Mahony, 'Fault location, isolation, and service restoration (FLISR) technique using IEC 61850 GOOSE', in *2013 IEEE Power & Energy Society General Meeting*, Vancouver, BC, Canada: IEEE, July 2013, pp. 1–6.

[2.34] [T. SCOPE, 'FLISR Technology for Minimising Power Outages and Improving Network Reliability', SCOPE Corporate Blog. [Online]. Available: https://scopetnm.blog/2022/03/24/flisr-technology-for-minimising-power-outages-and-improving-network-reliability/

[2.35] Y. G. Paithankar and S. R. Bhide, *Fundamentals of power system protection*. New Delhi: Prentice-Hall of India, 2007.

[2.36] A. Stankovski, B. Gjorgiev, L. Locher, and G. Sansavini, 'Power blackouts in Europe: Analyses, key insights, and recommendations from empirical evidence', *Joule*, vol. 7, no. 11, pp. 2468–2484, November 2023.

[2.37] C. Booth and K. Bell, 'Protection of transmission and distribution (T&D) networks', in *Electricity Transmission, Distribution and Storage Systems*, Elsevier, 2013, pp. 75–107.

[2.38] *IEC 60255-151 Measuring relays and protection equipment - Part 151: Functional requirements for over/under current protection*, International Standard, August 28, 2009. [Online]. Available: https://webstore.iec.ch/en/publication/1166

[2.39] ALSTOM, *Network Protection & Automation Guide*. ALSTOM Grid, 2011.

[2.40] V. C. Gungor *et al.*, 'Smart Grid Technologies: Communication Technologies and Standards', *IEEE Trans. Ind. Inform.*, vol. 7, no. 4, pp. 529–539, November 2011.

[2.41] B. A. Akyol, H. Kirkham, S. L. Clements, and M. D. Hadley, 'A Survey of Wireless Communications for the Electric Power System', Pacific Northwest National Lab. (PNNL), Richland, WA (United States), PNNL-19084, January 2010.

[2.42] Z. Fan *et al.*, 'Smart Grid Communications: Overview of Research Challenges, Solutions, and Standardization Activities', *IEEE Commun. Surv. Tutor.*, vol. 15, no. 1, pp. 21–38, 2013.

[2.43] R. Moxley and K. Fodero, 'High-Speed Distribution Protection Made Easy: Communications-Assisted Protection Schemes for Distribution Applications', *SEL J. Reliab. Power*, vol. 3, August 2012.

[2.44] M. Simon *et al.*, 'Protection Relay Applications Using the Smart Grid Communication Infrastructure', Working Group H2 of the IEEE Power System Relaying Committee (PSRC), 2011. [Online]. Available: https://www.pes-psrc.org/kb/report/061.pdf

[2.45] G. Michel *et al.*, 'Digital Communications for Relay Protection', Working Group H9 of the IEEE Power System Relaying (PSRC) Committee, 2011. [Online]. Available: https://www.pes-psrc.org/kb/report/064.pdf

[2.46] S. V. Achanta, K. Hao, and J. Fowler, 'Emerging Communications and Sensor Technologies That Advance Distribution Automation', presented at the Power and Energy Automation Conference, March 2019.

[2.47] B. K. Dash and J. Peng, 'Zigbee Wireless Sensor Networks: Performance Study in an Apartment-Based Indoor Environment', *J. Comput. Netw. Commun.*, vol. 2022, no. 1, p. 2144702, August 2022.

[2.48] National Grid, 'Substation configuration and build types'. [Online]. Available: https://www.nationalgrid.com/electricity-transmission/substation-configuration-and-build-types

[2.49] D. Parnell, 'An Introduction to Gas Insulated Electrical Substations', presented at the CED engineering, [Online]. Available: https://www.cedengineering.com/userfiles/E03-043%20-%20An%20Introduction%20to%20Gas%20Insulated%20Electrical%20Substations%20-%20US.pdf

[2.50] [H. C. Ferreira, L. Lampe, J. Newbury, and T. G. Swart, *Power Line Communications: Theory and Applications for Narrowband and Broadband Communications over Power Lines*. John Wiley & Sons, Ltd, 2010.

[2.51] D. W. Rieken and M. R. Walker II, 'Ultra Low Frequency Power-Line Communications Using a Resonator Circuit', *IEEE Trans. Smart Grid*, vol. 2, no. 1, pp. 41–50, March 2011.

[2.52] S. Galli, A. Scaglione, and Z. Wang, 'Power Line Communications and the Smart Grid', presented at the IEEE SmartGridComm'10, 2010, pp. 303–308.

[2.53] N. Pavlidou, A. J. Han Vinck, J. Yazdani, and B. Honary, 'Power line communications: state of the art and future trends', *IEEE Commun. Mag.*, vol. 41, no. 4, pp. 34–40, April 2003.

[2.54] [E. Kabalci and Y. Kabalci, Eds., *Smart Grids and Their Communication Systems*. in Energy Systems in Electrical Engineering. Singapore: Springer, 2019.

[2.55] G. Keiser, *Fiber Optic Communications*. Singapore: Springer, 2021. [Online]. Available: https://doi.org/10.1007/978-981-33-4665-9_13

[2.56] M. McGranaghan and F. Goodman, 'Technical and system requirements for Advanced Distribution Automation', in *CIRED 2005 - 18th International Conference and Exhibition on Electricity Distribution*, Turin, Italy, June 2005, pp. 1–5.

[2.57] V. C. Gungor and F. C. Lambert, 'A survey on communication networks for electric system automation', *Comput. Netw.*, vol. 50, no. 7, pp. 877–897, May 2006.

[2.58] X. Fang, S. Misra, G. Xue, and D. Yang, 'Smart Grid — The New and Improved Power Grid: A Survey', *IEEE Commun. Surv. Tutor.*, vol. 14, no. 4, pp. 944–980, 2012.

[2.59] C. Root, 'The New Relationship Between Electric Utilities and Telecommunications', T&D World. [Online]. Available: https://www.tdworld.com/overhead-transmission/article/21161057/the-new-relationship-between-electric-utilities-and-telecommunications

[2.60] S. V. Achanta, R. Bradetich, and K. Fodero, 'Speed and security considerations for protection channels', in *2016 69th Annual Conference for Protective Relay Engineers (CPRE)*, College Station, TX, USA, April 2016, pp. 1–9.

[2.61] Caregon Networks Ltd., 'Advanced Wireless Backhaul for the Smart Grid', June 2014. [Online]. Available: https://www.winncom.com/images/solutions/Ceragon_Solution_Brief_Utilities_Smart_Grid.pdf

[2.62] E. W. Allen, 'Measured time delay and re-synchronization time in digital microwave radio systems', *IEEE Trans. Power Deliv.*, vol. 9, no. 2, pp. 639–644, April 1994.

[2.63] B. J. Eggleton, M. J. Steel, and C. G. Poulton, *Semiconductors and Semimetals*, vol. 110. Elsevier, 2022.

[2.64] tanxinmeng, 'What Is Microwave?', Huawei. [Online]. Available: https://forum.huawei.com/enterprise/intl/en/thread/What-Is-Microwave/667273393667457024?blogId=667273393667457024

[2.65] 'What is Microwave Communication?'. [Online]. Available: https://lightyear.ai/tips/what-is-microwave-communication

[2.66] A. Yarali, 'Wireless Mesh Networking technology for commercial and industrial customers', in *2008 Canadian Conference on Electrical and Computer Engineering*, Niagara Falls, ON, Canada, May 2008, pp. 47–52.

[2.67] C. Gezer and C. Buratti, 'A ZigBee Smart Energy Implementation for Energy Efficient Buildings', in *2011 IEEE 73rd Vehicular Technology Conference (VTC Spring)*, Budapest, Hungary, May 2011, pp. 1–5.

[2.68] A. Y. Mulla, J. J. Baviskar, F. S. Kazi, and S. R. Wagh, 'Implementation of ZigBee/802.15.4 in Smart Grid communication and analysis of power consumption: A case study', in *2014 Annual IEEE India Conference (INDICON)*, December 2014, pp. 1–7.

[2.69] A. Gopstein, C. Nguyen, C. O'Fallon, N. Hastings, and D. A. Wollman, 'NIST Framework and Roadmap for Smart Grid Interoperability Standards, Release 4.0', *NIST*, February 2021. [Online]. Available: https://www.nist.gov/publications/nist-framework-and-roadmap-smart-grid-interoperability-standards-release-40

[2.70] P. Yi, A. Iwayemi, and C. Zhou, 'Developing ZigBee Deployment Guideline Under WiFi Interference for Smart Grid Applications', *IEEE Trans. Smart Grid*, vol. 2, no. 1, pp. 110–120, March 2011.

[2.71] E. Avşar and Md. N. Mowla, 'Wireless communication protocols in smart agriculture: A review on applications, challenges and future trends', *Ad Hoc Netw.*, vol. 136, p. 102982, November 2022.

[2.72] M. Lauridsen, I. Z. Kovacs, P. Mogensen, M. Sorensen, and S. Holst, 'Coverage and Capacity Analysis of LTE-M and NB-IoT in a Rural Area', in *2016 IEEE 84th Vehicular Technology Conference (VTC-Fall)*, September 2016, pp. 1–5.

[2.73] Agustin Pelaez, 'NB-IoT vs LTE-M: Here's What The Cellular IoT Buzz Is All About', Ubidots Blog. [Online]. Available: https://ubidots.com/blog/nb-iot-vs-lte-m/

[2.74] S. R. Yoffe *et al.*, 'Low latency wireless broadcast production over 5G'.

Chapter 3

Review of Challenges and Proposed Solutions for Distribution Network with DERs

3.1 Chapter overview

In this chapter, focus is upon the challenges introduced by distributed energy resources (DERs), both from the generation and energy storage perspectives. The primary area of review and discussion will be on challenges related to the protection of power networks when DER penetration increases. As DER integration becomes more widespread, traditional protection schemes face difficulties in maintain reliability, selectivity, and stability. These challenges can disrupt the functioning of the grid, leading to miscoordination in fault detection and increased risk of cascading failures. There may also be challenges due to widespread integration of electric vehicles and electric heat pumps, which may also benefit from the protection system described in this thesis, but a detailed analysis of this is not in the scope of this work.

A particular emphasis is placed on the issues that arise in fault location, isolation, and service restoration (FLISR), which is an emerging and crucial application in power networks that incorporate DERs. FLISR is a relatively new term, but similar functions have been around for many years, often under the umbrella term "Distribution Automation" or "Distribution Network

Automation". Other related terms include "Smart Grid" or "Active Network" management functions. For the purpose of this thesis the term FLISR is used. The presence of multiple and decentralised energy sources in the grid complicates the identification and isolation of faults, thus potentially leading to delays in restoration times and higher operational costs, possibly involving penalties if the system operator is deemed to be responsible for extended outages due to them having ineffective or defective protection and FLISR systems.

After identifying these challenges, the chapter reviews various solutions proposed by other researchers to address these issues. The solutions are compared based on the methods employed, the specific problems they aim to solve, and their respective advantages and disadvantages. Through this comparison, the effectiveness and limitations of each approach are highlighted, providing a comprehensive understanding of how DER-related challenges can be mitigated in modern power systems, while it will also be shown later the gaps and shortcomings in other proposed solutions that the solution proposed in this thesis can address.

3.2 Challenges due to penetration of DERs

3.2.1 Protection challenges

The increasing integration of DERs within distribution networks can present significant protection challenges that affect system performance under both normal and fault conditions. As DERs, including solar photovoltaic (PV) systems, wind turbines, and energy storage, become more prevalent, they alter the traditional dynamics of (typically unidirectional) power flow, leading to changes in the magnitude and directions of current. This can have an impact during both normal and faulted system states. This shift complicates the operation of protection devices, which are typically designed for unidirectional power flow, thereby impacting on the processes of fault detection, protection

sensitivity, discrimination and stability, and in some cases isolation mechanisms (e.g. if fault levels are exceeded, or faults need to be isolated by devices that do not have interrupting capabilities).

Additionally, the presence of DERs can result in voltage fluctuations, imbalances, and harmonic distortion, further complicating the operation of protection schemes. These changes may lead to maloperations of protection devices, such as unnecessary tripping, which can disrupt service and increase operational costs.

The following sections provide a detailed examination of the specific protection challenges that may be encountered due to high penetration of DERs in distribution networks. This analysis aims to inform the development of effective solutions, which is discussed in the next main section of this chapter. These proposed solutions are designed to address the identified challenges, ultimately contributing to the enhanced reliability and safety of modern distribution networks.

3.2.1.1 Sympathetic tripping

Sympathetic tripping is frequently cited as a significant challenge for protection networks that incorporate DERs. In electrical power systems, protection schemes are specifically designed to detect faults and isolate affected areas, thereby preventing damage to equipment and ensuring safety. However, under certain conditions, these devices may trip unnecessarily, a phenomenon sometimes termed sympathetic tripping (although they can trip incorrectly for other reasons). Sympathetic tripping is a class of maloperation of protection where there is usually a fault somewhere in the vicinity of the maloperating protection, but this is a fault that the specific protection (i.e. the protection that may trip sympathetically) should not react to. This issue poses a considerable challenge to system reliability, particularly in networks with DERs, where the integration of renewable energy sources can exacerbate the problem. Sympathetic tripping may apply to network protection and also protection used to protect DER/DG units and their interfaces to the grid [3.1].

Sympathetic tripping can occur when network relays activate due to variations in fault current magnitude or phase associated with remote or external faults. It can also happen if faults are on the system for a longer time than undervoltage protection is designed for and can result in DG interface protection tripping unnecessarily for remote network faults – situations for which the protection has not been designed for [3.2]. This phenomenon is sometimes also referred to as false tripping [3.3]. The implications of sympathetic tripping include unnecessary outages, diminished reliability and availability of the power grid, increased operational costs through more remedial activity and possibly penalties for loss of service to customers/generators, etc.

A primary cause of sympathetic tripping in systems with distributed generators (DGs) is the bidirectional nature of power flow introduced by these generators, particularly during faults on the network [3.4] – [3.5]. Conventional protection systems in distribution networks are designed for unidirectional power flow. Consequently, when a fault occurs, the current may exhibit a sufficiently high magnitude (which increases during a fault) but it may result in the direction/angle of the current being different to (even opposite to) the normal operational power flow and current angle. Conventional protection mechanisms, such as overcurrent protection, which focus solely on current magnitude, may misinterpret this condition. They may detect a current magnitude exceeding the predetermined pick-up setting, leading to relay tripping even in the absence of a fault within the specific section.

To illustrate this concept, consider Figure 3.1, which presents a single-line diagram of a portion of a distribution network comprising three buses: one utility, two DGs, and three overcurrent relays (OCRs). Assume a fault F occurs between Bus 1 and Bus 2. All generators, including the utility and DGs connected to bus 3 and bus 4, will generate fault current directed toward the fault location, as illustrated by the green lines in Figure 3.1. OCR2 and OCR3 can detect the fault current produced by DG 1 and DG 2. If the magnitude of the fault current exceeds the set pick-up current, these relays may activate,

despite the current flowing in the opposite direction. Consequently, in the event of fault F occurring between Bus 1 and Bus 2, in extreme cases, all three OCRs – OCR1, OCR2, and OCR3 – could potentially trip (particularly if the fault is not cleared by OCR1 quickly for some reason), even though only OCR1 should ideally respond. The activation of OCR2 and/or OCR3 in this scenario is classified as sympathetic tripping. Another issue could be the DG interface protection(s) tripping as the voltage may be depressed while the fault F is present on the system – and if OCR1 does not operate sufficiently quickly (i.e. within the time delay of the DG undervoltage protection) – then there is a risk of DG operation. This could also happen with significant unbalance and other conditions that may be caused by faults in the locality of the DG interface protection.

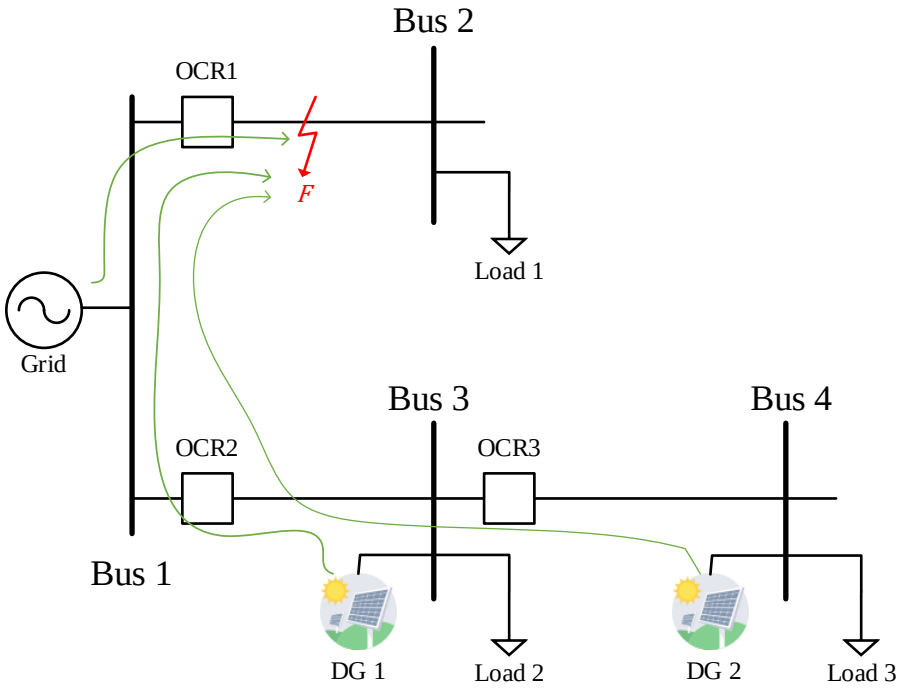

Figure 3.1: Example of sympathetic tripping

3.2.1.2 Protection blinding

Protection blinding occurs when relays are unable to detect faults due to diminished fault current levels measured by them, which could be caused by the presence of DERs in the vicinity of the fault [3.6].

Several factors may contribute to the phenomenon of protection blinding, primarily arising from alterations in the fault current profile of the power system due to presence of DER. These changes are largely driven by the DGs, especially non-synchronous sources such as solar PV systems, and the increasing amount of energy storage (also electric vehicles) could also contribute to changes in fault current profiles in the future. One significant factor leading to protection blinding is the reduced overall fault current contributions from DGs compared to grid infeeds from higher voltage levels, which are traditionally "strong" and provide high levels of fault current. Reductions in overall fault levels would be particularly evident in systems that are allowed to operate in islanded-mode in the future (and also may operate in grid-connected mode). This is not so common in many developed power systems, but could become more prevalent in the future. In traditional power systems, fault currents are predominantly supplied by synchronous generators (often connected to transmission systems, which would in turn supply fault current to distribution systems via transformers connected to the lower voltage systems), which are capable of delivering high fault current levels during system disturbances. In contrast, many DGs (and storage) typically utilise power electronic interfaces that do not provide the same of fault current [3.7]. Another contributing factor is the location of the fault in relation to the DG unit. If a fault occurs "downstream" of the DG unit with respect to the main grid infeed, the DG may effectively reduce the fault current observed by upstream protection devices. In such instances, the relay closest to the fault may fail to detect the presence of the fault (or may be slower in clearing that in should be) because the current is less than expected, or in extreme cases falls below its operational threshold |3.7|. This situation, sometimes referred to as 'under-reaching', is where the relay's zone of protection is effectively compromised due to the current contribution from the DG, and its potential to reduce "upstream" fault currents supplied from the grid (due to the DG supplying fault current and supporting the voltage at its point of connection, effectively increasing the

impedance presented to upstream relays and therefore the levels of fault current, which may slow down or "blind" upstream relays.

As illustrated in Figure 3.2, a DG is connected between protection relay R1 and R2, and the fault F is located downstream of the DG unit. In this configuration, the relative direction of the fault current supplied by the DG (denoted as $I_{f,DG}$), is from Bus 2 to fault, and voltage at Bus 1 and Bus 2 will be increased (but still depressed) compared to the fault situation of this system without any DG present. As a result, the current $I_{f,Grid}$) supplied from the grid will be relatively decreased due to the voltage being supported by DG. In some cases (particularly if the grid infeed is relatively low and the fault level from the DG is relatively high) then this reduction in fault current could lead to a situation where the protection relay R1 would operate more slowly than it should, or would not operate (e.g. in backup mode), resulting in blinding of the protection relay and prevention of its operation [3.8]. While in the diagram below R2 may operate correctly, in cases where R1 was required to operate in backup mode, then the operation of the overall protection system may be compromised.

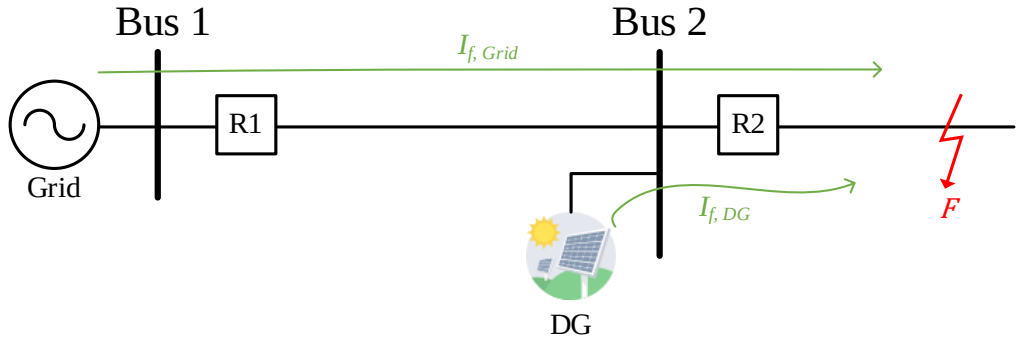

Figure 3.2: Example of protection blinding

3.2.1.3 Nuisance tripping

Nuisance tripping refers to the unintended or unnecessary activation of protective devices in the absence of a legitimate fault condition. Even in systems that do not incorporate DERs, protection mechanisms can experience

nuisance tripping due to a variety of factors. These factors include transient faults, inrush currents when transformers are energised, high currents associated with large motors starting directly, unbalance, harmonics, power quality issues [3.9] [3.10]. Note that many modern protection relays have functions to reduce or eliminate nuisance tripping, but it is still a risk for many systems. Furthermore, transient conditions in power systems, for example due to temporary disturbances in the system, such as lightning strikes or switching operations, may also cause protective devices to trip unnecessarily.

The integration of DERs introduces additional complexities in protection, both from introducing risks (such as harmonics and unbalance) and in terms of setting and coordination of protection devices. Traditional protection devices are typically designed to operate within specific voltage thresholds. However, the presence of overvoltage or undervoltage conditions – often resulting from fluctuating loads or the variability associated with DERs – can lead relays to misinterpret these voltage anomalies as fault conditions. This misinterpretation can result in unnecessary tripping, further complicating the operation of the power system and potentially leading to cascading failures if not managed appropriately [3.11] – [3.12].

One approach to "desensitising", protection is to make adjustments to protection settings, such as increasing time grading and/or thresholds to address operational errors in overcurrent protection devices when extensive amounts of DERs are connected to the protection system. However, this can lead to delays (or even non-operation) with respect to relay operation, which could lead to further problems or risks. These delays may result in the relay failing to respond in a timely manner to actual fault conditions, thereby increasing the risk of extensive damage to the system in the event of uncleared (or slowly cleared) faults, increasing the likelihood of nuisance tripping of other protection relays that should not operate for the fault in questions, tripping of generation unable to ride-through, etc. [3.13].

3.2.1.4 High impedance faults

High impedance faults (HIFs) present a distinct challenge in power system protection due to their characteristically low fault current magnitudes, which may fall below the threshold settings of conventional overcurrent protective devices. Such faults commonly arise when conductors come into contact with surfaces that restrict current flow, including dry soil, trees, or asphalt [3.14]. In these instances, the resulting low fault current is often inadequate to activate standard protective mechanisms, thereby leaving the fault undetected and posing significant risks to both equipment and public safety [3.15] – [3.17]. In certain cases, these devices may still operate; however, their response times are considerably delayed [3.18]. There can be dedicated protection to cater for this (such as sensitive earth fault) and other more costly schemes such as differential can also detect such faults, but in basic overcurrent protection schemes, this can be sometimes difficult to detect.

In this thesis, HIF detection was investigated through experimental validation. The study employed a maximum fault resistance of 50 Ω. The faulted section identification scheme demonstrates accurate and effective performance when the fault resistance is less than 40 Ω. Comprehensive details of the validation process and outcomes related to HIFs are presented in Chapter 5.

3.2.1.5 Weak infeeds

In future power systems, fault levels may decrease due to the widespread integration of DERs, with power electronics converter interfaces, at all levels of the grid, including transmission (e.g. offshore and onshore wind, solar farms etc.). These sources typically exhibit relatively low fault levels [3.19] – [3.20]. In some instances, this scenario can lead to outcomes similar to protection blinding, where certain protection schemes operate with delays or fail to operate entirely [3.21].

In this thesis, the performance of the faulted section identification scheme was evaluated under varying short-circuit levels. The lowest tested grid infeed short-circuit level was 10 MVA, for which the method continued to operate correctly and reliably. Further details regarding this aspect of the research, alongside the validation of HIFs fault identification, are provided in Chapter 5.

3.2.2 Challenges for FLISR applications

From the previous chapter, the emergence and applications of FLISR systems has been described. However, the protection and faulted section identification/location elements of FLISR schemes presented in the literature remain largely focused on traditional methods. These approaches continue to face significant challenges, as previously discussed, particularly in systems with a high penetration of DERs [3.22]. Moreover, several challenges related to circuit configuration can further impact performance such as:

- **Load sectionalising device locations:** strategic placement of these devices is crucial to effectively manage load distribution and address the intricacies of looped configurations, which can complicate fault isolation and service restoration processes.
- **Load transfers without protection devices:** altering loads through cuts, ties, and taps without corresponding protection devices. This issue can also arise during restoration actions following isolation, where configuration intended to restore service inadvertently bypasses protection coordination, increasing the likelihood of incorrect relay operations.
- **Formation of new loops during faults:** the inadvertent creation of new loops during short-circuit events can risk exceeding the equipment's withstand capabilities. Additionally, non-directional protection scheme may experience sympathetic tripping [3.4] – [3.5] .

The reliance on communication networks for monitoring and controlling the automation system can introduce vulnerabilities. Delays or failure in data

transmission can hinder the timely operation of FLISR, potentially compromising the system's effectiveness. Therefore, it is imperative to design communication infrastructures that ensure protection functions remain operational even in the event of communication degradations or failures [3.22] – [3.24].

3.3 Literature review of schemes and solutions proposed by other researchers

This section presents a critical literature review of solutions proposed by researchers to address some of the challenges associated with protection and FLISR systems, as discussed in the previous section.

The literature reveals a variety of strategies aimed at mitigating these challenges. In terms of protection-related issues, advanced and adaptive protection schemes are proposed to enhance fault detection, accelerate fault isolation, and improve the selectivity and sensitivity of protection devices. Such enhancements are essential for minimising system downtime and preventing cascading failures. With respect to FLISR, proposed solutions focus on improving fault detection and location accuracy, automating the isolation process, and expediting service restoration. These technologies aim to enhance the system's ability to respond swiftly and effectively to faults, thereby bolstering overall grid resilience and reducing outage durations.

Finally, this section, in addition to presenting an overview of existing and proposed solutions to the identified challenges, also lays the groundwork for the subsequent part of the research. It shows how the solutions proposed in this thesis build upon and extend the contributions of prior research. The novel approach introduced integrates and enhances various elements of previous work and studies/proposals, offering a more robust, adaptive, and resilient solution to the protection and FLISR challenges faced by modern power distribution networks with integration of DERs.

3.3.1 Protection solutions

The traditional design of protection schemes for distribution systems has been primarily developed for radial configurations, where the flow of power is unidirectional from source (typically the "upstream" grid via a transformer at a primary or grid supply substation) and loads are typically connected via individual (multi-section) radial feeders that supply loads directly or via other transformers. In contrast, modern and future electrical systems, such as microgrids, are characterised by multi-source and multi-loop configurations. In these modern setups, the applicability of traditional protection schemes may be significantly limited, as they may not function effectively under the complex operational conditions that arise in such environments.

To address these challenges, many novel protection schemes have been proposed and, in some cases, introduced, designed to operate effectively across a wide range of scenarios that may occur within modern networks. In this section of the thesis, several researched and proposed protection schemes are described, focusing on the methods employed and their contribution/novelty. Additionally, the advantages and limitations of each scheme are summarised and critiqued. This examination aims to provide a foundation and reference points for the scheme developed in this research, ensuring that the benefits and features of the scheme developed in this research address some of the perceived problems with network protection and build upon the reviewed and related advancements and research, thereby justifying the contribution to knowledge and the field required for the award of a PhD.

3.3.1.1 Adaptive protection schemes

The adaptive protection scheme represents one of the most extensively studied and implemented strategies in contemporary power system protection. This approach is characterised by its dynamic and flexible framework for the design and configuration of protection systems, enabling them to adjust to fluctuating network conditions. Such adaptability is particularly crucial in

modern power systems, where the integration of DERs presents new challenges to conventional protection mechanisms [3.25].

A comprehensive discussion of various methods and algorithms is presented in [3.26] [3.28]. Fundamentally, adaptive protection builds upon traditional protection schemes while incorporating the ability the modify settings in response to changing network conditions, such as load variations, fluctuations in DG capacity, and the operational modes of microgrids, which may alternate between grid-connected and islanded configurations.

In [3.26], a novel protection scheme is introduced that employs an adaptive overcurrent relay. This adaptive scheme is particularly useful in addressing protection challenges that emerge when the network operates in an islanded mode, a scenario where the potential fault current can vary unpredictably in both direction and magnitude. In such a mode, the fault current levels are often lower than those encountered under normal grid-connected conditions and can sometimes drop below the threshold required for detection and operation by traditional overcurrent relays. The method employed in the adaptive scheme is presented in the form of a flowchart in Figure 3.3, which outlines the algorithm's step-by-step operational logic.

The adaptive protection process begins with a detailed assessment of the relay settings to ensure they align with the real-time conditions and operational mode of the system, specifically adjusting the pickup current to be set at 1.5 times the maximum load current, through calculating load flows and short circuit levels. Once initial settings are in place, the algorithm actively monitors for any changes in the system's operating conditions. If no changes are detected, the relay settings remain consistent; however, if any significant changes are identified – such as variations in load or the status of DG connections – the system automatically recalibrates the relay settings to reflect the new environmental conditions. This real-time adjustment is facilitated by integration with SCADA, which enables continuous monitoring and rapid response to dynamic system changes.

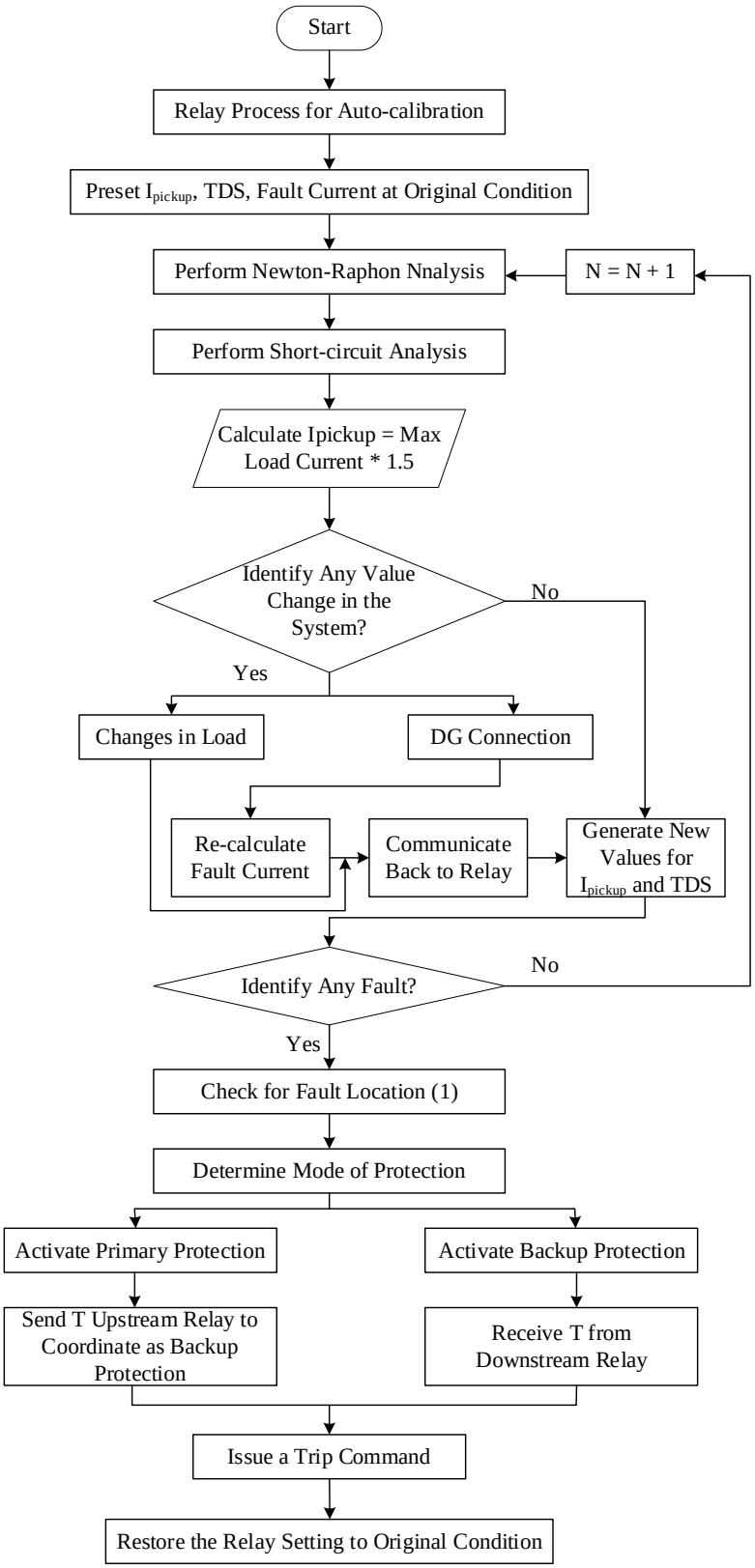

Figure 3.3: Algorithm of adaptive overcurrent protection as presented in [3.26]

To validate the effectiveness of this proposed adaptive overcurrent scheme, the authors employed the Electrical Transient Analyser Programme (ETAP) software and selected the IEEE 9-bus benchmark as the case study model. Simulation results indicate that the adaptive relay demonstrates superior performance compared to conventional overcurrent relays, with notable improvements in selectivity, reliability, and sensibility, as well as significantly faster operation speed. However, the system's reliance on real-time monitoring and calculation of load/short circuit levels introduces certain challenges, particularly the need for numerous sensors to enable continuous data collection across the network. While the simulation is this case study was limited to a 9-bus system, real-world distribution systems are generally much larger and more complex. This increased scale raises the potential for communication delays or data loss during transmission between sensors and control units, which could impact the performance of the adaptive protection scheme in practical applications.

Another adaptive overcurrent protection scheme is presented in [3.27], where the sequence components of both voltage and current are measured using voltage and current transformers to detect all types of faults. The current measurements are utilised to identify overcurrent situations, while voltage measurements are employed to monitor overvoltage or undervoltage conditions. When an overcurrent event occurs, it is detected by an overcurrent relay, which also determines the tripping time based on the Inverse IDMT characteristics [3.29]. If a disturbance in voltage is detected for a sustained duration, the CB is tripped using the appropriate command in response to overvoltage or undervoltage conditions. This algorithm distinctly separates the operational modes for grid-connected and islanded modes, as illustrated in Figure 3.4. This system also includes additional functionality, such as event reporting, data logging, and communication links. Wireless communication is recommended for centralised control due to its low installation cost, rapid deployment, high mobility, and ability to reach remote locations. However, in instances where a fault cannot be easily resolved, manual intervention is required for fault

clearance, followed by a "black start" procedure to restore the system to islanded mode after each manual clearance.

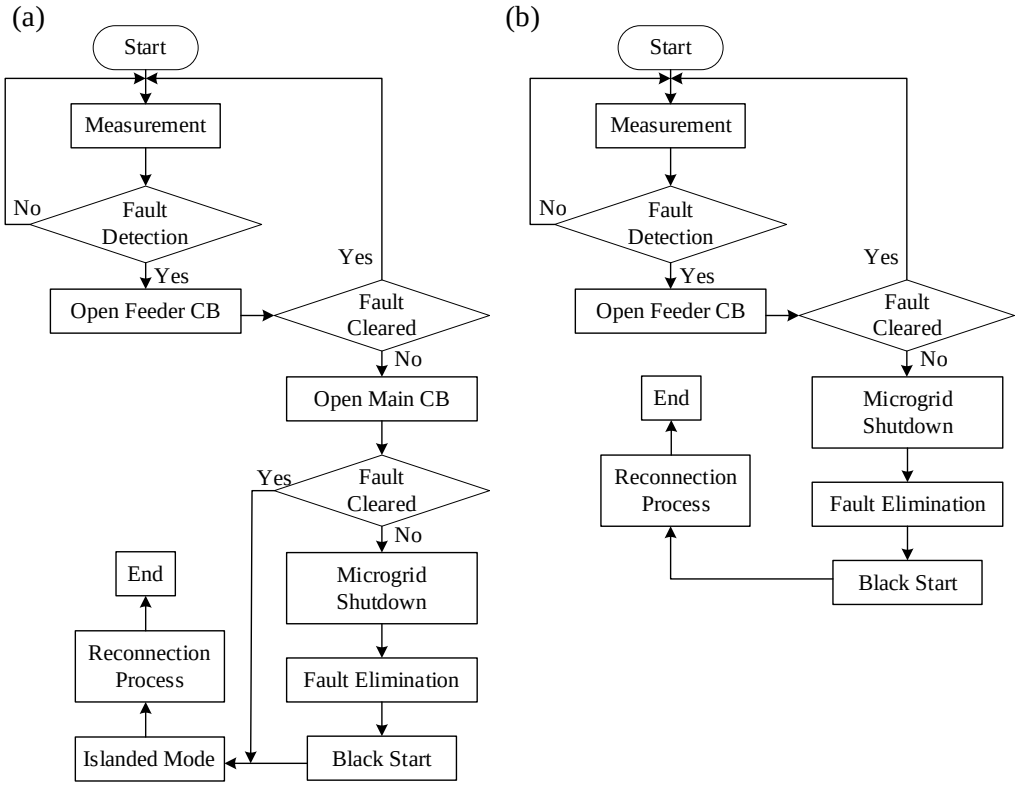

Figure 3.4: a) Protection scheme in grid-connected mode (b) Protection scheme in islanded mode of operation as presented in [3.27]

While the scheme demonstrates adaptability to different operating modes within a microgrid, it does not present experimental results under varying system configurations, nor does it consider situations such as non-fault load changes or disconnection of DGs. Moreover, although the settings are adjusted automatically in response to mode transitions, the initial configuration still requires manual input. This indicates that, in cases where the system topology is altered (even prior to the commencement of simulation), manual recalculations and reconfigurations are still necessary. As a result, the approach may be unsuitable and overly complicated to configure for systems characterised by frequency-changing topology and operational modes, which are typical features of modern microgrids, and in future may be more prevalent for "normal" grids.

The scheme presented in [3.28] introduces differential adaptive protection schemes capable of adjusting protection setting parameters in response to changes in the system's operational mode. The validation of this approach was conducted using DIgSILENT software, simulating practical conditions from a microgrid located in the Pedernales province of the Dominican Republic. The effectiveness of the differential adaptive scheme was compared to that of the conventional differential method under two distinct network conditions. The first scenario involved the microgrid being connected to the National Interconnected Electric System (SENI), while the second scenarios examined the microgrid in isolation, leaving a 15 GW PV plant as the sole power source for the microgrid. The results indicated that the adaptive differential scheme could trip significantly faster – 16 times quicker – than the conventional differential method when the microgrid was connected to the utility. This difference seems to be almost non-credible, but the authors state that an operating time of 320 ms can be taken for the standard differential, with 20 ms for the adaptive differential. During islanded mode the traditional method failed to clear faults due to its inability to identify the fault conditions in this scenario, resulting in protection blinding for the fault – again, this appears to be somewhat unrealistic as differential should operate with immunity to fault level changes. but this is what the authors state. In islanded mode, the adaptive method successfully detected the fault. Although the paper effectively highlights the performance advantages of adaptive differential protection over non-adaptive methods, it lacks a detailed explanation of how the system detects changes and how the algorithm adjusts to new situations. Additionally, it does not address the communication methods between the two measurement relays, which is crucial for understanding the overall functionality and costs of the adaptive protection scheme. Moreover, while the authors report a 16 times speed improvement of adaptive differential protection (20 ms vs. 320 ms), the comparison of the fastest response time of the adaptive method to a slower-case scenario from the conventional scheme may not provide a fully balanced assessment of overall effectiveness. A more balanced evaluation would involve

comparing average or median trip times under similar fault conditions and more detailed descriptions of various factors associated with the scheme.

A summary of the above protection schemes, plus several other various adaptive protection schemes that were reviewed (with reviews only presented in summary format due to the high number of papers in this field), is presented in Table 3.1. This table outlines the method employed in each scheme, as well as their associated benefits and limitations.

Table 3.1: Summary of proposed adaptive protection schemes

Reference	**Summary of Method**	**Contributions claimed**	**Limitations**
[3.26]	The approach adjusts relay settings in real time using SCADA-based monitoring, setting the pickup current at 1.5 times the maximum load, based on load flow and fault analysis.	The scheme improves protection under islanded conditions by enhancing sensitivity, selectivity, and speed through dynamic, system-aware relay behaviour.	The method relies on continuous data from multiple sensors and real-time communication, which may lead to delays or data loss in large-scale practical systems.
[3.27], [3.29]	The scheme uses sequence components of voltage and current to detect faults, combine overcurrent detection with voltage-based tripping logic.	Accommodates both grid-connected and islanded modes, and includes features such as event reporting, logging, and wireless communication	Lack of simulation under dynamic conditions, relies on manual initial setup, and is less suited for systems with frequent topological changes.
[3.28]	Apply differential adaptive protection that adjusts settings based on operational mode.	Validate via DIgSILENT using a real microgrid case study, and demonstrate significantly faster fault clearance, while maintain effective operation under both modes.	The paper omits explanation of detection and adjustment mechanisms, lacks detail on relay communication, and may present a skewed performance comparison.

Table 3.1 (cont.): Summary of proposed adaptive protection schemes

Reference	Summary of Method	Contributions claimed	Limitations
[3.30]	A centralised controller evaluates the fault current by analysing it against the cumulative generation input under normal operational conditions.	The scheme's accuracy is high when DG is connected to the grid. It is suitable for systems with large amount of DGs present.	Require high performance of PMUs. The recalculations are necessary whenever additional DGs or loads are connected.
[3.31]	Time Dial Setting (TDS) parameters in recloser are adjusted based on the ratio of recloser current (IR) to fuse current (IF).	Validation of the method using hardware-in-the-loop (HIL) simulation, ensuring the scheme's performance is practical and can be implemented.	Require validation under different topology such as variation of load or DG locations. May be too complex too set in a practical application.
[3.32]	The relay settings are calculated offline for both grid-connected and islanded modes. Once the network is operational, the relay settings dynamically adapt to the monitored conditions	Can reduce the operational time since the computations are pre-processed during the offline phase.	Fast detection of microgrid islanding is required. Reliable communication between numerical relay and CBs is necessary.
[3.33]	Incorporate an adaptive directional overcurrent relay (DOCR) and a directional earth fault relay.	Validate across various fault types and operational conditions of the system, including scenarios with and without DG penetration.	Require IEDs, a control centre, and real-time communication. Lack of backup protection mechanisms.

Overall, adaptive protection schemes are expected to operate effectively in all scenarios, including both grid-connected and islanded modes, while accommodating various conditions such as long changes, fault currents, and power flow variations. By functioning as smart self-monitoring systems,

adaptive protection schemes aim to perform all necessary functions automatically, which aim to facilitate enhanced overall system performance, reliability, and selectivity within networks.

However, the implementation of smart monitoring capabilities introduces a level of complexity that necessitates the integration of advanced intelligent technologies, often increasing cost, complexity and perhaps making it difficult to ensure the deterministic operation of the system under all possible scenarios. Specifically, these systems require multifunctional microprocessor or numerical relays, which must encompass a range of features, multiple setting options, and robust algorithm processing capabilities. Additionally, these relays should be able to interact seamlessly with other IEDs within the network. The flexibility of logic schemes is also essential, as these systems must adapt to real-time conditions.

The operational logic of adaptive protection requires that settings be adjusted in response to changing grid operations and conditions. Although some adaptive protection schemes can automatically recalibrate their settings, this process may still involve time-consuming calculations, especially when faced with new network situations. If a fault occurs immediately after a change in network conditions, the adaptive protection system may struggle to respond effectively, highlighting a potential vulnerability in its design. This challenge emphasises the importance of ensuring that adaptive protection systems are not only responsive but also capable of rapid recalibration to maintain system integrity.

History has shown that for more complex systems (not just protection), the possibility of (often human-introduced) errors increases, so this must be borne in mind when considering any "advanced" protection system, particularly given the highly-critical nature of protection functions in terms of maintaining supplies and avoiding dangerous conditions, and potential blackouts. The balance between complexity and simplicity and potential for error must always be maintained. One of the major benefits of the scheme developed in this

research is its simplicity, immunity from changing system configurations and conditions, and ease of application.

Moreover, the necessity for continuous monitoring of network conditions means that a substantial number of sensors are required to collect real-time data for adjusting relay settings. This requirement raises concerns about cost-effectiveness, as deploying numerous sensors can be financially burdensome. Additionally, high-speed communication infrastructure – and potentially high bandwidth for large data transmissions – is essential for optimal performance. However, a significant gap exists in the literature regarding the communication data requirements that are integral to the effective functioning of protection schemes.

In addition, the increasing integration of Internet of Thing (IoT) into power systems further complicates the landscape of adaptive protection. While IoT technologies offer enhanced monitoring and control capabilities, they also introduce cybersecurity challenges. Finally, the issue of standardisation and regulatory barriers remains a significant challenge in the field of adaptive protection. Currently, there is no universal standard governing the implementation and operation of adaptive protection schemes, which complicates their widespread adoption [3.34]. The lack of standardisation protocols can lead to inconsistencies in system performance and interoperability among different devices and manufacturers. As the industry continues to evolve, establishing universal standards will be crucial for overcoming these regulatory challenges and facilitating the integration of adaptive protection system into existing power distribution networks.

3.3.1.2 Directional-based solutions

In addition to adaptive protection methods, which rely on real-time (or periodic/responsive) adjustment of relay settings based on the topology and configuration of the power system, alternative approaches are also proposed and are attractive, particularly those that do not require complex schemes for dynamic setting coordination.

Given the protection challenges posed by DERs – notably bidirectional power flow and fluctuating fault levels in distribution networks – directional-based protection schemes offer a promising solution. One such method involves detecting the direction of faults using phasors derived from voltage and current measurements captured during fault conditions.

[3.35] provides a comprehensive overview of the fundamental principles and practical implementations of directional overcurrent protection. It explores various established techniques included using quadrature voltage combined with Maximum Torque Angle (MTA) settings, as well as symmetrical component analysis is to determine the direction of fault current. However, one of the main drawbacks of relying on voltage measurement is that it may fail to determine the fault direction when the fault occurs in close proximity to the relay, due to the substantial voltage collapse at the measurement point [3.36]. There is also the additional expense associated with providing voltage measurements. Notably, voltage measurements are not required in the scheme developed through this research.

Another paper proposes a novel algorithm for directional protection based on the cross-correlation of Fast Fourier Transform (FFT) components of voltage and current for each phase [3.37], as method illustrated in Figure 3.5. Fault detection is performed by applying the k-nearest neighbour (k-NN) algorithm to the instantaneous power sample is compared an adaptive threshold. Once a fault is detected, the direction is identified by applying cross-correlation between the voltage and current FFT components to determine whether the fault is in the forward or reverse direction with respect to the relay location. While the method demonstrates high accuracy and speed under various conditions, it lacks discussion on robustness against noisy measurement or signal distortion. The FFT should assist with this, but the method may be sensitive to time-window alignment, especially in system with rapidly changing dynamics. Moreover, it requires both voltage and current measurement devices, as mentioned before, which can be costly.

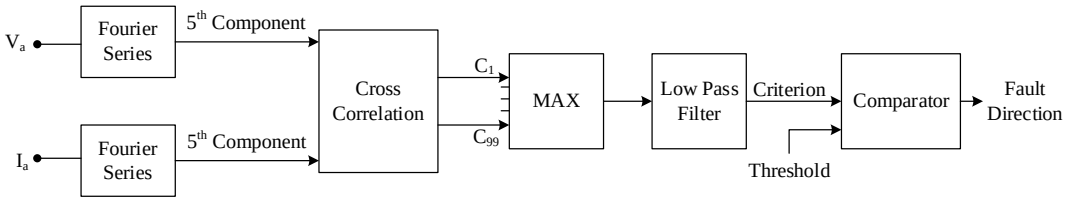

Figure 3.5: Directional protection using k-NN and cross-correlation (adapted from [3.37])

Furthermore, in voltage-based schemes, if a fault occurs in close proximity to the relay's measurement point, the polarisation function may be impaired due to significantly reduced voltage levels. This reduction can hinder the accurate determination of fault direction or phase in such 'close-in' fault scenarios [3.36]. Current angles may fluctuate slightly under normal conditions, depending on the nature of the loads and the power system from which the measurement is being taken. However, when faults occur, the current angle value will typically change considerable from its pre-fault value due to some or all of the load being short circuited and the system between the measuring point and the fault usually being mostly reactive in terms of its impedance (while loads and the power systems are normally more resistive, or controlled to be more resistive in nature). Consequently, current-only directional scheme may represent a good choice to determine the fault current direction and therefore location when comparing multiple measurements or solely directional voltage-based schemes.

The work presented in [3.38] introduces a fault direction estimation method based on the analysis of current waveforms in the time domain, utilising both pre-fault and during-fault current signals. However, the paper does not explicitly address the fault detection stage, which is a necessary precursor to any directional assessment. Moreover, the measurement of time-domain raw waveform signals inherently includes noise, harmonics, and potential frequency deviations, which could lead to maloperation of the protection system under certain conditions. In addition, the scheme requires knowledge of the power flow direction prior to determining fault direction. This is achieved through the

calculation of directional normal power (DNP), which relies on voltage measurements as reference. Therefore, the technique cannot be considered a truly current-only directional protection method as researchers said, as it still depends on voltage information during the pre-fault period for initial polarisation.

In [3.39] and [3.40], alternative schemes for determining current direction are described, including the use of Kalman filters and Discrete Fourier Transform (DFT) methods, as substitutes for direct time-domain signal processing. Both studies assume the pre-fault current is directed from the source towards the grid, as illustrated in Figure 3.6.

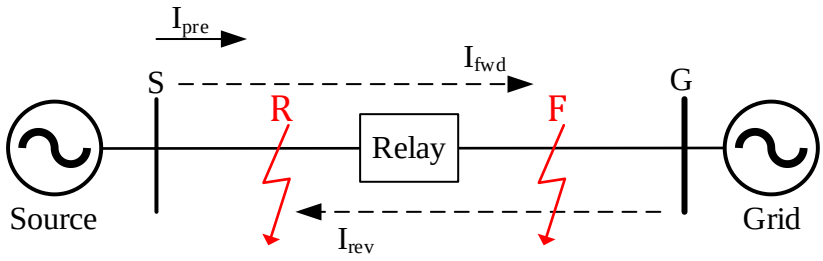

Figure 3.6: Directional relay: Forward (F) and reverse (R) fault (adapted from [3.40])

In [3.39], the Kalman filter is employed to estimate the current phasor, using the positive-sequence components of the pre-fault and during-fault current signals to determine whether the fault is in the forward or reverse direction. The overall process of fault direction estimation is depicted in Figure 3.7. However, similar to the approach in [3.38], this scheme does not specify when or how the phasor determination is triggered. It is also worth noting that although the Kalman filter is a well-known technique for signal estimation, it might not be the optimal choice in the context of harmonic distortions, computational speed, or algorithm complexity. These factors can limit its practical applicability, particularly under highly dynamic or distorted operating conditions. Furthermore, this method only evaluates the method under single-phase-to-earth and phase-to-phase faults, omitting more complex and

practically significant scenarios such as double-phase-to-earth and balanced three-phase faults. High-impedance faults are also not tested – the research reported in this publication only considers a fault resistance of 0.1 Ω – which may be insufficient to represent real-world fault conditions that often involve variable and higher fault impedances.

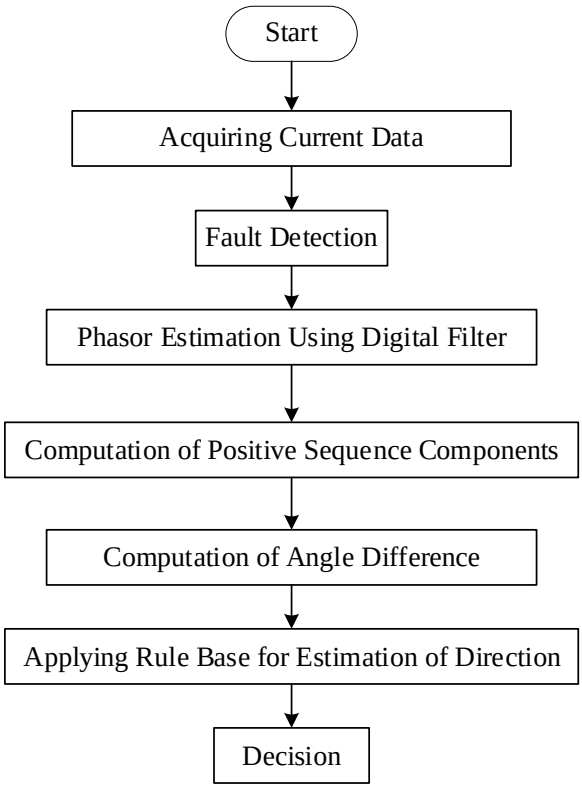

Figure 3.7: Flowchart diagram of relay algorithm described in [3.40]

In [3.40], a similar method is employed for fault direction determination, but with DFT used for phasor computation. DFT-based scheme inherently offers better noise rejection. Since DFT focuses on extracting the fundamental frequency components, it effectively filters out high-frequency noise and harmonic distortions, thereby increasing robustness against signa interference. Moreover, as the proposed relay is overcurrent-based, the pickup current is used as a threshold for fault detection. However, neither [3.39] nor [3.40] considers scenarios in which the power flow direction reverses. In such cases, the difference between forward and reverse faults may become ambiguous if the relay direction settings are not adjusted accordingly. Moreover, both studies

fail to consider non-fault disturbances such as load changes, which can also result in significant variations in current direction. Without explicit mechanisms to differentiate between genuine faults and operational disturbances, these schemes may be vulnerable to false tripping or exhibit a lack of security under practical conditions.

The study presented in [3.41] employs conventional overcurrent protection using Time Multiplier Settings (TMS) in combination with a basic directional relaying method, as previously described in [3.35]. This approach enables coordination among multiple overcurrent relays and helps to mitigate sympathetic tripping in bidirectional power systems. However, in multiple-infeed systems, power flow direction can vary depending on operating conditions. As such, prior knowledge of the power flow direction is essential for the method to function correctly. The validation in the referenced work is conducted using a fixed network topology or configuration, along with a constant load capacity. This limitation may lead to incorrect relay operation when applied to systems with dynamic configurations, which is a characteristic feature of modern distribution network with high penetration of DG.

[3.42] reports on a scheme which utilises the direction of negative sequence power, combined with the negative sequence current suppression strategy typically implemented in inverter-based DG, to determine fault direction. The approach estimates the fault direction based on the line impedance angle during the fault period. However, calculating the line impedance requires both voltage and current measurements, as previously discussed, which introduces additional costs and potential limitations. Voltage measurements, in particular, are known to be unreliable during close-in faults due to voltage collapse, and the reliance on multiple sensors significantly increases installation cost and complexity. Furthermore, the scheme's use of only the negative sequence component inherently prevents the detection of balanced faults, an omission that may be inadequate for practical deployment in realistic application environments.

Another pilot directional protection scheme that is solely current-based, utilising phasor measurements of the positive sequence fault current to

discriminate between internal and external faults is proposed in [3.43]. The method does not require prior knowledge of the system's power flow direction, as it relies on phase angle differences of the fault components before and after the fault event. However, the scheme depends on real-time communication to continuously exchange current phasor information between measurement locations. This imposes strict requirements on the communication infrastructure, particularly in terms of speed and latency, which are not addressed in the paper. The simulation studies conducted in the paper do not include single phase-to-earth faults, which are the most common fault type in practical distribution networks. Additionally, in systems where one source is weak or disconnected, the resulting current phase angle differences may be unreliable, thereby limiting the scheme's dependability under such operating conditions.

In [3.44], a novel method is proposed that introduces a directional protection scheme which does not rely on pilot communications or prior knowledge of system power flow direction. Instead, it determines the fault direction solely based on post-fault current. The approach utilises a "Directional Detector" (DD) to identify fault direction, with the algorithm shown in Figure 3.8. According to this method, if the computed DD – obtained via the S-Transform – yields a value of $+90^{o}$, the fault is classified as forward; conversely, a value of -90° indicates a reverse fault. The authors suggest that this scheme does not require prior knowledge of the power flow direction, enhancing its adaptability. However, no experimental validation is provided to support this statement. Additionally, the algorithm requires the fault current to stabilise before it can make a decision, preventing ultra-fast operation. This poses a significant limitation in scenarios involving situations such as close-in faults, where significant current distortions may occur during the initial transient phase. Delayed operation in such cases could result in system damage or safety hazards before the relay activates. Furthermore, the validation of the method is limited to offline simulations, and its robustness under real-time conditions remains uncertain. It is also important to note that the proposed scheme does not

include a defined mechanism for initial fault indication, focusing solely on fault direction estimation.

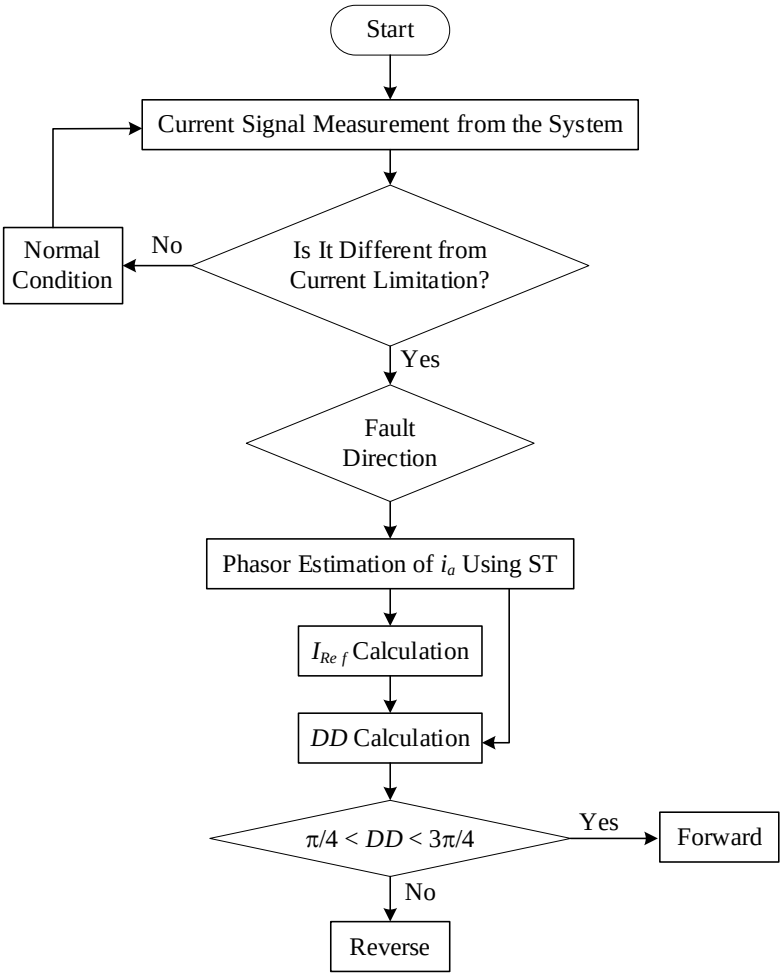

Figure 3.8: Directional protection algorithm proposed in [3.44]

Several other researchers have proposed directional-based protection schemes, which have also been reviewed. A summary of all the papers discussed above, as well as other reviewed works that were not described in detail, is presented in Table 3.2.

Table 3.2: Summary of directional-based schemes protection

Reference	Summary of Method	Contributions claimed	Limitations
[3.35]	Provide an overview of the existing directional protection techniques.	Explain the basic method used in practical relays.	The scheme requires both voltage and current measurements, leading to higher implementation costs. Voltage measurement are less reliable for close-in faults.
[3.37]	Utilise the k-NN algorithm for fault detection, followed by cross-correlation to determine the fault direction.	Detect faults extremely quickly ($<$ 1 ms) and determine fault direction within 8 ms with high accuracy.	Lacks discussion on robustness against noisy measurements and signal distortion, particularly in systems with rapidly changing dynamics. Additionally, it requires both voltage and current measurement devices, which may incur high installation costs and rely on accurate real-time data and communication infrastructure.
[3.38]	Fault direction estimation is based on the analysis of current waveforms in the time domain, utilising both pre- and during-fault current signals.	Uses a current-only based scheme, making it less susceptible to issues such as low voltage during close-in faults	The scheme does not address the fault detection stage, essential for directional assessment. Raw waveform signal measurements may include noise and harmonics, risking maloperation. The scheme relies on prior knowledge of power flow direction and uses voltage measurement for initial polarisation, making it not truly current-only.
[3.39]	Methods based on positive-sequence components and Kalman filter techniques are used to determine current direction	Only current-based scheme, eliminates the need for voltage measurements.	Lack of clarity on phasor determination triggering. The Kalman filter may not be optimal during excessive harmonic distortion or dynamic conditions. The study only considers simple fault types and low fault resistance.

Table 3.2 (cont.): Summary of directional-based schemes protection

Reference	Summary of Method	Contributions claimed	Limitations
[3.40], [3.45]	The method determines fault direction using DFT-based current phasor computation, following a principle similar to [3.39]	A current-only method with resilience to noise, harmonics, and distortion, incorporating a neutral setting to avoid maloperation under uncertain conditions.	The method does not account for power flow reversals or non-fault disturbances, increasing the risk of maloperation due to unclear fault direction and insufficient discrimination.
[3.41]	Uses overcurrent protection with adaptive and variable TMS setting alongside a basic directional relaying approach	Coordination application mitigates sympathetic tripping in systems with bidirectional power flow by ensuring selective and stable relay operation.	The method relies on prior knowledge of power flow direction, making it unsuitable for systems with dynamic configurations. Validation under fixed conditions may limit its practical applicability in modern network with high DG penetration.
[3.42]	Determines fault direction using negative sequence power and current suppression strategies in inverter-based DG, with estimation based on the line impedance angle during faults.	Does not require prior knowledge of power flow direction.	Requires both voltage and current measurements, increasing cost and complexity; voltage measurements are unreliable during close-in faults, and reliance on negative-sequence components may prevent detection of balanced 3-phase faults.

Table 3.2 (cont.): Summary of directional-based schemes protection

Reference	Summary of Method	Contributions claimed	Limitations
[3.43]	A fully current-based pilot protection scheme using phasor measurement of positive-sequence currents for pre- and during-fault current conditions to distinguish internal from external faults	Does not require prior knowledge of power flow direction, relying instead of phase angle difference of fault components before and after the events.	The scheme relies on real-time communication with strict latency requirements, which are not addressed in the paper. It is sensitive to noise, system unbalance, and may be unreliable with weak or disconnected sources. Common fault types like single-phase-to-earth fault are not considered in the validation.
[3.44]	Determines fault direction using a DD computed via the S-Transform.	Determines fault direction solely from post-fault current, without relying on pilot strategies or prior knowledge of power flow direction.	Lacks experimental validation and relies on stabilised fault current, delaying operation during severe transients. The method is only validated through offline simulations and lacks a mechanism for fault indication/initiation of operation.
[3.46]	Detects faults using current variation or step comparison, and determines fault direction based on the characteristic of pre- and post-fault current.	A current-only method capable of detecting faults very rapidly, in less than 1 cycle.	Requires prior knowledge of power flow direction, making it unsuitable for systems with variable configurations and operating modes.

Table 3.2 (cont.): Summary of directional-based schemes protection

Reference	Summary of Method	Contributions Claimed	Limitations
[3.47]	Uses overcurrent for fault detection, followed by comparison of the cosine of current angle differences, computed by Fourier Transform, between two relays in the pre- and post-fault periods to identify the faulted zone.	Suitable for grids with multiple infeed sources, requiring no prior knowledge of power flow direction and resistance to noise.	The method may not be sensitive to systems with weak infeed or low fault levels due to the use of overcurrent for fault detection. It is unsuitable for single-infeed systems, as the fault current angles are unreliable. There is no experimental validation using real-time HIL or communication.
[3.48]	Uses positive-sequence voltage and current to calculate the vector impedance (Z) matrix, which is then used to determine the fault direction.	Experimental validation is conducted across various scenarios, including different fault types, high fault impedance, power flow changes, and close-in faults, to assess the accuracy of the results.	Requires both voltage and current measurement sensors, increasing costs, and may be susceptible to noise and harmonic disturbances.

It can be observed that directional-based schemes are a viable solution for modern distribution networks with DGs, which often pose challenges to conventional protection systems – particularly in relation to sympathetic tripping and nuisance tripping. Unlike adaptive schemes, directional-based approaches do not necessarily require real-time setting reconfiguration, yet can still provide effective protection by determining the fault direction using voltage and/or current measurements.

However, voltage-based schemes face significant limitations in the case of close-in faults, where the voltage magnitude at the relay location may be

severely reduced, leading to inaccurate fault direction estimation. Moreover, the requirement for both voltage and current sensors increases the number of sensing devices, thereby raising the overall cost of the scheme. As a result, current-only directional protection schemes offer an attractive alternative. However, for non-unit systems – where a relay operates independently of others and typically has no communications – prior knowledge of the system's power flow direction is often essential for the fault detection process. This makes such methods less suitable for distribution networks with multiple infeeds and inherently variable, bidirectional power flows.

To overcome this, integrating communication to enable unit (pilot) protection, which allows for the localisation of faulted sections, becomes an attractive option. Even though some studies have proposed approaches that do not require communication or prior knowledge of power flow direction, these methods may still present certain limitations (as, for example, previously described in the thesis's review in [3.44]).

However, the majority of current-only, directional-based pilot protection schemes rely heavily on continuous data exchange, such as that used by differential schemes. This necessitates high-performance, low-latency communication links to prevent false tripping caused by phasor misinterpretation due to communications propagation delays. Furthermore, none of the reviewed work has demonstrated real-time validation e.g., using hardware-in-the loop (HIL) with actual communication systems, highlighting a research gap that the work in this thesis addresses.

There are several other AI-based and machine learning/intelligent protection schemes reported in the literature; however, these are not reviewed here as this work is focussed on a deterministic and logical form of faulted section identification for protection and/or monitoring applications; therefore comparison with such techniques, which have not been used in any practical applications to the knowledge of the author and supervisor, is not warranted. A review of applications of such techniques is contained in [3.49] – [3.52].

3.3.2 FLSIR solutions

As stated earlier, the adoption of FLISR systems is growing and in some cases they are becoming an integral component of modern distribution networks, aiming to enhance reliability by swiftly isolating faults and minimising service interruptions through minimising of isolation, accurate fault location and/or section identification, plus rapid and often automated network reconfiguration and restoration following faults. While FLISR is an emerging term, the functionality has been researched and introduced for many years, often with terms such as "distribution automation" or "distribution network automation" being applied. However, many existing FLISR implementations are built upon conventional protection schemes that present notable limitations, particularly in environments where the network configuration may change regularly, and the system may operate in islanded mode. The increasing integration of DERs further exacerbates these challenges, as traditional protection logic often struggles to accommodate bidirectional power flows and variable current contributions.

Studies presented in [3.53] – [3.54] illustrate the deployment of FLISR using fixed-time overcurrent protection, coordination with sectionalising devices and reclosers. While both publications provide comprehensive simulations demonstrating FLISR performance under fault scenarios, they adopt static protection setting that are preconfigured based on fixed network topologies. This approach, although effective under normal operating conditions, fails to account for changes in topology resulting from restoration actions or planned maintenance. Consequently, the preconfigured protection settings may become misaligned with the real-time network conditions, leading to coordination failures such as nuisance tripping or a failure to isolate genuine faults – challenges previously highlighted in earlier sections of this thesis. Moreover, in [3.53], non-directional protection schemes are also utilised, further increasing the risk of sympathetic and/or slow/non-tripping under such different scenarios and contexts.

To address the limitations posed by static protection settings, [3.55] proposes a protection scheme that leverages multiple setting groups for overcurrent relays, as displayed in Figure 3.9, allowing protection logic to adapt to changes in network topology. These setting groups are pre-calculated through offline studies and dynamically selected based on real-time topology updates received by a central controller. While this approach enhances flexibility and protection accuracy, the authors acknowledges that its successful operation depends heavily on an effective and highly reliable communication infrastructure to receive configuration changes and transmit control commands to the appropriate devices. This requirement may render the scheme costly and potentially infeasible in some application environments.

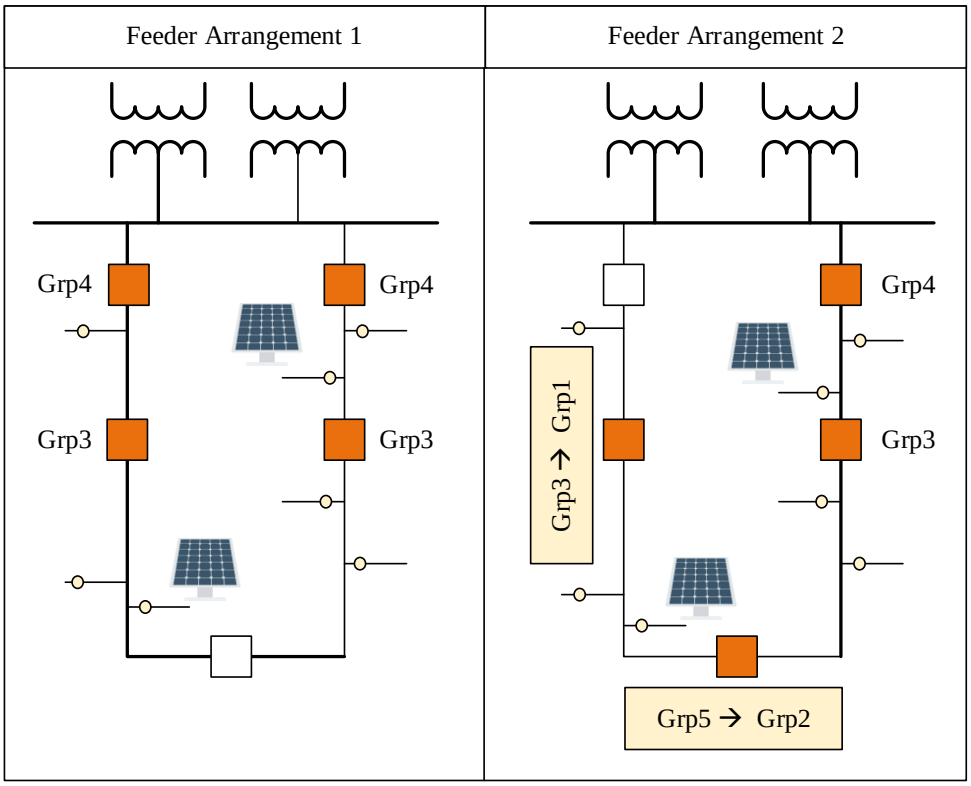

Figure 3.9: Setting group modifications as reported in [3.55]

Another related study, presented in [3.56], introduces an alternative semi-decentralised adaptive protection strategy, in which IEDs autonomously reconfigure their setting via IEC 61850-based GOOSE messaging, as shown in Figure 3.10. The scheme maintains a localised decision-making capability at

the substation and device level, while still depending on higher-level supervisory units as the Substation Automation Unit (SAU) to perform configuration management. Although this architecture improves response times and reduces dependency on a centralised Distribution Management System (DMS), it also introduces notable complexity. Coordinating peer IEDs using GOOSE in large-scale networks may pose challenges in terms of maintenance, scalability, and system integration.

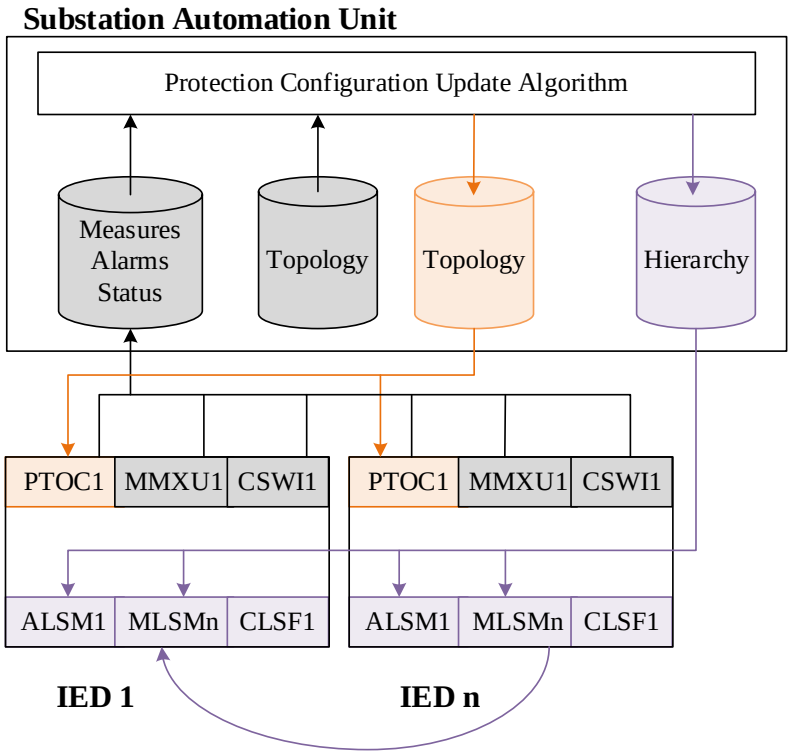

Figure 3.10: Protection configuration in a substation automation unit adapted from [3.56]

[3.57] introduces the operational concept of non-communicative FLISR, wherein devices operate purely based on local sensing and pre-programmed logic without any data exchange between components. While this approach mitigates challenges associated with communication links between IEDs, and offers a cost-effective solution requiring minimal communication infrastructure, it is inherently constrained in its capacity to handle complex fault scenarios.

Furthermore, no simulation-based demonstrations have been presented to substantiate the performance or reliability of this architecture.

These studies collectively highlight that while advanced and adaptive protection schemes have the potential to significantly improve FLISR system responsiveness in dynamic environments, they often introduce communication or architectural burdens that can hinder their practical deployment. This underscores the need for FLISR schemes that can maintain adaptability without excessive reliance on bandwidth-heavy, highly deterministic communication infrastructures or complex device-to-device coordination mechanisms.

3.4 Chapter summary

This chapter has presented protection and FLISR challenges associated with modern distribution systems incorporating DGs. In addition, various solution approaches proposed to address these challenges have been introduced and critically reviewed. With regard to protection challenges, adaptive protection has been explored as a promising approach, characterised by its ability to adjust protection settings in real-time in response to changes in network mode and topology. Furthermore, directional-bases schemes have been examined as a viable option, particularly for systems with bidirectional power flows. The advantages and limitations of these solutions have been analysed in order to identify research gaps that the work reported in this thesis seeks to address. Similarly, key methods related to FLISR application have also been evaluated, with a focus on those most relevant to the evolving characteristics of modern distribution networks.

Chapter references

[3.1] *Engineering Recommendation G99*, March 04, 2024. [Online]. Available: https://dcode.org.uk/assets/uploads/files/ENA_EREC_G99_Issue_1_Amendment_10_(2024).pdf

[3.2] J. Roberts, T. L. Stulo, and A. Reyes, 'Sympathetic Tripping Problem Analysis and Solutions', May 2002.

[3.3] V. Telukunta, J. Pradhan, A. Agrawal, M. Singh, and S. G. Srivani, 'Protection challenges under bulk penetration of renewable energy resources in power systems: A review', *CSEE J. Power Energy Syst.*, vol. 3, no. 4, pp. 365–379, December 2017.

[3.4] T. Seegers *et al.*, 'Impact of Distributed Resources on Distribution Relay Protection', August 2004.

[3.5] K. I. Jennett, C. D. Booth, F. Coffele, and A. J. Roscoe, 'Investigation of the sympathetic tripping problem in power systems with large penetrations of distributed generation', *IET Gener. Transm. Distrib.*, vol. 9, no. 4, pp. 379–385, 2015.

[3.6] T. Gallery, L. Martinez, and D. Klopotan, 'IMPACT OF DISTRIBUTED GENERATION ON DISTRIBUTION NETWORK PROTECTION', *ESBI Eng. Facil. Manag.*, 2005.

[3.7] M. S. Turiman, M. K. N. M. Sarmin, N. Saadun, L. C. Chong, H. Ali, and Q. Mohammad, 'Analysis of High Penetration Level of Distributed Generation at Medium Voltage Levels of Distribution Networks', in *2022 IEEE International Conference on Power Systems Technology (POWERCON)*, September 2022, pp. 1–6.

[3.8] B. J. Brearley and R. R. Prabu, 'A review on issues and approaches for microgrid protection', *Renew. Sustain. Energy Rev.*, vol. 67, pp. 988–997, January 2017.

[3.9] J. Lu, D. Zhao, and W. Han, 'Analysis and mitigation of inrush current-induced nuisance tripping in transformer protection', *Electr. Power Syst. Res.*, 2020.

[3.10] G. Escrivá-Escrivá, C. R. Porta, and E. C. W. de Jong, 'Nuisance tripping of residual current circuit breakers in circuits supplying electronic loads', *Electr. Power Syst. Res.*, vol. 131, pp. 139–146, February 2016.

[3.11] [W. G. Hartmann, 'How to nuisance trip distributed generation', in *Rural Electric Power Conference, 2003*, May 2003, pp. C5–C5.

[3.12] D. R. Bhise, R. S. Kankale, and S. Jadhao, 'Impact of distributed generation on protection of power system', in *2017 International Conference on Innovative Mechanisms for Industry Applications (ICIMIA)*, February 2017, pp. 399–405.

[3.13] A. B. Nassif, 'An Analytical Assessment of Feeder Overcurrent Protection With Large Penetration of Distributed Energy Resources', *IEEE Trans. Ind. Appl.*, vol. 54, no. 5, pp. 5400–5407, September 2018.

[3.14] 'High Impedance Faults'. [Online]. Available: https://www.e-cigre.org/publications/detail/402-high-impedance-faults.html

[3.15] J. Tengdin *et al.*, 'High Impedance Fault Detection Technology', PSRC working Group D15. [Online]. Available: https://www.pes-psrc.org/kb/report/083.pdf

[3.16] J. L. Blackburn and T. J. Domin, *Protective Relaying: Principles and Applications*, 4th ed. CRC Press, 2014.

[3.17] P. M. Anderson, *Power System Protection*. Wiley-IEEE Press, 1999. [Online]. Available: https://ieeexplore.ieee.org/book/5264125

[3.18] M. A. U. Khan and C. D. Booth, 'Detailed analysis of the future distribution network protection issues', *J. Eng.*, vol. 2018, no. 15, pp. 1150–1154, 2018.

[3.19] 'IEEE Guide for Protective Relay Applications to Transmission Lines', *IEEE Std C37113-2015 Revis. IEEE Std C37113-1999*, pp. 1–141, June 2016.

[3.20] M. Wang and Y. Chen, 'Weak Infeed Study and Protection Solution', presented at the 38th Annual Western Protective Relay Conference, Spokane, Washington, October 2011. [Online]. Available: https://na.eventscloud.com/file_uploads/136b969dbfc7734cdfd93780f709b85d_wan_pap.pdf

[3.21] A. Apostolov, 'Accelerated Transmission Line Protection for Systems with High Penetration of Inverter Based Resources', PAC World. [Online]. Available: https://www.pacw.org/accelerated-transmission-line-protection-for-systems-with-high-penetration-of-inverter-based-resources

[3.22] F. Friend *et al.*, 'Effect of Distribution Automation on Protective Relaying', in *2014 67th Annual Conference for Protective Relay Engineers*, College Station, TX, USA: IEEE, March 2014, pp. 193–228.

[3.23] 'FLISR and IEC 61850 GOOSE Communications over LTE networks using QoS and IP/MPLS', Energy Central. [Online]. Available: https://energycentral.com/c/iu/flisr-and-iec-61850-goose-communications-over-lte-network-using-qos-and-ipmpls

[3.24] J. Weikert, 'A Measured Approach to Distribution Automation for an Evolving Future', *Power Syst. Eng.*, 2023.

[3.25] K. Islam, D. Kim, and A. Abu-Siada, 'A review on adaptive power system protection schemes for future smart and micro grids, challenges and opportunities', *Electr. Power Syst. Res.*, vol. 230, p. 110241, May 2024.

[3.26] C. Chandraratne, T. Naayagi Ramasamy, T. Logenthiran, and G. Panda, 'Adaptive Protection for Microgrid with Distributed Energy Resources', *Electronics*, vol. 9, no. 11, Art. no. 11, November 2020.

[3.27] R. Sitharthan, M. Geethanjali, and T. Karpaga Senthil Pandy, 'Adaptive protection scheme for smart microgrid with electronically coupled distributed generations', *Alex. Eng. J.*, vol. 55, no. 3, pp. 2539–2550, September 2016.

[3.28] A. J. Taveras-Cruz *et al.*, 'Differential adaptive protection proposal to interconnect isolated microgrid to the primary electric grid: A case study in the Pedernales province', in *2024 12th International Conference on Smart Grid (icSmartGrid)*, May 2024, pp. 78–83.

[3.29] M. B. Delghavi and A. Yazdani, 'A control strategy for islanded operation of a Distributed Resource (DR) unit', in *2009 IEEE Power & Energy Society General Meeting*, July 2009, pp. 1–8.

[3.30] S. M. Brahma and A. A. Girgis, 'Development of adaptive protection scheme for distribution systems with high penetration of distributed generation', *IEEE Trans. Power Deliv.*, vol. 19, no. 1, pp. 56–63, January 2004.

[3.31] P. H. Shah and B. R. Bhalja, 'New adaptive digital relaying scheme to tackle recloser–fuse miscoordination during distributed generation interconnections', *IET Gener. Transm. Distrib.*, vol. 8, no. 4, pp. 682–688, April 2014.

[3.32] M. Khederzadeh, 'Adaptive setting of protective relays in microgrids in grid-connected and autonomous operation', in *11th IET International Conference on Developments in Power Systems Protection (DPSP 2012)*, in Conferences. April 2012, p. P14.

[3.33] R. C. S. P. Tambun, K. M. Banjar-Nahor, N. Hariyanto, F. S. Rahman, and R. Rahmani, 'Adaptive Protection Coordination Scheme for Distribution System under Penetration of Distributed Generation', in *2021 3rd International Conference on High Voltage Engineering and Power Systems (ICHVEPS)*, October 2021, pp. 355–360.

[3.34] P. Gupta, R. S. Bhatia, and D. K. Jain, 'Adaptive protection schemes for the microgrid in a Smart Grid scenario: Technical challenges', in *2013 IEEE Innovative Smart Grid Technologies-Asia (ISGT Asia)*, November 2013, pp. 1–5.

[3.35] J. Horak, 'Directional overcurrent relaying (67) concepts', in *59th Annual Conference for Protective Relay Engineers, 2006.*, April 2006, p. 13 pp.-.

[3.36] W. A. Elmore, *Protective Relaying: Theory and Applications*, CRC Press. Baton Rouge, 2004.

[3.37] G. Saleki, H. Samet, and T. Ghanbari, 'High-speed directional protection based on cross correlation of Fourier transform components of voltage and current', *IET Sci. Meas. Technol.*, vol. 10, no. 4, pp. 275–287, 2016.

[3.38] M. M. Eissa, 'Evaluation of a new current Directional Protection technique using field data', *IEEE Trans. Power Deliv.*, vol. 20, no. 2, pp. 566–572, April 2005.

[3.39] A. K. Pradhan, A. Routray, and S. Madhan Gudipalli, 'Fault Direction Estimation in Radial Distribution System Using Phase Change in Sequence Current', *IEEE Trans. Power Deliv.*, vol. 22, no. 4, pp. 2065–2071, October 2007.

[3.40] A. Ukil, B. Deck, and V. H. Shah, 'Current-Only Directional Overcurrent Protection for Distribution Automation: Challenges and Solutions', *IEEE Trans. Smart Grid*, vol. 3, no. 4, pp. 1687–1694, December 2012.

[3.41] J. S. Farkhani, M. Zareein, H. Soroushmehr, and H. M. SIEEE, 'Coordination of Directional Overcurrent Protection Relay for Distribution Network With Embedded DG', in *2019 5th Conference on Knowledge Based Engineering and Innovation (KBEI)*, February 2019, pp. 281–286.

[3.42] J. Zhang, B. Li, F. Chen, B. Li, X. Ji, and F. Xiao, 'Multi-terminal negative sequence directional pilot protection method for distributed photovoltaic and energy storage distribution network', *Int. J. Electr. Power Energy Syst.*, vol. 157, p. 109855, June 2024.

[3.43] W. Li, J. He, D. Zhang, and Q. Zhang, 'Directional pilot protection based on fault current for distribution network with Distributed Generation (DG)', *J. Eng.*, vol. 2017, no. 13, pp. 1327–1331, 2017.

[3.44] H. S. Hosseini, A. Koochaki, and S. H. Hosseinian, 'A Novel Scheme for Current Only Directional Overcurrent Protection Based on Post-Fault Current Phasor Estimation', *J. Electr. Eng. Technol.*, vol. 14, no. 4, pp. 1517–1527, July 2019.

[3.45] A. Ukil, B. Deck, and V. H. Shah, 'Current-Only Directional Overcurrent Relay', *IEEE Sens. J.*, vol. 11, no. 6, pp. 1403–1404, June 2011.

[3.46] H. Samet, T. Ghanbari, M. A. Jarrahi, and H. J. Ashtiani, 'Efficient Current-Based Directional Relay Algorithm', *IEEE Syst. J.*, vol. 13, no. 2, pp. 1262–1272, June 2019.

[3.47] J. Nsengiyaremye, B. C. Pal, and M. M. Begovic, 'Microgrid Protection Using Low-Cost Communication Systems', *IEEE Trans. Power Deliv.*, vol. 35, no. 4, pp. 2011–2020, August 2020.

[3.48] A. R. Adly and S. A. Kotb, 'A Novel Scheme for a Directional Relaying Based on Impedance Approach', in *2022 4th International Youth Conference on Radio Electronics, Electrical and Power Engineering (REEPE)*, March 2022, pp. 1–5.

[3.49] K. A and V. C, 'Design of adaptive protection coordination scheme using SVM for an AC microgrid', *Energy Rep.*, vol. 11, pp. 4688–4712, June 2024.

[3.50] D. Wu, D. Kalathil, M. M. Begovic, K. Q. Ding, and L. Xie, 'Deep Reinforcement Learning-Based Robust Protection in DER-Rich Distribution Grids', *IEEE Open Access J. Power Energy*, vol. 9, pp. 537–548, December 2022.

[3.51] M. Uzair, M. Eskandari, L. Li, and J. Zhu, 'Machine Learning Based Protection Scheme for Low Voltage AC Microgrids', *Energies*, vol. 15, no. 24, Art. no. 24, January 2022.

[3.52] M. Bakkar, S. Bogarra, F. Córcoles, A. Aboelhassan, S. Wang, and J. Iglesias, 'Artificial Intelligence-Based Protection for Smart Grids', *Energies*, vol. 15, no. 13, p. 4933, July 2022.

[3.53] G. P. Juvekar, E. Atienza, C. Kelley, and N. Malla, 'Power System Contingencies to Evaluate FLISR Systems'.

[3.54] P. D. Le, D. Minh Bui, C. C. Ngo, T. Phuong Nguyen, C. P. Huynh, and N. Minh Doan, 'A Proposed FLISR Approach for Distribution Networks with Distributed Generators', in *2020 IEEE International Conference on Power and Energy (PECon)*, December 2020, pp. 125–130.

[3.55] T. K. Barik, A. Padmanabhan, M. Bello, S. McGuinness, and P. Y. Chan, 'Multiple Setting Groups Based Adaptive Protection for Radial Distribution Feeder', in *2024 77th Annual Conference for Protective Relay Engineers (CFPR)*, March 2024, pp. 1–6.

[3.56] A. Alvarez de Sotomayor, D. Della Giustina, G. Massa, A. Dedè, F. Ramos, and A. Barbato, 'IEC 61850-based adaptive protection system for the MV distribution smart grid', *Sustain. Energy Grids Netw.*, vol. 15, pp. 26–33, September 2018.

[3.57] 'Distribution Automation Application: Fault Location, Isolation, and Service Restoration (FLISR) - Automatically minimize the impact of outages-within seconds.', selinc.com. [Online]. Available: https://selinc.com/solutions/p/flisr/#overview

Chapter 4

Faulted Section Identification Using Only Current Measurements

4.1 Chapter overview

Following the examination of protection challenges in future distribution networks and the review and analysis of modern and proposed/researched protection and FLISR schemes in Chapter 3, this chapter introduces the detailed operation of the scheme that has been developed for faulted section identification as part of this research. Key factors, such as the threshold for triggering the faulted section identification process, and the current angular and magnitudes changes (from pre- to during-fault conditions) used to identify the faulted section, are defined and quantified. For practical demonstration, a simplified system model – a 2-bus radial model with 2 sources and 2 loads at the medium voltage level, as illustrated in Figure 4.1 – is employed to aid in clearly explaining the principles of the proposed methodology, making the theoretical concepts easier to understand and apply. Other illustrations of operation using an 8-bus test system are also included later.

In the previous chapter, it was shown how the process of faulted section identification relies on comparative analysis of data obtained from multiple measurement points. However, it is important to note that data exchange is

very simple, consisting not of continuous streams of measurements, but simple packets of binary codes describing the pre- to during-fault transitions of current angles and magnitudes, and communication is only required during fault conditions (after the faulted section identification process is initiated). Consequently, this necessitates the exchange of data between measurement devices/relays positioned at different locations within the network – the scheme could be implemented in a distributed or centralised fashion. The selection of an appropriate communications technology/protocol for transmitting this data is therefore important.

This chapter also describes the data transfer process between measurement locations that is a fundamental part of the scheme. Furthermore, it reviews communications technologies that are generally applicable for protection systems in smart grid/distribution networks, followed by a summary and identification of relevant candidate communication technologies, with comments on their suitability for application to the scheme developed through this research.

4.2 System model to illustrate scheme operation

In summary, the faulted section identification process operates through comparing pre-fault current to during-fault current "directions" – or angular differences, from multiple locations, to identify the location (in terms of the faulted section) of the fault on a multi-section/feeder system. This is explained fully later in this chapter.

To facilitate a comprehensive understanding of the faulted section identification principle, this study utilises a simple 2-bus radial model, as illustrated in Figure 4.1. This model represents a medium voltage distribution system comprising two sources and two loads arranged in a radial configuration.

Two sources are used in most of the simulations and tests in this thesis for two reasons. Firstly, to test and evaluate the operation of the scheme when there are sources of fault current (e.g. generation or energy storage) connected at both "sides" of the faulted section. This will be increasingly common in future systems with distributed generation connected throughout the system. In reality, Source 1 in the diagram below may be a grid connection (e.g. a transformer connected to the higher voltage system), whereas Source 2 may in fact be made up of many small distributed energy resources (such as solar PV, energy storage, etc.) connected at various locations "downstream" from the fault location. Secondly, Source 2 is used to emulate situations where the generation connected throughout the overall section of distribution system may in fact be "net" exporting to the grid prior to a fault (i.e. the normal direction of power flow is reversed). Alternatively, in some countries, the distribution network may be operated routinely as a non-radial, "meshed" or interconnected network with two or more grid connection. The presence of Source 2 also allows demonstration and testing of operation under such scenarios.

The radial topology is found in the vast majority of traditional power distribution networks, where power flows from a source (typically a transformer connected to the higher voltage distribution/transmission system) indicated by Source 1 on the figure, to multiple loads through a series of interconnected components. While radial topologies are common, as described previous, the scheme will also function in an interconnected/meshed topology and/or systems with significant distributed generation connected, as for each section, the pre-fault power flow would still be in the same direction when measured at the terminals of each individual section of the network (as no loads are connected to any individual sections).

In this model illustrated in Figure 4.1, Sources 1 and 2 are interconnected through the line section from R1 to R2, with power flowing from R1 to R2 in normal circumstances prior to any fault (although the power could also flow from R2 to R1 and the operation of the faulted section identification process

would remain unaffected). Each bus is connected to a load as shown in the Figure 4.1.

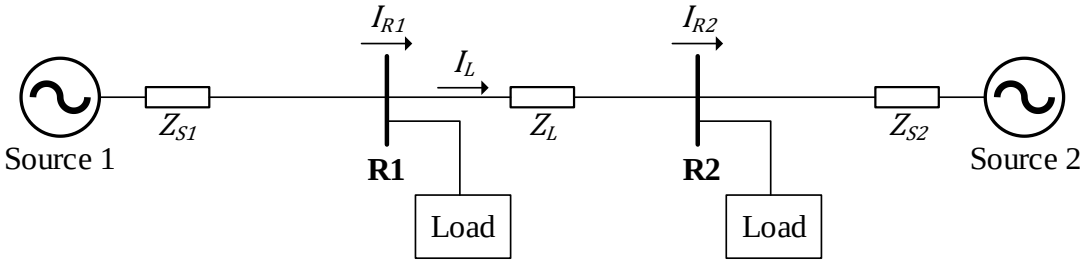

Figure 4.1: Single-line diagram of 2-bus system during normal conditions

In the section of system shown above, Z_{S1} represents the combined source impedance of Source 1 and its connecting line to Bus R1. Similarly, Z_{S2} denotes the source impedance of Source 2 and its associated line to Bus R2. The line impedance interconnecting Bus R1 and Bus R2 is represented by Z_L. The values of the system parameters are not important here, as this is simply used for explanation of the concept of operation. The values for all actual system parameters as used in simulations and case studies later in the thesis are included later.

The voltages at Source 1 and Source 2 are denoted as V_{S1} and V_{S2}, respectively. The current measured at the designated measurement points on the lines at Bus R1 and Bus R2 are represented by I_{R1} and I_{R2}. Additionally, I_L signifies the line current flowing between Bus R1 and Bus R2. Under normal operating conditions, I_L, I_{R1}, and I_{R2}, which are the current measured at the line section between Bus R1 and Bus R2, are assumed to be equal as expressed in Equation (4.1).

$$I_{R1} = I_{R2} = I_L \tag{4.1}$$

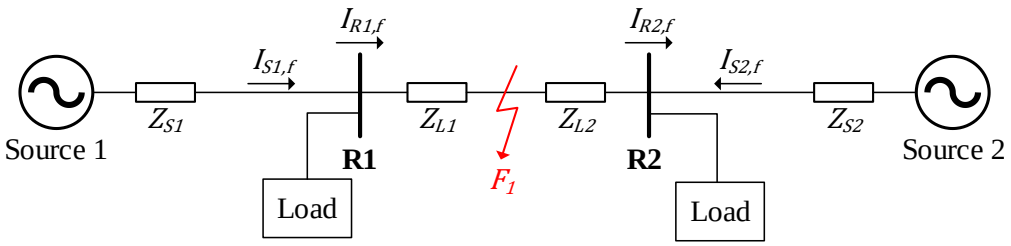

Figure 4.2: 2-bus system with internal fault F_1

However, when a fault F_1 occurs in the zone between Bus R1 and Bus R2, as shown in Figure 4.2, the line impedance between Bus R1 and Bus R2 (Z_L) is divided into two components, Z_{L1} and Z_{L2} as shown in Equation (4.2).

$$Z_{L1} + Z_{L2} = Z_L \tag{4.2}$$

The amplitudes of these impedances depend on the fault F_1 location.
During the fault condition, two fault component currents are calculated:

$$I_{S1,f} = \frac{V_{S1}}{Z_{S1} + Z_{L1}} \tag{4.3}$$

$$I_{S2,f} = \frac{V_{S2}}{Z_{S2} + Z_{L2}} \tag{4.4}$$

Here, $I_{S1,f}$ represents the fault current from Source 1 to the fault F_1 location, while $I_{S2,f}$ denotes the fault current from Source 2 to the fault F_1.

By applying the superposition theorem, when the fault occurs at F_1, the lines currents at both line ends can be expressed as:

$$I_{R1,f} = I_{R1} + I_{S1,f} = I_L + \frac{V_{S1}}{Z_{S1} + Z_{L1}} \tag{4.5}$$

$$I_{R2,f} = I_{R2} + I_{S2,f} = I_L - \frac{V_{S2}}{Z_{S2} + Z_{L2}} \tag{4.6}$$

I_L denotes the pre-fault current or the current in normal condition and $I_{R1,f}$, $I_{R2,f}$ represent the line fault currents measured by relays situated at Bus R1 and Bus R2, respectively. It is important to note that fault impedance and load impedances have been neglected for the purposes of this conceptual

explanation. Non-zero values for fault impedance are included in simulations and case studies presented later in the thesis.

In contrast to the internal fault scenario previously discussed, a case where fault F_2 is located between Bus R2 and Source 2 is considered, as depicted in the system illustrated in Figure 4.1. In this configuration, fault F_2 is external to the protected zone defined by the line connecting Bus R1 and Bus R2 (effectively between the measuring locations for the relays at these buses). This particular system with an external fault present on the system is presented in Figure 4.3.

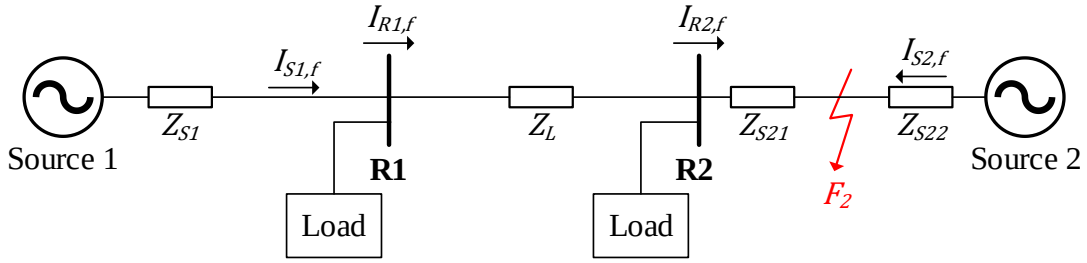

Figure 4.3: 2-bus system with external fault F_2

As the conditions of the system change, the parameters relevant to the analysis must also be adjusted. Notably, the line impedance between Bus R1 and Bus R2 remains consistent with the values illustrated in Equation (4.2). However, the line impedance between Bus R2 and Source 2 is divided into two distinct components; Z_{S21}, which represents the line impedance between Bus R2 and the fault location F_2, and Z_{S22}, which encompasses the line impedance from fault F_2 to Source 2, in addition to the impedance associated with Source 2 itself. The sizes of these impedances are contingent upon the specific location of fault F_2. The relationship among Z_{S2}, Z_{S21}, and Z_{S22} can be expressed mathematically in Equation (4.7).

$$Z_{S2} = Z_{S21} + Z_{S22} \tag{4.7}$$

Furthermore, the components of fault current during this fault condition can be represented as follows:

$$I_{S1,f} = \frac{V_{S1}}{Z_{S1} + Z_L + Z_{S21}} \tag{4.8}$$

$$I_{S2,f} = \frac{V_{S2}}{Z_{S22}} \tag{4.9}$$

In the context of the external fault illustrated in Figure 4.3, $I_{S1,f}$ denotes the fault current in the line from Source 1 to the fault location F_2, while $I_{S2,f}$ signifies the fault current supplied from Source 2 to the fault location F_2.

Similar to the internal fault case, the total current at each terminal of the line faulted section during the external fault condition can be determined using the superposition method. The fault currents measured by the relays at Bus R1 and Bus R2, denoted as $I_{R1,f}$ and $I_{R2,f}$ respectively, can be calculated using Equations (4.1), (4.8), and (4.9):

$$I_{R2,f} = I_{R1} + I_{S1,f} = I_L + \frac{V_{S1}}{Z_{S1} + Z_L + Z_{S21}} \tag{4.10}$$

$$I_{R2,f} = I_{R2} + I_{S1,f} = I_L + \frac{V_{S1}}{Z_{S1} + Z_L + Z_{S21}} \tag{4.11}$$

As stated earlier, fault impedance is neglected in this case, but is included in simulations and case studies presented later.

In summary, the simplified 2-bus radial system provides the framework for explaining the operation of the faulted section identification scheme in medium-voltage distribution systems. The full set of system parameters and data used in the simulation are presented in Chapters 5 and 6.

4.3 The Fourier Transform

As the system developed and presented in the thesis is concerned with measuring the magnitude and phase angles of currents, it is necessary to include a brief description of the Fourier Transform, as this is fundamental to measuring current in protection systems (particularly in systems that sample

currents digitally and also in systems where the fundamental current measurement must be extracted from "noisy" waveforms containing distortion (e.g. due to fault transients) and harmonics.

The Fourier Transform is a mathematical tool that decomposes any periodic waveform in the time domain into its constituent frequency components, and can extract specific components' (e.g. the fundamental component) magnitudes and phase values. It plays a fundamental role in numerous fields, including signal processing, physics, and engineering [4.1]. This transform allows for the decomposition of a signal into its constituent frequencies including harmonic, representing a function as a sum of sinusoidal waves, each characterised by distinct amplitudes and phases.

Additionally, due to its harmonic decomposition properties, the Fourier Transform is widely utilised as a filter for noise reduction or the mitigation/removal of harmonic distortion from "raw" measurement data. Such distortion often arises from non-linear loads, including DG drives, voltage source inverters (VSIs), current source inverters (CSIs), or phenomena such as transformer saturation, arcing loads, etc. By selectively filtering out specific frequencies associated with this distortion, the Fourier Transform allows for the extraction of the desired harmonic components from the input waveform [4.2]. Figure 4.4 illustrates harmonic decomposition achieved through the application of a 12-pulse rectifier.

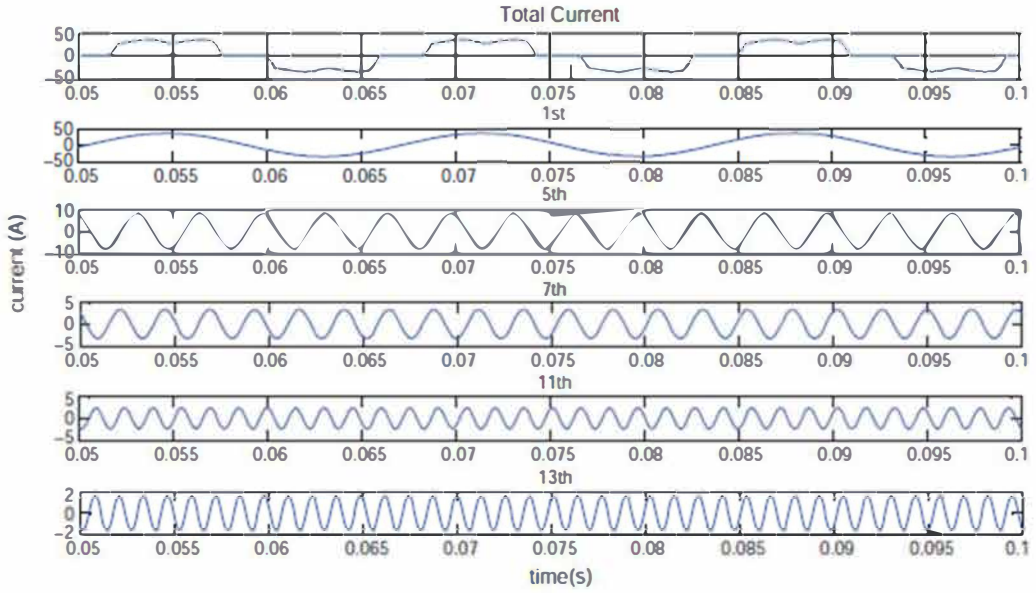

Figure 4.4: Harmonic components after decomposing: the fundamental (1st), 5th, 7th, 11th, 13th [4.2]

In practical applications, signals are often samples and exist in a discrete form – in protection, this would typically be as a result of an analogue measurement (e.g. from a current transformer) being sampled, within the relay or at the current transformer itself, to produce discrete numeric values for onward processing [4.3]. The Discrete Fourier Transform (DFT) is employed to analyse these discrete signals, particularly in the context of digital signal processing (DSP). The Fast Fourier Transform (FFT) is an efficient algorithm designed to compute the DFT, significantly reducing the computation complexity associated with this transform [4.2].

4.3.1 The Discrete Fourier Transform (DFT)

The DFT is a mathematical technique used to analyse the frequency content of discrete and finite in length signals [4.1]. Unlike the continuous Fourier Transform, which is used for continuous-time signals, the DFT operates on sampled data, making it particularly useful in DSP. The DFT converts a finite

sequence of time-domain into its frequency-domain representation, revealing the signal's spectral components. The DFT can be represented as follows:

DFT equation is

$$X[k] = \sum_{n=0}^{N-1} x[n] e^{-j2\pi kn/N} \tag{4.12}$$

And the inverse DFT (IDFT) equation is

$$x[n] = \frac{1}{N} \sum_{k=0}^{N-1} x[k] e^{j2\pi kn/N} \tag{4.13}$$

where $x[n]$ is the input signal in the time domain

$X[k]$ is the output signal in the frequency domain

N is the number of samples

$n = 0, 1, \ldots, N - 1$ is the frequency index

$k = 0, 1, \ldots, N - 1$ is the time index

Moreover, the DFT pair is commonly represented by simplified the exponential term as

For DFT equation:

$$X[k] = \sum_{n=0}^{N-1} x[n] W_N^{kn} \tag{4.14}$$

For IDFT equation:

$$x[n] = \frac{1}{N} \sum_{k=0}^{N-1} x[k] W_N^{-kn} \tag{4.15}$$

When $W_N = e^{-j2\pi/N}$

4.3.2 Magnitudes and angles of sine wave signal calculation using DFT

In practical applications, the DFT enables the calculation of both the magnitude and relative angle of a signal, as shown by the following equation.

The magnitude at the k^{th} bin – "bin" is a term referring to the k^{th} discrete harmonic frequency component of the input signal's frequency spectrum – is

$$|X[k]| = \sqrt{Re(X[k])^2 + Im(X[k])^2} \tag{4.16}$$

The angle at k^{th} bin is

$$\angle X[k] = \tan\left(\frac{Im(X[k])}{Re(X[k])}\right) \tag{4.17}$$

Where $Re(X[k])$ is the real part of DFT output signal

$Im(X[k])$ is the imaginary part of DFT output signal

In the developed system, the DFT is used to calculate the magnitude and relatively phase angles of the fundamental 50 Hz component of the measured phased currents. A sampling frequency of 1 kHz is used.

4.4 Initiating the faulted section identification process

For the faulted section identification process to function, there must be a significant change, greater than pre-determined thresholds, in the currents measured at any point within the overall system being monitored. Following the calculation of magnitude and phase for the current using the DFT, which is described in Section 4.3, the magnitudes and angles, calculated via the DFT, are analysed. The faulted section identification algorithm is only initiated by deviations greater than a specified threshold, which can be varied. Having the system more sensitive may result in more "triggering" of the system, but for non-fault transients, this will not be a problem, as ultimately the algorithm

will find no fault and reset, even though the system has ultimately been unnecessarily initiated. Selection of final values for thresholds may be carried out based on system studies to establish the nature of the primary system, but regardless of the values chosen, false operation of the system should never be a problem. This detection involves comparing a immediately-previous current measurements with the present measurements over a three-cycle moving window. The thresholds selected for the scheme and sued in all simulations are tests are as below:

$$\begin{aligned} &|I_n| < 0.8|I_0| \quad \text{or} \quad |I_n| > 1.2|I_0| \quad \text{or} \\ &\theta_n < \theta_0 - 3.6° \quad \text{or} \quad \theta_n > \theta_0 + 3.6° \end{aligned} \tag{4.18}$$

when

$|I_n|$ = magnitude of current measured 3 cycles after the initial measurement

$|I_0|$ = initial (or immediately-previous) magnitude of current

θ_n = phase angle of current measured 3 cycles after the initial measurement

θ_0 = initial (or immediately-previous) phase angle of current

As an example, consider a scenario where the current magnitude at point R1 in Figure 4.5 is 1 per unit (p.u.) under normal conditions. If a fault occurs as depicted, within three cycles (approximately 60 milliseconds (ms) in the UK electricity system with a frequency of 50 Hz), the current magnitude at point A rises to 1.5 p.u., representing 150% of the initial value. This exceeds the predefined upper threshold of 120%. As a result, this triggers the faulted section identification process to begin. The threshold could be adjusted to make the system more or less sensitive. If the system is made more sensitive, it may initiate operation for non-fault transients. This would not result in any significant issues, as if the system was to initiated but subsequently there was "no fault found" through the latter stages of the system's operation, then it would simply reset and await the next initiating transient. Tests for cases with non-fault load changes are included later in the thesis.

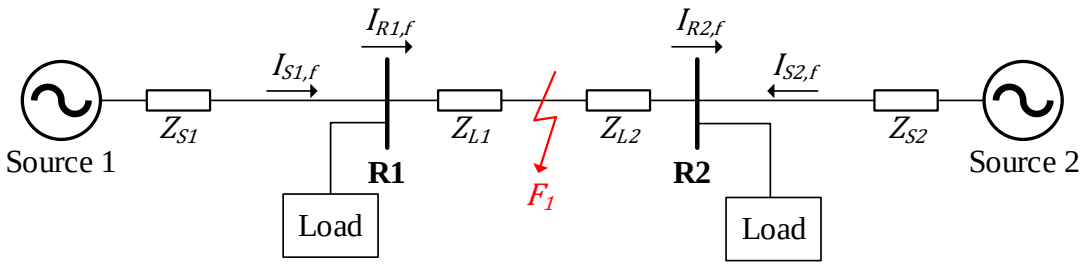

Figure 4.5: 2-bus system with internal fault

4.5 Faulted section identification

Once the pick-up threshold from Section 4.4 is triggered by a significant change in any current measurement, the faulted section identification process begins by comparing data between the two measurement points.

4.5.1 Calculation of current angle and magnitude changes

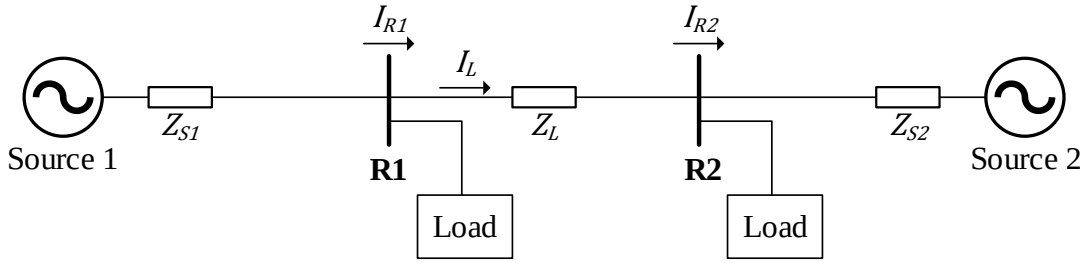

Figure 4.6: The case study system

Referring to the study system in Figure 4.6, the shift in magnitude and phase angle of the current for pre-fault to during-fault conditions can be calculated using the following equation.

Angle change:

$$\Delta\theta_{R1} = \theta_{R1,f} - \theta_{R1} \tag{4.19}$$

$$\Delta\theta_{R2} = \theta_{R2,f} - \theta_{R2} \tag{4.20}$$

Where θ_{R1} and θ_{R2} represent the angles of pre-fault (load) currents measured at points R1 and R2, and $\theta_{R1,f}$ and $\theta_{R2,f}$ signify the angles of the currents as measured during fault conditions.

Magnitude change:

$$\Delta|I_{R1}| = |I_{R1,f}| - |I_{R1}| \tag{4.21}$$

$$\Delta|I_{R2}| = |I_{R2,f}| - |I_{R2}| \tag{4.22}$$

Where $|I_{R1}|$ and $|I_{R2}|$ indicate the magnitudes of pre-fault (load) current measured at point R1 and point R2, and $|I_{R1,f}|$ and $|I_{R2,f}|$ denote the magnitudes of current measured under fault conditions.

4.5.2 Comparison of angular changes between pairs of measurement points (at line ends)

The faulted section identification is performed exclusively using current measurement data. Following the calculation of current angle changes at each measurement point, as detailed in Section 4.5.1, these results are compared from each section/line boundary to ascertain whether the identified faults are situated within, or external to, the monitored observation zone (which, as outlined earlier, would typically be a line or line section bounded by CTs). This analysis can be categorized into the following cases:

4.5.2.1 Internal fault scenario

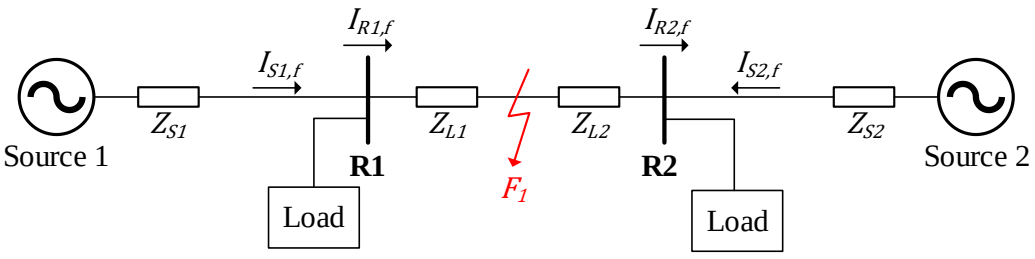

Figure 4.7: Fault F_1 (internal)

Consider a scenario where the single-line diagram presented in Figure 4.7 illustrates an internal fault scenario, and power within this part of the system flows from Source 1 to Source 2. The observation zone is defined by the area between Bus R1 and Bus R2, where the fault F_1 occurs along the line section connecting these two buses. To analyse this situation, through using measurements of relevant parameters from Bus R1 and Bus R2 and calculating the resulting angle changes, it is possible to derive a phasor diagram, as depicted in Figure 4.8. This phasor diagram visually represents the phase relationships of the currents and the voltages before and during the fault, providing a basis for fault analysis and identification within the defined zone. Note that while voltage measurements are not required in the actual system, the simulated voltages at each source/bus are shown in the diagram below for completeness.

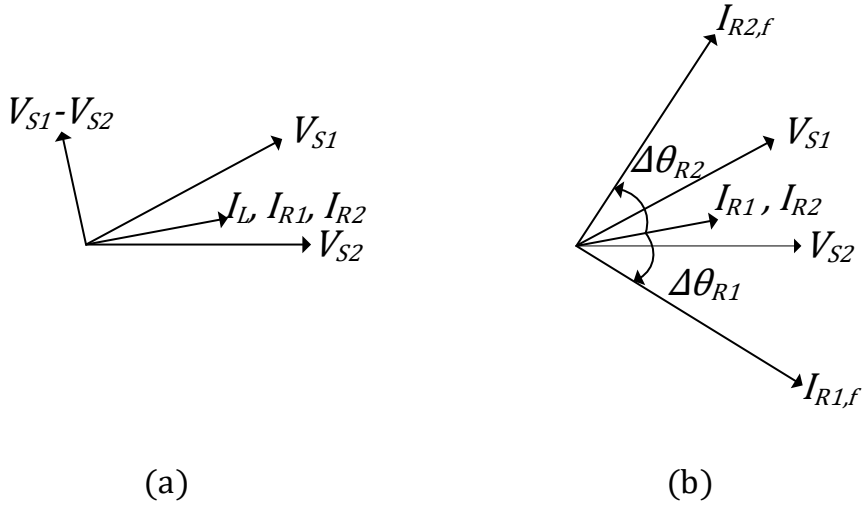

Figure 4.8: Phasor diagram of currents and voltages under (a) pre-fault (b) during-fault conditions for internal fault and left-to-right pre-fault power flow

Due to the lagging phase angle of $I_{R1,f}$ relative to I_{R1}, the current phase angle at Bus R1, transitioning from the pre-fault to during-fault conditions, undergoes a clockwise (CW) rotation on the phasor diagram. A clockwise rotation of a phasor will act to "decrease" its angle, while a counter-clockwise rotation of a phasor will result in an increase in its angle. Conversely, at Bus

R2, the current phase angle exhibits a counterclockwise (CCW) rotation from pre- to during-fault conditions. It can be inferred that the phase change between the pre-fault current and during-fault current at Bus R1 is negative ($-180° \leq \Delta\theta_{R1} < 0°$), while the phase angle change observed at Bus R2 is positive ($0° \leq \Delta\theta_{R2} < 180°$), as $I_{R2,f}$ leads I_{R2}. Consequently, it can be posited that the phase shifts at Bus R1 and Bus R2 exhibits differing rotation characteristics.

Conversely, if the system power flow is reversed, transitioning from Source 2 to Source 1, the phasor diagram of currents and voltages can be illustrated as shown in Figure 4.9.

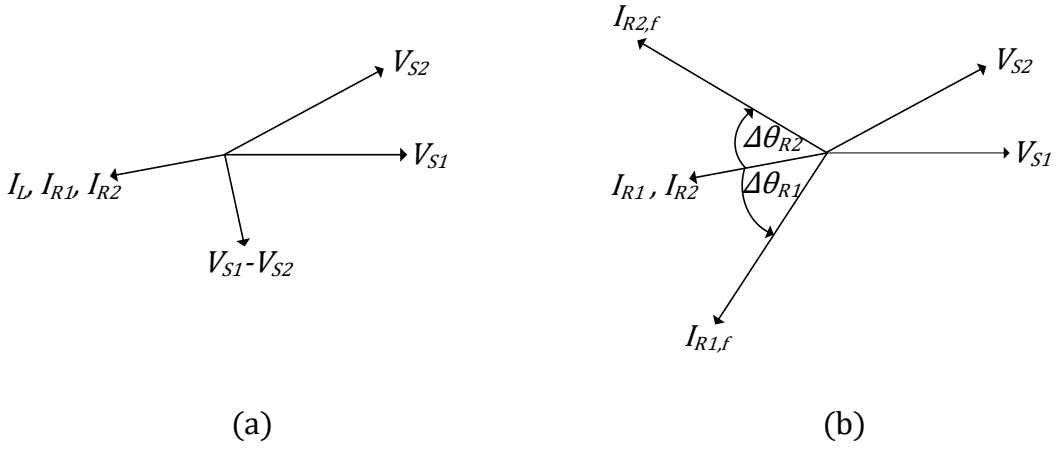

Figure 4.9: Phasor diagram of currents and voltages under (a) pre-fault (b) during-fault conditions for internal fault and right-to-left pre-fault power flow

It is evident that the starting positions and pre- to during-fault transitions of the voltage and current phasors in Figure 4.9, are effectively "reversed" compared to those of the previous example, when pre-fault power was flowing from Source 1 to Source 2, as depicted in Figure 4.8. Specifically, the current angle change measured at Bus R1 becomes a positive value, indicating a CCW rotation, whereas at Bus R2, while the current phase angle change measured at Bus R2 will display a negative value or CW rotation. However, upon comparing the current phase angle changes at both Bus R1 and Bus R2, it remains apparent that the phase rotations between pre- and during-fault

currents differ (that is, the directions of the phase angle changes are different for the currents measured at R1 and R2).

Therefore, it can be concluded that in the case of an internal fault, the current phase angle changes measured at both ends of the observation zone rotate in opposite directions (CW-CCW) or reflect differing values (positive-negative)

4.5.2.2 External fault scenario

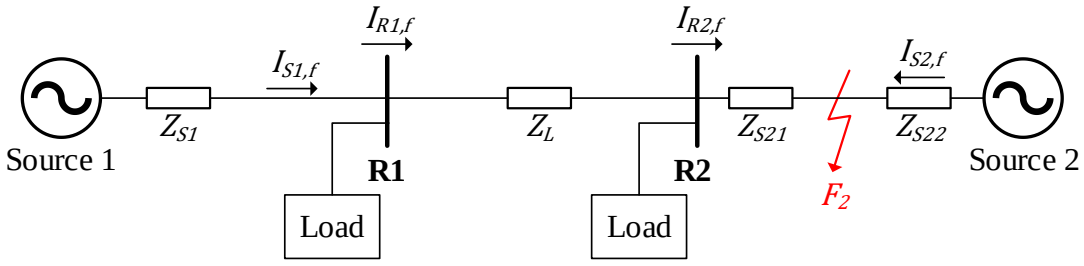

Figure 4.10: Fault F_2 (external)

Figure 4.10 illustrates the single-line diagram of an external fault scenario. Assume that the power flow within the system moves from Source 1 to Source 2, with the fault F_2 occurring on the line between Bus R2 and Source 2, while the observation zone remains the line between Bus R1 and Bus R2, similar to the internal fault case. The phasor diagram for the currents and voltage measured at Bus R1 and Bus R2 during the pre-fault and during-fault conditions can therefore be represented as follows:

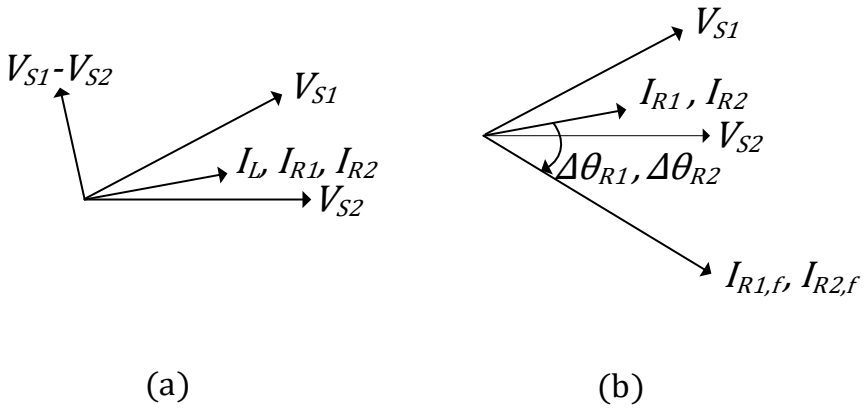

Figure 4.11: Phasor diagram of currents and voltages under (a) pre-fault (b) during-fault conditions when external fault and forward power flow direction

As shown in Figure 4.11, the measured $I_{R1,f}$ lags behind I_{R2}, resulting in a reduced current phase angle at Bus R1 during the fault occurred compared to the pre-fault condition. Consequently, the change in current phase shift, as calculated in Equation (4.19), is negative ($-180° \leq \Delta\theta_{R1} < 0°$), which can be described as a CW rotation. Simultaneously, the current angle change at Bus R2 during the fault also reflects a negative value, similarly indicating CW rotation, as $I_{R2,f}$ also lags behind I_{R2}, akin to the current data at Bus R1.

However, when the system power flow is directed from Source 2 to Source 1, the measured currents change accordingly. In this case, the during-fault current phase at Bus R1 ($I_{R1,f}$) now leads the pre-fault current phase at the same point (I_{R1}), causing the current angle change at Bus R1 to be positive ($0° \leq \Delta\theta_{R2} < 180°$), or to rotate CCW. Likewise, the measured current data at Bus R2 also shifts, with the current angle during the fault being greater than during normal condition. This results in a positive shift in the current phase angle. The phasor diagram of this event is shown in Figure 4.12.

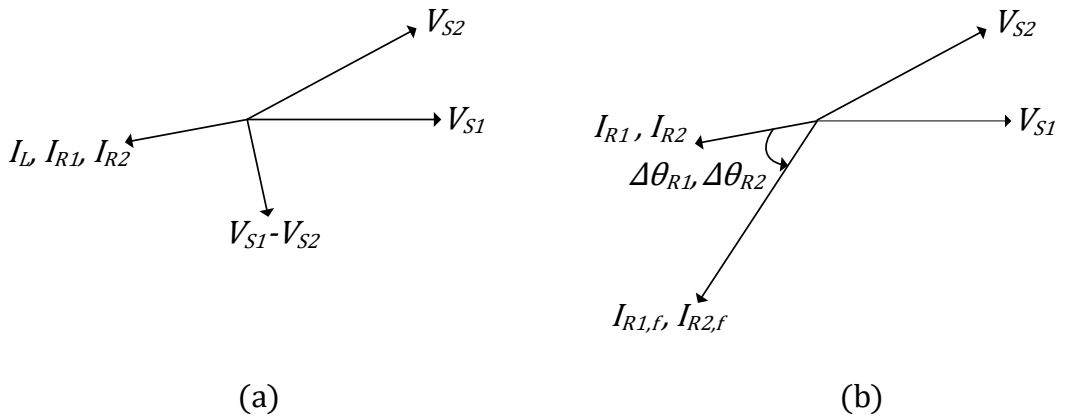

Figure 4.12: Phasor diagram of currents and voltages under (a) pre-fault (b) during-fault conditions when external fault and reversed power flow direction

It is evident that while the current angle changes at each measurement point undergo variation, a comparison reveals that these changes exhibit identical values (either both positive or both negative) and thus rotate in the same direction (CW-CW or CCW-CCW) when the fault occurs outside the observation zone. Therefore, it can be summarised that the current angle shifts measured at the boundaries of the zone during a fault, when compared to pre-fault situations, output similar results (positive-positive or negative-negative) and maintain a consistent rotational direction.

4.5.3 Comparison of magnitude changes between pairs of measurement points (at line ends)

However, the faulted section identification method based solely on current angle changes presents a potential limitation in scenarios involving low fault current conditions or instances where fault current is supplied from only one end of the feeder section. The current directional change comparison method remains most accurate when high fault current is injected from both ends of the feeder. If the fault levels are comparatively low, or if only end supplies the fault current as shown in Figure 4.13, the reliability of this technique, as described in Section 4.5.2, may be compromised [4.4].

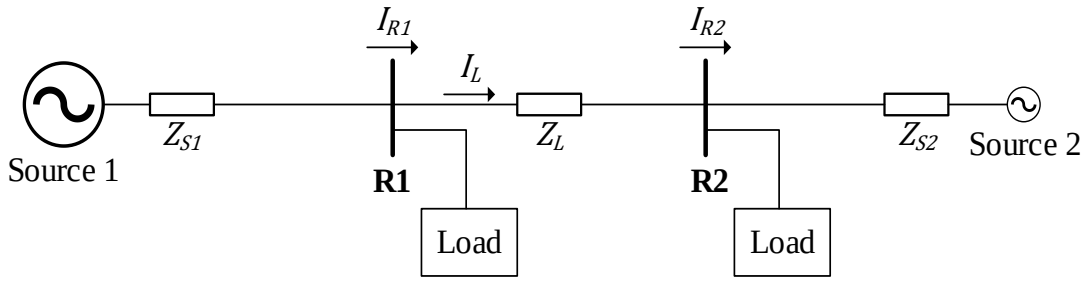

Figure 4.13: The system with Source 2 fault level relatively low

To address this limitation, changes in current magnitudes are employed to support the analysis, particularly in case where infeed occurs from only one end or when one infeed is exceptionally weak. Initial fault detection is still relied on measuring significant angular or magnitude "jumps", as detailed in Section 4.4, without the need for voltage measurements. It is important to note that the shift in current magnitudes is not applicable in scenarios where tapped loads exist between measurement points; however, it can serve as a confirmatory measure in cases of extremely weak source or in the absence of infeed from one boundary.

The comparative analysis of changes in current magnitudes proceeds as follows:

4.5.3.1 Internal fault scenario

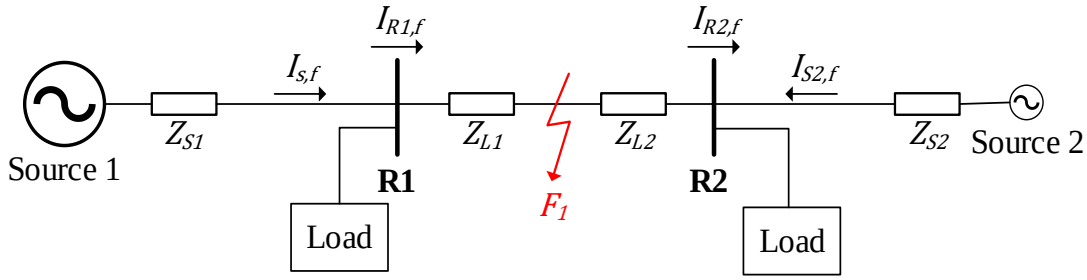

Figure 4.14: Fault F_1 when Source 2 fault level is relatively low

Assuming that scenario depicted in Figure 4.14, where Source 2 has an extremely low fault level, or disconnected, when a fault F_1 occurs on the line between Bus R1 and Bus R2. In this situation, Source 1 generates fault current that flows into the line between Source 1 and the fault location F_1, resulting in

an increased current magnitude measured at Bus R1 ($|I_{R1,f}|$). Consequently, since the current magnitude during the fault is greater than that during the pre-fault period, the change in current magnitudes at Bus R1 ($\Delta|I_{R1}|$) produces a positive value, as computed from Equation (4.21).

Conversely, due to the extremely low fault level of Source 2, the fault current generated is minimal. The current measured at Bus R2 has no contribution from Source 1, as it is located downstream of the fault F_1(although if the fault is resistive and/or of a certain type, e.g. phase-phase, there could be currents from source 2 circulating from Source 1 to loads and back to the fault). This leads to a reduction in the magnitude of $I_{R2,f}$. As a result, the change in current magnitude at Bus R2, as expressed in Equation (4.22), from pre- to during-fault, yields a negative value.

Nonetheless, when the changes in current magnitudes at both measurement points are compared, a difference is apparent (positive-negative).

If Source 2 has a relatively higher fault level than Source 1, fault current generated by Source 1 will be relatively less. Accordingly, the current magnitude measured at Bus R1 – which does not receive fault current from Source 2 – during the fault would decrease relative to the pre-fault condition. Thus, when calculating the change in current at Bus R1, it would be a negative value. At the same time, because Source 2 functions normally and is capable of generating fault current, the current magnitude at Bus R2 increases during the fault, leading to a positive change in current magnitude at Bus R2.

However, similar to the previous case when Source 1 has a higher fault level than Source 2, comparing the changes in current magnitudes at both buses reveals a difference (negative-positive).

Therefore, it can be concluded that when a fault occurs within the observation zone, the changes in current magnitudes measured at both ends of the zone will exhibit opposite values (positive-negative or negative-positive).

4.5.3.2 External fault scenario

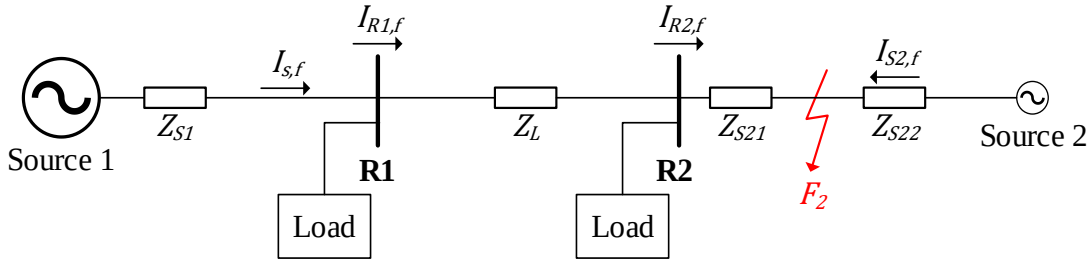

Figure 4.15: Fault F_2 when Source 2 fault level is relatively low

Let Figure 4.15 demonstrates the study case of an external fault scenario, when Source 2 has an extremely low fault level. When a fault F_2 occurs on the line between Bus R2 and Source 2, despite Source 2 generates minimal fault current, its position downstream of the fault means that it does not influence the current magnitudes measured at either Bus R1 and Bus R2. Both buses receive fault current from Source 1 as normal, resulting in increased current magnitudes during the fault condition compared to the normal operating state. Thereby, the changes in current magnitudes at both Bus R1 and Bus R2 is positive.

Again, if Source 1 experiences very low fault current, or disconnected while Source 2 operates normally, the occurrence of fault F_2 results in Source 1 generated negligible fault current at both Bus R1 and Bus R2. Furthermore, neither bus receives fault current from Source 2, as the fault F_2 acts as a barrier, leading to reduced current magnitudes during the fault relative to their pre-fault values. This results in a negative change in current magnitudes for both measurement points (negative-negative), as calculated by Equation (4.21) and (4.22).

When comparing the changes in current magnitudes at both measurement locations, it is evident that the values remain identical. Hence, it can be summarised that if the changes in current magnitudes during the fault condition and before the fault occurrence at the endpoints of the zone exhibit the same sign (positive-positive or negative-negative), and that the fault is located externally to the zone.

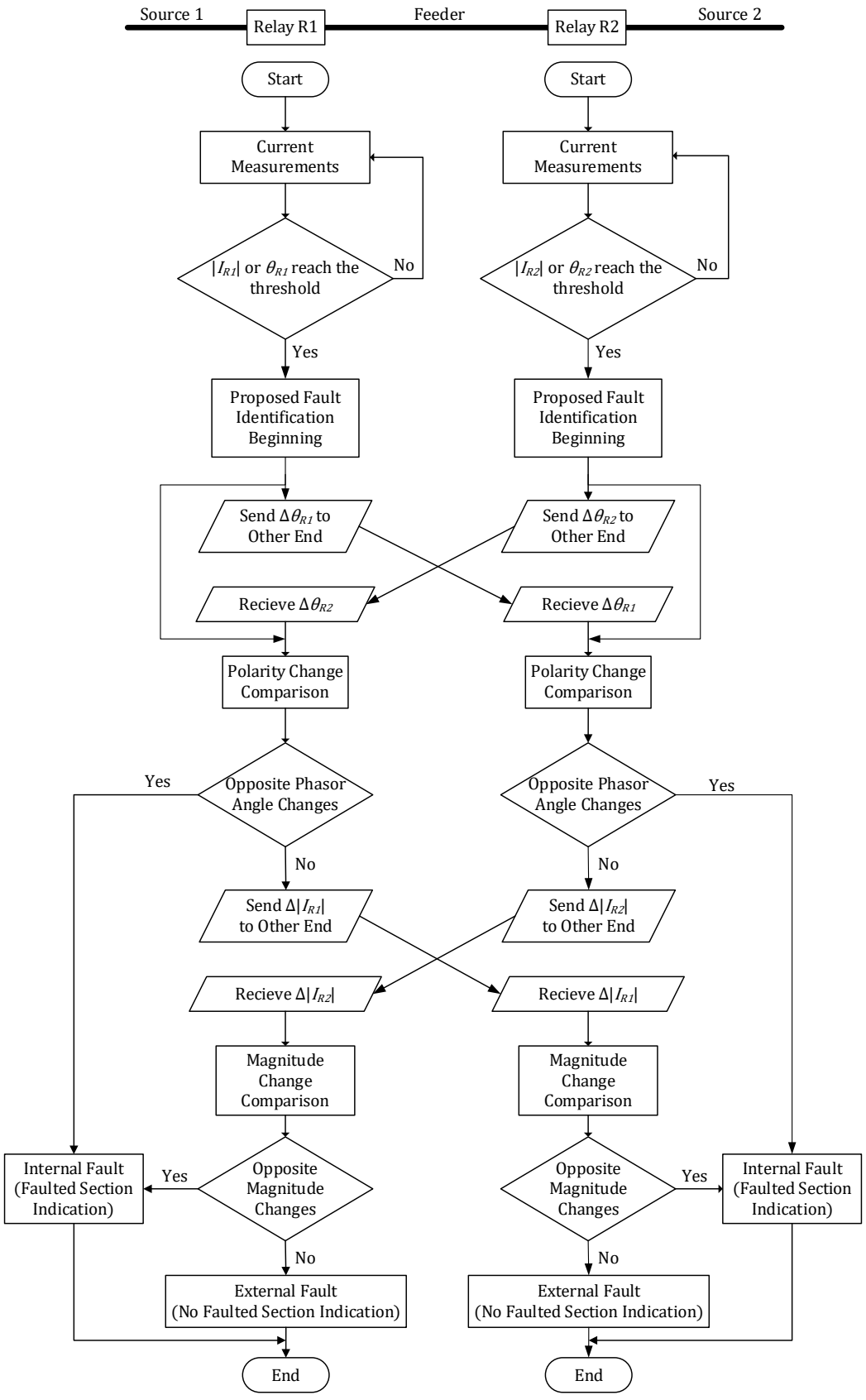

Figure 4.16: The flowchart for faulted section identification

The faulted section identification method discussed in Section 4.5 can be represented as a flowchart, as illustrated in Figure 4.16.

The method necessitates the implementation of a "moving window" approach along with a memory of previous measurements to accurately determine the characteristics and magnitudes of current angular and amplitude variations. A specific time duration may be required to compute the phasor quantities, which are derived using DFT in this scheme, enabling the identification of any shifts in relative angles and magnitudes. Furthermore, an appropriate communication system is essential for efficient data transmission, as outlined in the next section. While this process may take some time – typically one full cycle – to achieve a stable and precise result, it is highly effective in mitigating noise and harmonic distortions. Additionally, at distribution and microgrid levels, fault clearance times on the scale of several hundred milliseconds (ms) are generally acceptable, as extremely high-speed protection operations are not typically required.

4.6 Communications used within the faulted section identification scheme

A relatively simple transfer of simple short binary-code packets between measurement locations is adopted to ensure scheme efficiency and low communications requirements in terms of bandwidth and utilisation. As mentioned in the introduction, rather than transmitting continuous digitised versions of the analogue measurements continuously, the exchanged data is converted into a digital format using binary codes to represent the pre- to during-fault angular and magnitude changes of the current measured in the scheme [4.5]. Bandwidth requirements are minimised, and real-time data processing is significantly simplified, thereby optimising communication efficiency.

The process of converting the measured currents into the appropriate codes describing their transition behaviour is as follows:

Current phase angle changes:

- If the rotation of the current phase change is clockwise (CW), the corresponding binary code is assigned a value of '1'.
- If the rotation of the current phase change is counterclockwise (CCW), the corresponding binary code is assigned a value of '0'.

Current magnitude changes:

- If the current magnitude change is positive, the corresponding binary code is assigned a value of '1'.
- If the current magnitude change is negative, the corresponding binary code is assigned a value of '0'.

It is, however, important to note that the method outlined above may encounter an issue in situations where the binary code transmitted is '0'. This arises from the inherent limitations of the sensors associated with the relay. Specifically, when a decision-making element (relay) receives a '0' from its counterpart, it is uncertain whether this '0' has actually been sent from another measurement location or not (if the initial signal is a '0' it is effectively no different from the "no-signal" state). This situation poses challenges in accurately recognising the start the received packet of binary codes. To alleviate this, a supplementary signal known as the "flag signal" (effectively similar to a "starter" signal) has been developed. This is activated under the following circumstances:

- When a threshold is violated, as outlined in Section 4.4 – the initial packet flag signal is set to '1'.
- Conversely, if there are no alternations in the current or voltage, or if the fault identification threshold remains inactive, no flag signal is transmitted, resulting in no further action or analysis is taken.

The flag signal is transmitted simultaneously with the data signals describing current angle and magnitude changes. Consequently, the total size of the dataset packet of each relay sent from itself at one end of the feeder to another relay at the opposite end will consist of merely seven binary codes for the purpose of faulted section identification. This packet includes:

- 1st initial binary code for the flag signal (flag)
- 3 binary codes representing current phase angle changes ($\Delta\theta_A, \Delta\theta_B, \Delta\theta_C$)
- 3 binary codes representing current phase magnitude changes ($\Delta|I_A|, \Delta|I_B|, \Delta|I_C|$)

This compact data structure ensures efficient and precise faulted section identification while minimising difficulties in signal interpretation. It should be noted that communications systems often continually utilise a "watchdog" or other form of health-check signal on a periodic basis to ascertain the status of the communications system. In such cases different initial "starter" codes (e.g. a multi-bit unique string of binary numbers) may be required to allow the faulted section identification scheme to begin [4.6].

The process of faulted section identification using these codes in each relay can be illustrated using a flowchart and a logic diagram, as presented in Figure 4.17 and Figure 4.18, respectively.

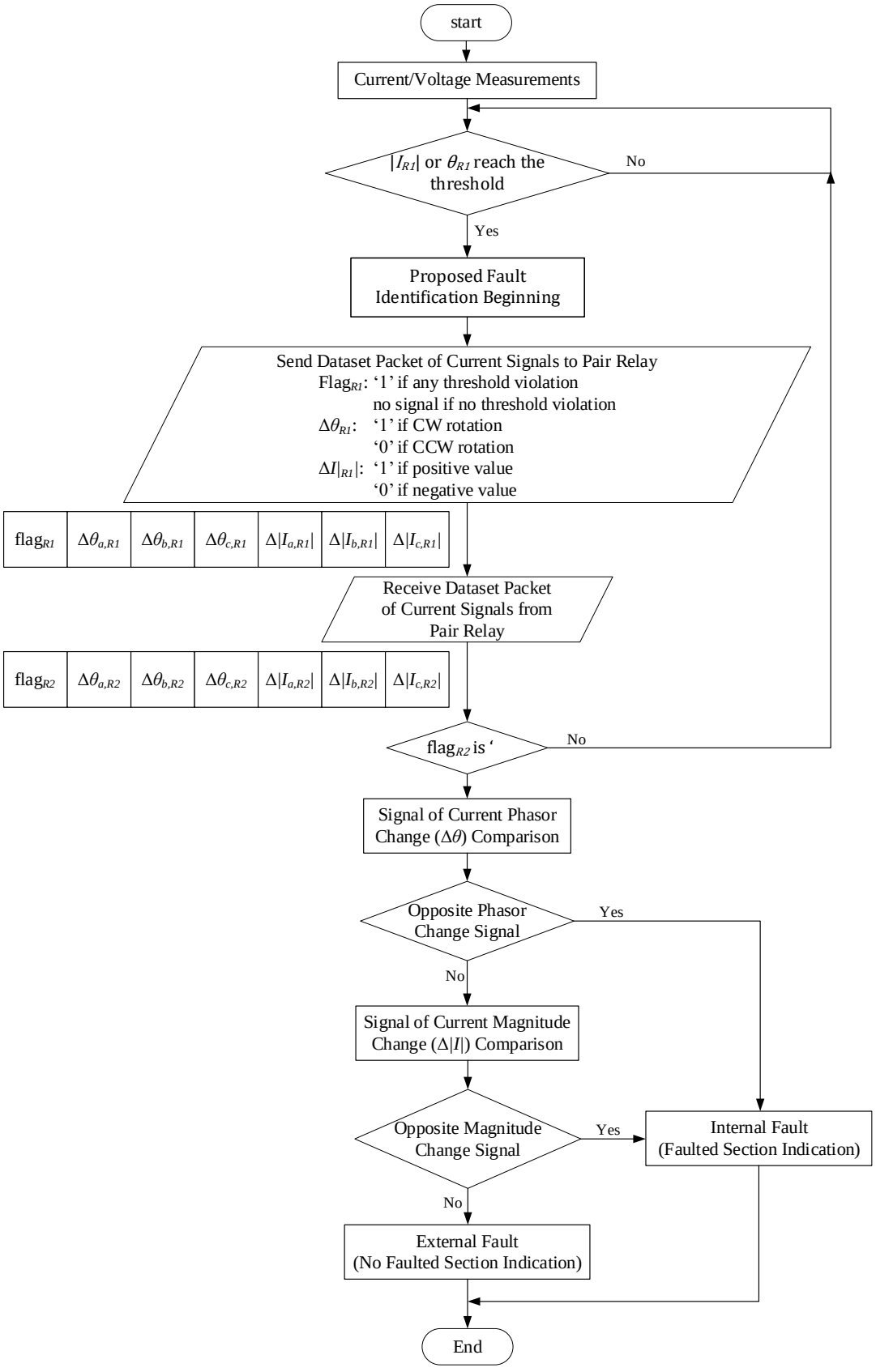

Figure 4.17: Flowchart of faulted section identification using communications

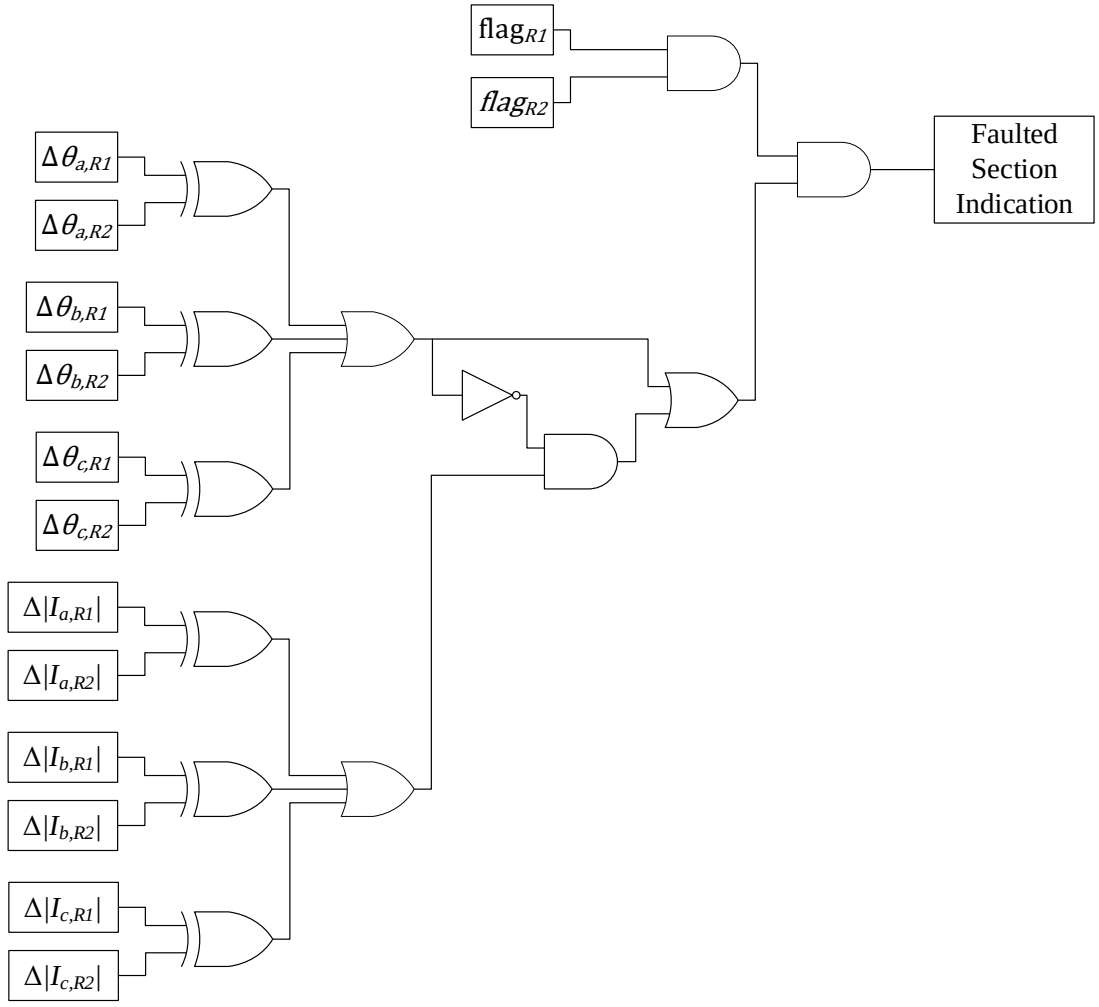

Figure 4.18: Logic Diagram for faulted section identification scheme

4.7 Chapter summary

In this chapter, a method for proposed faulted section identification in a distribution system featuring with dual sources of infeed is presented. This scheme utilises current data exclusively, and does not require voltage measurements, also the direction of power in the system (pre- or during fault) does not affect operation. The methodology is based on a comparative analysis between two measurement points located at the end of the feeder within the observation zone. The comparison is conducted by evaluating the variations in current data at each measurement point that occur during the fault, relative

to the data recorded under normal operating (before a fault happens) conditions.

Following the occurrence of a sudden change in current, the faulted section identification process commences by initially assessing the shift in current phase angles. It is determined that if the changes in current angles at both measurement points exhibit differing rotations (CW-CCW or CCW-CW) or differing values (positive-positive or negative-negative), the fault is identified as residing within the zone. Conversely, if the shifts in current phase angles at both measurement points demonstrate similar (positive-positive or negative-negative), the fault is presumed to be located outside the zone.

However, when the current angle changes at both measurement points are identical, this does not necessarily indicate the absence of a fault within the zone. If one of the sources at the endpoint has an extremely low fault level, it will contribute minimal fault current when a fault occurs (or, in some cases, may even behave as a load). Consequently, the current angle at any point downstream of the fault may become unreliable. This lack of reliability is reasoned by the exceedingly low current magnitude. Therefore, an additional faulted section identification scheme based on the comparison of changes in current magnitudes is introduced to enhance the reliability of the method, particularly when the comparison of current phase angle changes along proves insufficient.

If the changes in current magnitudes at both measurement points are opposite in sign (positive-negative or negative-positive), the fault is presumed to be internal. Conversely, if the changes in current magnitudes are identical (positive-positive or negative-negative), the fault is considered to be external to the observation zone or may not be a fault at all; however, other circumstances such as load changing may also cause sudden changes in current or voltage.

Additionally, this chapter provides an explanation of the study system design, the current magnitudes and phases calculation process and implementation, along with a flowchart of the faulted section identification

scheme. These elements are included to enhance the comprehensibility of the faulted section identification method.

This chapter has provided a detailed description of the communications used for the faulted section identification scheme. The approach utilises binary signals as the data exchanged between two relays, ensuring that the communication remains simple and efficient. This design allows for compatibility with various communication technologies, making it adaptable across multiple protection schemes without introducing unnecessary complexity. By maintaining a straightforward signalling structure, the method can be implemented with low-bandwidth communication systems, broadening the range of suitable technologies.

Chapter references

[4.1] 'The Scientist and Engineer's Guide to Digital Signal Processing'. [Online]. Available: https://www.dspguide.com/

[4.2] P. F. Ribeiro, C. A. Duque, P. M. da Silveira, and A. S. Cerqueira, *Power Systems Signal Processing For Smart Grids*, 1st ed. John Wiley & Sons, Ltd, 2013.

[4.3] W. Rebizant, J. Szafran, and A. Wiszniewski, *Digital Signal Processing in Power System Protection and Control*. London, 2011.

[4.4] J. J. Burke and D. J. Lawrence, 'Characteristics of Fault Currents on Distribution Systems', IEEE Power Engineering Review, vol. PER-4, no. 1, pp. 26–26, January 1984.

[4.5] P. Rajakrom, C. D. Booth, and Q. Hong, 'Current-only directional protection of distribution networks using low-cost communication', in *17th International Conference on Developments in Power System Protection (DPSP 2024)*, March 2024, pp. 1–7.

[4.6] bionicWolf7, 'Watchdog Service', Microsoft Learn. [Online]. Available: https://learn.microsoft.com/en-us/mdep/architecture/core-os/watchdog-service

Chapter 5

Simulations and Case Studies

5.1 Chapter overview

This chapter presents the simulation models developed using MATLAB/Simulink and corresponding results which serve to demonstrate and validate the faulted section identification scheme as well as the communication aspects introduced in Chapter 4. The chapter provides a detailed account of the settings and configurations applied to the measuring devices, which are termed "protection relays" in this chapter as this focuses on a protection application, although the system could be used for protection and/or monitoring/FLISR applications. The chapter presents and analyses the results of simulations for faults of various types, locations and impedances, referring to the benefits and features of the developed scheme.

5.2 Overview of MATLAB/Simulink simulation model

The medium-voltage 8-bus radial distribution system, operating at 11 kV line-line voltage (rms) with a frequency of 50 Hz, has been developed as a simulation-based study model using MATLAB/Simulink, as illustrated in Figure 5.1. The system consists of two power sources located at opposite ends. Source 1 is assumed to originate from the secondary side of a transformer connected to the transmission-level network of the utility, characterised by a fixed and high (maximum 250 MVA as per UK regulations [5.1] short-circuit level (except for the different short-circuit level in single-infeed system cases demonstrated in Section 5.4.2.3, where the fault level/infeed is varied). In contrast, Source 2 represents a smaller infeed (could be a connection to a neighbouring MV network, or another energy source). This is used to also investigate variable short-circuit levels from both "sides" of the faulted section. A controllable switch is positioned between Bus L8 and Source 2, allowing for the disconnection of Source 2 to emulate situations where there is only fault

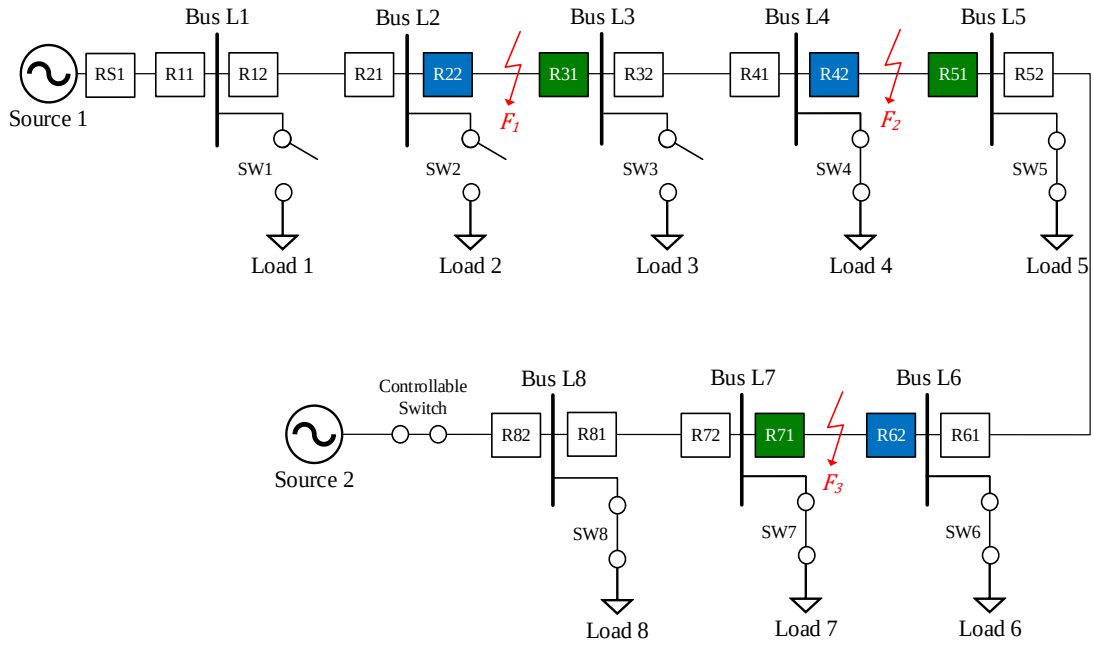

Figure 5.1: MATLAB/Simulink model used in case studies

infeed from one "side" for a fault on a section of network. Both of the sources are star-connected and solidly earthed.

The network incorporates fixed and constant-PQ balanced loads, which are connected to Bus L1, Bus L2, Bus L4, Bus L6, and Bus L8, each supporting a single load. Bus L3, Bus L5, Bus L7 are each connected to variable, constant-PQ, balanced loads, with switches allowing for disconnection of specific loads as needed this assists with investigating the performance of the system during load changes (non-fault transients). Additionally, measuring devices (or "protection relays" in a protection application of the scheme) are installed at both ends of the line sections between each interconnected bus, with each relay assumed to control a circuit breaker (CB) to facilitate the isolation of a faulty line section in the event of a disturbance. As mentioned elsewhere, the method could be used for protection applications and/or monitoring/FLISR applications. While protection application would require current-interrupting circuit breaker devices, an alternative may be to use non-fault interrupting devices (e.g. disconnectors) to isolate the faulted section, initially isolating the overall section of system with a circuit breaker (e.g. at the head or mid-point of the feeder) and rapidly re-configuring the system to isolate the faulted section using simple and cheap disconnectors, while the system has been isolated by the circuit breaker(s). This is also discussed in Chapter 7.

The line parameters used in the simulation model have been selected based on actual distribution line data, as documented in [5.2].

At the initial stage of the simulation, specific switching configurations are applied to control load connections within the system. Switches SW3, SW5, and SW7 are closed to connect Load 3, Load 5, and Load 7 to Bus L3, Bus L5, and Bus L7, respectively. Furthermore, the controllable switch between Bus L8 and Source 2 is maintained in a closed position to ensure that Source 2 remains connected to the system throughout the initial phase. A detailed summary of key simulation parameters, including line, load, and source are summarised in Table 5.1, with their respective values presented for use in the simulation model.

It is important to note that, within the MATLAB/Simulink environment, the algorithm is integrated into the same simulation framework. Consequently, communication latency between relays is neglected.

Table 5.1: Initial value of component's parameters in study system shown in Figure 5.1 [5.2]

Source			
Source	**Short-Circuit Level (MVA)**	**Initial Voltage Angle (degrees)**	**X/R ratio**
Source 1	250	10	5
Source 2	250	0	5

Load			
Load	**Type**	**Active Power (MW)**	**Reactive Power (MVAR)**
Load 1	Balanced PQ	3.50	0.70
Load 2	Balanced PQ	2.50	0.50
Load 3	Balanced PQ	1.00	0.20
Load 4	Balanced PQ	0.20	0.04
Load 5	Balanced PQ	0.20	0.04
Load 6	Balanced PQ	1.00	0.20
Load 7	Balanced PQ	2.50	0.50
Load 8	Balanced PQ	3.50	0.70
Total connected load in each case study for this section		7.40	1.48

Line Impedance				
From Bus	**To Bus**	**Line Length (km)**	**Resistance (Ω)**	**Reactance (Ω)**
Source 1	L1	1	0.182	0.335
L1	L2	1	0.182	0.335
L2	L3	1	0.182	0.335
L3	L4	1	0.182	0.335
L4	L5	1	0.182	0.335
L5	L6	1	0.182	0.335
L6	L7	1	0.182	0.335
L7	L8	1	0.182	0.335
L8	Source 2	1	0.182	0.335
Total line impedance		9	1.638	3.015

The results of voltage measured at each bus in normal condition are shown in Table 5.2, which are in allowable range of ±5% [5.3].

Table 5.2: Voltage results during normal condition

Bus Name	Bus Type	Voltage (p.u.)
Source 1	Swing	1.000
Bus L1	-	0.997
Bus L2	-	0.994
Bus L3	-	0.990
Bus L4	PQ	0.988
Bus L5	PQ	0.985
Bus L6	PQ	0.983
Bus L7	PQ	0.982
Bus L8	PQ	0.988
Source 2	Swing	1.000

5.3 Validation of simulation model performance

To validate the accuracy of the model employed in the MATLAB/Simulink simulation, a verification procedure has been undertaken in which the theoretical fault and load currents have been calculated for specific cases. These expected values have then been cross-checked against the outputs from the MATLAB/Simulink simulation. This comparison served to confirm that the model's performance and response to faults aligns with the anticipated physical behaviour of the system.

5.3.1 Validation of fault current generated by sources

When both sources are set to their maximum short-circuit levels (250 MVA for both sources 1 and 2), a balanced three-phase fault is applied on the line connecting Source 1 and Bus L1, with the fault located next to Source 1, (there

is no impedance on the line connected the Source and Bus), the fault can be theoretically calculated using

$$I_f = \frac{S_f}{\sqrt{3} \times V_L} \tag{5.1}$$

Here, S_f represents the short-circuit level of Source 1, which is given as 250 MVA, and the voltage base of the system model is 11 kV. Substituting these values into Equation (5.1) produce a theoretical fault current contributed from Source 1 of 13.12 kA.

$$I_{rms} = \frac{I_{peak}}{\sqrt{2}} \tag{5.2}$$

The phase-A current at relay RS1 in the MATLAB/Simulink simulation in response to the same balanced fault conditions is show in Figure 5.2, where the peak magnitude current value is 18.20 kA (after the initial DC offset current has subsided). This peak value can be converted into rms using Equation (5.2), resulting in a current of 12.87 kA. This simulated value can be considered to be in relatively close agreement with the theoretical value, thereby validating the accuracy of the simulation model. For Source 2, which has the same short-circuit level as Source 1 and yields identical simulation result, it can therefore be considered to produce equivalent behaviour to that of Source 1.

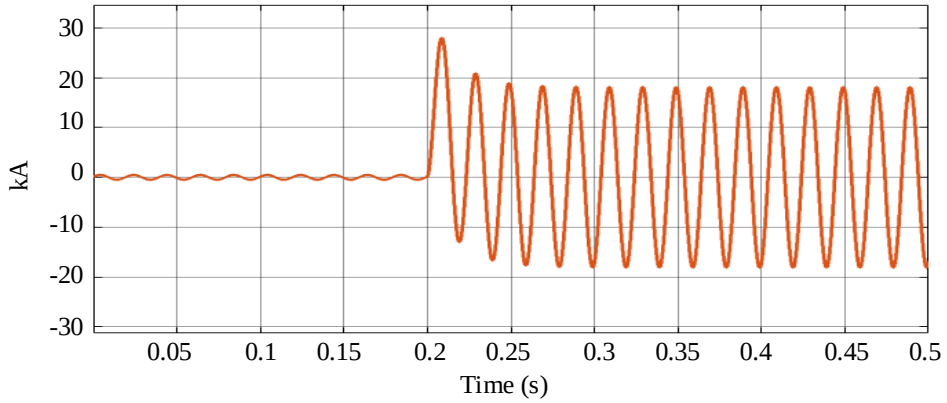

Figure 5.2: Phase-A fault current contributed by Source 1 for a balanced fault at t = 0.2 s (MATLAB/Simulink simulation)

5.3.2 Validation of during-fault current measured at an observed location

Based on the given short-circuit level and X/R ration of the source parameters, the source impedance of both Source 1 and Source 2, assumed to be identical, can be calculated using Equation (5.3):

$$Z_S = \frac{V_L^2}{S_f} \tag{5.3}$$

when S_f represents the short-circuit level, 250 MVA, and V_L is the voltage base, 11 kV. Substituting these values into the Equation (5.3) results in a source impedance of 0.484 Ω. Given that both sources have an X/R ratio of 5, the resulting complex source impedance is 0.0949 + j0.4746 Ω, and this value is identical for both sources under the specified conditions.

All switch configurations remain in their initial states, as displayed in Figure 5.1. Assuming a balanced fault occurs on the middle of the line connected to Bus L2 and Bus L3, to avoid any effect from loads (the loads between the source and the fault are all disconnected as shown in Figure 5.1). The phase currents at relay R22 during the fault condition are contributed only by Source 1. The theoretical magnitude of the current at R22 can be calculated as follows:

$$\left|I_{during-f}\right| = \frac{V_L}{\sqrt{3} \times Z_{eq}} \tag{5.4}$$

when and the equivalent impedance (Z_{eq}) is defined as the magnitude of sum of the source impedance (Z_S) and the line impedance between the source and the fault location. Using Equation (5.4), the theoretical current magnitude at relay R22 is 4.47 kA.

In the simulation, the phase-A during-fault current at each observed relay is presented in Figure 5.3, showing a peak value of 6.27 kA. By applying Equation (5.2) to convert this to a rms value, the result is 4.44 kA, which can be considered to be in close agreement with the corresponding theoretical calculation.

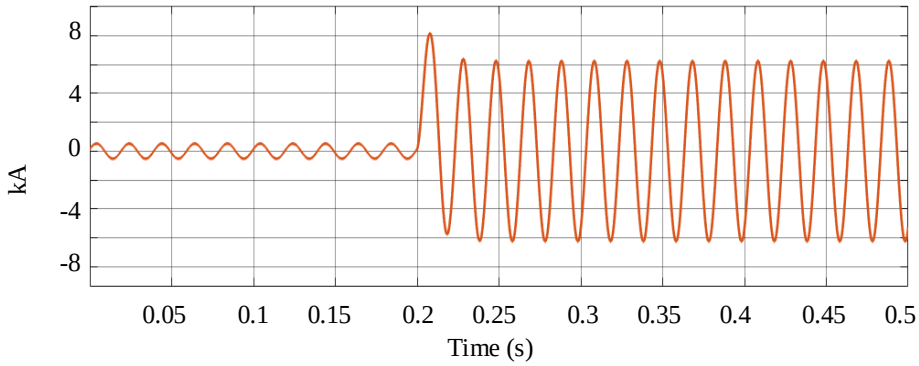

Figure 5.3: Phase-A current at relay R22 for a balanced fault at t = 0.2 s (MATLAB/Simulink simulation)

The alignment of calculated and simulated results indicates that the performance of the developed simulation model is both accurate and reliable. This consistency suggests that the model appropriately captures the expected system behaviour under faulted conditions and validates its suitability for further analysis and testing of the scheme.

5.4 Case studies of scheme operation

To evaluate and demonstrate the performance of the scheme, simulations reflecting a range of scenarios where faults occur at a specific time have been conducted. It is assumed that faults of all types occur at three specific locations: fault F_1 is on the line connecting Bus L2 and Bus L3, fault F_2 is on the line between Bus L4 and Bus L5, and fault F_3 is on the line connecting Bus L6 and Bus L7. The objective is to analyse the response of three "paired" (i.e. at each end of the 3 line sections specified above) relays R22 and R231, R42 and R51, and R62 and R71, positioned as illustrated in Figure 5.1.

To facilitate clear observation of the operation of these specified relays, all other relays in the system are configured not to trip their respective CBs, even if they detect a disturbance. This ensure that the analysis remains focused on the targeted relays and their fault-clearing (or remaining stable) response under the given conditions.

5.4.1 Double-infeed system results

To observe the operation of the relays in a system with multiple sources of infeed that will supply the fault current from both "ends" of the system, the controllable switch position between Bus L8 and Source 2 is set to closed, and Source 2 is therefore connected to the system model. This configuration enables a comprehensive assessment of scheme performance under conditions where more than one infeed is present. The simulation is subsequently conducted under various case study conditions to evaluate the effectiveness of the faulted section identification scheme across different scenarios.

5.4.1.1 Different fault locations

For the scenario involving different fault locations, all switches are configured as depicted in Figure 5.1. The short-circuit levels of both Source 1 and 2 are maintained at their initial values of 250 MVA. The experiment is divided into two sets:

For the first set of studies, the non-fault system power flows from Source 1 to Source 2, and fault F_1, F_2, and F_3 are introduced at their respective locations. Each fault is simulated at 10%, 50%, and 90% of the total line length for each respective line section.

For the second set of studies, the same fault locations are simulated, but the system power flow during pre-fault conditions is reversed and flows from Source 2 to Source 1.

Within each set of cases, all fault types, including balanced three-phase faults (3-PH), and unbalanced faults such as single-phase-to-earth faults (P-E), phase-to-phase faults (P-P), and double-phase-to-earth faults (P-P-E), are systematically applied. Each fault scenario is simulated with a fault resistance of 0.1 Ω. This approach provides a comprehensive assessment of the scheme's performance across varying fault conditions, fault types, and pre-fault power flow directions, enabling a thorough evaluation of its reliability and effectiveness in diverse operational scenarios.

5.4.1.1.1. Pre-fault system power flow from Source 1 towards Source 2

For the first case, a phase-A-to-earth (A-E) fault F_1 is placed 90% along the line between Bus L2 and Bus L3 at a time of 0.4 s. The simulation results for this scenario are presented in Figure 5.4 – Figure 5.6.

As shown in Figure 5.4, at relay R22, the phase angle of phase-A current ($\theta_{a,R22}$) shifts from 18.875° to -51.697° following the occurrence of fault F_1. This results in a current phase angle change for phase-A ($\Delta\theta_{a,R22}$) of -70.572°, indicating a clockwise (CW) rotation. In contrast, at relay R31, the phase polarisation of phase-A current ($\theta_{a,R31}$) changes from 18.875° to 118.336°, yielding a current phase angle change for phase-A ($\Delta\theta_{a,R31}$) of 99.461°, corresponding to a counterclockwise (CCW) rotation. Meanwhile, the current phase angles of phase-B and phase-C at both relays remain unchanged during fault F_1, indicating that there is no current phase angle change for these phases.

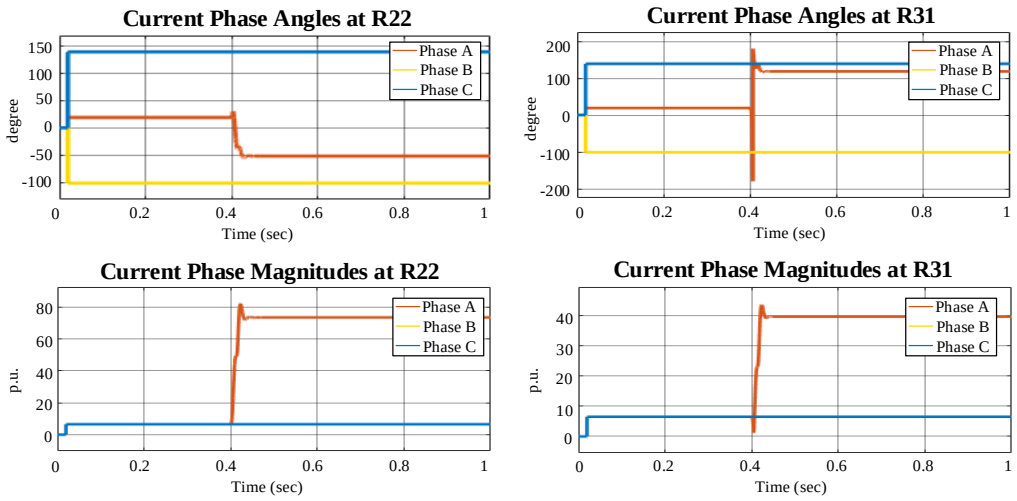

Figure 5.4: Current phase angle and current phase magnitude at relays R22 and R31 in double-infeed system when an A-E fault F_1 occurs, with pre-fault power flow from Source 1 towards Source 2

As the absolute value of phase-A angular change in both relays surpasses the predefined threshold (in Section 4.4) of 3.6° (that is a 1% angular change

in a 360° overall angular range), the faulted section identification process is initiated. By comparing the current phase angle changes at both relays, it is evident that their rotations differ (CW-CCW). This difference suggests that the fault is located within the line connecting Bus L2 and Bus L3, and the detected fault is classified as internal. Therefore, it is not necessary to incorporate an additional comparison of current phase magnitude change in the faulted section identification process.

The current phase angles and current phase magnitudes of the paired relays of R42 and R51, after processing through the DFT filter, when an A-E fault F_1 occurs, are presented in Figure 5.5.

At relay R42, the phase-A current angle ($\theta_{a,R42}$) shifts from 19.690° to 118.365° following the occurrence of fault F_1, resulting in a current phase angle change ($\Delta\theta_{a,R42}$) of 98.675°, indicating a CCW rotation. Similarly, at Relay R51, the phase-A current angle ($\theta_{a,R51}$) experiences the same shift from 19.690° to 118.365°, producing current phase angular shifts ($\Delta\theta_{a,R5-1}$) of 98.675°, also in a CCW direction. The current phase angles of phase-B and phase-C at both relays remain unchanged during fault F_1, indicating no current phase angle change for these phases. The fault identification process is triggered due to the value of the phase-A current shift of both relays exceeding the predefined threshold. When comparing the current phase angle shifts at both relays, the identical CCW-CCW rotation means that, in accordance with the algorithm, further analysis of the current phase magnitude change from pre-fault to during-fault at both ends is conducted. As observed in Figure 5.5, when fault F_1 occurs, the phase-A current magnitudes at both relays R42 and R51 ($|I_{a,R42}|$, $|I_{a,R51}|$) increase from the normal condition. Consequently, the current phase magnitude changes of phase-A for both relays ($\Delta|I_{a,R42}|$, $\Delta|I_{a,R51}|$) are alike (positive-positive), while the current magnitude change of phase-B and phase-C remain unchanged (with their values overlapping in Figure 5.5). Based on these comparisons, initially of phase angle change direction and subsequently of the changes in current magnitudes, it can be inferred that there is no fault

on the line between Bus L4 and Bus L5, and this is therefore classed as an external fault and no further action is necessary from these particular relays.

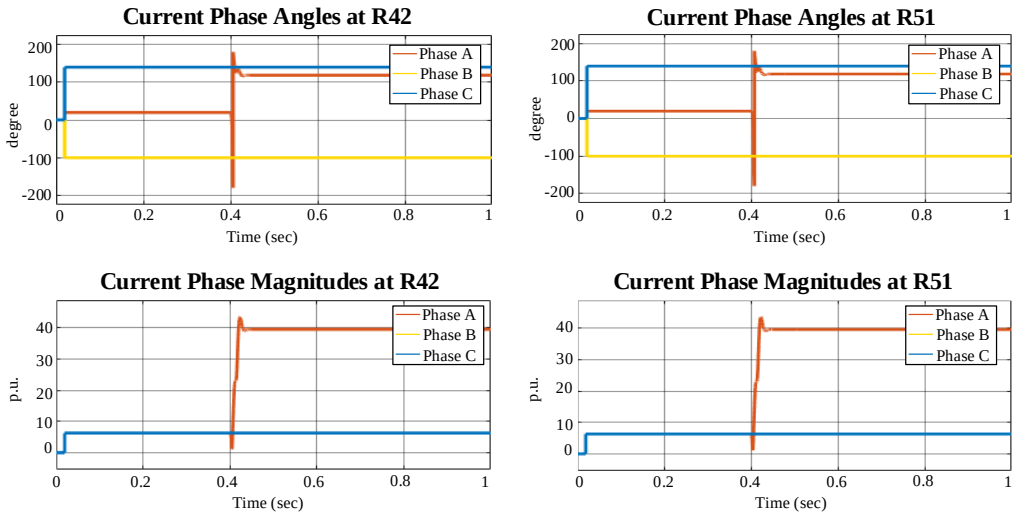

Figure 5.5: Current phase angles and current phase magnitudes at relays R42 and R51 in double-infeed system when an A-E fault F_1 occurs, with pre-fault power flow from Source 1 towards Source 2

For the final pair of relays, R62 and R71, the measured and calculated current phase angles and current phase magnitudes for the A-E fault F_1 scenario are shown in Figure 5.6.

At Relay R62, the measured phase-A current angle ($\theta_{a,R62}$) shifts from 26.046° to 118.842°, resulting in a current phase angle change ($\Delta\theta_{a,R62}$) of 92.796°, signifying a CCW rotational movement. Similarly, the current phase angular change at Relay R71 ($\Delta\theta_{a,R71}$) is computed as 92.796°, resulting from a shift in the phase-A current angle from 26.046° to 118.842° following the occurrence of fault F_1. This change leads to a CCW angular shift, which mirrors the behaviour observed at Relay R62. At the same time, the current phase angles of phase-B and phase-C at both relays remain unchanged, indicating no current phase angle for these phases. This identical CCW-CCW rotation means that, in accordance with the algorithm, further analysis of the current phase magnitude change from pre-fault to during-fault at both ends is conducted. As observed in Figure 5.6, the current magnitude of phase-A for both relays

$((|I_{a,R62}|, |I_{a,R71}|))$ increases when fault F_1 occurs, leading to a similar positive-positive current phase magnitude change. In contrast, the current magnitudes of phases-B and phase-C remain unchanged (with their values overlapping in Figure 5.6). Based on these comparisons, initially of phase angle change direction and subsequently of the changes in current magnitudes, it can be inferred that there is no fault on the line between Bus L6 and L7, and this is therefore classed as an external fault and no further action is necessary from these particular relays.

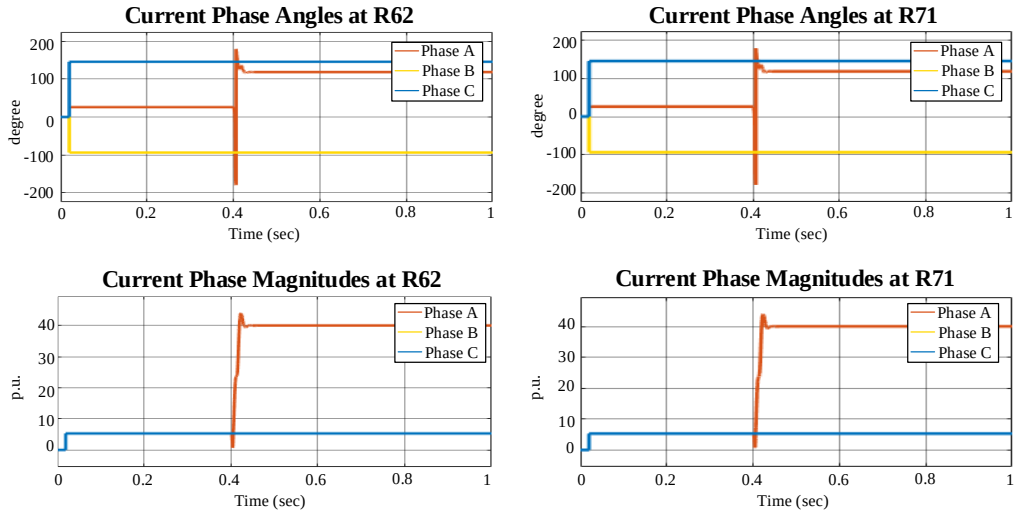

Figure 5.6: Current phase angles and current phase magnitudes at relays R62 and R71 in double-infeed system when an A-E fault F_1 occurs and system pre-fault power flows from Source 1 towards Source 2

In summary, based on the calculation and comparison of current angular and magnitude changes across all three sets of paired relays, it can be determined that the fault occurred on the line section between Bus L2 and Bus L3. The other two pairs of relay remained stable (detecting the fault but not tripping). For this case, Relays R22 and R31 would issue a trip command to their respective CBs, while the other relays will not.

As outlined in Section 4.6, the phase angle and magnitude change signals for each phase current that are exchanged between paired relays must be coded

into binary signals. Thus, the data signals sent between relays are summarised in Table 5.3.

Table 5.3: Summary of transmitted signals between each set of paired relays when pre-fault power flows from Source 1 towards Source 2 and A-E fault F_1 occurs

Relay	Flag Signal	Angle Change Signal	Angle Change Comparison Signal ($\Delta\theta_{abc}$)	Magnitude Change Signal	Magnitude Change Comparison Signal ($\Delta\|I_{abc}\|$)	Trip Signal
R22	1	1	1	1	0	1
R31	1	0		1		1
R42	1	0	0	1	0	0
R51	1	0		1		0
R62	1	0	0	1	0	0
R71	1	0		1		0

In addition, other fault types and locations – fault F_2 between Bus L4 and Bus L5, and Fault F_3 between Bus L6 and Bus L7, have also been simulated using the same procedures and conditions as outlined in detail in the previous pages. The results of the communicated signals between paired relays R22 and R31, R42 and R51, and R62 and R71, comprising the flag signals, result of comparing current angle and magnitude changes from pre-fault to during-fault conditions, and trip signals, are presented in Table 5.4.

Table 5.4: Summary of transmitted signals between each set of paired relays under various fault types and fault locations conditions for double-infeed system when pre-fault power flows from Source 1 towards Source 2

Fault			Flag Signal			$\Delta\theta_{abc}$			$\Delta\|I_{abc}\|$			Trip Signal		
Location	Type	At Line Percentage	Signals Between Paired Relays											
			L2-L3	L4-L5	L6-L7	L2-L3	L4-L5	L6-L7	L2-L3	L4-L5	L6-L7	L2-L3	L4-L5	L6-L7
Between Bus L2-L3	3-PH	10%	1	1	1	1	0	0	0	0	0	1	0	0
		50%	1	1	1	1	0	0	0	0	0	1	0	0
		90%	1	1	1	1	0	0	0	0	0	1	0	0

Table 5.4 (cont.): Summary of transmitted signals between each set of paired relays under various fault types and fault locations conditions for double-infeed system when pre-fault power flows from Source 1 towards Source 2

Fault			Flag Signal			$\Delta\theta_{abc}$			$\Delta\lvert I_{abc}\rvert$			Trip Signal		
Location	Type	At Line Percentage	Signal Between Paired Relay											
			L2-L3	L4-L5	L6-L7	L2-L3	L4-L5	L6-L7	L2-L3	L4-L5	L6-L7	L2-L3	L4-L5	L6-L7
Between Bus L2-L3	P-E	10%	1	1	1	1	0	0	0	0	0	1	0	0
		50%	1	1	1	1	0	0	0	0	0	1	0	0
		90%	1	1	1	1	0	0	0	0	0	1	0	0
	P-P	10%	1	1	1	1	0	0	0	0	0	1	0	0
		50%	1	1	1	1	0	0	0	0	0	1	0	0
		90%	1	1	1	1	0	0	0	0	0	1	0	0
	P-P-E	10%	1	1	1	1	0	0	0	0	0	1	0	0
		50%	1	1	1	1	0	0	0	0	0	1	0	0
		90%	1	1	1	1	0	0	0	0	0	1	0	0
Between Bus L4-L5	3-PH	10%	1	1	1	0	1	0	0	0	0	0	1	0
		50%	1	1	1	0	1	0	0	0	0	0	1	0
		90%	1	1	1	0	1	0	0	0	0	0	1	0
	P-E	10%	1	1	1	0	1	0	0	0	0	0	1	0
		50%	1	1	1	0	1	0	0	0	0	0	1	0
		90%	1	1	1	0	1	0	0	0	0	0	1	0
	P-P	10%	1	1	1	0	1	0	0	0	0	0	1	0
		50%	1	1	1	0	1	0	0	0	0	0	1	0
		90%	1	1	1	0	1	0	0	0	0	0	1	0
	P-P-E	10%	1	1	1	0	1	0	0	0	0	0	1	0
		50%	1	1	1	0	1	0	0	0	0	0	1	0
		90%	1	1	1	0	1	0	0	0	0	0	1	0
Between Bus L6-L7	3-PH	10%	1	1	1	0	0	1	0	0	0	0	0	1
		50%	1	1	1	0	0	1	0	0	0	0	0	1
		90%	1	1	1	0	0	1	0	0	0	0	0	1
	P-E	10%	1	1	1	0	0	1	0	0	0	0	0	1
		50%	1	1	1	0	0	1	0	0	0	0	0	1
		90%	1	1	1	0	0	1	0	0	0	0	0	1
	P-P	10%	1	1	1	0	0	1	0	0	0	0	0	1
		50%	1	1	1	0	0	1	0	0	0	0	0	1
		90%	1	1	1	0	0	1	0	0	0	0	0	1
	P-P-E	10%	1	1	1	0	0	1	0	0	0	0	0	1
		50%	1	1	1	0	0	1	0	0	0	0	0	1
		90%	1	1	1	0	0	1	0	0	0	0	0	1

From Table 5.4, it can be concluded that when the fault identification process is triggered (from flag signal is '1'), the current angle shift between pre-fault and during-fault comparison of the paired relays at the locations of the fault is consistently '1', indicating that the measured current angle changes of both ends are different. This allows the relays to identify the presence of an internal fault within their respective line sections, even when the fault is located close to the measurement point, leading them to issue a trip signal of '1' to their relevant CBs. This outcome confirms the accuracy of the scheme, demonstrating the reliability and effectiveness of the method.

5.4.1.1.2. Pre-fault system power flow from Source 2 towards Source 1

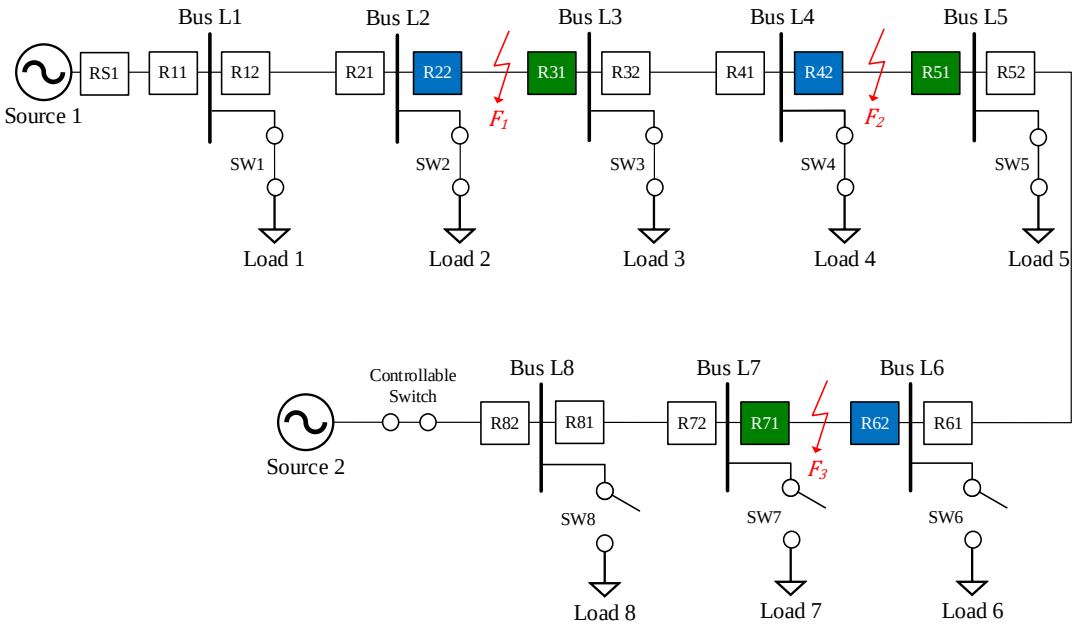

Figure 5.7: The study model for double-infeed system when power flows Source 1 towards Source 2

When the system power flow is reversed, directing from Source 2 to Source 1, this configuration is implemented by closing SW1, SW2 and SW 3 to connect Load 1, Load 2, and Load 3 to the system, while SW6, SW7, and SW8 are opened to disconnect Load 6, Load 7, and Load 8. The controllable switch connected to Source 2 remains closed, ensuring Source 2 stays connected to the

system. The model configuration for these scenarios is illustrated in Figure 5.7. Additionally, the voltage angle setting of both sources are swapped, with Source 1 set to 0° and Source 2 set to 10°, to ensure that the power flow direction is fully reversed.

To assess the system response under this condition, a phase-B-to-phase-C-to-earth (B-C-E) fault F_2 is applied at 10% of the line connecting Bus L4 and Bus L5, at t = 0.4 s. The results of this simulation are displayed in Figure 5.8 – Figure 5.10.

The first pair of Relays R22 and R31 results are displayed in Figure 5.8. The current phase angular of phase-B and phase-C of Relay R22 ($\theta_{b,R22}$, $\theta_{c,R22}$) during the fault F_2 period is 177.656° and 57.131°, respectively. These values are shifted from their pre-fault values of 86.046° and -33.954°, resulting in a current phase angle change ($\Delta\theta_{b,R22}$, $\Delta\theta_{c,R22}$) of 91.610° and 91.085°, respectively. This change corresponds to a CCW rotation for both phase currents, while the phase angle change of phase-A ($\Delta\theta_{A,R1}$) remains zero due to no changed value. Similarly, at Relay R31, the calculated current phase angle change for phase-B and phase-C ($\Delta\theta_{b,R31}$, $\Delta\theta_{c,R31}$) is 91.610° and 91.085°, respectively, also producing an CCW rotation for both phases, with no change in the current phase-A angle. The faulted section identification is started due to the absolute value of phase-B and phase-C current angle shift in both relays exceeding the threshold, then the current angle changes and current magnitude changes of both relays are compared. Since the current angle change rotation of both relays is in the same direction, further analysis of current phase magnitude change between pre-fault and during-fault comparison is necessary. From Figure 5.8, it is observed that when fault F_2 occurs, the current phase magnitude shifts of phase-B and phase-C at both relays increases from the initial values under normal condition, while there is stable value in the magnitude of phase-A current. Hence, when comparing the current phase magnitude changes across all phases for both relays, the results appear identical characteristics. This observation suggested that the disturbance did not occur on the line connected Bus L2 and Bus L3.

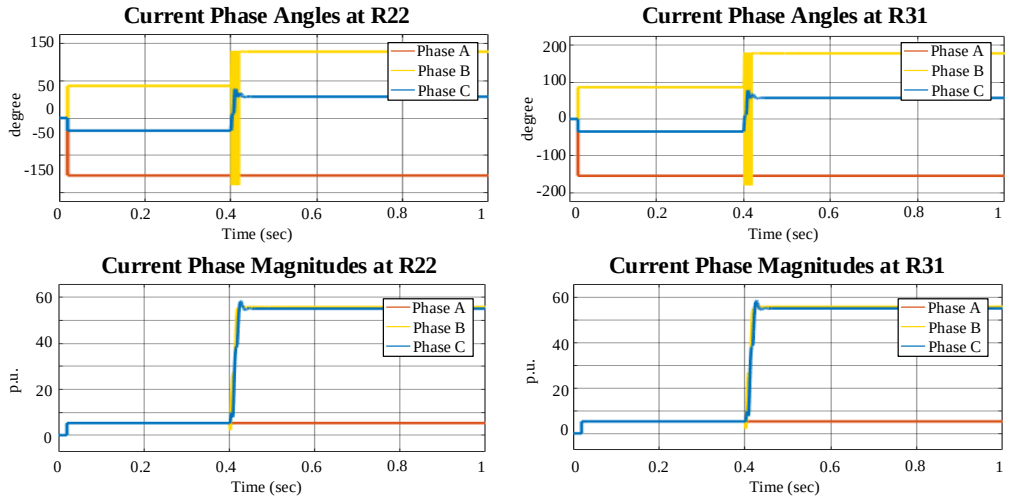

Figure 5.8: Current phase angle and current phase magnitude at Relay R22 and R31 in double-infeed system when a B-C-E fault F_2 occurs, with pre-fault power flow from Source 2 towards Source 1

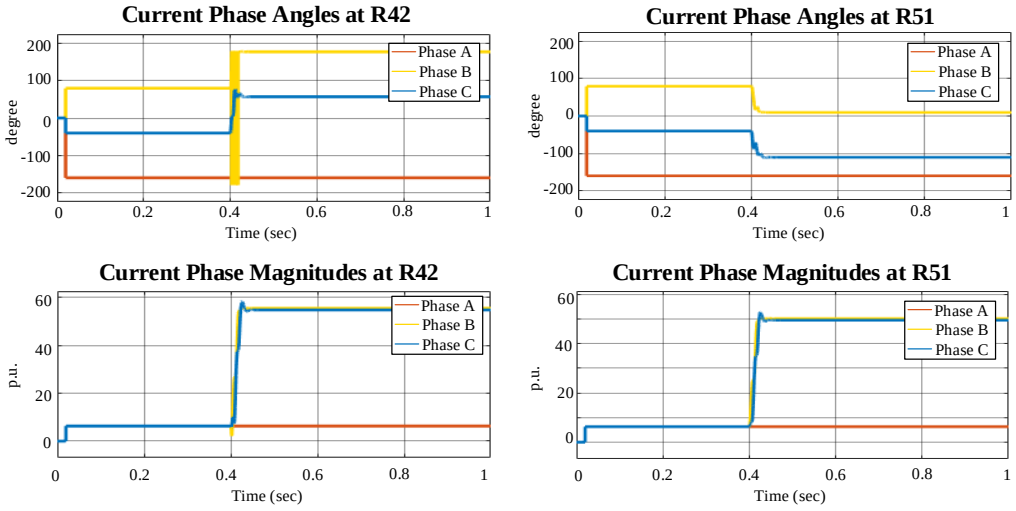

Figure 5.9: Current phase angle and current phase magnitude at Relay R42 and R51 in double-infeed system when a B-C-E fault F_2 occurs, with pre-fault power flow from Source 2 towards Source 1

Figure 5.9 presents the results for the second paired relays of R42 and R51. When fault F_2 occurs, at relay R42, the current phase angle of phase-B (F_2) shifts from 72.690° to 177.518°, whereas phase-C ($\theta_{c,R42}$) shifts from -40.310° to 56.975°. Thus, the computed current phase-B and phase-C angular shifts

($\Delta\theta_{b,R42}$, $\Delta\theta_{c,R42}$) are 97.828° and 97.286°, both indication a CCW rotation, while the phase-A current angle remains stable when fault happened. However, at relay 51, the current phase angle change for phase-B ($\Delta\theta_{b,R51}$) measured as -70.111° and for phase-C ($\Delta\theta_{c,R51}$) is 70.454°. These values a derived from the phase angle shifts during the fault, where the phase-B current angle changes from 79.690° to 9.579°, and the phase-C current angle shifts from -40.310° to -110.764°, both exhibiting a CW rotation. Same as the first paired relays, the faulted section identification is started due to the absolute value of phase-B and phase-C current angle shift in both relays exceeding the threshold. When comparing the direction of current angle changes between pre-fault and during-fault from the two relays, the opposite CCW-CW rotation is observed, signifying the presence of a fault within the monitored zone line connecting Bus L4 and Bus L5 without requiring further current phase magnitude change comparison between pre- and during-fault of the two relays for confirmation.

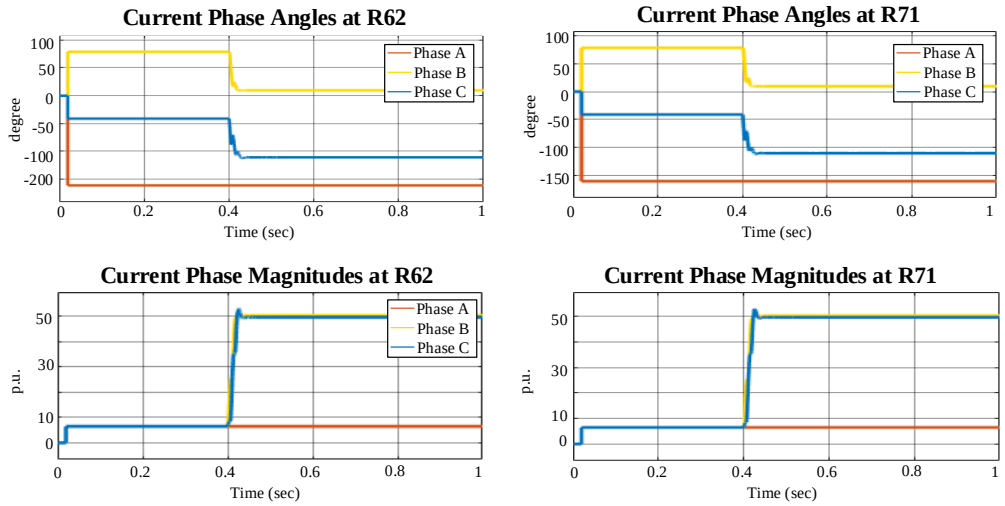

Figure 5.10: Current phase angle and current phase magnitude at Relay R62 and R71 in double-infeed system when a B-C-E fault F_2 occurs, with pre-fault power flow from Source 2 towards Source 1

For the final paired relays, R62 and R71, the results are displayed in Figure 5.10. At relay R62, the phase-B current angle ($\theta_{b,R62}$) changes from 78.875 to 9.597° due to fault F_2, resulting in a current phase angle change ($\Delta\theta_{b,R62}$)

of -69.278°, indicating a CW rotation, and phase-C current angle ($\theta_{c,R62}$) changes from -41.125° to -110.743°, resulting in a current phase angular shift ($\Delta\theta_{c,R62}$) of -69.618° or CW rotation. At the same time, relay R71 calculates the phase-B and phase-C current angular changes ($\Delta\theta_{b,R71}$, $\Delta\theta_{c,R71}$) as -69.278° and -69.618°, respectively, which is conducted to the same angle change direction as at relay R62. Meanwhile, the current phase angle of phase-A at both relays remains unchanged during the fault, indicating no current phase angle change for this phase. Same as others, the faulted section identification is started due to the absolute value of phase-B and phase-C current angle shift in both relays exceeding the threshold. When comparing the current phase angle shifts of both relays, the identical phase angle change rotations (CW-CW) informed that further analysis using current phase magnitude change between fault and normal conditions comparison is necessary. As depicted in Figure 5.10, when fault F_2 occurs, the current magnitudes of phase-B and phase-C at both ends of R62 and R71 increase. Therefore, the current phase magnitude changes of phase-B and phase-C for both relays are similar (positive-positive), while the current magnitude of phase-B remain stable despite fault occurrence. Based on this computation, it can be concluded that the fault did not occur on the line connected Bus L6 and Bus L7, as the similar current phase magnitude change suggests that the fault is external to this line section.

As the results from faulted section identification analysis of all three paired relays, it can be summarised that the fault occurred solely within the line section connected Bus L4 and Bus L5. Therefore, the relays at both boundaries of this zone correctly issue a trip command to their respectively CBs, while no actions were taken by the other relays in other zones. Furthermore, the flag signals, current phase angle changes, and current phase magnitude changes between before and fault periods can be represented as binary codes, as shown in Table 5.5.

Table 5.5: Summary of transmitted signals between each set of paired relays when the pre-fault power flows from Source 2 towards Source 1 and B-C-E fault F_2 occurs

Relay	Flag Signal	Angle Change Signal	$\Delta\theta_{abc}$	Magnitude Change Signal	$\Delta\lvert I_{abc}\rvert$	Trip Signal
R22	1	0	0	1	0	0
R31	1	0		1		0
R42	1	0	1	1	0	1
R51	1	1		1		1
R62	1	1	0	1	0	0
R71	1	1		1		0

Moreover, other fault types and fault locations have also been demonstrated with the simulation results summarised in Table 5.6.

Based on the experimental results presented in Table 5.4 and Table 5.6, the algorithm demonstrates consistent and reliable performance under a wide range of operating conditions. Regardless of the system power flow direction, the location of the fault – including close-in faults – or the type of fault applied, the algorithm consistently identifies the correct faulted section and issues the trip signal to the appropriate CBs within that zone. This confirms both the accuracy and selectivity of the scheme, validating its effectiveness in isolating internal faults while maintaining system stability.

Table 5.6: Summary of transmitted signals between each set of paired relays under various fault types and fault locations conditions for double-infeed system when pre-fault power flows from Source 2 towards Source 1

Fault			Flag Signal			$\Delta\theta_{abc}$			$\Delta\lvert I_{abc}\rvert$			Trip Signal		
Location	Type	At Line Percentage	Signal Between Paired Relay											
			L2-L3	L4-L5	L6-L7	L2-L3	L4-L5	L6-L7	L2-L3	L4-L5	L6-L7	L2-L3	L4-L5	L6-L7
Between Bus L2-L3	3-PH	10%	1	1	1	1	0	0	0	0	0	1	0	0
		50%	1	1	1	1	0	0	0	0	0	1	0	0
		90%	1	1	1	1	0	0	0	0	0	1	0	0
	P-E	10%	1	1	1	1	0	0	0	0	0	1	0	0
		50%	1	1	1	1	0	0	0	0	0	1	0	0
		90%	1	1	1	1	0	0	0	0	0	1	0	0
	P-P	10%	1	1	1	1	0	0	0	0	0	1	0	0
		50%	1	1	1	1	0	0	0	0	0	1	0	0
		90%	1	1	1	1	0	0	0	0	0	1	0	0
	P-P-E	10%	1	1	1	1	0	0	0	0	0	1	0	0
		50%	1	1	1	1	0	0	0	0	0	1	0	0
		90%	1	1	1	1	0	0	0	0	0	1	0	0
Between Bus L4-L5	3-PH	10%	1	1	1	0	1	0	0	0	0	0	1	0
		50%	1	1	1	0	1	0	0	0	0	0	1	0
		90%	1	1	1	0	1	0	0	0	0	0	1	0
	P-E	10%	1	1	1	0	1	0	0	0	0	0	1	0
		50%	1	1	1	0	1	0	0	0	0	0	1	0
		90%	1	1	1	0	1	0	0	0	0	0	1	0
	P-P	10%	1	1	1	0	1	0	0	0	0	0	1	0
		50%	1	1	1	0	1	0	0	0	0	0	1	0
		90%	1	1	1	0	1	0	0	0	0	0	1	0
	P-P-E	10%	1	1	1	0	1	0	0	0	0	0	1	0
		50%	1	1	1	0	1	0	0	0	0	0	1	0
		90%	1	1	1	0	1	0	0	0	0	0	1	0
Between Bus L6-L7	3-PH	10%	1	1	1	0	0	1	0	0	0	0	0	1
		50%	1	1	1	0	0	1	0	0	0	0	0	1
		90%	1	1	1	0	0	1	0	0	0	0	0	1
	P-E	10%	1	1	1	0	0	1	0	0	0	0	0	1
		50%	1	1	1	0	0	1	0	0	0	0	0	1
		90%	1	1	1	0	0	1	0	0	0	0	0	1
	P-P	10%	1	1	1	0	0	1	0	0	0	0	0	1
		50%	1	1	1	0	0	1	0	0	0	0	0	1
		90%	1	1	1	0	0	1	0	0	0	0	0	1
	P-P-E	10%	1	1	1	0	0	1	0	0	0	0	0	1
		50%	1	1	1	0	0	1	0	0	0	0	0	1
		90%	1	1	1	0	0	1	0	0	0	0	0	1

5.4.1.2 Different fault resistance scenarios

In this set of tests, the maximum fault resistance is set to 50 Ω. The short-circuit levels of both Source 1 and Source 2 are maintained at their initial values of 250 MVA. The experiments are conducted under two system power direction conditions: one where the pre-fault power is flowing from Source 1 towards Source 2, and the other where the flow is reversed. Additionally, all fault types are simulated at different fault location, specifically at fault F_1 is at the midpoint between Bus L2 and Bus L3, fault F_2 is at the centre between Bus L4 and Bus L5, and fault F_3 is on the middle between Bus L6 and Bus L7. The fault resistance is varied systematically over several values – 10, 20, 30, 40, and 50 Ω – to assess the effectiveness of the scheme under this range of conditions.

5.4.1.2.1 Pre-fault system power flow from Source 1 towards Source 2

The voltage angle of Source 1 is set to 10°, while that of Source 2 is set to 0°, ensuring that the pre-fault system power flows from Source 1 towards Source 2. All switching configurations remain unchanged from the initial state shown in Figure 5.1. Different types of fault are introduced at between Bus L2 and L3 (F_1), between Bus L4 and Bus L5 (F_2), and between Bus L6 and Bus L7 (F_3) individually. As before, all faults are applied at t = 0.4 s. The transmitted signals between the paired relays for the lines connecting Bus L2-L3, Bus L4-L5, and Bus L6-L7 are summarised in Table 5.7.

The results outlined in Table 5.7 indicate that the faulted section identification process is successful for tested fault resistances up to and including 30 Ω, representing the maximum value for which correct operation was observed. As the fault resistance increases, the resulting fault current decreases, such that the abrupt change in current (both in angle change and magnitude change) no longer exceeds the predefined threshold required to trigger the fault identification process. These findings suggest that the fault

identification scheme maintains acceptable performance in terms of both reliability and selectivity for faults with moderately high impedance. As noted elsewhere, the thresholds for initiation could be modified to make the system more sensitive, but this would come at the expense of increased operation (but the system should still never maloperate). These configurations of thresholds could be considered on a case-by-case basis.

Table 5.7: Summary of relayed signals between each set of paired relays under various fault types, fault locations, and fault resistances conditions for double-infeed system when pre-fault power flows from Source 1 towards Source 2

Fault			Flag Signal			$\Delta\theta_{abc}$			$\Delta\lvert I_{abc}\rvert$			Trip Signal		
Location	Type	Fault Resistance (Ω)	Signal Between Paired Relay											
			L2-L3	L4-L5	L6-L7	L2-L3	L4-L5	L6-L7	L2-L3	L4-L5	L6-L7	L2-L3	L4-L5	L6-L7
Between Bus L2-L3	3-PH	10	1	1	1	1	0	0	1	0	0	1	0	0
		20	1	1	1	1	0	0	1	0	0	1	0	0
		30	1	1	1	1	0	0	1	0	0	1	0	0
		40	0	0	0	-	-	-	-	-	-	-	-	-
		50	0	0	0	-	-	-	-	-	-	-	-	-
	P-E	10	1	1	1	1	0	0	1	0	0	1	0	0
		20	1	1	1	1	0	0	1	0	0	1	0	0
		30	1	1	1	1	0	0	1	0	0	1	0	0
		40	0	0	0	-	-	-	-	-	-	-	-	-
		50	0	0	0	-	-	-	-	-	-	-	-	-
	P-P	10	1	1	1	1	0	0	1	0	0	1	0	0
		20	1	1	1	1	0	0	1	0	0	1	0	0
		30	1	1	1	1	0	0	1	0	0	1	0	0
		40	0	0	0	-	-	-	-	-	-	-	-	-
		50	0	0	0	-	-	-	-	-	-	-	-	-
	P-P-E	10	1	1	1	1	0	0	1	0	0	1	0	0
		20	1	1	1	1	0	0	1	0	0	1	0	0
		30	1	1	1	1	0	0	1	0	0	1	0	0
		40	0	0	0	-	-	-	-	-	-	-	-	-
		50	0	0	0	-	-	-	-	-	-	-	-	-
Between Bus L4-L5	3-PH	10	1	1	1	0	1	0	0	1	0	0	1	0
		20	1	1	1	0	1	0	0	1	0	0	1	0
		30	1	1	1	0	1	0	0	1	0	0	1	0
		40	1	1	1	0	1	0	0	1	0	0	1	0
		50	0	0	0	-	-	-	-	-	-	-	-	-

Table 5.7 (cont.): Summary of relayed signals between each set of paired relays under various fault types, fault locations, and fault resistances conditions for double-infeed system when pre-fault power flows from Source 1 towards Source 2

Fault			Flag Signal			$\Delta\theta_{abc}$			$\Delta\lvert I_{abc}\rvert$			Trip Signal		
Location	Type	Fault Resistance (Ω)	Signal Between Paired Relay											
			L2-L3	L4-L5	L6-L7	L2-L3	L4-L5	L6-L7	L2-L3	L4-L5	L6-L7	L2-L3	L4-L5	L6-L7
Between Bus L4-L5	P-E	10	1	1	1	0	1	0	0	1	0	0	1	0
		20	1	1	1	0	1	0	0	1	0	0	1	0
		30	1	1	1	0	1	0	0	1	0	0	1	0
		40	1	1	1	0	1	0	0	1	0	0	1	0
		50	0	0	0	-	-	-	-	-	-	-	-	-
	P-P	10	1	1	1	0	1	0	0	1	0	0	1	0
		20	1	1	1	0	1	0	0	1	0	0	1	0
		30	1	1	1	0	1	0	0	1	0	0	1	0
		40	1	1	1	0	1	0	0	1	0	0	1	0
		50	0	0	0	-	-	-	-	-	-	-	-	-
	P-P-E	10	1	1	1	0	1	0	0	1	0	0	1	0
		20	1	1	1	0	1	0	0	1	0	0	1	0
		30	1	1	1	0	1	0	0	1	0	0	1	0
		40	1	1	1	0	1	0	0	1	0	0	1	0
		50	0	0	0	-	-	-	-	-	-	-	-	-
Between Bus L6-L7	3-PH	10	1	1	1	0	0	1	0	0	1	0	0	1
		20	1	1	1	0	0	1	0	0	1	0	0	1
		30	0	0	1	-	-	1	-	-	1	-	-	1
		40	0	0	0	-	-	-	-	-	-	-	-	0
		50	0	0	0	-	-	-	-	-	-	-	-	0
	P-E	10	1	1	1	0	0	1	0	0	1	0	0	1
		20	1	1	1	0	0	1	0	0	1	0	0	1
		30	0	0	1	-	-	1	-	-	1	0	0	1
		40	0	0	0	-	-	-	-	-	-	-	-	-
		50	0	0	0	-	-	-	-	-	-	-	-	-
	P-P	10	1	1	1	0	0	1	0	0	1	0	0	1
		20	1	1	1	0	0	1	0	0	1	0	0	1
		30	0	0	1	-	-	1	-	-	1	0	0	1
		40	0	0	0	-	-	-	-	-	-	-	-	-
		50	0	0	0	-	-	-	-	-	-	-	-	-
	P-P-E	10	1	1	1	0	0	1	0	0	1	0	0	1
		20	1	1	1	0	0	1	0	0	1	0	0	1
		30	0	0	1	-	-	1	-	-	1	0	0	1
		40	0	0	0	-	-	-	-	-	-	-	-	-
		50	0	0	0	-	-	-	-	-	-	-	-	-

5.4.1.2.2 Pre-fault system power flow from Source 2 towards Source 1

When the system configurations are changed to ensure the power flow direction is reversed – from Source 2 towards Source 1. Similar to forward system power flow, different types of fault are introduced at t = 0.4 s in fault locations between Bus L2 and L3 (F_1), between Bus L4 and Bus L5 (F_2), and between Bus L6 and Bus L7 (F_3) individually in each scenario. The test results under various conditions for different fault resistance cases, when the system power flows from Source 2 towards Source 1, are provided in Table 5.8.

The results shown in Table 5.7 and Table 5.8 show that, for HIF conditions, regardless of the system pre-fault direction of power flow, the angular rotations are in different directions, and this results in their comparison signal registering a value of '1'. This indication alone is sufficient for the relays to issue a trip signal ('1') to their relevant CBs without the need to verify the results of the current magnitude change comparison signal in the faulted zone. However, if that fault resistance is extremely high (typically greater than 30 Ω), the relays may be unable to operate as expected, due to the very small changes in both current angles and magnitudes, which fail to reach the predefined threshold required to initiate the faulted section identification process. In such cases, other protection techniques may be required (e.g. sensitive earth fault), but this may be a limit for other types of protection too (such as directional and differential).

These findings highlight the robust performance, reliability, and selectivity of the method, demonstrating its capability to accurately detect and isolate internal faults, even in the presence of moderately HIF conditions, where conventional protection methods may struggle to operate effectively.

Table 5.8: Summary of relayed signals between each set of paired relays under various fault types, fault locations, and fault resistances conditions for double-infeed system when pre-fault power flow is reversed

Fault			Flag Signal			$\Delta\theta_{abc}$			$\Delta\lvert I_{abc}\rvert$			Trip Signal		
Location	Type	Fault Resistance (Ω)	Signal Between Paired Relay											
			L2-L3	L4-L5	L6-L7	L2-L3	L4-L5	L6-L7	L2-L3	L4-L5	L6-L7	L2-L3	L4-L5	L6-L7
Between Bus L2-L3	3-PH	10	1	1	1	1	0	0	1	0	0	1	0	0
		20	1	1	1	1	0	0	1	0	0	1	0	0
		30	1	0	0	1	-	-	1	-	-	1	-	-
		40	0	0	0	-	-	-	-	-	-	-	-	-
		50	0	0	0	-	-	-	-	-	-	-	-	-
	P-E	10	1	1	1	1	0	0	1	0	0	1	0	0
		20	1	1	1	1	0	0	1	0	0	1	0	0
		30	1	0	0	1	-	-	1	-	-	1	-	-
		40	0	0	0	-	-	-	-	-	-	-	-	-
		50	0	0	0	-	-	-	-	-	-	-	-	-
	P-P	10	1	1	1	1	0	0	1	0	0	1	0	0
		20	1	1	1	1	0	0	1	0	0	1	0	0
		30	1	0	0	1	-	-	1	-	-	1	-	-
		40	0	0	0	-	-	-	-	-	-	-	-	-
		50	0	0	0	-	-	-	-	-	-	-	-	-
	P-P-E	10	1	1	1	1	0	0	1	0	0	1	0	0
		20	1	1	1	1	0	0	1	0	0	1	0	0
		30	1	0	0	1	-	-	1	-	-	1	-	-
		40	0	0	0	-	-	-	-	-	-	-	-	-
		50	0	0	0	-	-	-	-	-	-	-	-	-
Between Bus L4-L5	3-PH	10	1	1	1	0	1	0	0	1	0	0	1	0
		20	1	1	1	0	1	0	0	1	0	0	1	0
		30	1	1	1	0	1	0	0	1	0	0	1	0
		40	1	1	1	0	1	0	0	1	0	0	1	0
		50	0	0	0	-	-	-	-	-	-	-	-	-
	P-E	10	1	1	1	0	1	0	0	1	0	0	1	0
		20	1	1	1	0	1	0	0	1	0	0	1	0
		30	1	1	1	0	1	0	0	1	0	0	1	0
		40	1	1	1	0	1	0	0	1	0	0	1	0
		50	0	0	0	-	-	-	-	-	-	-	-	-
	P-P	10	1	1	1	0	1	0	0	1	0	0	1	0
		20	1	1	1	0	1	0	0	1	0	0	1	0
		30	1	1	1	0	1	0	0	1	0	0	1	0
		40	1	1	1	0	1	0	0	1	0	0	1	0
		50	0	0	0	-	-	-	-	-	-	-	-	-

Table 5.8 (cont.): Summary of relayed signals between each set of paired relays under various fault types, fault locations, and fault resistances conditions for double-infeed system when pre-fault power flow is reversed

Fault			Flag Signal			$\Delta\theta_{abc}$			$\Delta\lvert I_{abc}\rvert$			Trip Signal		
Location	Type	Fault resistance (Ω)	Signal Between Paired Relay											
			L2-L3	L4-L5	L6-L7	L2-L3	L4-L5	L6-L7	L2-L3	L4-L5	L6-L7	L2-L3	L4-L5	L6-L7
Between Bus L4-L5	P-P-E	10	1	1	1	0	1	0	0	1	0	0	1	0
		20	1	1	1	0	1	0	0	1	0	0	1	0
		30	1	1	1	0	1	0	0	1	0	0	1	0
		40	1	1	1	0	1	0	0	1	0	0	1	0
		50	0	0	0	-	-	-	-	-	-	-	-	-
Between Bus L6-L7	3-PH	10	1	1	1	0	0	1	0	0	1	0	0	1
		20	1	1	1	0	0	1	0	0	1	0	0	1
		30	0	0	1	-	-	1	-	-	1	-	-	1
		40	0	0	0	-	-	-	-	-	-	-	-	-
		50	0	0	0	-	-	-	-	-	-	-	-	-
	P-E	10	1	1	1	0	0	1	0	0	1	0	0	1
		20	1	1	1	0	0	1	0	0	1	0	0	1
		30	0	0	1	-	-	1	-	-	1	0	0	1
		40	0	0	0	-	-	-	-	-	-	-	-	-
		50	0	0	0	-	-	-	-	-	-	-	-	-
	P-P	10	1	1	1	0	0	1	0	0	1	0	0	1
		20	1	1	1	0	0	1	0	0	1	0	0	1
		30	0	0	1	-	-	1	-	-	1	0	0	1
		40	0	0	0	-	-	-	-	-	-	-	-	-
		50	0	0	0	-	-	-	-	-	-	-	-	-
	P-P-E	10	1	1	1	0	0	1	0	0	1	0	0	1
		20	1	1	1	0	0	1	0	0	1	0	0	1
		30	0	0	1	-	-	1	-	-	1	0	0	1
		40	0	0	0	-	-	-	-	-	-	-	-	-
		50	0	0	0	-	-	-	-	-	-	-	-	-

5.4.1.3 Different short-circuit level scenarios

The variation of short-circuit level in the system has been conducted to evaluate the effectiveness of the method under a range of scenarios. Several scenarios are considered and analysed in the following sections. In this section, dual infeed systems are considered, with one of the infeeds becoming progressively weaker in terms of its fault level contribution. In order to further

test the system, later in section 5.4.2, scenarios where there is only one infeed, with variable fault levels, are considered.

The scenarios include double-infeed but with one infeed being weak. Such weak infeed condition can pose challenges for conventional protection schemes [5.4].

For this experiment, Source 2 is assumed to be a weak infeed with a minimum short-circuit level of 10 MVA. The short-circuit level of Source 2 is varied across a range of values including 10, 50, 100, 150, and 200 MVA. The experiment is divided into two sets of scenarios: one where the system pre-fault power flows from Source 1 to Source 2, and another where the pre-fault power flow direction is reversed. In each test, a fault with a resistance of 0.1 Ω is introduced at three different locations: fault F_1 at the midpoint of Bus L2 and Bus L3, fault F_2 at the middle of Bus L4 and L5, and fault F_3 at the centre of the Bus L6 and L7.

5.4.1.3.1. Pre-fault system power flow from Source 1 towards Source 2

The system configurations are set as shown in Figure 5.1, resulting power flows from Source 1 to Source 2. Various fault types, and fault locations are introduced individually in each simulation case with various short-circuit level at Source 2 at t = 0.4 s of simulated time. The simulation results for these scenarios including the flag signals, the relayed signals of the current angle change between normal and fault periods comparison ($\Delta\theta_{abc}$), the current magnitude change between pre-fault and during-fault condition comparison ($\Delta|I_{abc}|$), and the corresponding trip signals for each paired relay, are described in Table 5.9.

Table 5.9: Summary of transmitted signals between each set of paired relays under various fault types, fault locations, and short-circuit level of Source 2 conditions for double-infeed system when pre-fault power flows from Source 1 towards Source 2

Fault		Short-circuit Level at Source 2 (MVA)	Flag Signal			$\Delta\theta_{abc}$			$\Delta\lvert I_{abc}\rvert$			Trip Signal		
			Signal Between Paired Relay											
Location	Type		L2-L3	L4-L5	L6-L7	L2-L3	L4-L5	L6-L7	L2-L3	L4-L5	L6-L7	L2-L3	L4-L5	L6-L7
Between Bus L2-L3	3-PH	10	1	1	1	1	0	0	0	0	0	1	0	0
		50	1	1	1	1	0	0	0	0	0	1	0	0
		100	1	1	1	1	0	0	0	0	0	1	0	0
		150	1	1	1	1	0	0	0	0	0	1	0	0
		200	1	1	1	1	0	0	0	0	0	1	0	0
	P-E	10	1	1	1	1	0	0	0	0	0	1	0	0
		50	1	1	1	1	0	0	0	0	0	1	0	0
		100	1	1	1	1	0	0	0	0	0	1	0	0
		150	1	1	1	1	0	0	0	0	0	1	0	0
		200	1	1	1	1	0	0	0	0	0	1	0	0
	P-P	10	1	1	1	1	0	0	1	0	0	1	0	0
		50	1	1	1	1	0	0	0	0	0	1	0	0
		100	1	1	1	1	0	0	0	0	0	1	0	0
		150	1	1	1	1	0	0	0	0	0	1	0	0
		200	1	1	1	1	0	0	0	0	0	1	0	0
	P-P-E	10	1	1	1	1	0	0	0	0	0	1	0	0
		50	1	1	1	1	0	0	0	0	0	1	0	0
		100	1	1	1	1	0	0	0	0	0	1	0	0
		150	1	1	1	1	0	0	0	0	0	1	0	0
		200	1	1	1	1	0	0	0	0	0	1	0	0
Between Bus L4-L5	3-PH	10	1	1	1	0	1	0	0	0	0	0	1	0
		50	1	1	1	0	1	0	0	0	0	0	1	0
		100	1	1	1	0	1	0	0	0	0	0	1	0
		150	1	1	1	0	1	0	0	0	0	0	1	0
		200	1	1	1	0	1	0	0	0	0	0	1	0
	P-E	10	1	1	1	0	1	0	0	0	0	0	1	0
		50	1	1	1	0	1	0	0	0	0	0	1	0
		100	1	1	1	0	1	0	0	0	0	0	1	0
		150	1	1	1	0	1	0	0	0	0	0	1	0
		200	1	1	1	0	1	0	0	0	0	0	1	0
	P-P	10	1	1	1	0	1	0	0	1	0	0	1	0
		50	1	1	1	0	1	0	0	0	0	0	1	0
		100	1	1	1	0	1	0	0	0	0	0	1	0
		150	1	1	1	0	1	0	0	0	0	0	1	0
		200	1	1	1	0	1	0	0	0	0	0	1	0

Table 5.9 (cont.): Summary of transmitted signals between each set of paired relays under various fault types, fault locations, and short-circuit level of Source 2 conditions for double-infeed system when pre-fault power flows from Source 1 towards Source 2

Fault		Short-circuit Level at Source 2 (MVA)	Flag Signal			$\Delta\theta_{abc}$			$\Delta\lvert I_{abc}\rvert$			Trip Signal		
			Signal Between Paired Relay											
Location	Type		L2-L3	L4-L5	L6-L7	L2-L3	L4-L5	L6-L7	L2-L3	L4-L5	L6-L7	L2-L3	L4-L5	L6-L7
Between Bus L4-L5	P-P-E	10	1	1	1	0	1	0	0	0	0	0	1	0
		50	1	1	1	0	1	0	0	0	0	0	1	0
		100	1	1	1	0	1	0	0	0	0	0	1	0
		150	1	1	1	0	1	0	0	0	0	0	1	0
		200	1	1	1	0	1	0	0	0	0	0	1	0
Between Bus L6-L7	3-PH	10	1	1	1	0	0	1	0	0	0	0	0	1
		50	1	1	1	0	0	1	0	0	0	0	0	1
		100	1	1	1	0	0	1	0	0	0	0	0	1
		150	1	1	1	0	0	1	0	0	0	0	0	1
		200	1	1	1	0	0	1	0	0	0	0	0	1
	P-E	10	1	1	1	0	0	1	0	0	0	0	0	1
		50	1	1	1	0	0	1	0	0	0	0	0	1
		100	1	1	1	0	0	1	0	0	0	0	0	1
		150	1	1	1	0	0	1	0	0	0	0	0	1
		200	1	1	1	0	0	1	0	0	0	0	0	1
	P-P	10	1	1	1	0	0	1	0	0	1	0	0	1
		50	1	1	1	0	0	1	0	0	0	0	0	1
		100	1	1	1	0	0	1	0	0	0	0	0	1
		150	1	1	1	0	0	1	0	0	0	0	0	1
		200	1	1	1	0	0	1	0	0	0	0	0	1
	P-P-E	10	1	1	1	0	0	1	0	0	0	0	0	1
		50	1	1	1	0	0	1	0	0	0	0	0	1
		100	1	1	1	0	0	1	0	0	0	0	0	1
		150	1	1	1	0	0	1	0	0	0	0	0	1
		200	1	1	1	0	0	1	0	0	0	0	0	1

As indicated by the results in Table 5.9, even in a system model comprising sources with low short-circuit level, the faulted section identification process is successfully initiated when a fault occurs, as the during-fault current behaviours reaches the threshold required to trigger the faulted section identification process. The relays within the monitored line section where the locates detect a difference in current angle change between the pre-fault and

during-fault rotation at both ends of the zone. This dissimilarity enables the relays to identify the presence of a fault within the zone, thereby generating a trip signal to activate the CBs. In contrast, the relays in other zones do not issues a trip signal, as they do not detect the presence of an internal fault within their corresponding line sections.

5.4.1.3.2. Pre-fault system power flow from Source 2 towards Source 1

When the system configurations are set as displayed in Figure 5.7, also the voltage angles of Source 1 and Source 2 are alternated, with Source 1 set to 0°, and Source 2 set to 10°, the system power flow direction is reversed. Various types of faults were introduced at different locations (F_1, F_2, F_3) under the variation of short-circuit level at Source 2, the simulation results including the flag signals, the relayed signals of the current angle change between normal and fault periods comparison ($\Delta\theta_{abc}$), the current magnitude change between pre-fault and during-fault condition comparison ($\Delta|I_{abc}|$), and the corresponding trip signals for each paired relay are presented in Table 5.10.

As the results from Table 5.10, even in the simulated system including source whose low short-circuit level, the monitored line section's relays remain capable of detecting faults when they occur no matter how system power flow direction is. This is achieved by measuring the polarisation change through a pre-fault and during-fault stages comparison ($\Delta\theta_{abc}$) of the phase currents at both ends of the zone. The comparison yields a value of '1' when an internal fault is presented. For relays measuring from other line sections, the current angle change rotation results are an identical value, producing a '0' output. Consequently, only the CBs at the ends of the faulted line section would receive a trip signal from their own relays to isolate the faulty section, in a protection application of the faulted section identification scheme. These findings demonstrate the reliability and security of the scheme, ensuring effective fault detection and isolation even in systems with low fault level infeed.

Table 5.10: Summary of transmitted signals between each set of paired relays under various fault types, fault locations, and short-circuit level of Source 2 conditions for double-infeed system when pre-fault power flows from Source 1 towards Source 2

Fault		Short-circuit Level at Source 2 (MVA)	Flag Signal			$\Delta\theta_{abc}$			$\Delta\lvert I_{abc}\rvert$			Trip Signal		
			Signal Between Paired Relay											
Location	Type		L2-L3	L4-L5	L6-L7	L2-L3	L4-L5	L6-L7	L2-L3	L4-L5	L6-L7	L2-L3	L4-L5	L6-L7
Between Bus L2-L3	3-PH	10	1	1	1	1	0	0	0	0	0	1	0	0
		50	1	1	1	1	0	0	0	0	0	1	0	0
		100	1	1	1	1	0	0	0	0	0	1	0	0
		150	1	1	1	1	0	0	0	0	0	1	0	0
		200	1	1	1	1	0	0	0	0	0	1	0	0
	P-E	10	1	1	1	1	0	0	0	0	0	1	0	0
		50	1	1	1	1	0	0	0	0	0	1	0	0
		100	1	1	1	1	0	0	0	0	0	1	0	0
		150	1	1	1	1	0	0	0	0	0	1	0	0
		200	1	1	1	1	0	0	0	0	0	1	0	0
	P-P	10	1	1	1	1	0	0	1	0	0	1	0	0
		50	1	1	1	1	0	0	0	0	0	1	0	0
		100	1	1	1	1	0	0	0	0	0	1	0	0
		150	1	1	1	1	0	0	0	0	0	1	0	0
		200	1	1	1	1	0	0	0	0	0	1	0	0
	P-P-E	10	1	1	1	1	0	0	0	0	0	1	0	0
		50	1	1	1	1	0	0	0	0	0	1	0	0
		100	1	1	1	1	0	0	0	0	0	1	0	0
		150	1	1	1	1	0	0	0	0	0	1	0	0
		200	1	1	1	1	0	0	0	0	0	1	0	0
Between Bus L4-L5	3-PH	10	1	1	1	0	1	0	0	0	0	0	1	0
		50	1	1	1	0	1	0	0	0	0	0	1	0
		100	1	1	1	0	1	0	0	0	0	0	1	0
		150	1	1	1	0	1	0	0	0	0	0	1	0
		200	1	1	1	0	1	0	0	0	0	0	1	0
	P-E	10	1	1	1	0	1	0	0	0	0	0	1	0
		50	1	1	1	0	1	0	0	0	0	0	1	0
		100	1	1	1	0	1	0	0	0	0	0	1	0
		150	1	1	1	0	1	0	0	0	0	0	1	0
		200	1	1	1	0	1	0	0	0	0	0	1	0
	P-P	10	1	1	1	0	1	0	0	1	0	0	1	0
		50	1	1	1	0	1	0	0	0	0	0	1	0
		100	1	1	1	0	1	0	0	0	0	0	1	0
		150	1	1	1	0	1	0	0	0	0	0	1	0
		200	1	1	1	0	1	0	0	0	0	0	1	0

Table 5.10 (cont.): Summary of transmitted signals between each set of paired relays under various fault types, fault locations, and short-circuit level of Source 2 conditions for double-infeed system when pre-fault power flows from Source 2 towards Source 1

Fault		Short-circuit Level at Source 2 (MVA)	Flag Signal			$\Delta\theta_{abc}$			$\Delta\lvert I_{abc}\rvert$			Trip Signal		
			Signal Between Paired Relay											
Location	Type		L2-L3	L4-L5	L6-L7	L2-L3	L4-L5	L6-L7	L2-L3	L4-L5	L6-L7	L2-L3	L4-L5	L6-L7
Between Bus L4-L5	P-P-E	10	1	1	1	0	1	0	0	0	0	0	1	0
		50	1	1	1	0	1	0	0	0	0	0	1	0
		100	1	1	1	0	1	0	0	0	0	0	1	0
		150	1	1	1	0	1	0	0	0	0	0	1	0
		200	1	1	1	0	1	0	0	0	0	0	1	0
Between Bus L6-L7	3-PH	10	1	1	1	0	0	1	0	0	0	0	0	1
		50	1	1	1	0	0	1	0	0	0	0	0	1
		100	1	1	1	0	0	1	0	0	0	0	0	1
		150	1	1	1	0	0	1	0	0	0	0	0	1
		200	1	1	1	0	0	1	0	0	0	0	0	1
	P-E	10	1	1	1	0	0	1	0	0	0	0	0	1
		50	1	1	1	0	0	1	0	0	0	0	0	1
		100	1	1	1	0	0	1	0	0	0	0	0	1
		150	1	1	1	0	0	1	0	0	0	0	0	1
		200	1	1	1	0	0	1	0	0	0	0	0	1
	P-P	10	1	1	1	0	0	1	0	0	1	0	0	1
		50	1	1	1	0	0	1	0	0	0	0	0	1
		100	1	1	1	0	0	1	0	0	0	0	0	1
		150	1	1	1	0	0	1	0	0	0	0	0	1
		200	1	1	1	0	0	1	0	0	0	0	0	1
	P-P-E	10	1	1	1	0	0	1	0	0	0	0	0	1
		50	1	1	1	0	0	1	0	0	0	0	0	1
		100	1	1	1	0	0	1	0	0	0	0	0	1
		150	1	1	1	0	0	1	0	0	0	0	0	1
		200	1	1	1	0	0	1	0	0	0	0	0	1

However, if the source's short-circuit capacity is extremely small, relying solely on current phase change between before and during fault condition comparison for faulted sectioned identification may not be sufficient. This is because the angular measurement from an extremely low-magnitude current (approaching zero) may not be reliable enough [5.5]. Therefore, current phase magnitude change through pre-fault and during-fault comparison is

incorporated as an additional decision-making criterion. The simulations and analysis related to this is discussed further in Section 5.4.2.

5.4.1.4 Load changes without fault scenarios

This simulation is conducted to evaluate the response of the scheme under non-fault disturbances, specifically during load change events. The objective is to verify that the scheme does not maloperate (e.g. issue trip signals when not required in a protection application, or identify a faulted section in a monitoring application where no fault exists) when the system undergoes normal operational variations, such as the connection or disconnection of loads, in the absence of any fault conditions. This assessment is crucial for validating the security, dependability, and robustness of the algorithm, ensuring it remains stable and non-intrusive during normal system transients.

For this simulation, the short-circuit levels of both Source 1 and Source 2 are maintained at their maximum value of 250 MVA. The study is divided into two parts: one is which system power flows from Source 1 towards Source 2, and the other where the power flow direction is reversed, i.e. from Source 2 towards Source 1. During the simulation, the magnitudes of Load 3, Load 5, and Load 7 are varied to simulate load-changing scenarios.

Importantly, in each test case, only one load is modified or disconnected at a time, and this process is repeated across multiple individual cases to evaluate the scheme's response to a variety of load variation events.

5.4.1.4.1. Pre-fault system power flow from Source 1 towards Source 2

The simulation involves adjusting the levels of Load 5 and Load 7 to 50% and 90% of their full-load ratings. Additionally, simulations are also conducted that includes complete load disconnections through opening switches SW5 and SW7 to emulate sudden load loss.

As an example, the simulated results for immediate load loss at Load 7 by opening switch SW7 at t = 0.4 s, are presented in Figure 5.11.

As illustrated in Figure 5.11, when Load 7 is disconnected, every measuring device (relay) in the system experiences the disturbance, as evidenced by changes in their current angles and a drop in their current magnitudes. However, only the current angle variation at relays R62 and R71 are sufficient to trigger the faulted section identification process. The angle shift in all three phases recorded by both relays is identical, with a value of 4.771°. Both relays correctly determine that the disturbance lies outside their respective monitored line section, as the current angular shifts and magnitude changes before and after the disturbance exhibit identical behaviour. Therefore, neither relay initiates a trip signal. The currents measured the other relays do not exhibit significant enough changes to surpass the predefined threshold, meaning the scheme is not activated, and no protective actions, or actions to indicate that a faulted section has been identified, are taken.

For other scenarios of load changes in Load 5 and Load 7, their simulated results of the actual signals comprising the current angle shift between normal and after load change conditions comparison signal ($\Delta\theta_{abc}$), the current magnitude change between pre- and during-disturbance periods comparison signal ($\Delta|I_{abc}|$), and the trip signals of each paired relay, are listed in Table 5.11.

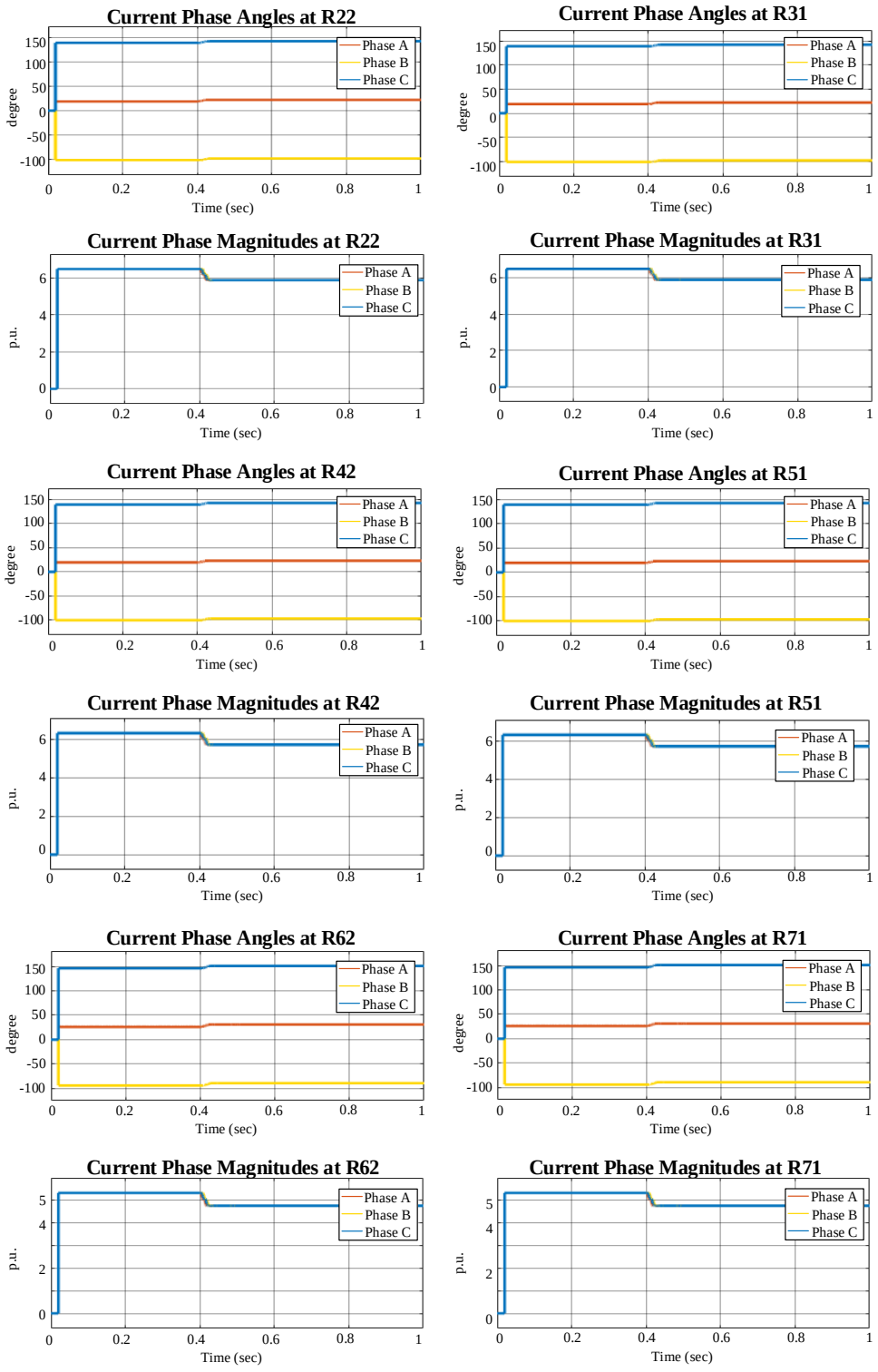

Figure 5.11: Current phase angle and current phase magnitude at observed relays in double-infeed system when Load 7 is disconnected to the system and pre-fault system power flow from Source 1 towards Source 2

Table 5.11: Summary of transmitted signals between each set of paired relays under various load changes scenarios when pre-fault power flows from Source 1 towards Source 2

Load Change at	Capacity of Full Load	Flag Signal			$\Delta\theta_{abc}$			$\Delta\lvert I_{abc}\rvert$			Trip Signal		
		Signal Between Paired Relay											
		L2-L3	L4-L5	L6-L7	L2-L3	L4-L5	L6-L7	L2-L3	L4-L5	L6-L7	L2-L3	L4-L5	L6-L7
Load 5	No Load	0	0	0	-	-	-	-	-	-	-	-	-
	50%	0	0	0	-	-	-	-	-	-	-	-	-
	90%	0	0	0	-	-	-	-	-	-	-	-	-
Load 7	No Load	0	0	1	-	-	0	-	-	0	-	-	0
	50%	0	0	0	-	-	-	-	-	-	-	-	-
	90%	0	0	0	-	-	-	-	-	-	-	-	-

5.4.1.4.2. Pre-fault system power flow from Source 2 towards Source 1

The same procedure as the forward system power flow direction is applied to Load 3 and Load 5, where their load levels are adjusted to 50% and 90% of their full-load capacities, and disconnection is simulated by opening SW3 and SW5, respectively.

The simulated results for this situation, including the current angle shift between normal and after load change conditions comparison signal ($\Delta\theta_{abc}$), the current magnitude change between pre- and after-load change periods comparison signal ($\Delta|I_{abc}|$), and the trip signals of each paired relay, are displayed in Table 5.12.

In the load change without fault scenarios in Table 5.12, it is observed that all relays detect the electrical disturbance resulting from the variation or disconnection of loads. Solely the relays located at both ends of the line section connecting Bus L2 and Bus L3 trigger the operation of the algorithm when Load 3 is abruptly disconnected. However, in every instance, the algorithm correctly determines that the disturbance does not originate within the

respective observed zones of those relays. As a result, no trip signals are issued, and the system continues to operate without interruption.

Table 5.12: Summary of transmitted signals between each set of paired relays under various load changes scenarios when pre-fault power flows from Source 2 towards Source 1

Load Change at	Capacity of Full Load	Flag Signal			$\Delta\theta_{abc}$			$\Delta\lvert I_{abc}\rvert$			Trip Signal		
		Signal Between Paired Relay											
		L2-L3	L4-L5	L6-L7	L2-L3	L4-L5	L6-L7	L2-L3	L4-L5	L6-L7	L2-L3	L4-L5	L6-L7
Load 3	No Load	1	0	0	0	-	-	0	-	-	0	-	-
	50%	0	0	0	-	-	-	-	-	-	-	-	-
	90%	0	0	0	-	-	-	-	-	-	-	-	-
Load 5	No Load	0	0	0	-	-	-	-	-	-	-	-	-
	50%	0	0	0	-	-	-	-	-	-	-	-	-
	90%	0	0	0	-	-	-	-	-	-	-	-	-

In all other scenarios, the changes observed – both in terms of current angle and magnitude – do not exceed the predefined thresholds required to initiate the faulted section identification process. Consequently, the scheme is not activated, and no protection or faulted section identification action are taken.

This outcome highlights the security, accuracy, and discrimination capability of the scheme to remain stable and not to identify that a fault has occurred on a section during non-fault disturbances events, thus ensuring the stability and reliability of the overall system under normal non-fault transients.

5.4.2 Single-infeed system results

In cases where one of the infeeds has extremely low fault level, or is not in service, or indeed does not exist (e.g. in radial systems), the system has a single fault infeed, which is common in traditional power distribution systems. Under such conditions, when a fault occurs, the loads and lines downstream of the fault (for solid short circuits) will not receive power on the faulted phase(s) due to the voltage at the point of the upstream fault being zero (again for solid

short circuits). Consequently, the current phase angle measured "downstream" of the fault location becomes either impossible to measure or highly uncertain, making it unreliable for accurate faulted section identification using this scheme [5.5].

Therefore, relying solely on current angle change from pre-fault to during fault conditions for faulted section identification may not be sufficient. To enhance decision-making, current phase magnitude change comparison (effectively a simple differential comparison) is incorporated as a secondary "check" within the algorithm. This magnitude-based comparison is applied when the angle change comparison signifies a result of '0', indicating that no fault has been detected within the section from angle-change comparisons. To evaluate the fault identification scheme under this condition, the system model in Figure 5.1 is used for demonstration, with the same configuration as used in previous case studies. However, the controllable switch between Bus L7 and Source 2 is opened, thereby disconnecting Source 2 from the system, as displayed in Figure 5.12.

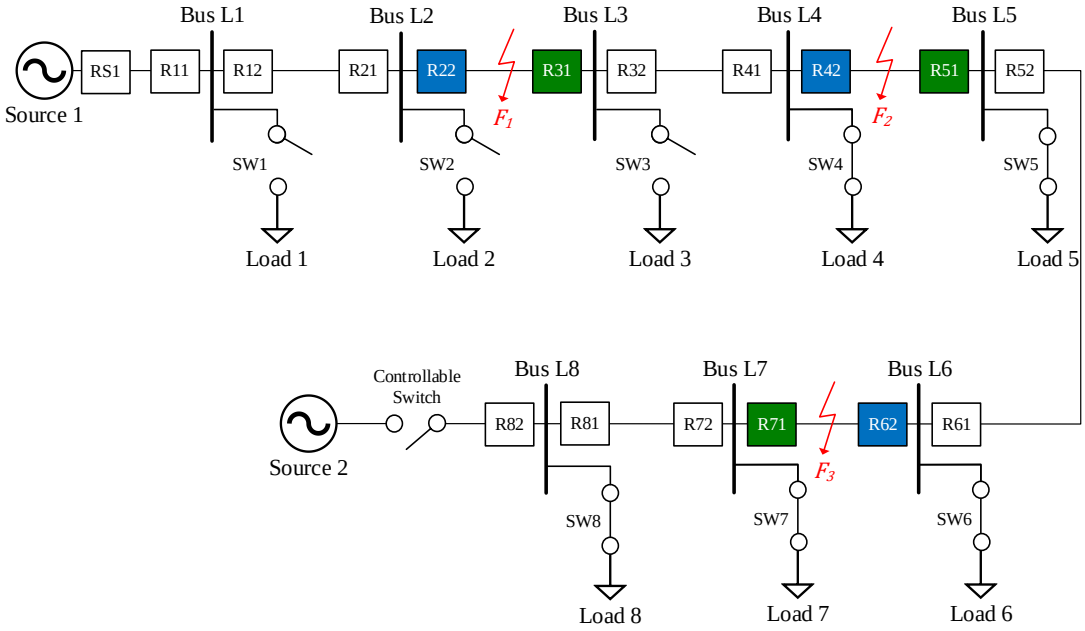

Figure 5.12: MATLAB/Simulink model used in single-infeed system case studies

5.4.2.1 Different fault location scenarios (single-infeed system)

Similar to the double-infeed scenario simulation, the single-infeed simulation with different fault locations is conducted to evaluate the performance of the scheme under various fault conditions along the distribution lines, including close-in faults. The simulation considers fault F_1 between Bus L2 and Bus L3, fault F_2 between Bus L4 and Bus L5, and fault F_3 between Bus L6 and Bus L7, occurring at 10%, 50%, and 90% of the line section length within each monitoring zone.

For all cases, Source 1 maintains has a short circuit level of 250 MVA, with a voltage angle of 10°. Each simulation case incorporates different fault types, including balanced three-phase faults (3-PH) and unbalanced faults such as single-phase-to-earth (P-E) faults, phase-to-phase faults (P-P), and double-phase-to-earth faults (P-P-E), to ensure a comprehensive assessment of the scheme's reliability and effectiveness.

For example, a phase-B-to-earth (B-E) fault F_3 occurs at 90% of the line section length between Bus L6 and Bus L7 at simulated time of 0.4 s. The results for this scenario are presented in Figure 5.13 – Figure 5.15.

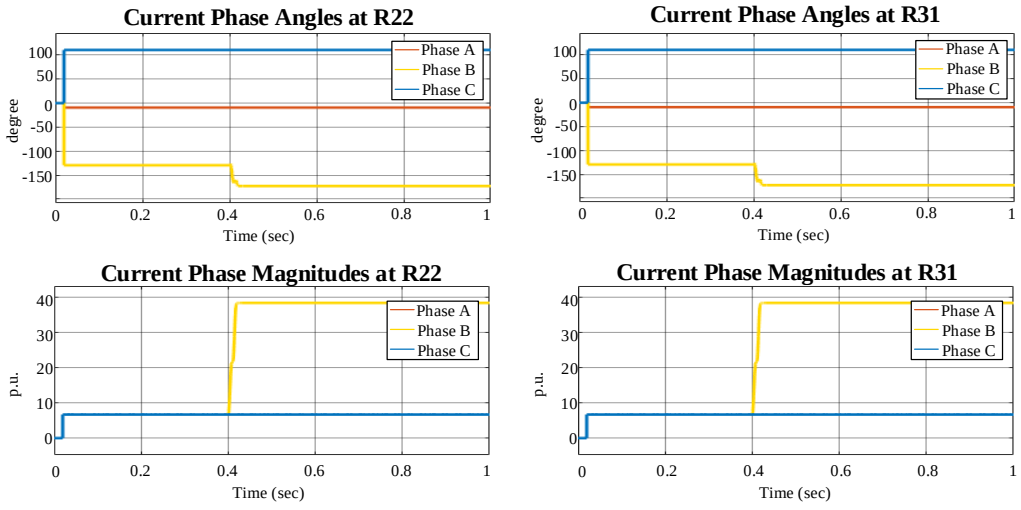

Figure 5.13: Current phase angle and current phase magnitude at relays R22 and R31 in single-infeed system when a B-E fault F_3 occurs

As observed in Figure 5.13, when a B-E fault F_3 is introduced, the faulted section identification process is initiated. The phase-B current angular changes between the pre-fault and during-fault conditions as measured at relays R22 and R31 ($\Delta\theta_{b,R22}$, $\Delta\theta_{b,R31}$) and exhibits the same rotational direction at both, specifically a CW rotation. These results are from a phase angle change of -43.323°, transitioning from -129.473° before the fault to -172.796° when fault occurs, which is sufficient to initiate the process. Since the current angle change comparison indicates that both relays the same rotational direction, it is necessary to incorporate current magnitude change between fault and normal periods comparison for further analysis. However, when examining the current magnitude at both relays, it is observed that upon fault occurrence, the phase-B current magnitude of both relays increases. Consequently, when comparing these values, the results confirm that the fault does not occur on the line section between Bus L2 and Bus L3.

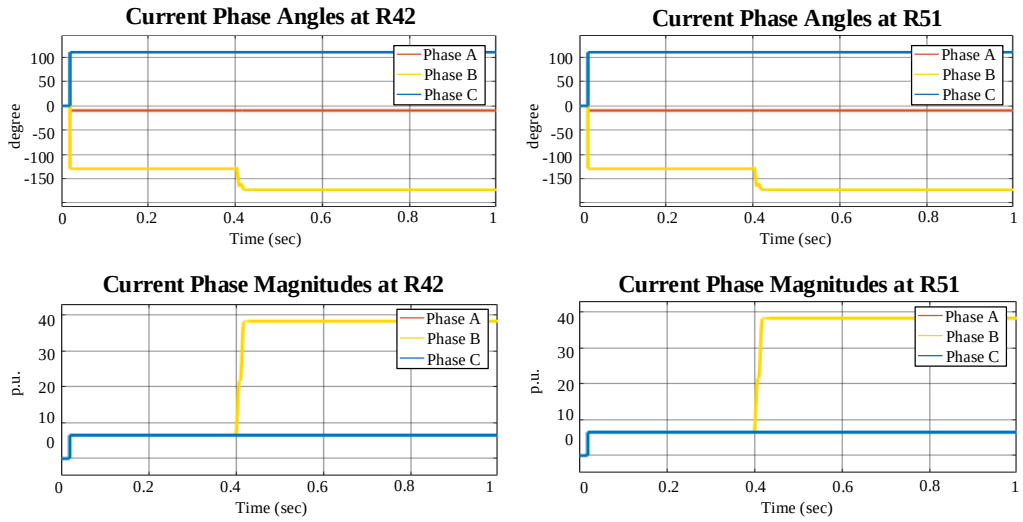

Figure 5.14: Current phase angle and current phase magnitude at relays R42 and R51 in single-infeed system when a B-E fault F_3 occurs

As for the paired relays (R22 and R31), relays R42 and R51 produce identical results, as illustrated in Figure 5.14. The fault identification process is initiated when B-E fault F_3 occurs, both relays measured a phase-B current phase angle of -172.876° during the fault, compared to the normal condition

value of -129.552°. This results in a calculated phase-B current phase angular change ($\Delta\theta_{b,R42}$, $\Delta\theta_{b,R51}$) of -43.322°, indicating a CW rotation for both relays. Given that the current angle change phase comparison yields identical results, further analysis using current magnitude change of pre- and during-fault comparison is required. However, upon the examination of the current magnitude values, it is observed that when the fault F_3 occurs, the phase-B current magnitude increases at both relays. This comparison suggests that the fault is external from Bus L4-L5 zone, as a fault within this line section would have resulted in a different magnitude change pattern.

For the final set of relays, R62 and R71, the experimental results in Figure 5.15 indicate that when a B-E fault F_3 occurs, the operation of the algorithm is initiated. Relay R62 measures a phase-B current angle change ($\Delta\theta_{b,R62}$) of -43.276°, corresponding to a CW rotation. This shift results from a transition in the normal condition value from -129.768° to -173.044° during the fault. At the same time, Relay R71 records a phase-B current angle change ($\Delta\theta_{b,R71}$) of -54.891°, also exhibiting a CW rotation, which shifts from -129.769° to 175.340 °. Since the current angle change comparison indicates identical rotation direction as both ends, the initial conclusion would suggest that the fault is external to the observed zone between Bus L6 and Bus L7. This behaviour is influenced by the significant reduction in current magnitude at Relay R71, which is positioned downstream of the fault. During the fault, the current at R71 decreases dramatically, approaching zero, making the measured current angular unreliable for use in current angle change between before and fault periods comparison within the scheme. In contrast, the current at R62 (upstream of the fault) increases, as it receives fault current generated from Source 1. When comparing the current magnitude change between pre-fault and during-fault at both relays ($\Delta|I_{b,R62}|$, $\Delta|I_{b,R71}|$), a clear difference emerges: while the current magnitude upstream of the fault (R62) increases, the current magnitude downstream of the fault (R71) significantly decrease, approaching zero during the fault period. This behaviour is used as an additional decision-

making criterion for faulted section identification, particularly when the current angle change comparison alone is insufficient or misleading (or to decide the fault as external).

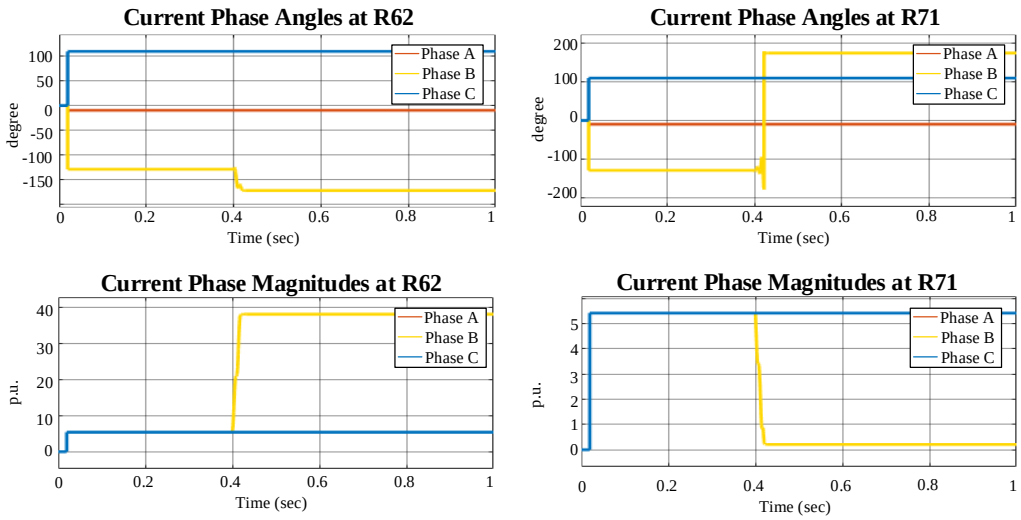

Figure 5.15: Current phase angle and current phase magnitude at relays R62 and R71 in single-infeed system when a B-E fault F_3 occurs

For relays R62 and R71, although the current angle change comparison suggests that the fault is external, the current magnitude change comparison shows a marked difference in the magnitudes of the measured current. Based on this, it can be concluded that the fault is internal to the line connecting Bus L6 and Bus L7.

Based on the fault identification analysis of all three pairs of relays, it is concluded that the fault is on the line section between Bus L6 and Bus L7. Consequently, only the CBs within this zone receive a trip signal of '1' to isolate the faulty section in a protection application, while the CBs at other buses remains inactive. In a monitoring/FLISR application, the faulted section would be identified and used to reconfigure/repair/restore the system.

As described earlier, to minimise communications bandwidth and simply communications, the actual signals transmitted between paired relays, as well as the trip signals sent to the CBs, are represented using binary codes. Therefore, the results presented above are summarised in Table 5.13.

Table 5.13: Summary of transmitted signals when a B-E Fault F_3 occurs

Relay	Flag Signal	Angle Change Signal	Angle Change Comparison Signal ($\Delta\theta_{abc}$)	Magnitude Change Signal	Magnitude Change Comparison Signal ($\Delta\|I_{abc}\|$)	Trip Signal
R22	1	1	0	1	0	0
R31	1	1		1		0
R42	1	1	0	1	0	0
R51	1	1		1		0
R62	1	1	0	1	1	1
R71	1	1		0		1

Furthermore, other fault types and fault F_1 (between Bus L2-L3), fault F_2 (between Bus L4-L5), have also been simulated to evaluate the performance of the scheme under various fault locations conditions. The test results for these scenarios are shown in Table 5.14.

Table 5.14: Summary of transmitted signals between each set of paired relays under various fault types and fault locations conditions

Fault			Flag Signal			$\Delta\theta_{abc}$			$\Delta\lvert I_{abc}\rvert$			Trip Signal		
Location	Type	At Line Percentage	Signal Between Paired Relay											
			L2-L3	L4-L5	L6-L7	L2-L3	L4-L5	L6-L7	L2-L3	L4-L5	L6-L7	L2-L3	L4-L5	L6-L7
Between Bus L2-L3	3-PH	10%	1	1	1	0	0	0	1	0	0	1	0	0
		50%	1	1	1	0	0	0	1	0	0	1	0	0
		90%	1	1	1	0	0	0	1	0	0	1	0	0
	P-E	10%	1	1	1	0	0	0	1	0	0	1	0	0
		50%	1	1	1	0	0	0	1	0	0	1	0	0
		90%	1	1	1	0	0	0	1	0	0	1	0	0
	P-P	10%	1	1	1	1	0	0	1	0	0	1	0	0
		50%	1	1	1	1	0	0	1	0	0	1	0	0
		90%	1	1	1	1	0	0	1	0	0	1	0	0
	P-P-E	10%	1	1	1	0	0	0	1	0	0	1	0	0
		50%	1	1	1	0	0	0	1	0	0	1	0	0
		90%	1	1	1	0	0	0	1	0	0	1	0	0
Between Bus L4-L5	3-PH	10%	1	1	1	0	0	0	0	1	0	0	1	0
		50%	1	1	1	0	0	0	0	1	0	0	1	0
		90%	1	1	1	0	0	0	0	1	0	0	1	0
	P-E	10%	1	1	1	0	0	0	0	1	0	0	1	0
		50%	1	1	1	0	0	0	0	1	0	0	1	0
		90%	1	1	1	0	0	0	0	1	0	0	1	0
	P-P	10%	1	1	1	0	1	0	0	1	0	0	1	0
		50%	1	1	1	0	1	0	0	1	0	0	1	0
		90%	1	1	1	0	1	0	0	1	0	0	1	0
	P-P-E	10%	1	1	1	0	0	0	0	1	0	0	1	0
		50%	1	1	1	0	0	0	0	1	0	0	1	0
		90%	1	1	1	0	0	0	0	1	0	0	1	0
Between Bus L6-L7	3-PH	10%	1	1	1	0	0	0	0	0	1	0	0	1
		50%	1	1	1	0	0	0	0	0	1	0	0	1
		90%	1	1	1	0	0	0	0	0	1	0	0	1
	P-E	10%	1	1	1	0	0	0	0	0	1	0	0	1
		50%	1	1	1	0	0	0	0	0	1	0	0	1
		90%	1	1	1	0	0	0	0	0	1	0	0	1
	P-P	10%	1	1	1	0	0	1	0	0	1	0	0	1
		50%	1	1	1	0	0	1	0	0	1	0	0	1
		90%	1	1	1	0	0	1	0	0	1	0	0	1
	P-P-E	10%	1	1	1	0	0	0	0	0	1	0	0	1
		50%	1	1	1	0	0	0	0	0	1	0	0	1
		90%	1	1	1	0	0	0	0	0	1	0	0	1

As observed from results in Table 5.14, it can be concluded that the fault identification process operates accurately over a range of conditions. Although the comparison of current phase angle change between pre-fault and during-fault condition at both ends of a line section may fail to detect an internal fault, due to the significant difference in current magnitudes at each end pre- and during-fault periods comparison results in the system correctly identifying the faulted section. When the current magnitude change comparison yields a result of '1', indicating a significant difference in current magnitude characteristics between the pre-fault and during-fault conditions, the scheme is still able to accurately determine the presence of an internal fault within the observed zone. This confirms the effectiveness and the reliability of the proposed method, even in cases where angle-based detection alone is insufficient.

Note that in certain phase-to-phase (P-P) fault scenarios for single infeed systems, the comparison of current angles from pre- to during-fault conditions across measuring devices at each line section end remains effective for identifying the faulted section. This is because, during phase-phase faults, as long as there is a three-phase connected load (star or delta) connected downstream from the phase-phase fault location, then current will "flow" from the source through the healthy phase and return, via the load connections, to the fault location via the faulted phases, and the currents on the faulted phases will be out of phase with the currents flowing from the source upstream of the fault. So, if measurements are taken from both ends of the faulted section, the faulted section will be correctly identified. This will be the case when there are infeeds from only one, or both, of the ends of the system. In the case where there are no loads or other phase-phase connections (e.g., transformers) downstream of the phase-phase fault location, then no currents will flow "back" to the fault from downstream. In such cases, the supplementary magnitude change comparison element of the algorithm should successfully identify the faulted section.

5.4.2.2 Different fault resistance scenarios (single-infeed system)

The scheme was tested in a single-infeed system with varying to assess its performance in detecting HIFs. In this experiment, the short-circuit level of Source 1 was maintained at 250 MVA, with a voltage angle of 10°. The simulation was conducted by introducing faults at different locations, specifically between Bus L2-L3 (F_1), Bus L4-L5 (F_2), and Bus L6-L7 (F_3) at t = 0.4 s. Each fault was assigned a fault resistance of 10, 15, 20, 25, and 30 Ω to evaluate the impact of HIF conditions on the scheme. Table 5.15 outlines the simulation results for different fault resistance scenarios.

Table 5.15: Summary of communicated signals under various fault types, fault locations, and fault resistances conditions in single-infeed system

Fault			Flag Signal			$\Delta\theta_{abc}$			$\Delta\lvert I_{abc}\rvert$			Trip Signal		
Location	Type	Fault Resistance (Ω)	Signal Between Paired Relay											
			L2-L3	L4-L5	L6-L7	L2-L3	L4-L5	L6-L7	L2-L3	L4-L5	L6-L7	L2-L3	L4-L5	L6-L7
Between Bus L2-L3	3-PH	10	1	1	1	1	0	0	1	0	0	1	0	0
		15	1	1	1	1	0	0	1	0	0	1	0	0
		20	0	0	0	-	-	-	-	-	-	-	-	-
		25	0	0	0	-	-	-	-	-	-	-	-	-
		30	0	0	0	-	-	-	-	-	-	-	-	-
	P-E	10	1	1	1	1	0	0	1	0	0	1	0	0
		15	1	1	1	1	0	0	1	0	0	1	0	0
		20	0	0	0	-	-	-	-	-	-	-	-	-
		25	0	0	0	-	-	-	-	-	-	-	-	-
		30	0	0	0	-	-	-	-	-	-	-	-	-
	P-P	10	1	1	1	1	0	0	1	0	0	1	0	0
		15	1	1	1	1	0	0	1	0	0	1	0	0
		20	0	0	0	-	-	-	-	-	-	-	-	-
		25	0	0	0	-	-	-	-	-	-	-	-	-
		30	0	0	0	-	-	-	-	-	-	-	-	-
	P-P-E	10	1	1	1	1	0	0	1	0	0	1	0	0
		15	1	1	1	1	0	0	1	0	0	1	0	0
		20	0	0	0	-	-	-	-	-	-	-	-	-
		25	0	0	0	-	-	-	-	-	-	-	-	-
		30	0	0	0	-	-	-	-	-	-	-	-	-

Table 5.15 (cont.): Summary of communicated signals under various fault types, fault locations, and fault resistances conditions in single-infeed system

Fault			Flag Signal			$\Delta\theta_{abc}$			$\Delta\lvert I_{abc}\rvert$			Trip Signal		
Location	Type	Fault Resistance (Ω)	Signal Between Paired Relay											
			L2-L3	L4-L5	L6-L7	L2-L3	L4-L5	L6-L7	L2-L3	L4-L5	L6-L7	L2-L3	L4-L5	L6-L7
Between Bus L4-L5	3-PH	10	1	1	1	0	0	0	0	1	0	0	1	0
		15	1	1	1	0	1	0	0	1	0	0	1	0
		20	1	1	1	0	1	0	0	1	0	0	1	0
		25	1	1	1	0	1	0	0	1	0	0	1	0
		30	1	0	0	0	-	-	0	-	-	0	-	-
	P-E	10	1	1	1	0	0	0	0	1	0	0	1	0
		15	1	1	1	0	1	0	0	1	0	0	1	0
		20	1	1	1	0	1	0	0	1	0	0	1	0
		25	1	1	1	0	1	0	0	1	0	0	1	0
		30	1	0	0	0	-	-	0	-	-	0	-	-
	P-P	10	1	1	1	0	1	0	0	1	0	0	1	0
		15	1	1	1	0	1	0	0	1	0	0	1	0
		20	1	1	1	0	1	0	0	1	0	0	1	0
		25	1	1	1	0	1	0	0	1	0	0	1	0
		30	1	0	0	0	-	-	0	-	-	0	-	-
	P-P-E	10	1	1	1	0	0	0	0	1	0	0	1	0
		15	1	1	1	0	1	0	0	1	0	0	1	0
		20	1	1	1	0	1	0	0	1	0	0	1	0
		25	1	1	1	0	1	0	0	1	0	0	1	0
		30	1	0	0	0	-	-	0	-	-	0	-	-
Between Bus L6-L7	3-PH	10	1	1	1	0	0	0	0	0	1	0	0	1
		15	1	1	1	0	0	0	0	0	1	0	0	1
		20	1	1	1	0	0	0	0	0	1	0	0	1
		25	0	0	0	-	-	-	-	-	-	-	-	-
		30	0	0	0	-	-	-	-	-	-	-	-	-
	P-E	10	1	1	1	0	0	0	0	0	1	0	0	1
		15	1	1	1	0	0	0	0	0	1	0	0	1
		20	1	1	1	0	0	0	0	0	1	0	0	1
		25	0	0	0	-	-	-	-	-	-	-	-	-
		30	0	0	0	-	-	-	-	-	-	-	-	-
	P-P	10	1	1	1	0	0	1	0	0	1	0	0	1
		15	1	1	1	0	0	1	0	0	1	0	0	1
		20	1	1	1	0	0	1	0	0	1	0	0	1
		25	0	0	0	-	-	-	-	-	-	-	-	-
		30	0	0	0	-	-	-	-	-	-	-	-	-
	P-P-E	10	1	1	1	0	0	0	0	0	1	0	0	1
		15	1	1	1	0	0	0	0	0	1	0	0	1
		20	1	1	1	0	0	0	0	0	1	0	0	1
		25	0	0	0	-	-	-	-	-	-	-	-	-
		30	0	0	0	-	-	-	-	-	-	-	-	-

As displayed in Table 5.15, the scheme remains capable of detecting a fault correctly when the fault resistance is no more than 15 Ω. This is because, at higher fault resistance, the absolute values of the changes in current angle and current magnitude may fail to reach the predefined threshold, thereby preventing the initiation of the fault identification process. As mentioned previously, the thresholds for initiation could be modified to make the system more sensitive, but this would come at the expense of increased operation (but the system should still never maloperate). These configurations of thresholds could be considered on a case-by-case basis. In such cases, no signal exchange occurs between the paired relays. However, when the fault identification process is initiated, the analysis of current angle changes between pre- and during-fault conditions may not be reliable, as the fault current is supplied only from one end (upstream of the fault), and there is no fault current contribution from the downstream side. As a result, the current angle downstream of the fault may not exhibit the expected change (as would be expected if there was a fault infeed from this direction). Nevertheless, the current magnitude on the downstream side consistently decreases (even if not significantly close to zero, due to the characteristic of HIFs [5.6]). This ensures that the analysis of current magnitude change between pre- and during-fault conditions remains accurate and dependable. As a result, only the CBs associated with the faulted section are activated by issuing a trip signal ('1') in a protection application, thereby isolating the fault without impact other parts of the system. This demonstrates the selectivity and precision of the method in accurately identifying and isolating fault, even under challenging HIF conditions.

5.4.2.3 Different short-circuit level scenarios (single-infeed system)

For the demonstration of the single-infeed system, the short-circuit level is varied to simulate fault conditions in a weak infeed system.

In this experiment, the fault level of Source 1 is varied, to include levels of at 10, 50, 100, 150, and 200 MVA. The switching configuration remain unchanged, as shown in Figure 5.12, and various fault types are introduced at different locations: between Bus L2-L3 (F_1), Bus L4-L5 (F_2), and Bus L6-L7 (F_3). Each fault occurs at simulated time of 0.4 s during the simulation. The experiment results of relays signals exchanged between each paired relay, including the flag signals, the signals of current angle change before and during fault period comparison ($\Delta\theta_{abc}$), signals of current magnitude change pre-fault and during-fault condition comparison ($\Delta|I_{abc}|$), and trip signals are depicted in Table 5.16.

As the results from Table 5.16 illustrate, when different type of fault occurs under various short-circuit levels, the fault identification is initiated, then the current angle change comparison signals between normal and fault conditions consistently return a value of '0', indicating that no internal disturbance within the corresponding observed zones – an outcome which reflect incorrect analysis decision. However, the algorithm is still able to correctly identify the internal fault by relying on the comparison of current magnitude change between the pre-fault and fault periods. In these cases, a '1' value is obtained, signifying a difference in current magnitude at the upstream and downstream ends of the faulted section. These results confirm the effectiveness and dependability of the scheme, highlighting its ability to accurately detect and isolate faults even under challenging conditions associated with different inertia infeed system.

Table 5.16: Summary of communicated signals under various fault types, fault locations, and short-circuit level of the source in single-infeed system

Fault		Short-circuit Level at Source 2 (MVA)	Flag Signal			$\Delta\theta_{abc}$			$\Delta\lvert I_{abc}\rvert$			Trip Signal		
			Signal Between Paired Relay											
Location	Type		L2-L3	L4-L5	L6-L7	L2-L3	L4-L5	L6-L7	L2-L3	L4-L5	L6-L7	L2-L3	L4-L5	L6-L7
Between Bus L2-L3	3-PH	10	1	1	1	0	0	0	1	0	0	1	0	0
		50	1	1	1	0	0	0	1	0	0	1	0	0
		100	1	1	1	0	0	0	1	0	0	1	0	0
		150	1	1	1	0	0	0	1	0	0	1	0	0
		200	1	1	1	0	0	0	1	0	0	1	0	0
	P-E	10	1	1	1	0	0	0	1	0	0	1	0	0
		50	1	1	1	0	0	0	1	0	0	1	0	0
		100	1	1	1	0	0	0	1	0	0	1	0	0
		150	1	1	1	0	0	0	1	0	0	1	0	0
		200	1	1	1	0	0	0	1	0	0	1	0	0
	P-P	10	1	1	1	1	0	0	1	0	0	1	0	0
		50	1	1	1	1	0	0	1	0	0	1	0	0
		100	1	1	1	1	0	0	1	0	0	1	0	0
		150	1	1	1	1	0	0	1	0	0	1	0	0
		200	1	1	1	1	0	0	1	0	0	1	0	0
	P-P-E	10	1	1	1	0	0	0	1	0	0	1	0	0
		50	1	1	1	0	0	0	1	0	0	1	0	0
		100	1	1	1	0	0	0	1	0	0	1	0	0
		150	1	1	1	0	0	0	1	0	0	1	0	0
		200	1	1	1	0	0	0	1	0	0	1	0	0
Between Bus L4-L5	3-PH	10	1	1	1	0	0	0	0	1	0	0	1	0
		50	1	1	1	0	0	0	0	1	0	0	1	0
		100	1	1	1	0	0	0	0	1	0	0	1	0
		150	1	1	1	0	0	0	0	1	0	0	1	0
		200	1	1	1	0	0	0	0	1	0	0	1	0
	P-E	10	1	1	1	0	0	0	0	1	0	0	1	0
		50	1	1	1	0	0	0	0	1	0	0	1	0
		100	1	1	1	0	0	0	0	1	0	0	1	0
		150	1	1	1	0	0	0	0	1	0	0	1	0
		200	1	1	1	0	0	0	0	1	0	0	1	0
	P-P	10	1	1	1	0	1	0	0	1	0	0	1	0
		50	1	1	1	0	1	0	0	1	0	0	1	0
		100	1	1	1	0	1	0	0	1	0	0	1	0
		150	1	1	1	0	1	0	0	1	0	0	1	0
		200	1	1	1	0	1	0	0	1	0	0	1	0

Table 5.16 (cont.): Summary of communicated signals under various fault types, fault locations, and short-circuit level of the source in single-infeed system

Fault		Short-circuit Level at Source 2 (MVA)	Flag Signal			$\Delta\theta_{abc}$			$\Delta\|I_{abc}\|$			Trip Signal		
			Signal Between Paired Relay											
Location	Type		L2-L3	L4-L5	L6-L7	L2-L3	L4-L5	L6-L7	L2-L3	L4-L5	L6-L7	L2-L3	L4-L5	L6-L7
Between Bus L4-L5	P-P-E	10	1	1	1	0	0	0	0	1	0	0	1	0
		50	1	1	1	0	0	0	0	1	0	0	1	0
		100	1	1	1	0	0	0	0	1	0	0	1	0
		150	1	1	1	0	0	0	0	1	0	0	1	0
		200	1	1	1	0	0	0	0	1	0	0	1	0
Between Bus L6-L7	3-PH	10	1	1	1	0	0	0	0	0	1	0	0	1
		50	1	1	1	0	0	0	0	0	1	0	0	1
		100	1	1	1	0	0	0	0	0	1	0	0	1
		150	1	1	1	0	0	0	0	0	1	0	0	1
		200	1	1	1	0	0	0	0	0	1	0	0	1
	P-E	10	1	1	1	0	0	0	0	0	1	0	0	1
		50	1	1	1	0	0	0	0	0	1	0	0	1
		100	1	1	1	0	0	0	0	0	1	0	0	1
		150	1	1	1	0	0	0	0	0	1	0	0	1
		200	1	1	1	0	0	0	0	0	1	0	0	1
	P-P	10	1	1	1	0	0	1	0	0	1	0	0	1
		50	1	1	1	0	0	1	0	0	1	0	0	1
		100	1	1	1	0	0	1	0	0	1	0	0	1
		150	1	1	1	0	0	1	0	0	1	0	0	1
		200	1	1	1	0	0	1	0	0	1	0	0	1
	P-P-E	10	1	1	1	0	0	0	0	0	1	0	0	1
		50	1	1	1	0	0	0	0	0	1	0	0	1
		100	1	1	1	0	0	0	0	0	1	0	0	1
		150	1	1	1	0	0	0	0	0	1	0	0	1
		200	1	1	1	0	0	0	0	0	1	0	0	1

5.4.2.4 Load changes without fault scenarios (single-infeed system)

Similar to the double-infeed scenarios, simulations involving load variation without the presence of faults were conducted to evaluate the performance of the scheme under non-fault conditions. The aim was to confirm whether the algorithm continues to operate correctly when subjected to typical operational

disturbances. The initial switching configuration was maintained as shown in Figure 5.12, with Source 1 set to a short-circuit level of 250 MVA and a voltage angle of 10°.

In each test case, Load 5 and Load 7 were independently modified to represent 50% and 90% of their full-load capacities, including complete disconnection, which was achieved by opening switch SW5 and SW7, respectively, in order to isolate the corresponding loads. An example of the simulation results – when switch SW7 is open to disconnected Load 7 at t = 0.4 s – is shown in Figure 5.16.

As illustrated in Figure 5.16, when isolating Load 7, both the current phase angle and current magnitude at all relays exhibit observable changes, with are sufficiently to trigger the fault identification process. However, upon comparing the current angle change and current magnitude change between each relay and its paired relays, the algorithm correctly determines that the disturbance lies outside of their respective monitored zones. Consequently, no relay issues a trip command.

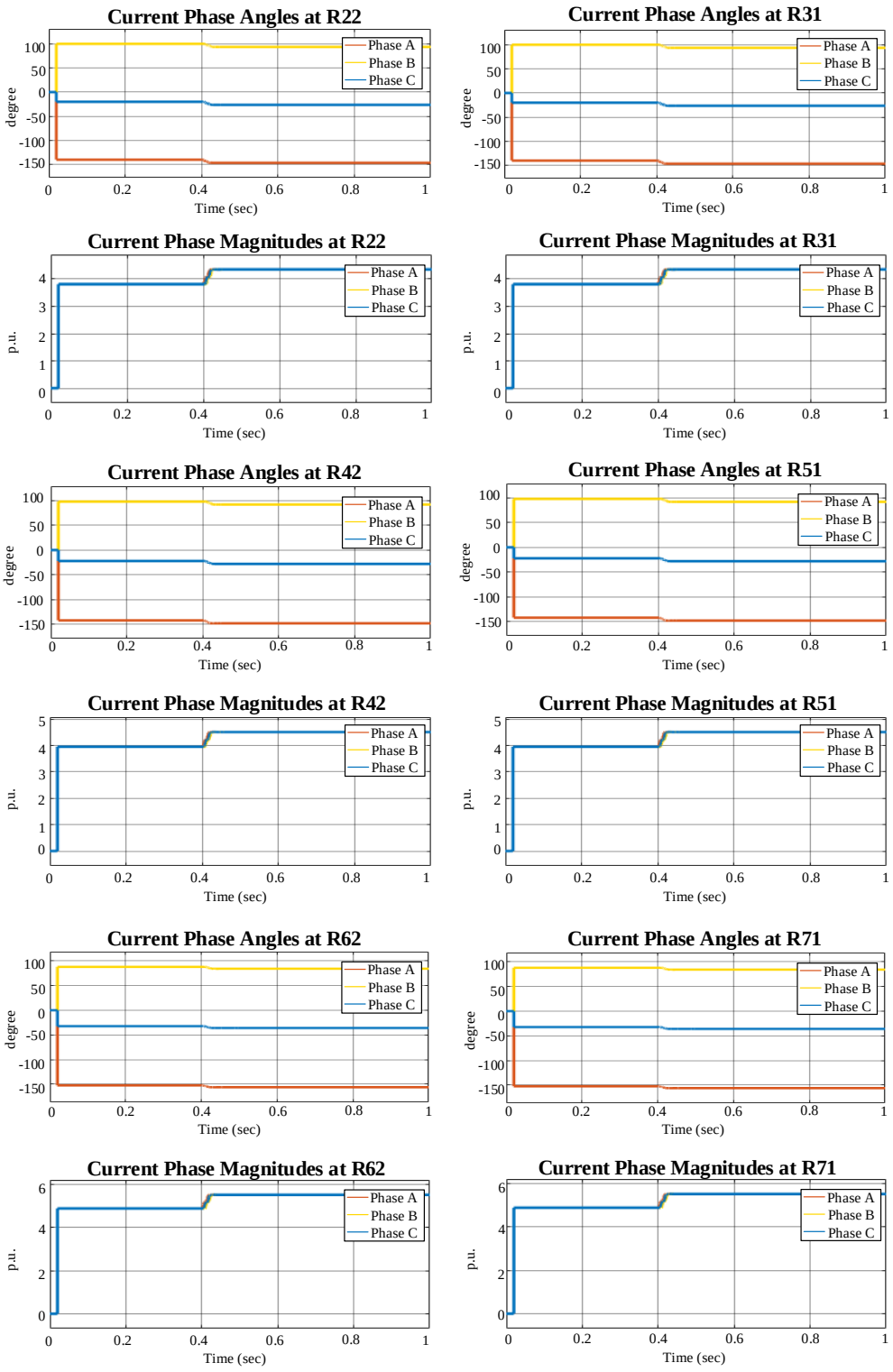

Figure 5.16: Current phase angle and current phase magnitude at observed relays in single-infeed system when Load 7 is reduced to 50% of full-load rating

For other scenarios of load changes in Load 5 and Load 7, their simulated results of the actual signals comprising the current angle shift between normal and disturbance conditions comparison signal ($\Delta\theta_{abc}$), the current magnitude change between normal and load change periods comparison signal ($\Delta|I_{abc}|$), and the trip signals of each paired relay, are listed in Table 5.17.

Table 5.17: Summary of transmitted signals between each set of paired relays under various load changes scenarios in single-infeed system

Load Change at	Capacity of Full Load	Flag Signal			$\Delta\theta_{abc}$			$\Delta\|I_{abc}\|$			Trip Signal		
		Signal Between Paired Relay											
		L2-L3	L4-L5	L6-L7	L2-L3	L4-L5	L6-L7	L2-L3	L4-L5	L6-L7	L2-L3	L4-L5	L6-L7
Load 5	No Load	0	0	0	-	-	-	-	-	-	-	-	-
	50%	0	0	0	-	-	-	-	-	-	-	-	-
	90%	0	0	0	-	-	-	-	-	-	-	-	-
Load 7	No Load	1	1	1	0	0	0	0	0	0	0	0	0
	50%	0	0	0	-	-	-	-	-	-	-	-	-
	90%	0	0	0	-	-	-	-	-	-	-	-	-

In the load change scenarios without the presence of faults, with the exception of the Load 7 disconnection scenario, which demonstrated in Figure 5.17, the current at all relays in the other cases exhibits noticeable variation in response to load changes. however, these changes are not sufficiently large to initiate the fault identification process, and as a result, the scheme is not activated.

These results underscore the scheme's strong security, sensitivity, and selectivity. The relays are capable of recognising changes in system conditions while accurately distinguishing between actual faults and routine load fluctuations, thereby maintain systems stability and ensuring reliable operation under non-fault conditions.

5.5 Chapter summary

This chapter has presented a set of comprehensive case studies showing the operation of the faulted section estimation scheme for a variety of conditions. Off-line simulations using the MATLAB/Simulink software have been used to highlight and analyse the scheme operation and to evaluate its performance and limits of performance. The simulation scenarios included variations of fault location within the same faulted line section – covering a range of positions including close-in faults – to assess the scheme's sensitivity and discriminative capabilities. Variation of fault resistance was also carried out to evaluate the scheme's effectiveness for a range of fault resistances and to establish the limits of the system's ability to correctly identify faults and faulted sections in terms of fault resistance, noting that the sensitivity of the system could be increased to make it more sensitive, but this may result in more operation for non-fault transients – but not maloperation. The influence of different short-circuit levels on the scheme's operation was also examined, including situations where one infeed is strong, one is progressively weaker, and situations where only a single infeed is present (again, varying its infeed levels across a range).

The results confirm that, regardless of fault type or location, and for a wide range of fault levels and infeed permutations, the system can operate correctly to identify the faulted section correctly (and remain stable for non-fault transients) in the vast majority of cases. It is only in scenarios where there is very low infeed form one end, or a low infeed from a single source, where the operation of the system may be compromised. In such cases, current magnitude change analysis between pre- during-fault conditions is conducted as a supplementary check and successfully identifies faults based on the different current behaviour observed at the upstream and downstream ends of the faulted zone, even when angle-based detection fails.

This chapter also reported on the scheme's performance in response to non-fault disturbances, such as sudden load changes. The results shows that although the scheme identifies such transients and in some cases initiates the

faulted section detection algorithm, no unnecessary trip signals or identification of faulted sections were produced, as no fault is detected on the system from analysis of angular and magnitude changes.

Overall, the simulation outcomes demonstrate that the protection scheme exhibits high reliability, selectivity, and robustness across a wide range of operational and fault conditions.

Chapter references

[5.1] J. Berry and P. Aston, 'Determination of Short Circuit Duty for Switchgear on the WPD Distribution System'. May 2017. [Online]. Available: https://www.nationalgrid.co.uk/downloads-view-reciteme/3482

[5.2] T. Haggis and P. Booth, 'Network Design Manual'. E.ON UK, December 2006. [Online]. Available: https://www.yumpu.com/en/document/read/8953808/network-design-manual-eon-uk

[5.3] *IEEE Standard for Interconnection and Interoperability of Distributed Energy Resources with Associated Electric Power Systems Interfaces*, April 2018.

[5.4] A. Apostolov, 'Accelerated Transmission Line Protection for Systems with High Penetration of Inverter Based Resources', PAC World. [Online]. Available: https://www.pacw.org/accelerated-transmission-line-protection-for-systems-with-high-penetration-of-inverter-based-resources

[5.5] J. J. Burke and D. J. Lawrence, 'Characteristics of Fault Currents on Distribution Systems', *IEEE Power Eng. Rev.*, vol. PER-4, no. 1, pp. 26–26, January 1984.

[5.6] D. Hou, 'High-Impedance Fault Detection—Field Tests and Dependability Analysis', presented at the 36th Annual Western Protective Relay Conference, Spokane, Washington, October 2009.

Chapter 6

Hardware-in-the-Loop Test Using RTDS

6.1 Chapter overview

Building upon the software simulation demonstration presented in Chapter 5, this chapter introduces real-time hardware-in-the-loop (HIL) testing to assess the practical applicability of the faulted section identification scheme in an "actual" (although experimental and laboratory-based) environment. The HIL laboratory setup incorporates a model developed in RSCAD for implementation in a Real-Time Digital Simulator (RTDS). Within this arrangement, an actual communication and computing hardware are utilised to implement the faulted section identification scheme and to facilitate data exchange between the two measuring devices (or relays). The testing validation process is conducted using various cases covering different fault locations and fault types, ensuring a comprehensive evaluation of the proposed scheme under diverse operating conditions and in a more realistic environment (compared to offline simulation as reported in Chapter 5) with actual hardware "in the loop".

6.2 The HIL experimental arrangement

To enhance the demonstration and validation of the faulted section identification scheme's performance, a HIL experimental arrangement has been created, and corresponding case studies have been executed using this arrangement in the laboratory at the University of Strathclyde. An overview of the laboratory is illustrated in Figure 6.1. The real-time dynamic behaviour of the power system, under both normal operating conditions and fault scenarios, are emulated using the RTDS [6.1]. The algorithm for the faulted section identification scheme, initially developed in MATLAB/Simulink, has been converted into a C++ code file and executed using Visual Studio software [6.2] to facilitate its integration with RSCAD.

To enable real-time date exchange, output current signals from the simulated current transformers (CTs) positioned between Bus 2 and Bus 3 are transmitted to separate computers via the Gigabit Transceiver Network – Socket (GTNET-SKT) cards. These cards serve as a real-time communication interface, enabling bidirectional data transfer between the RTDS and external computational units [6.3]. The communication between these components is establish using Ethernet communication, ensuring high-speed and reliable data transmission. Each processor, running the faulted section identification algorithm, receives the relevant data, processes it, and displays the results in real time, demonstrating the operation of the faulted section identification scheme in real time.

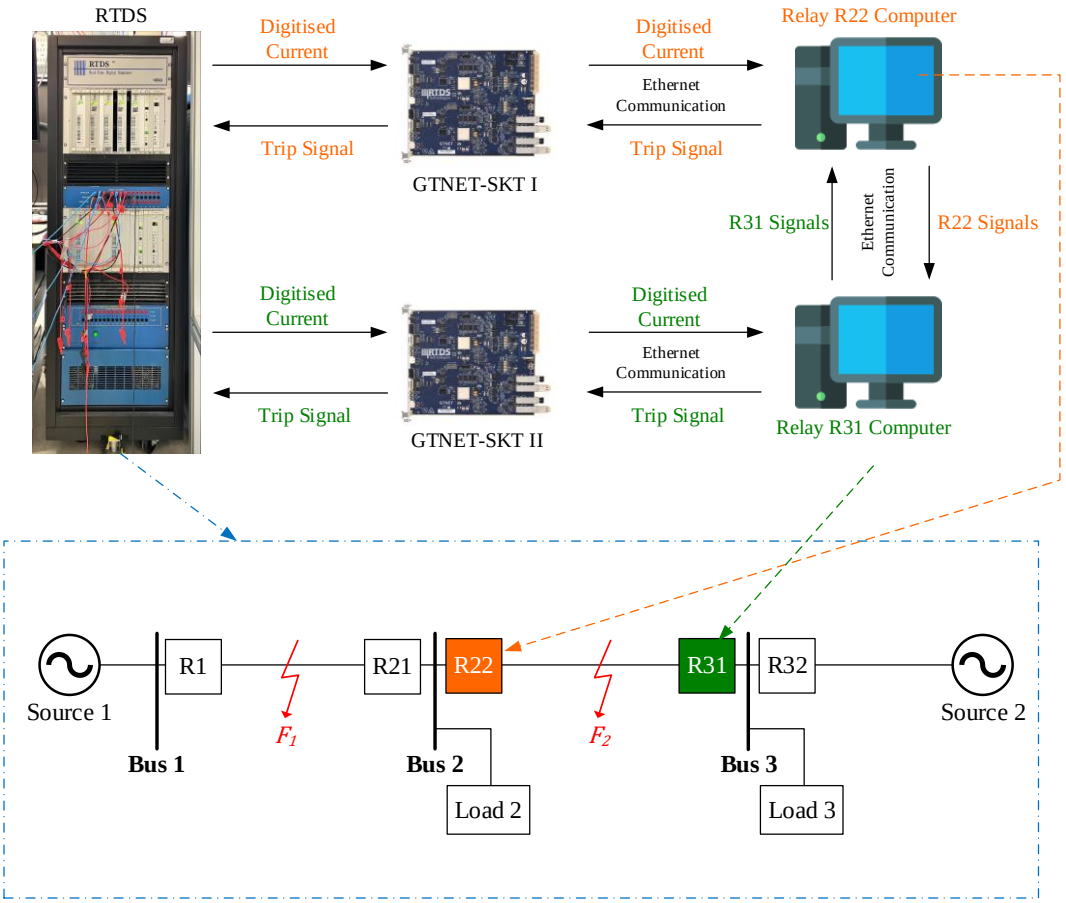

Figure 6.1: HIL laboratory arrangement and corresponding RSCAD model

As illustrated in Figure 6.1, the simulated model represents an 11 kV, 50 Hz system with radial configuration consisting of three buses, incorporating two power sources (which are modelled using ideal voltage sources with equivalent impedances to emulate different fault levels) located at opposite ends of the system, as used in the offline simulation studies presented earlier. The power flow direction is set up to ensure that power is flowing from Source 1 towards Source 2 in normal conditions, while two different (and variable) loads are individually connected to Bus 2 and Bus 3. Additionally, the RSCAD system includes five measurement locations (denoted as numbered "relays") positioned as shown in the figure. The line impedance is based on actual data from an 11 kV distribution line datasheet [6.4]. The parameters for each system component are provided in Table 6.1.

Two relays, R22 and R31, located at opposite ends of the line connecting Bus 2 and Bus 3, are interfaced with the RTDS via the GTNET-SKT card to facilitate the operation and testing of the algorithm. The measurement data transfer process in the HIL test is initiated by the RTDS, which generates three-phase current signals (that are digitised) representing the waveform at relay R22 and transmits them to the first computer/processor hosting the algorithm for relay 22 via the GTNET-SKT I card. Similarly, the RTDS sends three phase current waveform data from relay R31 to the second computer/processor, which runs the algorithm for relay 31, via GTNET-SKT II.

Upon receiving the waveform data, the algorithm extracts current magnitudes and current angles using the Discrete Fourier Transform (DFT) method, as described in Chapter 4. When the faulted section identification scheme is initiated by a violation of the pre-determined thresholds as described in Section 4.4, each relay triggers, sends a flag signal and proceeds to calculates its measured current magnitude and angle changes to codify and then communicate to the corresponding "paired" relay, as detailed in Section 4.6, to complete the process faulted section identification via comparison of the pre- to during-fault changes. This may then lead to a trip signal in a protection application, or a "no fault found" situation and resetting of the system, if initiation is due to an external fault or a non-fault transient. If there is deemed to be a fault on the monitored section, each relay sends the trip signal back to the RTDS via the GTNET-SKT interface, representing tripping action for the corresponding relays in a protection application.

To assess the effectiveness of the scheme, the experiment considers a scenario in which a single fault occurs at a specific time. In this case, fault F_1 is simulated at the middle of the line between Bus 1 and Bus 2 to observe the system's response (which is monitoring the line between Bus 2 and 3) to an external fault, while fault F_2 is introduced at the middle of the line between Bus 2 and Bus 3 to evaluate the scheme's performance in detecting and responding to an internal fault. The fault resistances are shown in Table 6.1.

Since the focus of this experiment is on assessing and demonstrating the behaviours of R22 and R31, it is assumed that the other relays in the system remain inactive when a fault occurs on the line between Bus 1 and 2 – although in practice the actual system may contain many relays, and there is also a question over whether the algorithm could be implemented in a centralised or distributed fashion in an actual application. This ensures that the test isolates and evaluates the performance of the scheme, in terms of it identifying the faulted section correctly, without interference from other protection elements in the system.

Notably, the communication between system components within the laboratory setup at the University of Strathclyde has been established using standard Ethernet communication. As outlined elsewhere in Chapter 2, there are various communications technology options for an actual implementation, and this would depend on a variety of factors including the utility's existing system and the details of the application (e.g. urban vs rural, distance between locations etc). Experimental results from the HIL implementation indicate that the measured latency does not exceed 8 ms, which is not a problem for distribution-level applications, where fault clearance times of several 10s or even 100s of ms are acceptable. In an FLISR application, very fast (less than 1 cycle) operating times would also not be required, so no communications issues are evident or anticipated.

Table 6.1: Initial parameters of system model for the HIL test [6.4]

Source characteristics				
Source	**Impedance (Ω)**		**Voltage Angle (degree)**	
Source 1	0.1736 + j0.9848		10	
Source 2	0.1736 + j0.9848		0	
Load characteristics				
At Bus	**Type**	**Active Power (MW)**	**Reactive Power (MVAR)**	
2	Balanced PQ	2.5	0.5	
3	Balanced PQ	5.0	1.0	
Total Load		7.5	1.5	
Line Impedance				
From Bus	**To Bus**	**Line Length (km)**	**Resistance (Ω)**	**Reactance (Ω)**
1	2	3	0.546	1.005
2	3	3	0.546	1.005
3	Source 2	3	0.546	1.005
Total		9	1.638	3.015
Fault				
Fault	**Resistance (Ω)**	**Location**		
F_1	0.1	Mid-point of line from Bus 1 – Bus 2		
F_2	0.1	Mid-point of line from Bus 2 – Bus 3		

6.3 Validation of HIL model performance

To evaluate the accuracy of the model used in the HIL testing, a verification process has been carried out by calculating, manually and analytically, the expected fault current generated by each source and fault currents at the point of fault for a specific fault condition. These calculated values have then been compared with the results obtained from the HIL simulation. This comparative analysis was performed to confirm that the model exhibits behaviour consistent with the theoretical and physical characteristics of the system under faulted conditions.

6.3.1 Validation of sources' fault current contributions

Assuming a balanced three-phase fault occurs on the line between Bus 1 and Bus 2, with the fault location positioned very close to Relay R1, the line impedance can be reasonably neglected. Under this assumption, the fault current contributed by Source 1 ($I_{f,S1}$) can be calculated as

$$Z_{S1} = j\frac{V_s}{\sqrt{3} \times I_{f,S1}} \tag{6.1}$$

By substituting the impedance parameter of Source 1, which are 0.1736 + j0.9848 Ω and voltage of the system (11 kV line-line rms), into Equation (6.1), the calculated magnitude of the fault current generated by Source 1 is 6.35 kA per phase.

The phase-A current at R1, recorded as part of the HIL testing results for a fault occurring at the same location, is illustrated in Figure 6.2. The measured peak value of the waveform is 8.92 kA. This value is then converted to its rms equivalent using Equation (6.2).

$$I_{rms} = \frac{I_{peak}}{\sqrt{2}} \tag{6.2}$$

Accordingly, the phase-A current rms value measured at R1 is calculated to be 6.31 kA, which shows a close agreement with the theoretical calculation. For Source 2, which has the same source impedance as Source 1 and yields identical HIL testing result, it can therefore be considered to produce equivalent behaviour to that of Source 1. Note that the calculated and measured fault currents are calculated/made several cycles after fault inception and therefore represent the sustained fault current "after" the DC offset from the source has subsided.

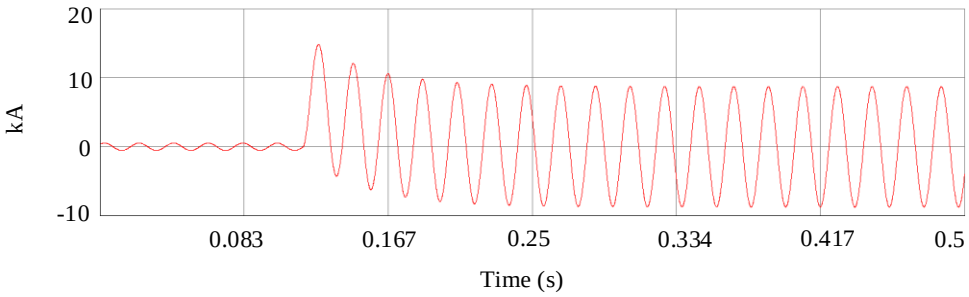

Figure 6.2: Phase-A fault current contributed by Source 1 in HIL demonstration when a balanced fault occurs at t = 0.118 s

6.3.2 Validation of fault currents measured at relay locations

Assuming a balanced fault F_1 occurs at the mid-point of the line connecting Bus 1 and Bus 2, the currents measured at relays R22 and R31 during the fault condition will be supplied solely by Source 2 as Source 1 will be short-circuited (and supplying current to the "other" side of the fault). As both relays are located along the same line segment, and "downstream" of the fault point if we view the system as "flowing" from right to left, the measured currents at both relays are expected to be identical and can be calculated as follows:

$$Z_{eq} = j\frac{V_s}{\sqrt{3} \times I_{during-f}} \tag{6.3}$$

In this case, the equivalent impedance (Z_{eq}) is defined as the sum of the Source 2 impedance and the line impedance between Source 2 and the fault location, which totals 1.554 + j3.490 Ω. Substituting this value into Equation (6.3) yields a calculated current at R22 and R31 of 1.66 kA. Note that this calculation neglects the load current that may be drawn by loads connected at Bus 2 and 3 during the fault, but in practice some currents will be drawn by these loads during the fault (although the voltages will be depressed due to the short circuit on the system).

This theoretical value can be compared with the current measured during HIL testing, as shown in Figure 6.3, where the peak current values of each phase were recorded as 2.33 kA at R32, and 2.16 kA at both R22 and R31 (which is effectively the current through the line connecting bus 3 and 2), and 2.13 kA at R21. Converting the R22 and R31 values to rms equivalents using Equation (6.2) results in a rms current of 1.53 kA, which is relatively close to the analytically calculated value. For completeness and, as mentioned earlier, there will be some current drawn by the loads connected at bus 2 and bus 3. From the RTDS simulation, the magnitudes of the rms load currents at bus 2 and 3 during the fault are 118.28 A and 26.39 A, respectively. These load currents have been calculated by measuring the currents at relays R32 and R21. For example, load current from bus 3 is equal to the current at R32 minus the current at R31. While the current from bus 2 to the load is the current measured at R22 – the current measured at R21. These values for load currents during this fault, which when added to the line current of 1.53 kA gives a total current of 1.65 kA, which is very closely aligned with the calculated value of 1.65 kA stated earlier (which neglected the loads).

A close alignment between the analytical and simulated current values indicates that the model responds relatively accurately during disturbances, and does not exhibit instability or anomalous behaviour. This step was essential to validate that the simulation environment provides a sound basis for evaluating the performance of the scheme. The results confirm that the model is suitable for real-time implementation, and that it can be confidently used to assess relay operation under a wide range of fault scenarios.

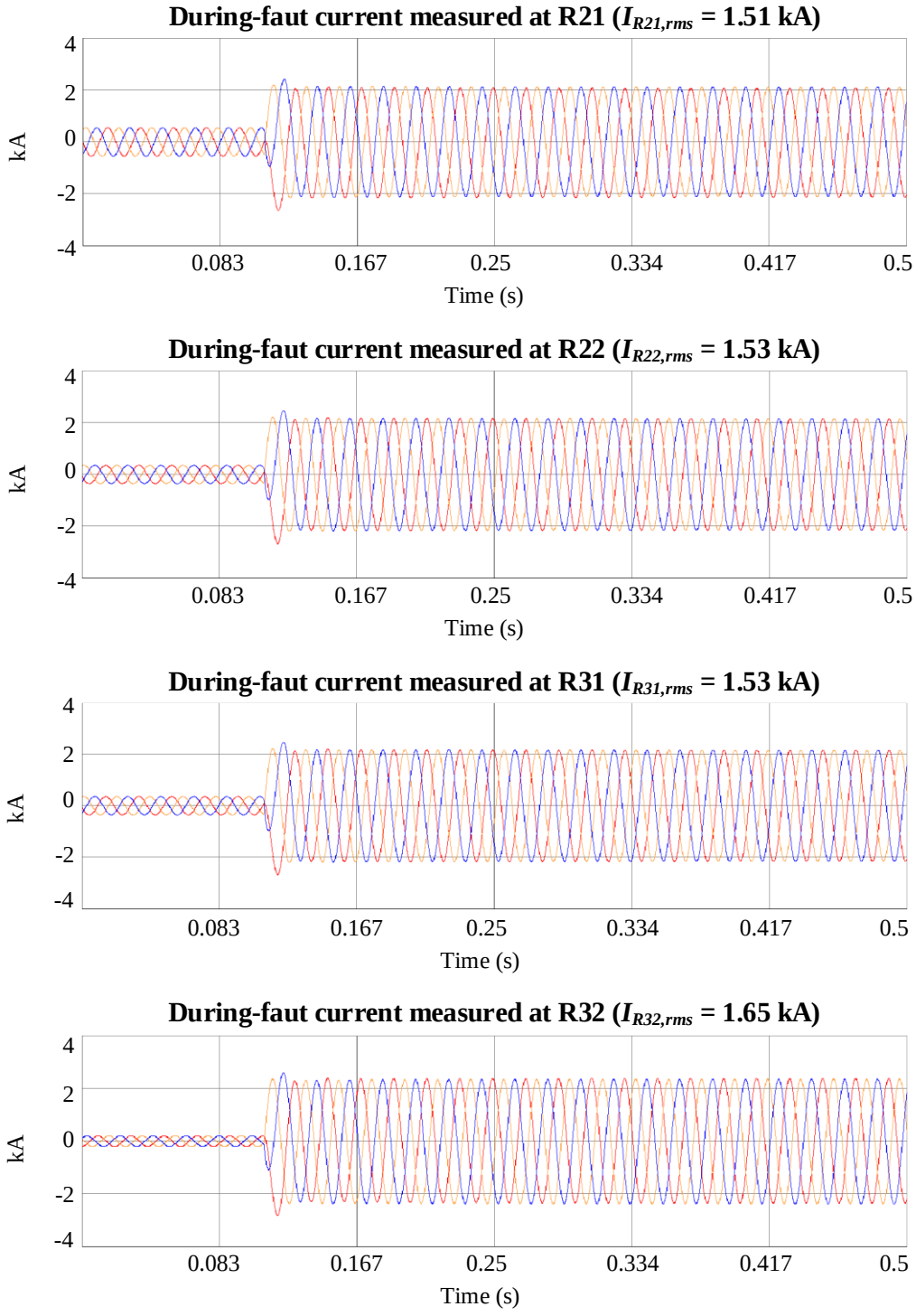

Figure 6.3: Current measured at various locations in the HIL simulations when a balanced fault occurs at t = 0.110 s

6.4 RTDS test results for balanced faults

Using the HIL simulation arrangement, three-phase balanced faults have been simulated at various locations within the modelled system. The results of the calculated actual data exchanged between relays R22 and R31 are presented in Figures 6.4 – 6.11.

6.4.1 Results for fault between Bus 1 and Bus 2

When fault F_1 occurs on the line between Bus 1 and Bus 2, the results observed at relays R22 and R31 are presented in Figure 6.4 – Figure 6.5 and Figure 6.6 – Figure 6.7, respectively. It is noted that the waveform results for this case are shown in Figure 6.3 in Section 6.3.2.

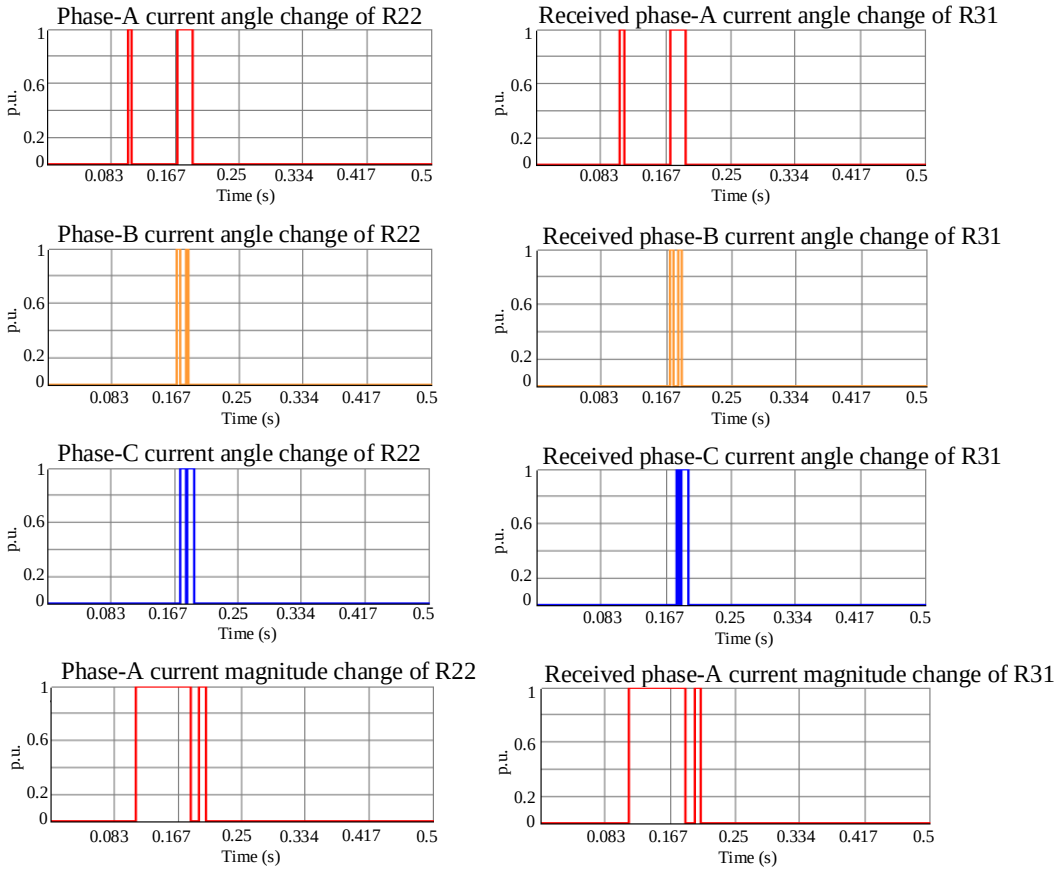

Figure 6.4: The results at relay R22 when balanced fault F_1 occurs

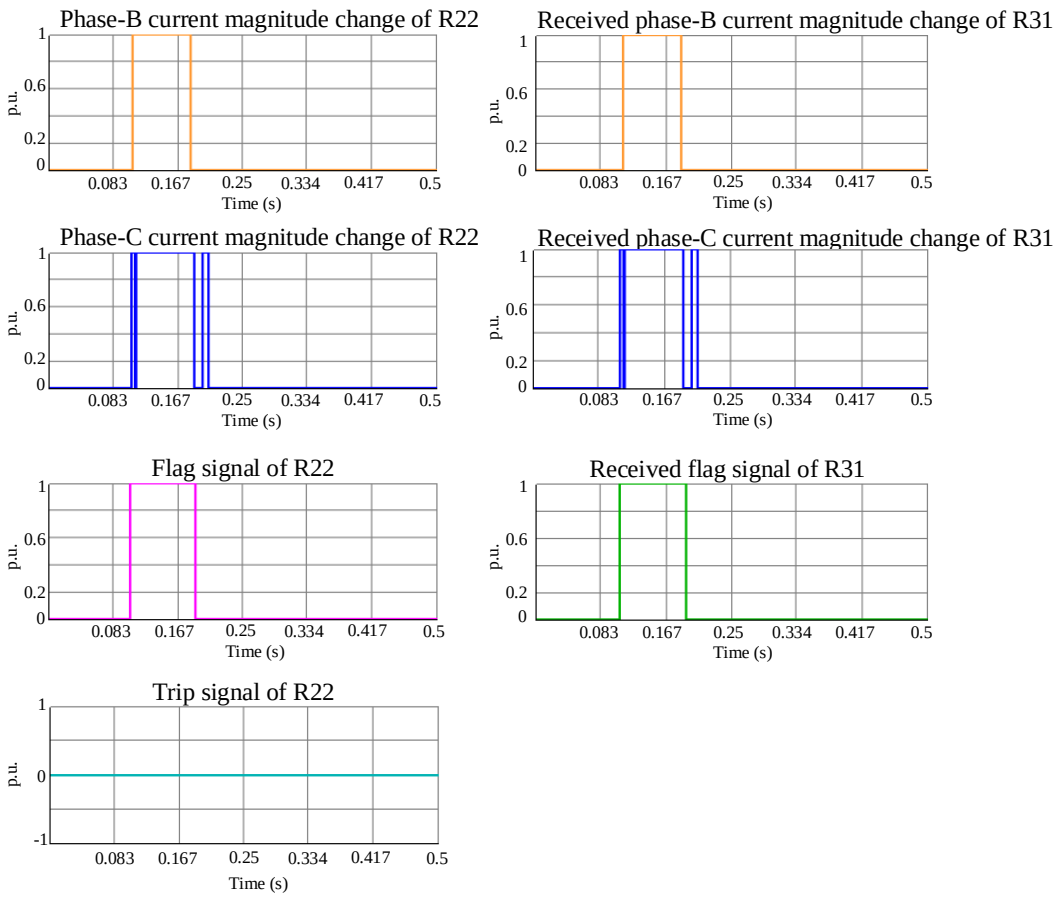

Figure 6.5: The results at Relay R22 when balanced fault F_1 occurs

As shown in Figure 6.4 and Figure 6.5, when fault F_1 occurs at t = 104.0 ms, the flag signal of R22 changes from '0' to '1' at t = 104.2 ms, indicating that an initiating threshold has been violated. Note that, as the algorithm uses a 3-cycle (60 ms) moving window to process transients, the flag to indicate the presence of an "initiating" transient will reset after approximately 60 ms as the fault currents stabilise at their post-fault values. At this point, relay R22 transmits its calculated data – comprising the flag signal (flag_{R22}), three signals indicative of the current phase angle changes ($\Delta\theta_{a,R22}$, $\Delta\theta_{b,R22}$, $\Delta\theta_{c,R22}$), and three signals indicative of the current phase magnitude changes ($\Delta|I_{a,R22}|$, $\Delta|I_{b,R22}|$, $\Delta|I_{c,R22}|$) – to relay R31. Simultaneously, R22 waits to receive data from relay R31, which arrives at t = 107.2 ms, as indicated by the flag signal of R31 (flag_{R31}) changing to '1'. The faulted section identification algorithm of

R22 then compares its own calculated current phase angle changes and calculated current phase magnitude changes with those received from its corresponding, or "paired" relay at the other end of the line section (R31).

It is clear that the current phase angle changes for all three phases at R22 register a value of '0', indicating a counterclockwise (CCW) phase rotation. Similarly, the current phase angle changes for all three phases at R31 are also '0', confirming that both relays detect an identical phase shift direction. Note that there are some temporary transient behaviours just after the fault where the signal is temporarily in the wrong state, but the "stable" output after the initial transient period is correct. Consequently, the algorithm proceeds to compare the current magnitude changes of both relays. It is noted that the current phase magnitude changes for all three phases at R22 switch from '0' to '1', signifying an increase in measured current magnitude due to the fault current contributed from both sources. Likewise, the current phase magnitude changes received from R31 also register a value of '1', verifying that an equivalent current magnitude increase is observed at both relays.

Accordingly, since both R22 and R31 detect current phase angle changes in the same direction and current phase magnitude changes, the fault is deemed to be located outside of the zone (line connecting Bus 2 and Bus 3). As a result, relay R22 does not issue a trip command (in a protection application – the signal could also be used for monitoring/FLISR application), and the trip signal remains at '0'.

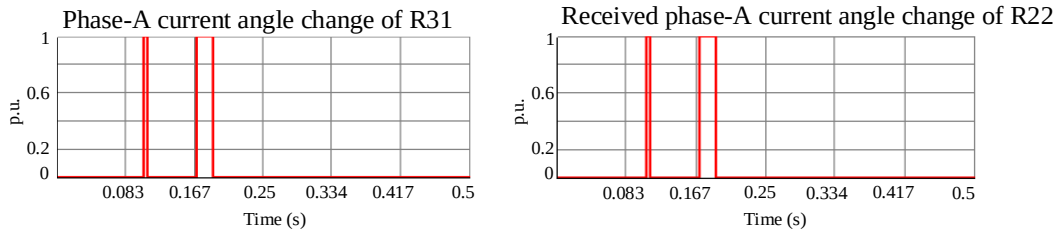

Figure 6.6: The results at relay R31 when balanced fault F_1 occurs

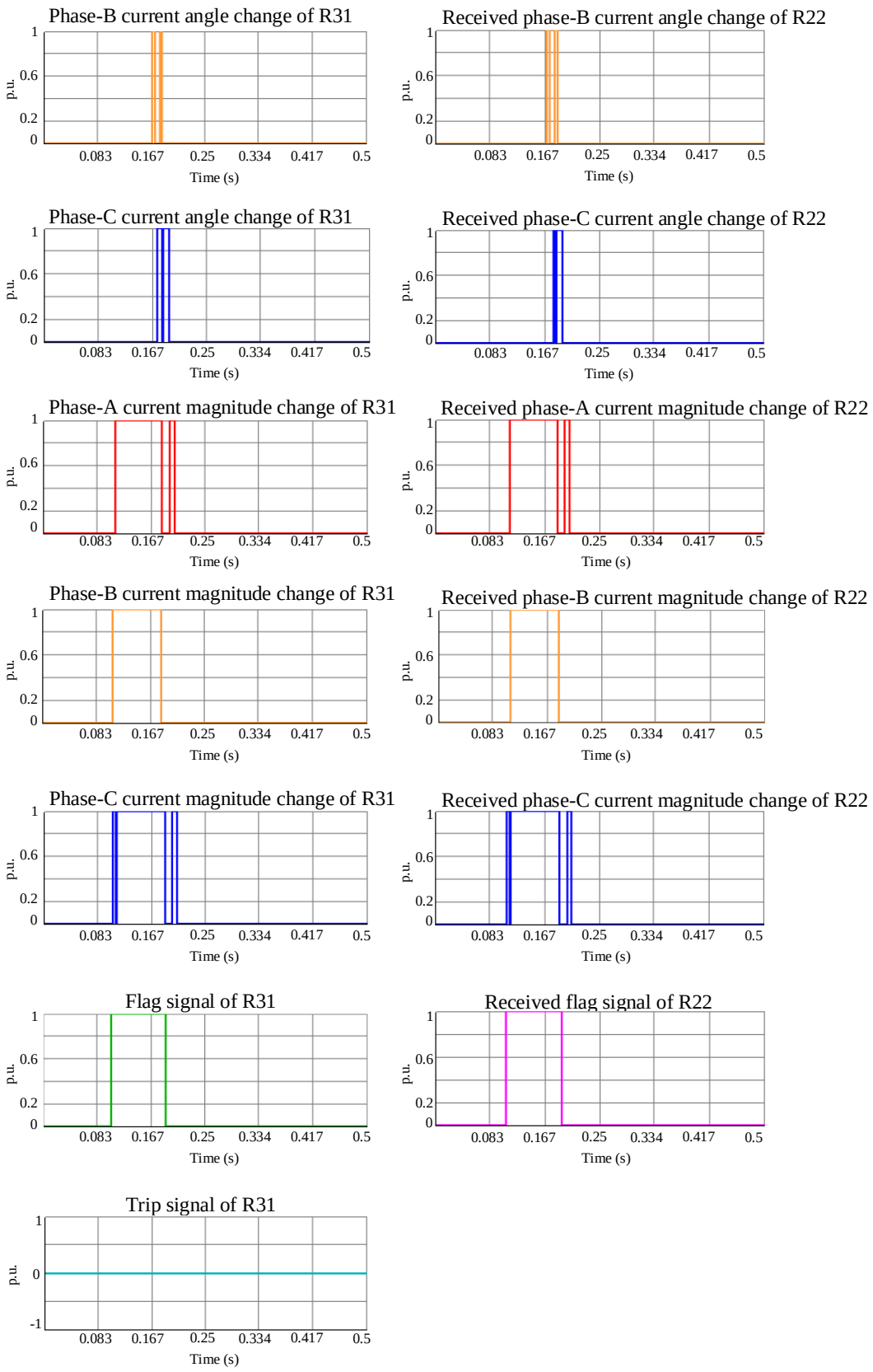

Figure 6.7: The results at relay R31 when balanced fault F_1 occurs

Furthermore, the results observed at relay R31 are shown in Figure 6.6 and Figure 6.7. The flag signal at R31 ($\mathbf{flag}_{R31}$) changes from '0' to '1' at t = 104.4 ms, after which R31 transmits its calculated current information to its paired relay, R22, while waiting to receive data from R22, which arrives at t = 106.3 ms. The algorithm at R31 then executes the same comparative analysis between its own current data and the data received from R22 (CCW-CCW). The results are consistent with those obtained at relay R22 – the current phase angle changes and current phase magnitude changes in each phase at R31 and R22 are identical.

This confirms that fault F_1 is external to the monitored line section connecting Bus 2 and Bus 3, and therefore, relay R31 also does not issue a trip signal or indication to FLISR that the faulted section is on the monitored line section, similar to relay R22, ensuring that the scheme correctly identifies that fault location to be external and prevents unnecessary tripping for a protection application or incorrect indication in a monitoring/FLISR application.

6.4.2 Results for fault between Bus 2 and Bus 3

When fault F_2 arises on the line connecting Bus 2 and Bus 3, the corresponding outcomes recorded at relays R22 and R31 are illustrated in Figure 6.8 – Figure 6.9 and Figure 6.10 – Figure 6.11, respectively.

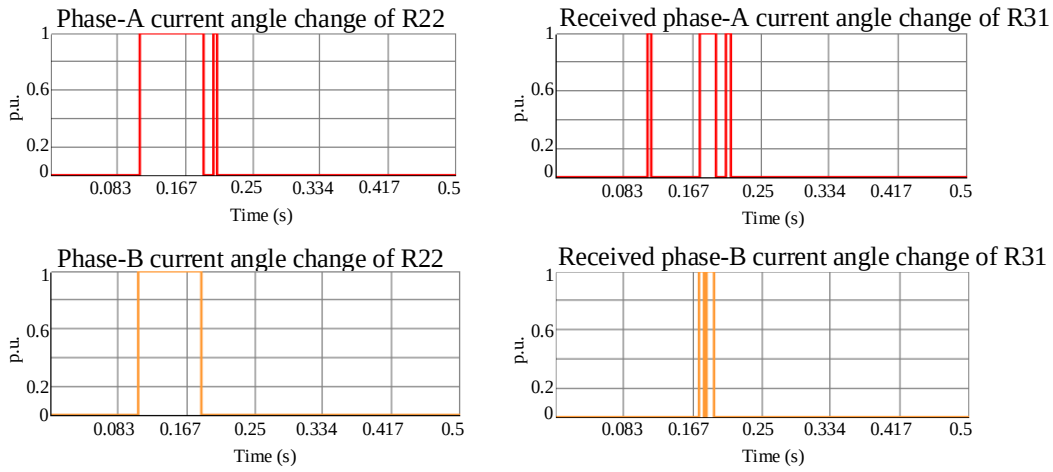

Figure 6.8: The results at relay R22 when balanced fault F_2 occurs

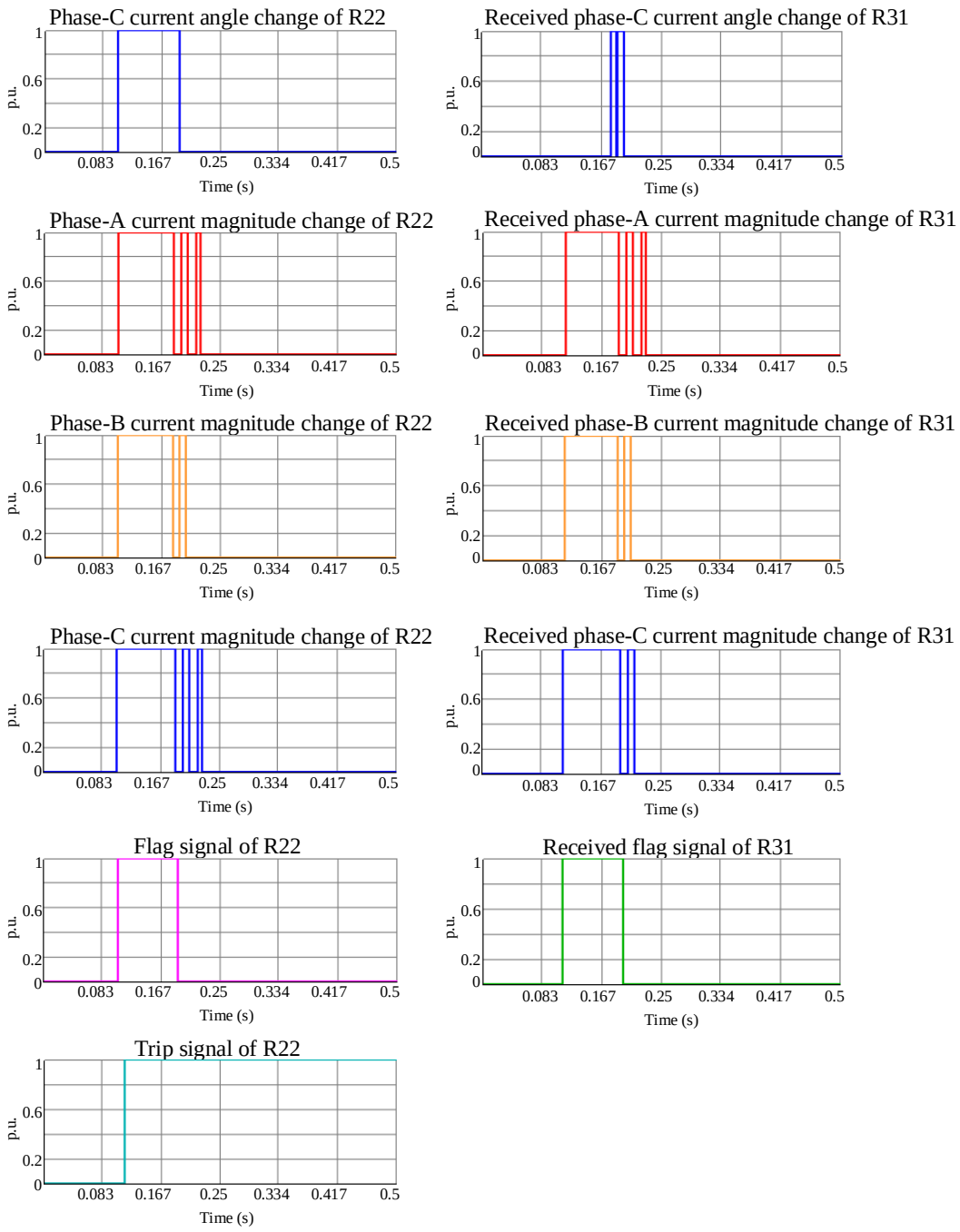

Figure 6.9: The results at relay R22 when balanced fault F_2 occurs

As illustrate in Figure 6.8 – Figure 6.9, fault F_2 occurs at t = 105.2 ms. Shortly after, the flag signal of R22 is triggered to '1' due to the changes violating thresholds as described before. Subsequently, relay R22 transmits the flag signal ($\mathbf{flag}_{R22}$), three calculated values of current phase angle changes ($\Delta\theta_{a,R22}$, $\Delta\theta_{b,R22}$, $\Delta\theta_{c,R22}$), and three calculated values of current phase

magnitude changes ($\Delta|I_{a,R22}|$, $\Delta|I_{b,R22}|$, $\Delta|I_{c,R22}|$) to relay R31 immediately while awaiting the corresponding data from R31. Upon receiving the signal from relay R31 at t = 111.6 ms, relay R22's algorithm compares its own current phase information with that of its paired relay.

The current phase angle changes in all three phases at R22 ($\Delta\theta_{a,R22}$, $\Delta\theta_{b,R22}$, $\Delta\theta_{c,R22}$) transition from '0' to '1', indicating a clockwise (CW) rotation of the current phase angle upon fault occurrence. Conversely, the received data from relay R31 show that the current phase angle changes ($\Delta\theta_{a,R31}$, $\Delta\theta_{b,R31}$, $\Delta\theta_{c,R31}$) during the fault is '0', signifying a CCW rotation of the current phase angle. The discrepancy in current phase angle changes suggests a difference in angle shift rotation (CW at one end of the line, CCW at the other), which is attributed to the fault currents being generated by different sources at either end of the system and "flowing" towards the fault with different angles. Based on this observation, without comparison of current phase magnitude changes, it can be inferred that the fault is located within the zone (the line section connecting Bus 2 and Bus 3). Consequently, relay R22 triggers the trip signal (for a protection application – it would merely be indicating the faulted line section in a monitoring/FLISR application), setting it to '1' at t = 114.9 ms. The time delay between faulted notification and trip signal initiation/faulted section identification signal at relay R22 is 9.7 ms, which is acceptable and very fast (less than 1 cycle) for distribution protection system. Note that there are some temporary transient behaviours just after the fault where the signal is temporarily in the wrong state, but the "stable" output after the initial transient period is correct. This could be easily catered for by introducing stabilising delays in the algorithm.

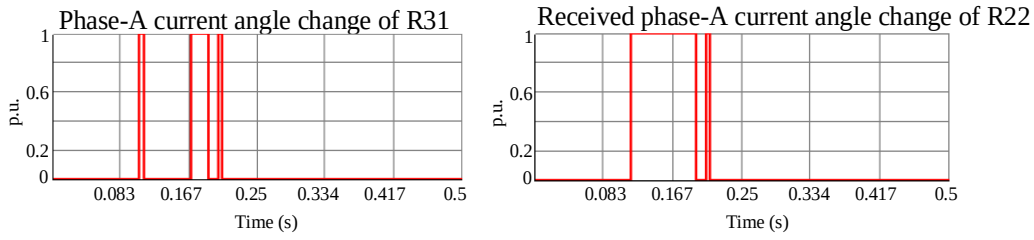

Figure 6.10: The results at relay R31 when balanced fault F_2 occurs

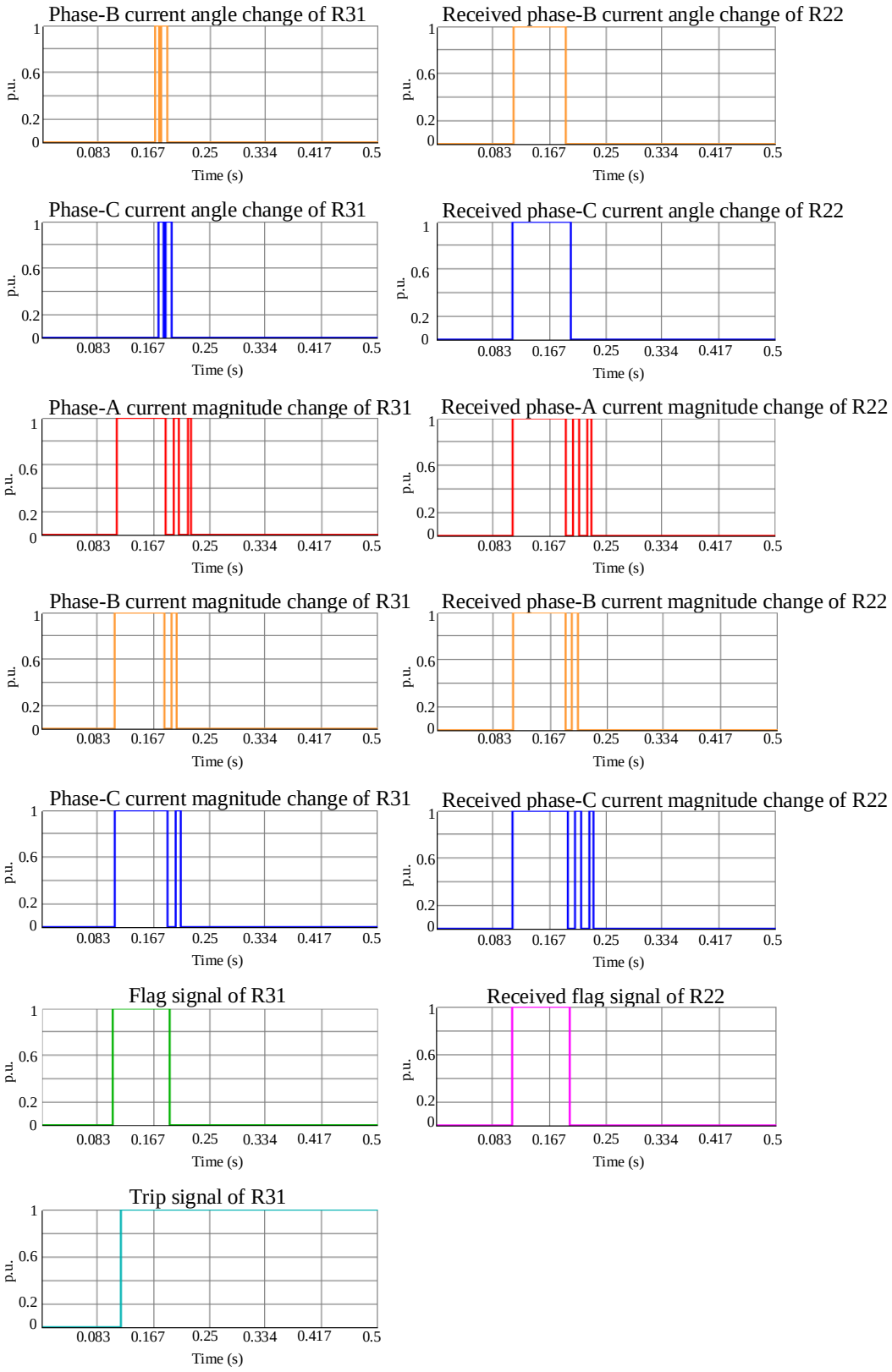

Figure 6.11: The results at relay R31 when balanced fault F_2 occurs

Figure 6.10 – Figure 6.11 present the response of relay R31 to fault F_2. When the fault occurs, the flag signal of R31 (flag_{R31}) also changes from '0' to '1' at t = 105.7 ms, consistent with the behaviour observed in flag_{R22}. Relay R31 then transmits its computed current data to relay R22, while awaiting the corresponding dataset in return. At t = 110.8 ms, relay R31 receives the current information from R22, allowing the algorithm to execute a comparative analysis.

The results confirm that the current phase angle changes in each of its three phases differ from those of its paired relay; the phase angles at R31 rotate CCW, while those at R22 rotate CW. This distinction in phases angle behaviour reinforces the conclusion that fault F_2 is located in the zone between Bus 2 and Bus 3. As a result, relay R31 also triggers its trip/faulted section identification signal, setting it to '1' at t = 113.9 ms, which is time for faulted section identification process before issuing trip signal is 8.2 ms, ensuring a fast fault-clearing response in a protection application, or a fast identification of the faulted line section in a monitoring/FLISR application.

6.5 RTDS test results for unbalanced faults

Unbalanced faults are introduced at various locations within the RTDS/HIL model. The fault conditions include single-phase-to-earth (A-E, B-E, C-E), phase-to-phase (A-B, B-C, C-A) and double-phase-to-earth (A-B-E, B-C-E, C-A-E) faults. The results of the calculated data for relays R22 and R31 are illustrated in Figures 6.12 – 6.19.

6.5.1 Results for fault between Bus 1 and Bus 2

When fault F_1 occurs on the line between Bus 1 and Bus 2, the results observed at relays R22 and R31 are presented in Figure 6.12 – Figure 6.13 and Figure 6.14 – Figure 6.15, respectively.

Assuming fault F_1 is a phase-A-to-earth (A-E) fault, its behaviour is illustrated in Figure 6.12 – Figure 6.13. When the fault occurs at t = 120.2 ms,

the flag signal of R22 ($\mathbf{flag}_{R22}$) is initiated, changing to '1' at t = 122.2 ms. Immediately after this, relay R22 transmits a packet of computed current data to relay R31 while simultaneously preparing for the next stage of the faulted section identification process. Upon receiving the signal from relay R31 at t = 124.3 ms, as indicated by the received $\mathbf{flag}_{R31}$ = '1' at this time, the algorithm in R22 compares the received signal with its own data.

The comparison reveals that the phase-A current angle shift ($\Delta\theta_{a,}$) for both R22 and R31 is '0', indicating that the phase-A current angles (after the transient of fault state) rotate CCW when fault condition, while the current angle changes for phases B and C remain unchanged. Since the current angular changes at both relays are identical, the next step involves analysing the current magnitude changes to further validate the fault location.

The analysis of the current magnitude changes shows that for both relay R22 and R31, measured values of phase-A current magnitude increase (switching from '0' to '1'), confirming the occurrence of a fault, whereas phase-B and phase-C values remain unchanged. However, as the fault current magnitude increases at both relays, it suggests that the fault is not located within the observed line section connecting Bus 2 and Bus 3. Consequently, relay R22 does not initiate a trip signal, preventing incorrect tripping/faulted section identification.

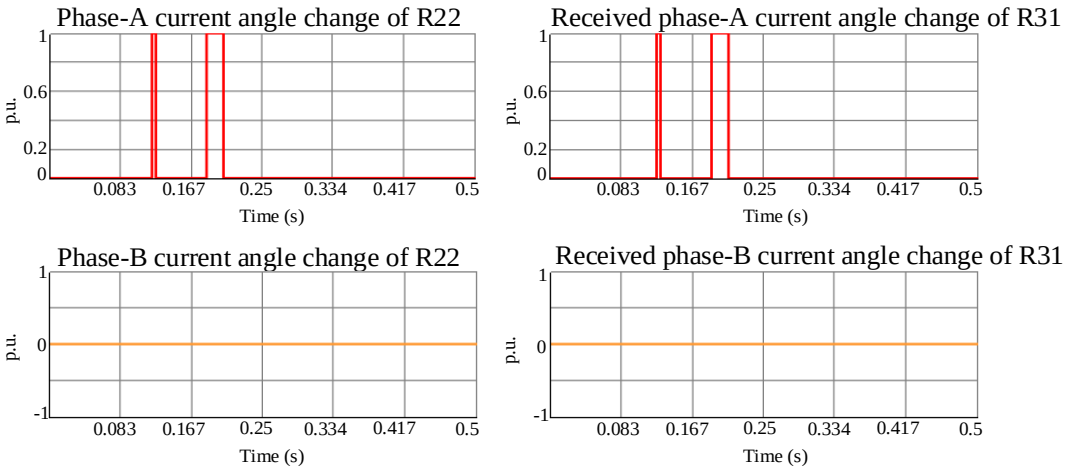

Figure 6.12: The results at relay R22 when phase-A-to-earth fault F_1 occurs

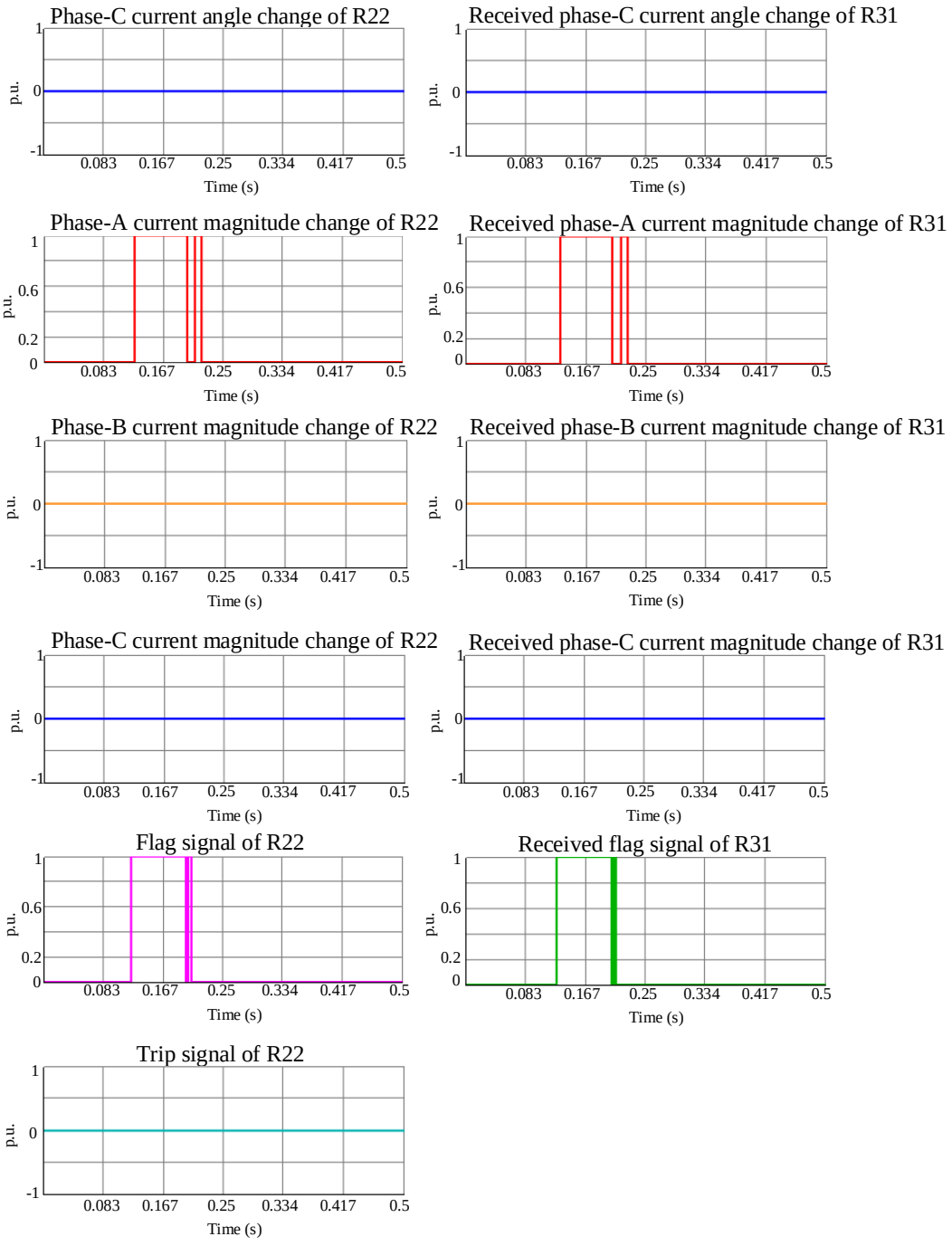

Figure 6.13: The results at relay R22 when phase-A-to-earth fault F_1 occurs

Similarly, the algorithm of relay R31 detects a system disturbance at t = 120.3 ms and subsequently transmits its computed current data to relay R22, while simultaneously changing its flag signal to '1' at t = 122.3 ms. Upon receiving the current data from R22 at t = 124.2 ms, the fault analysis process

begins. The results obtained from relay R31 mirror those of relay R22 - both relays detect identical current phase angle change rotations (CCW-CCW), leading to further verification using current phase magnitude comparison. The outcome of this comparison confirms that the current magnitude changes at both relays match, further supporting the conclusion that the fault is external to the protected/monitored zone between Bus 2 and Bus 3. As a result, relay R31 neither initiate a trip signal nor indicates that its monitored line section is faulted for monitoring/FLISR applications. The results observed at relay R31 are presented in Figure 6.14 – Figure 6.15.

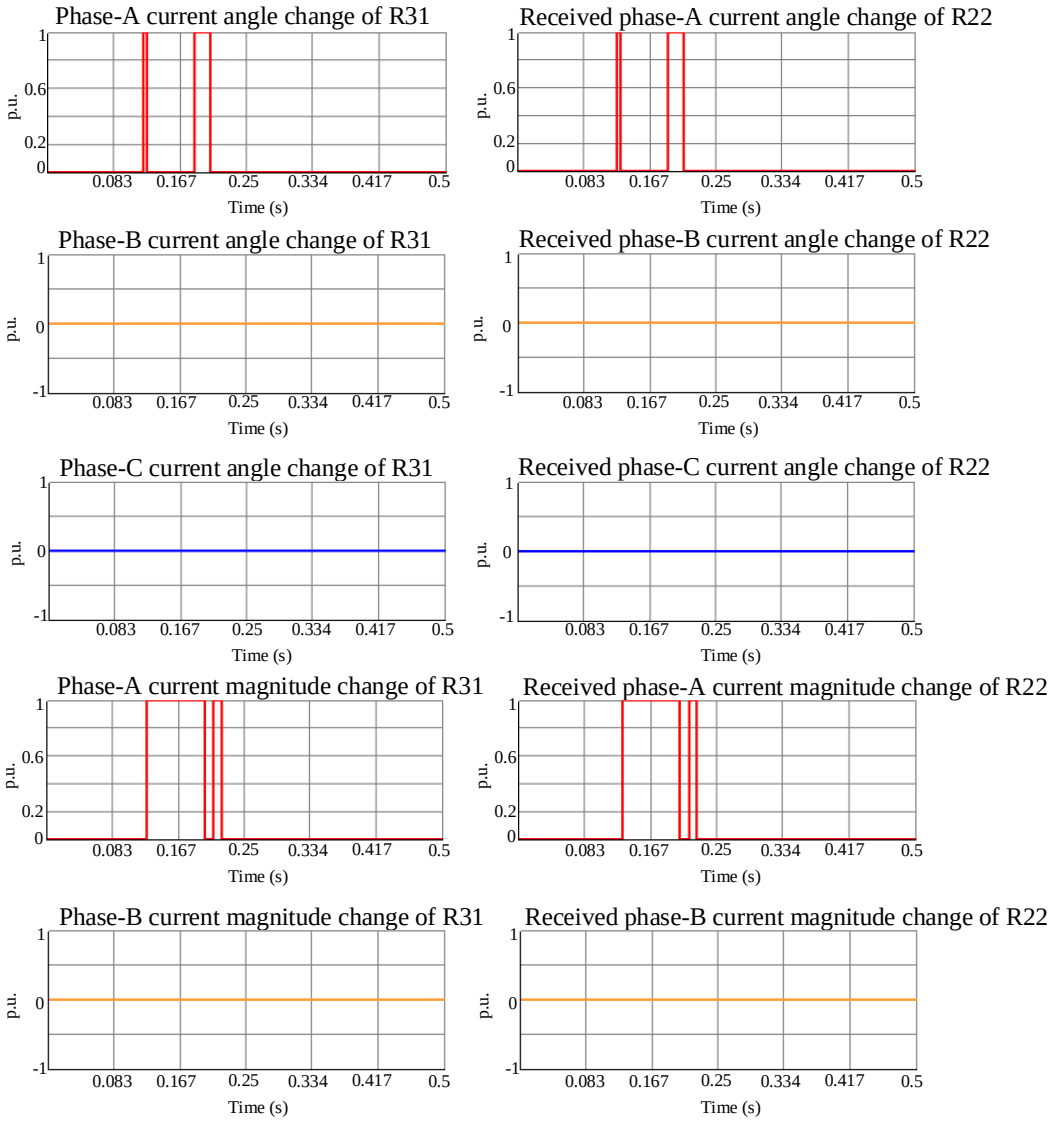

Figure 6.14: The results at relay R31 when phase-A-to-earth fault F_1 occurs

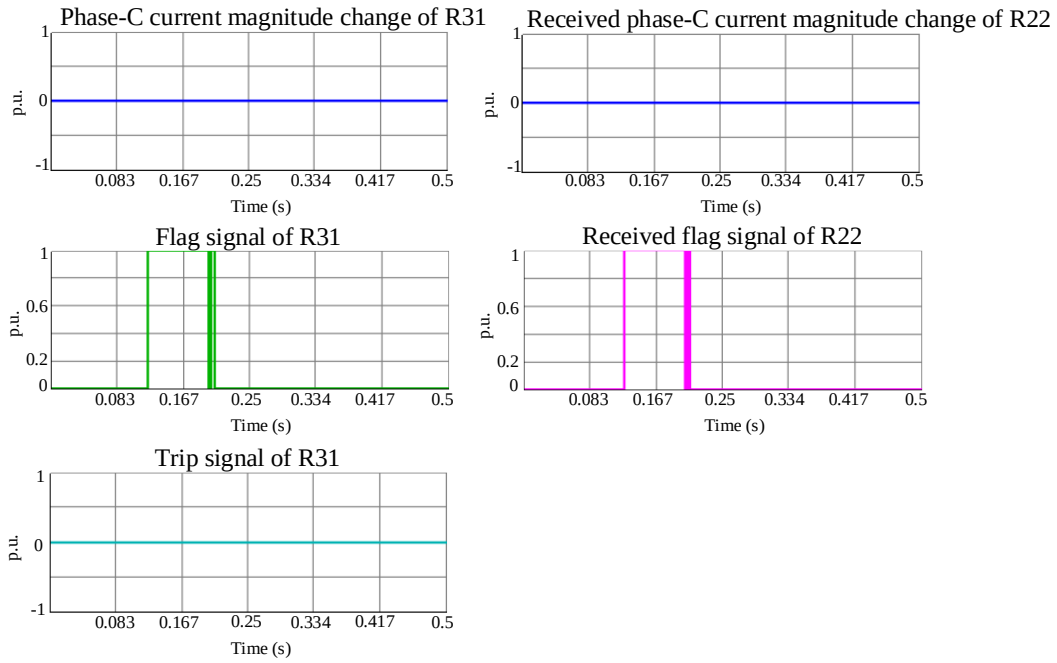

Figure 6.15: The results at relay R31 when phase-A-to-earth fault F_1 occurs

Additional fault types have been tested within the HIL simulation. The results of computed signal observed at relay R22 and R31 are summarised in Table 6.2. The findings indicate that when different fault types occur on the line between Bus 1 and Bus 2, the flag signals of both relays are triggered to '1', initiating the exchange of current angle changes and current magnitude changes between the two relays. However, upon comparing the current data from both relays, it is observed that all values are identical. This confirms that no fault is present within the zone between Bus 2 and Bus 2. Accordingly, neither relay R22 nor relay R31 issues a trip signal nor indicates that the monitored section is faulted, ensuring that the scheme functions correctly and does not indicate that there is a fault on its monitored line section.

Table 6.2: The results for relay R22 and relay R31 for different F_1fault types

Fault Type	Relay	Flag Signal	Current Angle Change Signal Value for phases A, B, and C			Current Magnitude Change Signal Value for phases A, B, and C			Fault identification/ initiation time (ms)	Identification time (ms)
			A	B	C	A	B	C		
B-E	R22	1	-	0	-	-	1	-	119.1	-
	R31	1	-	0	-	-	1	-	119.1	-
C-E	R22	1	-	-	0	-	-	1	117.6	-
	R31	1	-	-	0	-	-	1	117.6	-
A-B	R22	1	0	0	-	1	1	-	113.1	-
	R31	1	0	0	-	1	1	-	113.2	-
B-C	R22	1	-	0	0	-	1	1	105.0	-
	R31	1	-	0	0	-	1	1	105.2	-
C-A	R22	1	0	-	0	1	-	1	113.7	-
	R31	1	0	-	0	1	-	1	113.8	-
A-B-E	R22	1	0	0	-	1	1	-	119.9	-
	R31	1	0	0	-	1	1	-	120.0	-
B-C-E	R22	1	-	0	0	-	1	1	105.6	-
	R31	1	-	0	0	-	1	1	105.7	-
C-A-E	R22	1	0	-	0	1	-	1	110.4	-
	R31	1	0	-	0	1	-	1	110.3	-

As shown in Table 6.2, regardless of the type of fault F_1 on the line between Bus 1 and Bus 2, relays R22 and R31, which monitor the line connecting Bus 2 and Bus 3, detect the resulting disturbance, causing their respective flag signals to change from '0' to '1'. However, upon performing a comparison of the current angle change and current magnitude change data between the two relays, either relay issues a trip signal, as the fault is identified to have occurred outside their zone of monitoring.

6.5.2 Results for fault between Bus 2 and Bus 3

When fault F_2 occurs on the line between Bus 1 and Bus 2, the results observed at relays R22 and R31 are illustrated in Figure 6.16 – Figure 6.17 and Figure 6.18 – Figure 6.19, respectively.

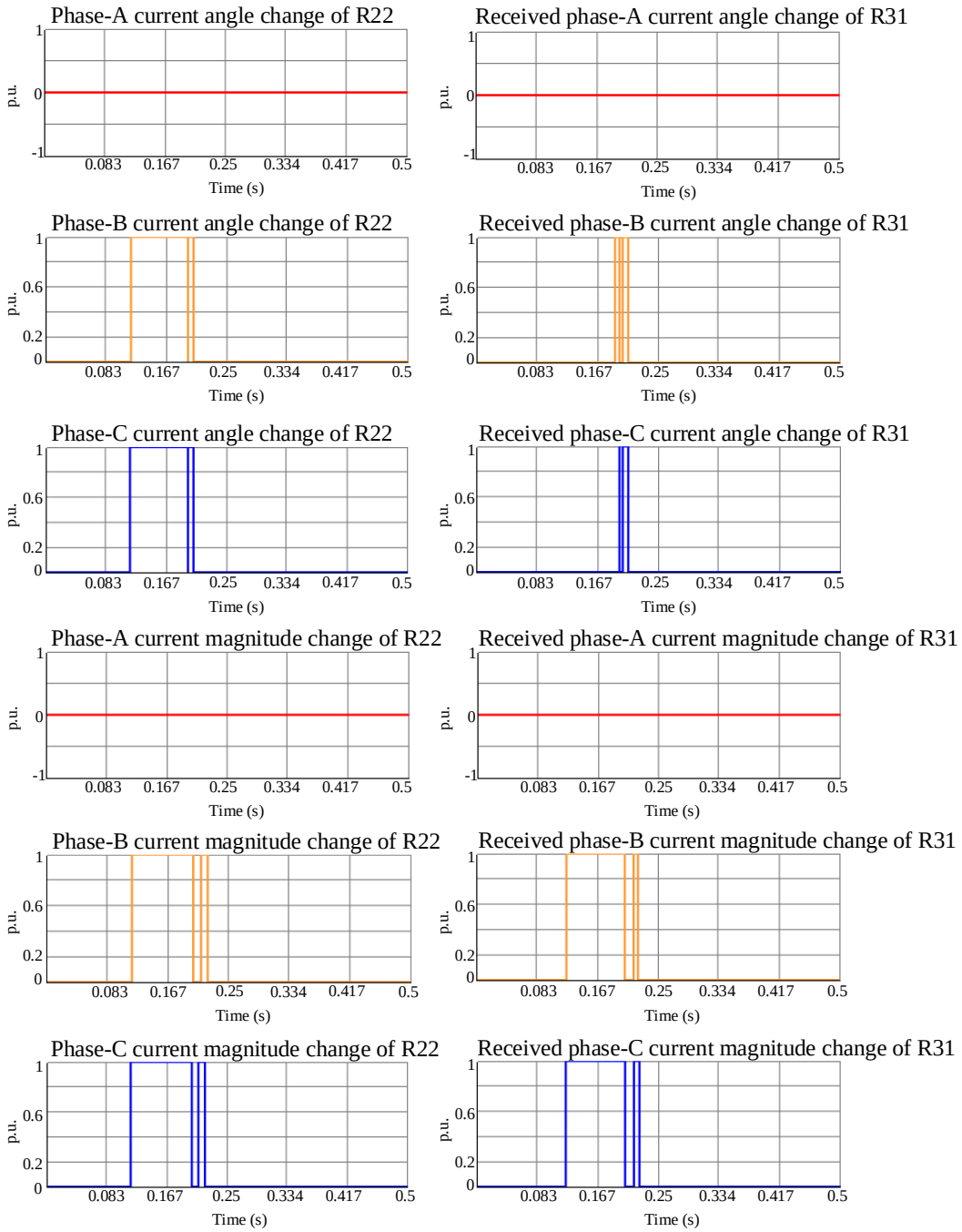

Figure 6.16: The results at relay R22 when phase-B-to-phase-C fault F_2 occurs

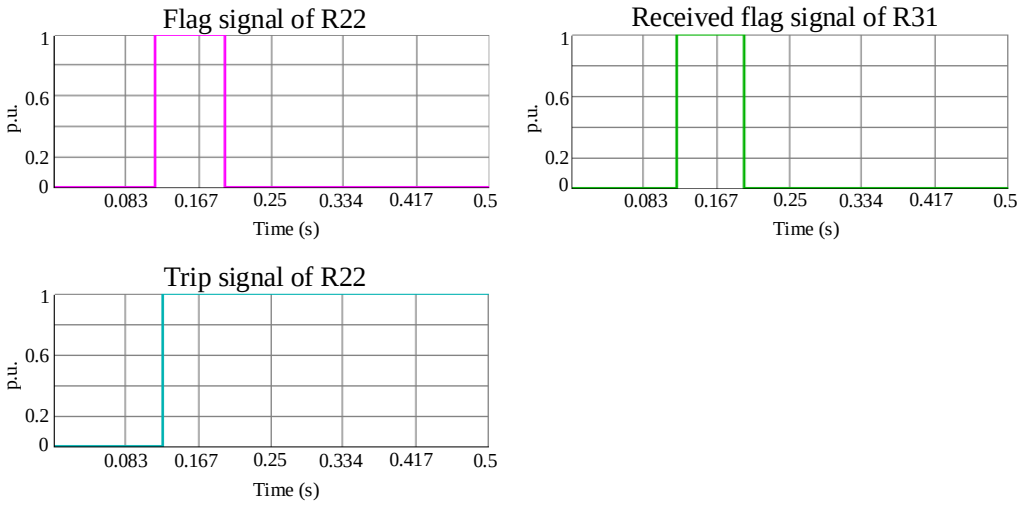

Figure 6.17: The results at relay R22 when phase-B-to-phase-C fault F_2 occurs

For the scenario where Fault F_2 is a phase-B-to-phase-C (B-C) fault, its behaviour is presented in Figure 6.16 – Figure 6.17. Following the fault occurrence at t = 115.4 ms, the algorithm at relay R22 triggers the flag signal, setting it to '1', and immediately transmits a packet of computed current data to its paired relay at t = 116.4 ms. Shortly after, relay R22 receives the corresponding data from relay R31 at t = 120.4 ms. Upon comparing the received data as part of the faulted section identification process, it is observed that the phase-B and phase-C current angle changes at R22 ($\Delta\theta_{b,R22}$, $\Delta\theta_{c,R22}$) register a value of '1', revealing a CW rotation. In contrast, the phase-B and phase-C current angle changes at R31 ($\Delta\theta_{b,R31}$, $\Delta\theta_{c,R31}$) indicate '0' value, signifying a CCW movement. Meanwhile, the phase-A current angle changes at both relays remain unchanged at '0'.

Given the observed discrepancy in current angle changes between the two relays, it can be inferred that the fault is located within the observed zone of the line between Bus 2 and Bus 3. Consequently, relay R22 initiates a trip signal and indicates that its monitored line section is faulted for monitoring/FLISR applications at t = 125.4 ms, based solely on the detection of current angle change differences (CW-CCW). As the distinction in angle

changes alone is sufficient to identify the fault, the current magnitude change comparison is not utilised in this case.

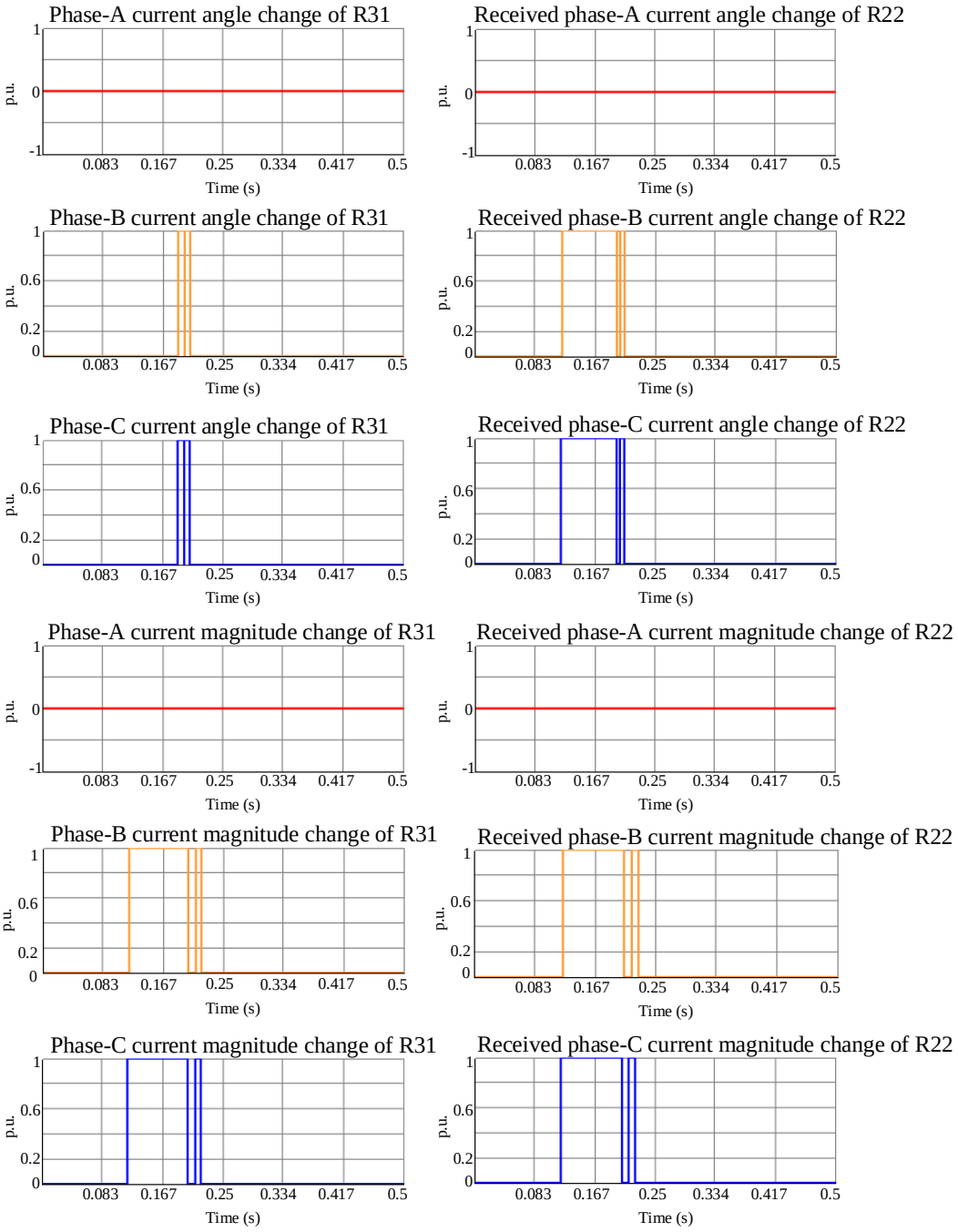

Figure 6.18: The results at relay R31 when phase-B-to-phase-C fault F_2 occurs

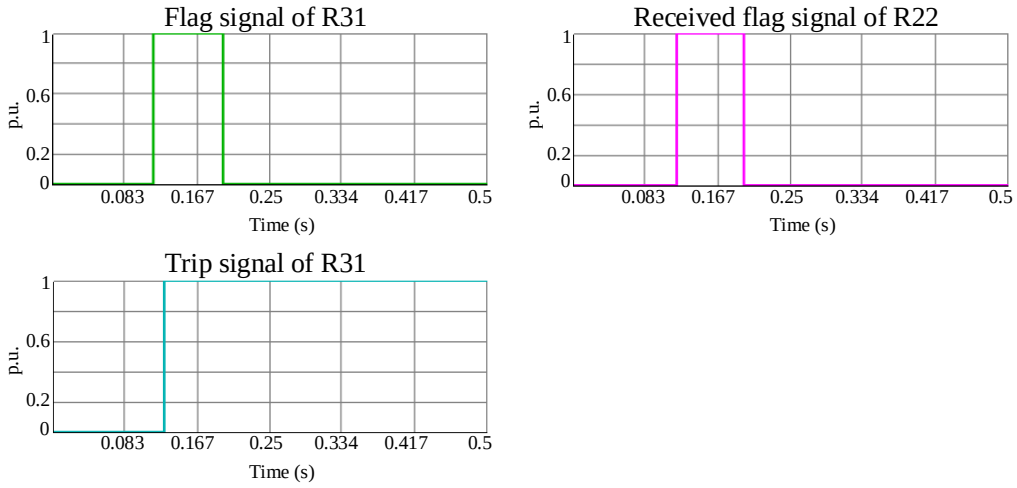

Figure 6.19: The results at relay R31 when phase-B-to-phase-C fault F_2 occurs

Similarly, as shown in Figure 6.18 – Figure 6.19, the algorithm at relay R31 detects the signal change and subsequently trigger its flag signal, setting it to '1' at t = 116.6 ms, before transmitting a dataset of computed current information to relay R22. Upon receiving the data from its paired relay at t = 118.6 ms, the algorithm at relay R31 performs a comparative analysis of current angle changes. The results of this comparison mirror those observed at relay R22 – the phase-B and phase-C current angle changes differ between R22 and R31, confirming the presence of a fault within the line connecting Bus 2 and Bus 3. Therefore, the relay R31 issues a trip signal, and indicates that it observed line section is faulted for monitoring/FLISR applications at t = 128.6 ms, ensuring that the faulted section is effectively isolated. Note that there are some temporary transient behaviours just after the fault where the signal is temporarily in the wrong state, but the "stable" output after the initial transient period is correct.

In addition to the previously-examined fault scenarios, other fault types, including single-phase-to-earth (A-E, B-E, C-E), phase-to-phase (A-B, C-A), and double-phase-to-earth (A-B-E, B-C-E, C-A-E) faults, were also tested within the HIL simulation, and the results are presented in Table 6.3. The analysis demonstrates that when various types of fault conditions arise on the

line connecting Bus 2 and Bus 3, the flag signals of relay R22 and R31 are activated, prompting the exchange of current angle and magnitude data between the two relays.

By evaluating the current data, it was consistently observed that there was always a difference in at least one phase's current angle shift. This observation confirms the presence of an internal fault within the monitored zone of Bus-B-Bus-C. Hence, the algorithms of relays R22 and R31 generate a trip signal with a value of '1', which is then sent back to the RTDS in every instance.

Moreover, the time delay between fault and trip signal initiation at both relays were recorded to be no greater than 25 ms. This measured latency is considered sufficiently fast for protection applications in distribution networks, ensuring a timely and reliable fault-clearing response.

Table 6.3: The results for relays R22 and R31 for different F_2 fault type

Fault Type	Relay	Flag Signal	Current Angle Change Signal Value for phases A, B, and C			Current Magnitude Change Signal Value for phases A, B, and C			Fault identification/ initiation time (ms)	Identification time (ms)
			A	B	C	A	B	C		
A-E	R22	1	1	-	-	1	-	-	121.0	129.7
	R31	1	0	-	-	1	-	-	120.8	140.9
B-E	R22	1	-	1	-	-	1	-	109.0	119.7
	R31	1	-	0	-	-	1	-	108.8	123.8
C-E	R22	1	-	-	1	-	-	1	117.6	126.8
	R31	1	-	-	0	-	-	1	117.8	130.8
A-B	R22	1	1	1	-	1	1	-	115.7	126.8
	R31	1	0	0	-	1	1	-	115.8	131.6
C-A	R22	1	1	-	1	1	-	1	111.3	125.4
	R31	1	0	-	0	1	-	1	111.5	121.5
A-B-E	R22	1	1	1	-	1	1	-	106.2	117.2
	R31	1	0	0	-	1	1	-	106.4	121.2
B-C-E	R22	1	-	1	1	-	1	1	103.2	112.3
	R31	1	-	0	0	-	1	1	103.4	116.4
C-A-E	R22	1	1	-	1	1	-	1	105.5	114.5
	R31	1	0	-	0	1	-	1	105.7	117.5

6.6 Chapter summary

This chapter has presented the HIL/RTDS experimental arrangements, real-time models, actual communications, and a range of results to validate the effectiveness of the proposed faulted section identification scheme. Validation of the power system model was also used by calculating theoretical results for a fault condition and comparing with the RTDS model output – very close alignment was found between calculated and simulated values and therefore

the performance of the model can be deemed accurate and valid. The investigation involved various fault types introduced at different locations within the system, with a particular focus on the line connected between Bus 2 and Bus 3. The flag signals, current phase angle changes, and current magnitude changes were analysed to determine the fault location and to distinguish between internal and external faults.

The results demonstrated that when a fault occurred outside the monitored zone, the relays correctly identified the condition and did not initiate a trip signal. Conversely, when the fault was within the monitored line section, the relays detected discrepancies in current phase angle shifts or current magnitude changes, leading to the activation of the trip signal.

While resistive faults and faults were there are weak/single infeeds were not included due to the time required to simulate and set up on the RTDS/HIL arrangement (and the limited availability of this facility), Chapter 6 has shown results for such scenarios using the offline simulation facilities. It is believed that the RTDS/HIL simulations would show similar results, so accordingly only a limited set of scenarios has been used – but this still shows the practical application of the system in a credible hardware/real-time context.

Furthermore, the communication latency between fault detection and trip signal generation was observed to be within 25 ms, ensuring a fast and reliable response suitable for protection applications in distribution networks. These results highlight the accuracy, selectivity, and efficiency of the proposed approach, confirming its practical applicability for real-time power system protection and/or monitoring and FLISR applications.

Chapter references

[6.1] 'Real-Time Simulation with the RTDS Simulator'. [Online]. Available: https://www.rtds.com/

[6.2] 'Visual Studio: IDE and Code Editor for Software Developers and Teams', Visual Studio. [Online]. Available: https://visualstudio.microsoft.com

[6.3] RTDS Technologies, 'GTNETx2: The RTDS Simulator's Network Interface Card', RTDS Technologies. [Online]. Available: https://knowledge.rtds.com/hc/en-us/articles/360034788593-GTNETx2-The-RTDS-Simulator-s-Network-Interface-Card

[6.4] T. Haggis and P. Booth, '*Network Design Manual*'. E.ON UK, December 2006.

Chapter 7

Conclusions and Future Work

7.1 Conclusions

A faulted section identification scheme has been proposed and comprehensively demonstrated in this thesis. The scheme operates solely based on current measurements and makes decisions through the comparison of simplified data exchanged via a basic communication link between two relays located at either end of the line section, although there are options to implement the system in a centralised fashion too (as described later). This approach offers a cost-effective alternative for protection and/or monitoring systems, encompassing applications in automation and fault location, isolation and service restoration (FLISR), both of which represent key emerging trends in the evolution of modern distribution networks.

The scheme is particularly well-suited to address the challenges posed by modern power distribution systems with multiple infeeds. These challenges include the reduction of system strength and short-circuit levels due to widespread integration of renewable energy sources and inverter-interfaced generators – phenomena that can be observed at virtually all system levels. Conventional protection and monitoring systems often struggle to perform reliably under such conditions.

The research has been contextualised within the broader landscape of related studies in both protection schemes and communication technologies. A

comprehensive literature review has been conducted, highlighted various developed schemes along with their benefits and limitations, some of which had been identified as potential research gaps relevant to the proposed work.

As noted, the proposed method enables cost-effectiveness by eliminating the need for voltage measurement sensors. Moreover, the decision-making process is based on highly simplified data, which in turn allows for a variety of communication technologies to be employed. This flexibility enables authorities to optimise both the cost-effectiveness and performance of the system. Furthermore, as the scheme is inherently based on digitised data, it is particularly well-suited for integration with modern digital equipment, aligning with the ongoing transition towards digital substations and smart grid infrastructures.

The scheme has demonstrated its reliability, selectivity, and accuracy through non-real-time simulation conducted in MATLAB/Simulink software. The simulated model represents a radial system with multiple buses. Various test scenarios are reported, including changes in fault location within the same line section to evaluate the scheme's performance against close-in faults; variation in fault resistance to assess its response to high impedance faults (noting that the scheme may not be initiated under extremely high fault resistance due to threshold limitations, which can be adjusted by the user); variations in short-circuit levels to examine effectiveness in weak infeed conditions; and load variations without faults to test system security.

Additionally, the scheme provides fast and accurate identification of faulted sections, as demonstrated through real-time hardware-in-the-loop (HIL), testing using Real Time Simulator (RTDS). These tests incorporated actual communication systems to validate the reliability, selectivity, and accuracy of the scheme within the time constraints appropriate for distribution protection and monitoring system.

7.2 Future work

The fault identification/protection scheme presented in this thesis has been described, demonstrated and validated within a defined scope to facilitate clear demonstrations of its performance and efficiency under a range of scenarios. However, real-world distribution systems exhibit a wide range of characteristics beyond the scope considered in this study, which may introduce additional challenges and complexities to the proposed research.

To enhance the practicality and applicability of the research, future work has been outlined as described in the following sections.

7.2.1 Future validation and practical consideration for IIDG-based systems

The tests and validation presented in Chapters 5 and 6 could be extended to applications where the power system incorporates converter-interfaced energy sources. These converters are usually inverters for generators but some applications, such as storage which may supply fault current, may have bi-directional converters. One of the key challenges for conventional protection schemes in future power systems is their reliance on fault currents, which may be significantly constrained by inverter-interfaced distributed generation (IIDG), such as solar PV. Unlike traditional protection, the proposed faulted section identification scheme, which relies on solely on current measurements, has demonstrated its ability to operate effectively even in conditions with reduced fault currents. This feature makes it particularly suitable for weak networks, where conventional protection methods often struggle due to lower short-circuit levels.

However, while the scheme has been extensively tested using a variety of source parameters in simulation and HIL testing, these parameters – although derived from actual sources values within the system – were not obtained from actual IIDG sources with inverters modelled – they were modelled as ideal

sources with variable source impedances to vary the fault level. Since the characteristic of actual IIDG units, such as their fault current contribution and dynamic response, particularly in the short time periods immediately following fault inception, are among the most influential factors affecting conventional protection performance, incorporating real-world data and/or including high-fidelity models of converter-interfaced sources into future simulation and validation exercises would be highly beneficial. Future work should focus on testing the scheme with practical IIDG parameters sets to ensure its applicability in realistic operating conditions. Related work that could be used to inform this future activity includes [7.1] – [7.2].

7.2.2 Investigation of applicability to isolated, or unearthed distribution systems

The research presented in this thesis has focused solely on the application of the faulted section identification scheme in earthed distribution systems. However, in some countries such as Norway or areas requiring particularly reliable and continuous supplies power (e.g. hospitals and mines), systems are sometimes operated completely isolated from earth. This means that for a phase-earth fault there will be no return path for fault current and therefore no fault current will circulate from the source through the fault and back to the source. Other systems are operated with impedance-earthed neutral configurations [7.3], where fault current characteristics may be significantly lower and systems behave differently compared to earthed systems during faults, while some systems are operated with "resonant-earthing" or "Petersen Coils" which match the fault path impedance with an earthing/neutral impedance (an inductor) which is "tuned" to eliminate an earth fault by providing a cancellation effect to the capacitive current during earth faults [7.4].

Accordingly, future work should investigate its performance in unearthed systems, where challenges such as low fault current magnitudes, sustained

overvoltages during single-phase-to-earth faults, and uncertain fault current/power directionality may arise [7.5]. These characteristics can affect the reliability of directional current measurements, which are central to the proposed method.

7.2.3 Expanding to more complex application systems

Given that incorporating actual IIDG parameters would represent more realistic future system behaviour and characteristics, future research should extend simulations to more complex power system configurations to further evaluate the robustness and applicability of the proposed faulted section identification scheme. While some of the cases studies in this thesis utilised a radial 8-bus system, future simulations could explore more intricate network topologies, such as ring or mesh systems or benchmark standard system, for example, the IEEE 34-bus Test Feeder [7.6], which better represent real-world power networks. These configurations would enable a more comprehensive assessment of the scheme's performance under both fault-induced and non-fault-induced system dynamics.

Notably, a preliminary investigation has already been conducted by the author of this thesis using a ring-type system, which was modified version of the IEEE 33-bus benchmark system [7.7] – [7.8]. Details of this can be found in [7.9]. This work provides an initial understanding of how the scheme operates in a more interconnected network. However, further studies incorporating varying system parameters, fault locations, and operational conditions are necessary to fully establish its effectiveness. By integrating more complex simulation environments, future research can provide deeper insights into the scheme's scalability and adaptability in practical and future power systems. Having said this, as long as the measurement and communication infrastructure exists, there should be no issue with the applicability or operation of the system presented in the thesis, but this work would be useful in evaluating the system's

applicability and perhaps with evaluating the economics/cost-benefit of the system in a realistic and representative scenario.

7.2.4 Expanding HIL testing to more complex systems

While the MATAB/Simulink simulation in this study incorporated complex system configurations and various fault scenarios, the HIL testing was conducted using RTDS with a relatively simple power system. The primary objective of the HIL experiments was to verify the fundamental applicability of the proposed fault identification scheme in a real-time environment, utilising hardware and actual communications protocols and systems for data transfer between measuring locations. Consequently, a simple radial 3-bus system with relatively-standard fault conditions was used.

Future work should focus on extending the HIL testing to more complex system configurations, aligning with the more diverse and wide-ranging set of conditions explored in the MATLAB/Simulink simulations. This includes investigating high-impedance faults, the integration of IIDGs, and potentially other more complex networks, as outlined previously. Furthermore, the inclusion of additional power system components such as transformers should be examined – particularly cases involving primary or current transformer saturation (which should not be numerous, but are still worthy of evaluation) – to assess the scheme's robustness under a wider range of realistic operational conditions.

Expanding the HIL framework to incorporate more complex networks and fault scenarios will provide a more comprehensive validation of the scheme's performance. This would ensure a more rigorous assessment of its practical feasibility in modern distribution networks and enhance confidence in its deployment practically.

7.2.5 Exploring alternative communication technologies for protection systems

As discussed in Chapter 2 and 4, various communication applications are relevant and potentially applicable to the proposed faulted section identification scheme for protection and monitoring/FLISR applications. However, in this research, validation using HIL testing was conducted using only wired Ethernet connections, which were chosen due to availability in the university laboratory. Ethernet is a communications technology similar to those commonly used in practical protection systems, such as power line communication or fibre optics. While Ethernet is a viable and representative option, future developments in power system protection are expected to incorporate a broader range of communication technologies, including increasingly wireless solutions [7.10] – [7.12].

A promising direction for future research would be to explore alternative communication methods, particularly wireless technologies, to expand the available options for protection schemes. For instance, integrating private 4G/5G networks into the HIL setup would allow for an early assessment of their feasibility in protection applications. This would provide insights into their performance under different conditions, and include investigation and evaluation of parameters such as latency, reliability, and resilience to interference. By investigating these emerging technologies (from a protection application perspective), this reach can contribute to the advancement of protection schemes, ensuring their adaptability to the evolving power system infrastructures.

7.2.6 Enhancing protection system resilience through back-up protection for communication failures

The proposed protection scheme has been designed to ensure that communication between relays remains as simple and low-bandwidth as possible, with robustness against varying latency and no requirements for extremely fast/fixed latency performance levels. This approach minimises the amount of data exchanged, making the signalling process more efficient and well-suited for modern digital infrastructures. However, despite its efficiency, the scheme still relies on communication for its operation. In the event of communication failure, relays would be unable to exchange signals, potentially compromising the effectiveness of the protection system.

To address this limitation, developing a back-up protection scheme operating independently of communication should be considered. The additional layer of protection would ensure system reliability under scenarios where communication is disrupted or unavailable. Potential solutions could involve localised decision-making methods, such as adaptive overcurrent protection or other non-communication-based techniques, to provide fault detection and isolation when the primary scheme is inoperative. Investigating and integrating such back-up mechanisms will enhance the robustness of the protection system, ensuring its resilience against communication failures while maintaining the advantages of the proposed digital-friendly scheme. Finally, in distribution applications, there may still be some definite time protection (for example at the main infeed point) that would be expected to provide an ultimate level of back-up, albeit operating relatively slowly and isolating much more of the network than necessary/desirable, but providing back-up protection nonetheless.

7.2.7 Improving faulted section identification to include more accurate fault location

One potential limitation of the proposed fault identification scheme is its approach to fault isolation, which focuses on identifying and isolating the faulted zone or line section rather than pinpointing the exact fault location. While this method is effective for ensuring system reliability and rapid fault clearance, it may present challenges in certain maintenance scenarios. The scheme is particularly well-suited for overhead line networks, where faults can often be visually inspected, allowing maintenance personnel to locate and repair the fault efficiently. However, in underground cable systems or complex network configurations where visual inspection is not feasible, additional fault localisation techniques may be required to complement existing approaches.

Future research can explore ways to enhance fault pinpointing capabilities, particularly in environments where direct visual inspection is impractical. This could involve integrating complementary fault location algorithms or leveraging advanced sensing technologies, such as travelling wave-based methods or machine learning-driven fault estimation techniques. By addressing these challenges, the scheme can be further improved to support a wider range of power distribution networks, ensuring both efficient fault isolation and practical maintenance procedures across different system topologies. Note that some of this may require more accurate measurement and/or higher-performance communications, but it is still worthy of investigation.

7.2.8 Implementing the algorithm in a physical relay and testing in a microgrid

While simulations and HIL testing provide valuable insights into the feasibility of the proposed fault identification scheme, the most definitive way to demonstrate its practical applicability is through implementation in a real protection relay and testing in an actual power system environment. Deploying

the algorithm in a physical relay would allow for an evaluation of its real-time performance, response time, and compatibility with existing protection infrastructures. Additionally, integrating the scheme with FLISR systems would enable a more comprehensive assessment of its potential role in enhancing distribution system reliability and automation [7.13].

To facilitate this, an initial step could involve testing the scheme in a microgrid, which serves as a controlled yet realistic environment that reflects key characteristics of modern power systems. Microgrids incorporate both traditional and IIDGs, making them an ideal testbed to assess the algorithm's effectiveness under different operating conditions. By conducting real-world experiments in such a setting, the research can bridge the gap between theoretical validation and large-scale implementation, ensuring the scheme's readiness for practical deployment in future distribution networks with advanced automation systems.

7.3 Economic and cost-benefit analysis of the proposed scheme

The proposed faulted section identification method, which utilises solely current measurements, with no need for time synchronisation nor polarising voltage measurements, potentially offers several economic advantages. Firstly, there should be faster and more discriminative isolation of faults. There should be with largely uniform operation times in terms of faulted section identification across the entire network, negating the often-undesirable impact of time-graded overcurrent protection at distribution voltages, which can sometimes result in fault clearance times of several hundreds of milliseconds or more.

This faster operation times can therefore minimise damage to equipment, reduce the risk of fires and other consequential damage, reduced risk to personnel, the public and wildlife, reduce the requirement for and stress

associated with fault ride-through for connected generation, storage and other devices, etc. This could all have significant economic benefit. If the system is fully or partially blacked out, the knowledge of faulted sections can be used to minimise fault finding time and to more efficiently reconnect the system. During restoration, any faults remaining on the system (e.g. after a major storm) would be known and the system could be used in either protection or monitoring mode to assist with restoration from severely damaged/degraded states.

Other economic benefits may be associated with the simplicity of the scheme – requiring no detailed design or setting (minimising staff and time required to assess, configure and apply settings) and reducing risk of incorrect settings/configurations leading to incorrect/undesired/slow operation after deployment. While communications is required for the system and will attract a cost, the design of the scheme - comparing data between measurement points at both ends of a line section and transmitting this information as binary codes, instead of streaming continuous analogue or phasor data - not only simplifies the communication process but also allows for the selection of cost-effective communication technologies (which is tailored to the desired balance between performance and cost) that meet the low-latency demands essential for protection systems in distribution networks.

Another potential economic benefit of this method is the reduction in costs associated with implementation (for example compared to directional, differential or phasor-based protection). The scheme's reliance solely on current measurements eliminates the need for voltage sensors, thereby decreasing both equipment and installation expenses. Furthermore, as the scheme does not require continuous communication between all nodes, it inherently minimises the risk of communication failure leading to incorrect protection decisions, enhancing system reliability without incurring additional costs. Finally, no timing/synchronisation is needed, so no GPS or other clock/synchronisation methods would be required.

The ability to implement the scheme on both centralised and distributed architectures allow flexibility and potential cost savings. However, the scheme's characteristics shows a slight preference for distributed architectures, particularly in the context of FLISR application [7.13]. It effectively reduces communication costs associated with wide-area coverage, by facilitating relay-to-relay communication within specific zones for localised fault discrimination autonomously, without needing to forward data to a central controller. This reduces latency issues, especially for long or remote feeders. This decentralised approach also mitigates the risk of a single point of failure associated with centralised communication backbone, thereby enhancing overall system resilience [7.14] [7.15]. However, the distributed approach requires embedded logic and processing capability at each line section, which may introduce higher initial costs compared to a centralised scheme, particularly in large-scale networks. For applications that demand comprehensive system monitoring, such as those involving stability analysis, maintenance planning, or high penetration of RES, a centralised architecture may prove more appropriate. This is especially relevant when integrating grid-edge resources into an advanced Distribution Management System (DMS) or when supporting grid-forming capabilities, where central visibility and coordination play a critical role [7.16] – [7.17].

In term of protection performance, the method offers highly targeted isolation by pinpointing the exact faulted line section, enabling the disconnection of only the faulted segment while preserving service to unaffected areas. This contributes to a significant reduction in extent of outages and minimising the impact upon customers. This target isolating contributes to a decrease in Customer Minutes Lost (CML) and Customer Interruptions (CI). For example, as reported by UK Power Networks, in the year 2022/2023, the average CML was 28.8 minutes per customer per year, and the average CI was 37.2 interruptions per 100 customers per year [7.18]. By improving fault detection and isolation, the scheme has the potential to lower these figures,

enhancing customer satisfaction and reducing penalties associated with service interruptions.

While the requirement to install current sensors at both boundaries of line sections may incur initial costs, these are offset by the elimination of voltage measurement devices and the benefits of simplified communication infrastructure (for example when compared with directional or differential schemes). The overall reduction in equipment complexity, settings and configuration and the associated decrease in the need to update/maintain/test settings on an ongoing basis further contribute to the cost-effectiveness of the protection scheme.

The method could be used for protection applications and/or monitoring/FLISR applications as mentioned several times elsewhere in the thesis. While protection application would require current-interrupting devices (which would incur costs), the other benefits listed elsewhere may justify this expense. An alternative may be to use non-fault interrupting devices (e.g. disconnectors) to isolate the faulted section, initially isolating the overall section of system with a circuit breaker (e.g. at the head or mid-point of the feeder) and rapidly re-configuring the system to isolated the faulted section using simple and cheap disconnectors, while the system is de-energised, having been isolated initially by circuit breaker(s).

In summary, the faulted section identification method offers a cost-effective solution for enhancing the reliability and efficiency of distribution network protection. Its design minimises infrastructure and operational costs while providing flexibility in communication and architecture choices, making it a financially viable option for modern power systems.

Chapter references

[7.1] X. Shi, H. Zhang, C. Wei, Z. Li, and S. Chen, 'Fault Modeling of IIDG Considering Inverter's Detailed Characteristics', *IEEE Access*, vol. 8, pp. 183401–183410, 2020.

[7.2] C. Fang, L. Mu, Z. Wang, and G. Chen, 'Analysis of Grid-Forming IIDG's Transient- and Steady-State Fault Model', *IEEE Trans. Smart Grid*, vol. 13, no. 2, pp. 1187–1199, March 2022.

[7.3] G. Zhu, 'Earthing Systems', Surge Protective Device. [Online]. Available: https://lsp.global/earthing-systems/

[7.4] H. H. Brown and E. T. B. Gross, 'Practical experience with resonant grounding', *Electr. Eng.*, vol. 70, no. 8, pp. 674–674, August 1951.

[7.5] W. Zhang, X. Xiao, Y. Wang, T. Zheng, H. Zhao, and H. Wang, 'Charging-Transient Based SLG Fault Location in Neutral-Unearthed Distribution System', in *2011 Asia-Pacific Power and Energy Engineering Conference*, March 2011, pp. 1–4.

[7.6] IEEE standard, 'Resources – IEEE PES Test Feeder'. [Online]. Available: https://cmte.ieee.org/pes-testfeeders/resources/

[7.7] M. E. Baran and F. F. Wu, 'Network reconfiguration in distribution systems for loss reduction and load balancing', *IEEE Trans. Power Deliv.*, vol. 4, no. 2, pp. 1401–1407, April 1989.

[7.8] S. H. Dolatabadi, M. Ghorbanian, P. Siano, and N. D. Hatziargyriou, 'An Enhanced IEEE 33 Bus Benchmark Test System for Distribution System Studies', *IEEE Trans. Power Syst.*, vol. 36, no. 3, pp. 2565–2572, May 2021.

[7.9] P. Rajakrom, C. D. Booth, and Q. Hong, 'Current-only directional protection of distribution networks using low-cost communication', in *17th International Conference on Developments in Power System Protection (DPSP 2024)*, March 2024, pp. 1–7.

[7.10] M. M. Eissa and M. H. A. Awadalla, 'Centralized protection scheme for smart grid integrated with multiple renewable resources using Internet of Energy', *Glob. Transit.*, vol. 1, pp. 50–60, 2019.

[7.11] [M. M. Eissa, I. A. Ali, and K. M. Abdel-Latif, 'Wi-Fi protected access for secure power network protection scheme', *Int. J. Electr. Power Energy Syst.*, vol. 46, pp. 414–424, March 2013.

[7.12] T. Bartman, B. Rowland, and L. Rogers, 'Expanding Protection and Control Communications Networks With Wireless Radio Links', in *2019 IEEE Rural Electric Power Conference (REPC)*, April 2019, pp. 39–45.

[7.13] [A. A. Shobole and M. Wadi, 'Multiagent systems application for the smart grid protection', *Renew. Sustain. Energy Rev.*, vol. 149, p. 111352, October 2021.

[7.14] ['Busbar protection | Hitachi Energy'. [Online]. Available: https://www.hitachienergy.com/products-and-solutions/substation-automation-protection-and-control/substation-automation-systems/protection-solutions/busbar-protection

[7.15] H. Watanabe, I. Shuto, K. Igarashi, P. Beaumont, and K. Okuno, 'An enhanced decentralised numerical busbar protection relay utilising instantaneous current values from high speed sampling', in *2001 Seventh International Conference on Developments in Power System Protection (IEE)*, April 2001, pp. 133–136.

[7.16] 'Wide Area Monitoring Protection & Control Solutions' [Online]. Available: https://www.gevernova.com/grid-solutions/services/catalog/wampac-solutions.htm

[7.17] R. Das *et al.*, 'Centralized Substation Protection and Control', IEEE PES Power System Relaying Commitee, Report of Working Group K15 of the Substation Protection Subcommitee, December 2015.

[7.18] 'Network reliability | UK Power Networks Annual Review 2023'. [Online]. Available: https://annualreview2023.ukpowernetworks.co.uk/annualreview2023/operational-performance/network-reliability